(12)

TECHNICAL REPORT NO. 11893 (LL-146)

FEASIBILITY ANALYSIS AND EVALUATION OF AN ADAPTIVE TRACKED VEHICLE SUSPENSION AND CONTROL SYSTEM

FINAL REPORT

See 1473

JUNE 1975

Contract No. DAAE07-72-C-0176

by Robert M. Salemka
National Water Lift Company
A Division of Pneumo Corporation

and

Ronald R. Beck
Surface Mobility Division

TACOM

MOBILITY SYSTEMS LABORATORY

U.S. ARMY TANK AUTOMOTIVE COMMAND Warren, Michigan

FEASIBILITY ANALYSIS AND EVALUATION OF AN ADAPTIVE TRACKED VEHICLE SUSPENSION AND CONTROL SYSTEM

Final Report No. 11893 (LL-146)

by

Robert M. Salemka

National Waterlift Company
A Division of Pneumo Corporation

and

Ronald R. Beck

US Army Tank Automotive Command

Contract No. DAAE07-72-C-0176

June 1975

TABLE OF CONTENTS

TABLE OF CONTENTS (cont'd)

FIGURES

FIGURES cont'd PAGE

FIGURES cont'd

FIGURES cont'd

2.0 ABSTRACT

This study shows that adaptive control of the jounce damping characteristics of the first and last wheel of a tracked vehicle can cause a significant improvement in performance. This improvement resulted in an overall 30 percent reduction in average pitching rate of the hull, as measured on the simulation of the MICV vehicle traversing the JEA bump course.

Verification testing of the computer model with actual performance data of the MICV vehicle showed good correlation of peak amplitudes and hull resonance. This data also confirmed that the actual dampers are working well below recommended levels.

A proposed method of mechanizing and testing the adaptive control on an actual vehicle is presented along with system schematics and preliminary performance specifications for the critical components.

3.0 INTRODUCTION

3.1 Purpose

The primary purpose of this study was to investigate the feasibility of using adaptive damping to improve the suspension characteristics of a tracked vehicle. Secondary purposes were to develop an analog computer model which could be used for more complete evaluation by TACOM and to propose a method of mechanization of the adaptive principle for actual hardware testing.

3.2 Vehicle and Terrain

The MICV vehicle running on the JEA bump course was selected as a candidate vehicle and terrain. The primary reason was the availability of test data of pitch and heave while traversing the bump course as well as high speed movies showing detail motion of the track, wheels, and hull. The suspension system has a dual rate mechanical spring rate which is as soft as a hydropneumatic system.

3.3 Adaptive Control

The adaptive control was achieved by switching the jounce damping relief valve between two different relief pressure points as a function of pitching rate of the hull. When the hull was pitching up, the damping was reduced on the front wheels and increased on the rear wheels. When the hull was pitching down the process was reversed. A modification using the heave rate of the hull was also tested by switching the damping control on the summed signal of the pitch rate times a constant plus the vertical heave velocity. The constant was determined by the distance between the wheel and the center of gravity of the hull. Careful consideration was given to the sign of the summation so that a positive heave signal would tend to reduce the damping on both the front and rear wheel and negative heave would increase the damping on both the front and rear wheels. Other modifications investigated included the bi-level damping control in the jounce direction, and full adaptive control on the first, second and sixth wheel.

3.4 Describing Equations

Two sets of describing equations have been developed. The first set assumes the availability of quite large analog or digital computer capabilities. The second set is less complete and tailored around the limitations of a modestly sized analog computer.

The major improvement of these describing equations over previous simulations is that the ground force is considered to act on the wheel at right angles to the local slope of the ground profile. Previous studies were done with the ground force acting vertically up regardless of the slope of the bump.

The effects of the track have also been included for the first time. This effect has been found to have a major impact on the dynamic behavior of the hull primarily due to an apparent change of stiffness of the suspension system due to the track. A difference of almost 2:1 in pitching frequency of the hull has been measured with and without the track.

3.5 Computer Model

The analog computer model differs from previous models principally because of the use of the direction of the ground force vector acting to rotate the hull. The previous studies treated the ground force vector as a vertical force only. Thus the torque to the hull was essentially proportional to the ground force. In actual practice the torque is a function of both the magnitude and the direction of the ground force. The other major difference is the inclusion of the track and track tensioning device.

A Systron Donner Model 80H analog computer was used for the simulation. One hundred and four internal amplifiers were supplemented with an additional forty-two external amplifiers for the simulation.

3.6 Proposed Mechanization

An existing tracked vehicle already equipped with hydro-pneumatic suspension has been selected as ideally suited for the mechanization of adaptive damping; main reasons were the degree of improvement to be expected, the ease and cost of rework, and the applicability of the results.

The suggested design of the test hardware will result in a system with adaptive damping on the two front and two rear wheels with hull pitch, heave and roll sensors combining signals to cause switching of the damping solenoids. This system is flexible enough so that all combinations of sensors and switching solenoids can be used or deleted for system evaluation.

Hardware testing is expected to be done with emphasis placed on the quality of the ride and the life expectancy of the dampers.

4.0 DISCUSSION

4.1 Computer Simulation

4.1.1 Candidate Terrain

In the early phases of the study, a number of candidate terrains were considered. Availability, comparative test data, and ease of implementation were the controlling factors effecting the choice. By mutual agreement with the cognizant TACOM engineers, it was decided to use the JEA bump course for the NWL studies to be followed by a final evaluation by TACOM using the number 12 rocky Fort Knox course from RRC9.

The JEA bump course is an existing terrain simulation which NWL has used in past simulations and for which comparative performance data on the MICV vehicle has been taken. The details of the obstacles and course are shown on Figure 26. Use of this course gives a data base from which relative comparisons can be made.

4.1.2 System Equations

The describing equations used to simulate the system are included in Appendix "A" of this report.

The basic philosophy has been to simulate only one side of the hull, neglecting all roll characteristics. This simplifies the problem to three degrees of freedom.

A unique feature of this simulation as opposed to previous studies, was that the vector direction of the ground force with respect to the center of gravity of the hull has been considered. This causes a difference in pitching motion on the hull which is quite significant. The difference between the spring torque on the road arm and the corresponding ground reaction component due to road arm angle has also been considered.

The effects of track tension and track inertia on the performance characteristics have been included. A discussion of the simulation is included in Appendix "A".

4.1.3 One Wheel Study

The physical limitation of the size of the computer required some simplifications of the describing functions for the system. To select which parameters could be simplified without affecting final results, a single wheel of the suspension system was simulated. The simulation was initially made without regard to usage of computer components but rather to give the best mathmatical model that was achievable. This model was then used as a comparison against various simplifications to determine the best model that could be made.

The major result of this study was that the centripetal force and tangential acceleration force vectors could be modeled quite closely by a single acceleration acting at a fixed radius from the center of gravity of the hull. This distance roughly corresponds to the nominal steady state distance between the center of gravity of the hull and the centerline of the wheel.

4.1.4 Computer Equations

The original system equations were simplified to accommodate the available computer. These equations along with the detailed computer simulation diagrams are included in Appendix "B" of this report.

By careful selection of variables, the horizontal motion was removed from the equations of motion. This reduced the system to only two degrees of freedom. These were rotation and vertical motion.

The ground profile was built into an electrical circuit as a separate ground profile generator. Twelve separate leads were used to generate the magnitude and slope for each of the six wheels so that the proper sequencing of each bump under each of the six wheels could be properly simulated.

4.1.5 Verification of Model

The computer model was set up to simulate the physical characteristics of the MICV vehicle. This model was then run across the JEA bump course and the results compared with actual test data from the vehicle. The results may be seen by comparing Figures 9.0, 9.1 and 8.0. It appears that the actual 15 mph test run falls between the 10 mph and 15 mph computer runs.

The damping pressure had to be reduced to a 600 psi relief pressure before the computer runs began to have the amplitude and acceleration magnitudes of the actual test data. This reduction in pressure level is substantiated by other test data which indicates that the actual damping pressure was considerably lower than the design level or the damping level demonstrated in bench testing.

The performance of the simulation is felt to be a good match with the actual performance of the vehicle.

The base line system established by this comparison is summarized in Figures 1 and 2. The 5, 10, 15, 20, 25, 30 and 35 mph speed runs are shown in Figures 7.0, 8.0, 9.1, 10.0, 11.0, 12.0 and 13.0.

4.1.6 <u>Performance Factor</u>

An average pitch rate of the hull over the bump course has been selected as a comparative performance factor for use of these studies for the following reasons:

a) It is very simple to generate.

b) Pitch rate is the single most sensitive source of input disturbance to the vehicle.

c) An actual gunner ignores sharp peaks in pitch rate. Time on target is more a function of average pitch rate.

d) In general a suspension system that reduces pitching will allow a man to perform his tasks more accurately, allowing the gun stabilization system to realize its full potential.

Figures 1 and 2 show this performance factor plotted against speed for the different configurations.

4.1.7 Improved Non-Adaptive System

The suspension system was optimized relative to the selected performance factor prior to incorporating the adaptive damping system. The results are summarized in Figures 1 and 2. The detail computer traces are shown in Figures 7.2, 8.2, 9.3, 10.2, 11.2, 12.2 and 13.2. These studies indicate a considerable improvement in pitch rate if the damping pressure relief point is increased to 1200 psi from the apparent present value of 600 psi, and an orifice is included for increased rebound damping. The relative improvement due to increasing the jounce damping and rebound damping is shown in Figure 2.

The average velocity was reduced to .54 of the base line system with more improvement in high speed operation than low speed.

4.1.8 Adaptive Damping

Incorporation of adaptive damping control shows an overall average of 30% improvement over an optimized system without adaptive damping. This is summarized in Figure 1. Detail performance curves are shown in Figures 7.3, 8.3, 9.4, 10.3, 11.3, 12.3, and 13.3. Figure 1 shows a tendency for more improvement at the low speed runs than at the higher speeds.

4.1.8.1 The mechanization of the adaptive damping control was to switch levels of the jounce damping relief valve between high damping and low damping based on the sign of the pitch rate of the hull. The bi-level damping curve is shown in Figure 6.

Figure 4 shows the damping curve for the base line system and Figure 5 shows the damping curve for the optimized system without adaptive control.

4.1.8.2 An investigation showed that switching the level of rebound damping rather than jounce damping was less effective. The results are better than simple jounce damping at the same level but not as good as adaptive jounce damping. No data is included.

4.1.8.3 Pitch rate control plus heave velocity of the hull is shown in Figure 1. The data shows a very slight improvement in average pitch rate between 15 and 25 mph, and a slight loss of performance above 25 mph.

The overall effect seems to be little difference in performance between having the additional heave velocity signal and not having it. It should be pointed out however that this particular terrain does not stimulate the vertical resonance frequency of the hull and that perhaps under these admittedly special conditions, the heave signal could show a tremendous improvement.

The detail performance difference between the pitch rate adaptive and the pitch rate plus heave rate adaptive control can be seen by comparing Figures 7.3, 8.3, 9.4, 10.3, 11.3, 12.3, and 13.3 with 7.4, 8.4, 9.5, 10.4, 11.4, 12.4, and 13.4.

4.1.9 <u>Sensitivity Study</u>

A sensitivity study was made to determine the effects on the suspension system of variations in the road arm angle and spring rate. To some degree the two parameters are related since the apparent vertical stiffness of the suspension is proportional to the torsional stiffness and inversly proportional to the cosine of the road arm angle. The main difference between the two parameters is that the torsional stiffness controls the total energy stored in the suspension system or the peak force at the jounce bump stop, while the road arm angle controls the shape of the energy curve, making it initially stiff, then softer as the road arm angle swings through zero degrees; then stiffer as the road arm swings up to the jounce stop.

4.1.9.1 The effects of suspension stiffness were studied for 750, 900, 1100, and 2000 in-lb/deg stiffness. The base line is 1000 in-lb/deg. Any rate less than 750 caused the wheel to toggle over to the rebound stop due to the 44° road arm angle yielding a bigger change in effective ground force than the corresponding change in force from the spring.

The results show the improvement in ride that can be achieved with a softer suspension. As may be expected, the softer spring yields a lower disturbance to the hull. The improvement however becomes less and less as the hull speed is increased until, at 30 mph there is almost no difference between a 750 in-lb/deg suspension and a 2000 in-lb/deg suspension. Detail performance curves are shown in groups of four from Figure 14.1 through Figure 19.4.

4.1.9.2 The effects of road arm angle were studied for 39°, 44°, and 49°. This is the angle with respect to the hull waterline and represents the static position of the road arms with the hull on level ground and at rest. The 44° angle is the base line system.

The results show that the more nearly horizontal case (30°) results in less heave and pitch velocity but a greater total pitch angle up to a speed of about 20 mph. Above 20 mph the differences in ride are inconclusive.

The steeper angles had higher pitch and heave acceleration and velocity peaks, but less total pitch angle. The ride appeared to be rougher.

The performance curves for these cases are shown in groups of three from Figure 20.1 through 25.3.

4.1.10 Track Tension

The track tension equations are developed in detail as part of Appendix "A" and "B".

Track tension had the effect of quadrupling the effective stiffness of the suspension system. With the suspension damping set to a very low value, the system was excited and allowed to ring down. With the track tension activated, the pitch resonant frequency was measured at 1.4 Hz. With the track tension effects removed, this frequency dropped to .70 Hz. Because of this tremendous difference in apparent track tension, the behavior of the vehicle across the bump course was drastically different with and without the effects of track tension.

All evaluation data was taken with the track tension active. Had the data been evaluated without the track tension, the pitch amplitudes would be greatly reduced, the pitch rates would be down, and there would be much poorer correlation between the actual vehicle and the simulation. Sample runs were made but the data is not included in this report.

4.2 Proposed Mechanization

In order to properly evaluate the proposed adaptive concept design, certain background considerations must be kept in mind, particularly in terms of the candidate test rig and suspension components that are chosen.

The first point that should be made is that comparison of vehicle performances both equipped with, and without the adaptive damping control feature must be based on optimal configurations of each. That is, if the existing vehicle damping characteristics are not optimum for the basic and conventionally damped system, two situations can occur. First, the adaptive system may exhibit performance advantages that exist only because the conventional system is not optimum. Secondly, the adaptive system may not be able to achieve the maximum performance improvement of which it may be capable. Implicit in these two statements is the fact that previous work has shown that best performance of the adaptive system is achieved when it is incorporated into the optimum conventional system.

The theoretical work also confirmed the validity of the basic rationale for the adaptive system. When a moving vehicle encounters ground disturbances, nonlinear periodic motions of the suspended mass result. The suspension system must damp out these motions by the generation of velocity-dependent forces. In a conventional system, these forces are also generated when an undisturbed hull traverses the ground disturbance. The suspension damping thus not only removes disturbances in the hull, but contributes to the source of those disturbances, when it reacts to the original ground disturbance. The adaptive concept recognized this anomaly by postulating the following control philosophy: the damping force should only exist when the local hull velocity is in a direction opposite to the damping force. As an example, consider a jounce damper on #1 wheel when it encounters a bump. The upward motion of the wheel creates an upward acting force on the hull due to the damper as well as the winding up of the spring. This increased force causes increased disturbance to the hull. After the bump has been traversed, the damping action acts to remove the periodic motion which is induced in the hull because its force is now always in the opposite direction to the hull motion. The adaptive function removes the damping force when the bump is first encountered, but applies it when the bump has been traversed.

These comments apply only when the suspension system can swallow the ground disturbance. That is, when the ground disturbance does not demand wheel travels greater than the suspension capability. With large obstructions in particular, the suspension system must generate forces large enough to move the hull away from the obstruction, so that the wheel does not bottom out on the bump stop. This situation demonstrates the desirability of having an adaptive control system that can be switched out under certain conditons. It also points to the main advantages of an adaptive system, which are to smooth out the relatively small disturbances in order to provide a better gun firing platform, increase riding comfort, and reduce heating of the damping mechanism.

With respect to the damper heating problem it should be pointed out that reducing the damping force invariably increases the heating effect. Numerous tests, as well as simulation programs have demonstrated this phenomenon. This has to do with the resonance characteristics of the vehicle in pitch heave and roll. With no damping at all, the hull motions become so severe that the suspension components are damaged. However, in this case, the heating is zero. Increasing the damping from zero results in a peak in the heating rate at very low damping levels. The heating effect then drops continuously, again becoming zero when infinite damping is reached. At some specific damping level, the ride motion becomes less severe, and the heat dissipation capability of the suspension is least exercised. With adaptive damping added, the damping level could presumably be increased, allowing for a rough but mobile characteristic over severe terrain when the adaptive system disconnected.

The desirability of a high damping level also is a factor when the suspension spring characteristics are optimized.

For the best ride, the spring rate must be as low as possible, since it, too, induces disturbances to the hull. This is not desirable when traversing severe terrain, however, but can be offset by having high damping levels.

Concept Design Goals

Previous work has indicated the feasibility and potential advantages of an adaptive system. The concept design proposed is intended to confirm these results by hardware testing and answer certain questions not answered by previous work. These goals are summarized as follows:

1) Evaluate the adaptive system as initially conceived.
2) Subject the system to terrain and operating modes not covered by previous work.
3) Evaluate the use of heave velocity sensing.
4) Evaluate the use of roll velocity sensing.
5) Determine the effect of adaptive damping on front wheels only.
6) Evaluate fail-safe feature.
7) Provide for recording of all dynamic quantities of interest.
8) Measure dynamic performance of sensors and solenoids.
9) Evaluate different levels of sensor switch bias offset.
10) Evaluate drive selection of damping mode.
11) Evaluate variable spring rate provision.
12) Evaluate damping levels.

4.2.1 System Schematic

The proposed integrated adaptive suspension and control system is shown schematically on S-2850023, and Figures 28.0 and 29.0

It is proposed to rework the damping valve section of an existing hydropneumatic system to incorporate the solenoid valves for bi-level damping control. This rework would be done on the front and rear units of the suspension system. The addition of two rate gyros for pitch and roll, one vertical rate gyro for heave, and the associated electrical logic and switching console completes the major portion of the adaptive system.

An additional solenoid is proposed to connect the hydraulic side of the springs of the first and second units through a manual selection switch. This allows for a manual selection of two different spring rates for the loading wheels. The system is completed with the addition of electrical manual shut-off switches which will allow the vehicle to be run with various combinations of front wheel control only, front and rear wheel control, pitch control with or without heave control, with or without roll control, or no adaptive damping at all.

A complete evaluation of the adaptive damping concept can be made by electrically switching the system into the various modes of operation with no mechanical changes to the system while traversing the same terrain on the same day in the same vehicle.

The proposed system has been optimized for maximum integration, simplicity, flexibility, and ease of conversion.

The system integrates easily into existing hardware and requires only the acquisition of a few additional parts all of which, with the exception of the reworked damper valve and special electrical logic package, are standard existing hardware with proven performance characteristics.

The controlled damping is proposed to be added to both the front and rear wheels. Computer studies indicate that the system will work quite well on just the front wheels. Both front and rear wheels however can be incorporated with very little added effort and it is felt that under conditions not tested on the computer, such as undulating terrain, that both front and rear wheel control may be needed. The rear wheel adaptive damping may be switched out for evaluation of the benefit derived by this additional control.

Pitch and roll rate sensors and a vertical accelerometer make up the sensors for the system. Rate sensors have been selected on the basis of proven performance and system simplicity. A solid state accelerometer is available which has the capability of extending the life expectancy well above the 1000 hour level of the rate sensor, but the electronic circuit would have to be extended to include an integrator with proportional feedback to offset the long term drift problem,and the physical mounting of the accelerometer within the vehicle hull would become more critical.

The six solenoids used by the system are all identical. A conventional off-the-shelf type valve manufactured by NWL for a number of aircraft and ground vehicle applications is being used. The high flow requirements of the spring rate selector solenoids are accommodated by a pilot operated valve which is driven by the solenoid valve.

Fail safe features are inherently included in this type of system. The solenoid valves are of the normally closed type so that with no electrical power, the system will automatically revert to a conventional hydropneumatic suspension system. (Reference Figure 27.0)

4.2.2 System Evaluation

Low amplitude switching of the solenoids could cause excess wear to the components, reducing their operating life. This is circumvented by the use of a small bias offset on the rate detector and summing circuit. Thus, a discrete pitching rate level must be reached before any switching of the solenoids takes place.

The rate signals from the pitch, roll and heave sensors are summed with an adjustable weighting factor given to each signal. The resulting signal will determine the solenoid position for each of the four variable damping solenoids. Because of the difference in sign of the summation and also to increase the overall reliability, each solenoid will have its own summing network.

The solenoid valve used for varying the effective spring rate for the first two wheels is triggered by a manual on-off switch. This allows the solenoid to run on normal vehicle power without any power conditioners being used.

In actual application, the valve and line restriction and inertial impedance will tend to have a dynamic effect on the modified spring rate. For slow acting disturbances such as undulating terrain, the lower spring rate will be apparent. For fast acting disturbances such as blocks or rocks, the oil transfer between the units will be delayed and the wheel will have its normal high stiffness, even when the lower rate is requested by the solenoid.

4.2.3 Sensor Trade-Off Study

4.2.3.1 Sensor Types. Standard angular rate gyros are used to indicate directly the required pitch and roll rate information. A linear accelerometer is used for the vertical (heave) direction. Linear rate sensors are not commercially available. The acceleration signal is integrated electronically to obtain the heave rate.

4.2.3.2 Rate Gyros. Angular rates of up to 60 deg/sec can occur on the hull, but the signal of interest is only in the plus and minus 5 deg/sec range. A 5 deg/sec sensor can be used, and the pickoff will be against its stops beyond this range. The characteristics of a rate gyro allow this to occur without degradation in performance.

4.2.3.3 Accelerometer. The electronic circuitry to obtain the vertical rate from the accelerometer is the critical part of this component. Very low drift requirements are necessary. Commercially available I.C. components are available, but additional circuitry is required to filter out high frequency components of the signal due to noise. Proportional feedback which has the effect of canceling out very low frequencies is also required to compensate for long term drift inherent in such a system.

4.2.3.4 Switching Logic. The local velocity of the hull at each damped wheel is required. Figure 31.0 shows the switching logic to be used.

4.2.3.5 Simplification. The complexity of the concept design is increased due to the need for examining the validity of the simplifications which the simulation study showed feasible. For instance, it is anticipated that only pitch rate will be needed ultimately to obtain most of the adaptive damping effect.

4.2.4 <u>Performance Specifications</u>

4.2.4.1 Appendix C gives the rate gyro specifications.

4.2.4.2 Accelerometer specification TBD.

4.2.4.3 Damper Valve. Figure 30.0 shows the damper valve design. This is an in-house design and manufacture. Additional data for design is contained in R-1649.

4.2.4.4 Electronics. TBD. This is in-house design and assembly.

4.2.4.5 Suspension Units. Existing NWL designed and manufactured units are to be used. See Section 5.0.

4.2.4.6 Solenoid Valve. This is a standard NWL Model 3785 unit.

4.2.5 <u>Hardware Testing</u>

4.2.5.1 Test Conditions Selection. The following conditions will be selected:

1) Jounce damping levels on the first and last wheel locations on both sides of the vehicle.

2) Removal of heave rate logic.

3) Removal of roll rate logic.

4) Spring rate modification to the #1 and #2 road wheel suspensions, by means of manual controls or, as an alternate, automatic control.

5) Damper valve damping pressure levels.

4.2.5.2 <u>Test Instrumentation</u>

1) A 15 channel tape recorder will be used to measure the following variables.

a. Damper pressure levels (4).

b. Pitch, roll and heave sensor rate signals, (3).

c. Voice-over recording of test condition, (1).

d. Solenoid logic signals (4).

e. Suspension cylinder pressures (2).

f. Vehicle speed.

5.2.5.3 <u>Terrain Selection</u>

1) Bump course

2) Cross-country terrain

3) Ditches

5.0 <u>CONCLUSIONS</u>

5.1 A pitch rate adaptive system can be expected to yield a 30% improvement in average pitch rate over a comparable non-adaptive system.

5.2 The addition of heave rate to the pitch rate signal shows only a marginal improvement between 15 and 25 mph. This control loop might become significant under the special operating conditions of undulating terrain being traversed at a speed which will excite the vertical resonance of the suspension system.

5.3 The most improvement of the pitch rate adaptive system can be expected from a vehicle with a soft suspension system.

5.4 The track tension device is so important to the characteristic behavior of the vehicle that it should be included as part of the suspension system design.

6.0 <u>RECOMMENDATIONS</u>

6.1 Pitch rate adaptive damping should be tried on an actual vehicle.

6.2 A vehicle with a soft suspension, preferably a hydro-pneumatic system, should be used.

6.3 Heave rate adaptive damping should be incorporated with the pitch rate damping in such a fashion that it may be switched on or off for comparative performance.

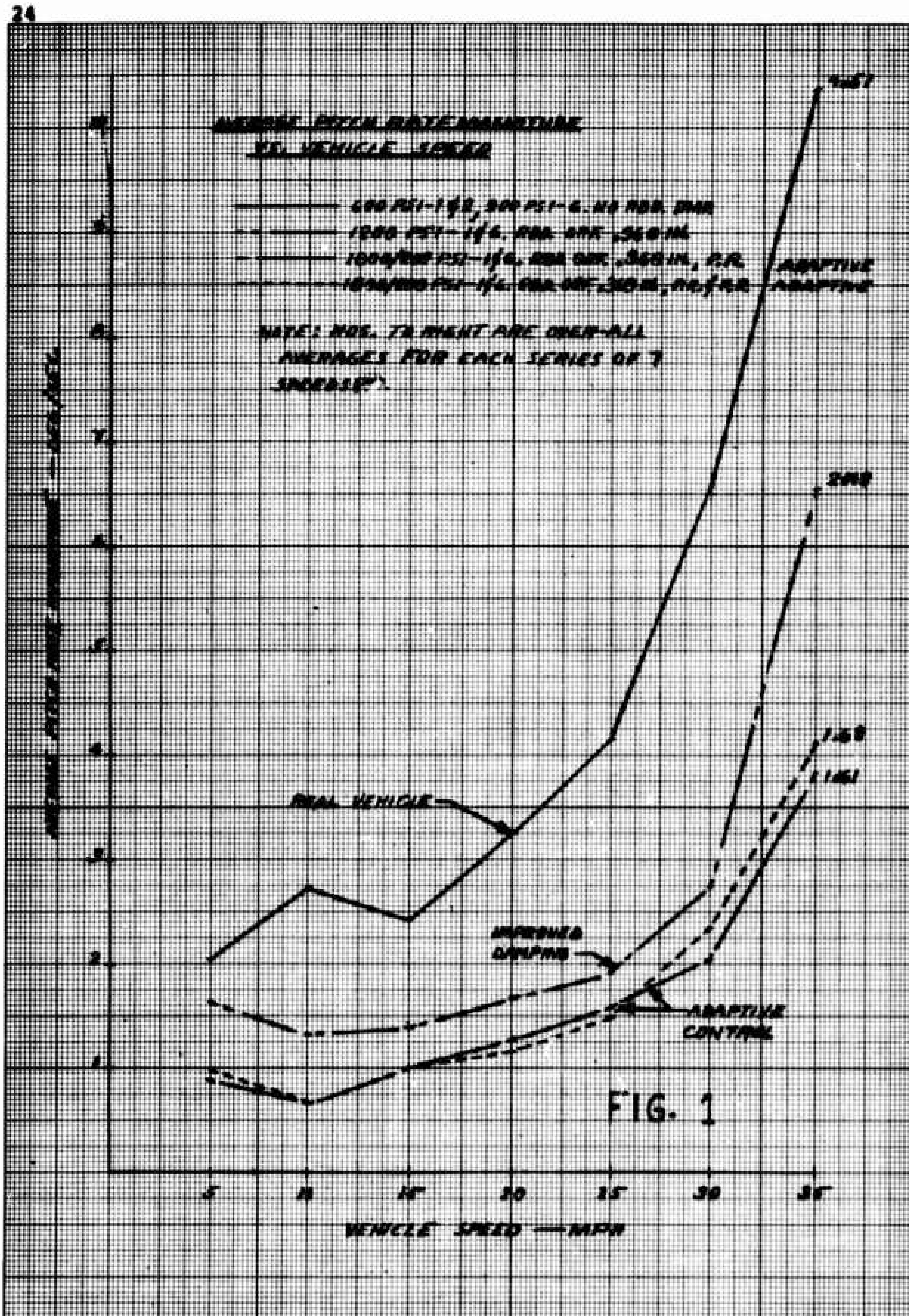
AVERAGE PITCH RATE MAGNITUDE
VS. VEHICLE SPEED
ADAPTIVE
NOTE: NOS. TO RIGHT ARE OVER-ALL
AVERAGES FOR EACH SERIES OF 7
SPEEDS
REAL VEHICLE
IMPROVED
DAMPING
ADAPTIVE
CONTROL
1.69
5
10
15
20
25
30
35
VEHICLE SPEED — MPH

FIG. 1

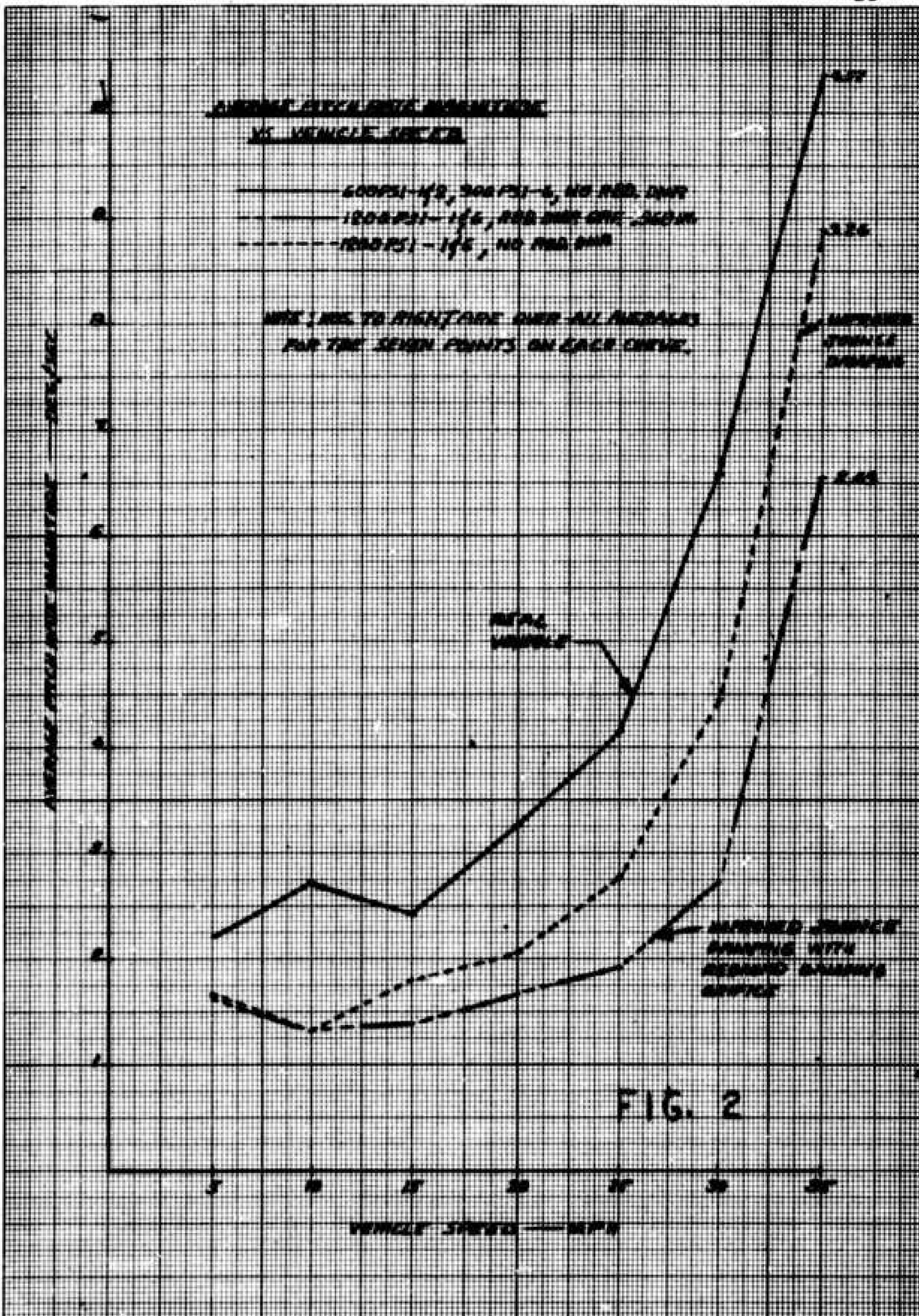

FIG. 2

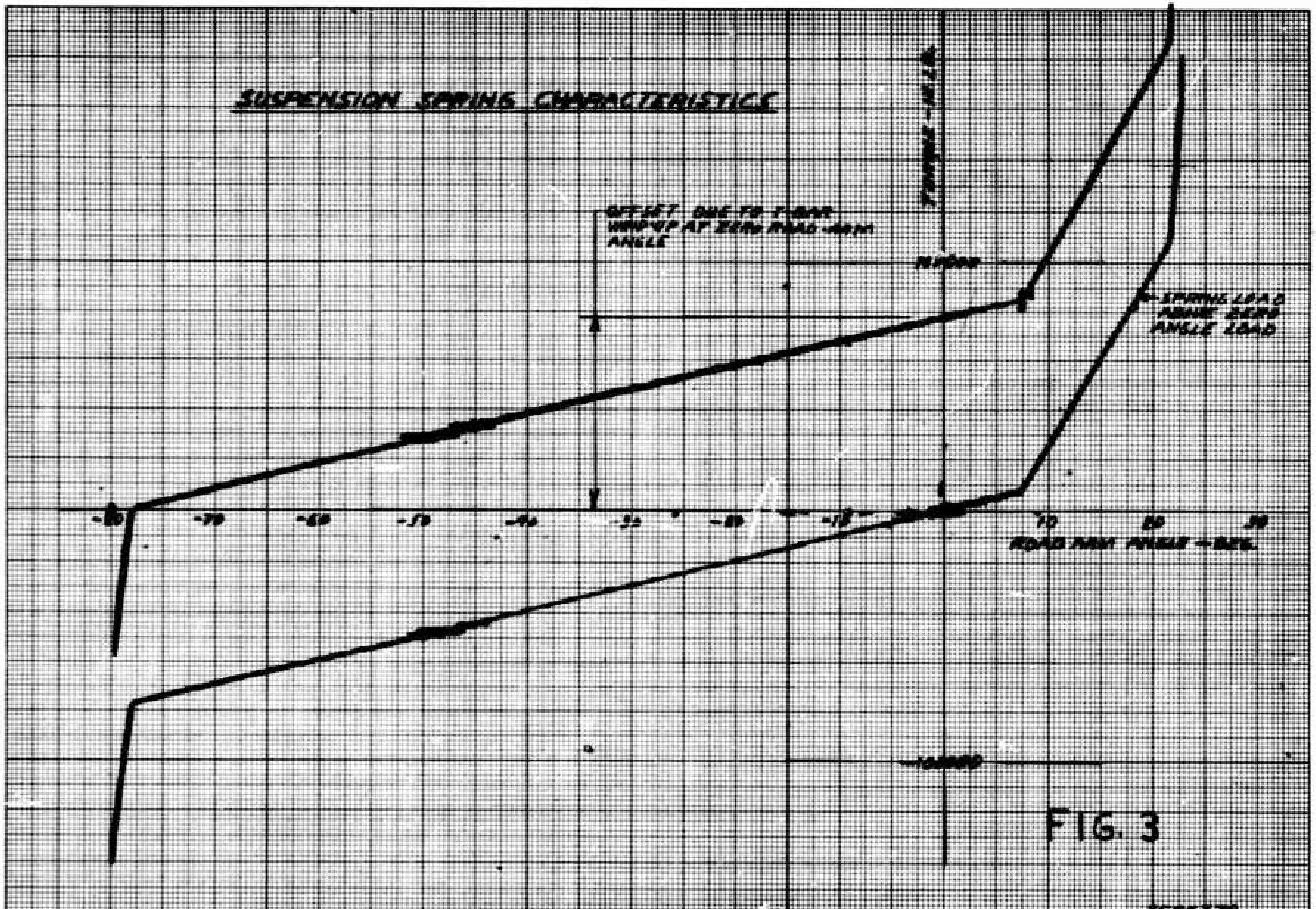
SUSPENSION SPRING CHARACTERISTICS
TORQUE — IN. LB.
OFFSET DUE TO T-BAR WIND-UP AT ZERO ROAD ARM ANGLE
SPRING LOAD ABOVE ZERO ANGLE LOAD
-80
-70
-60
-50
-40
-30
-20
-10
10
20
30
ROAD ARM ANGLE — DEG.

FIG. 3

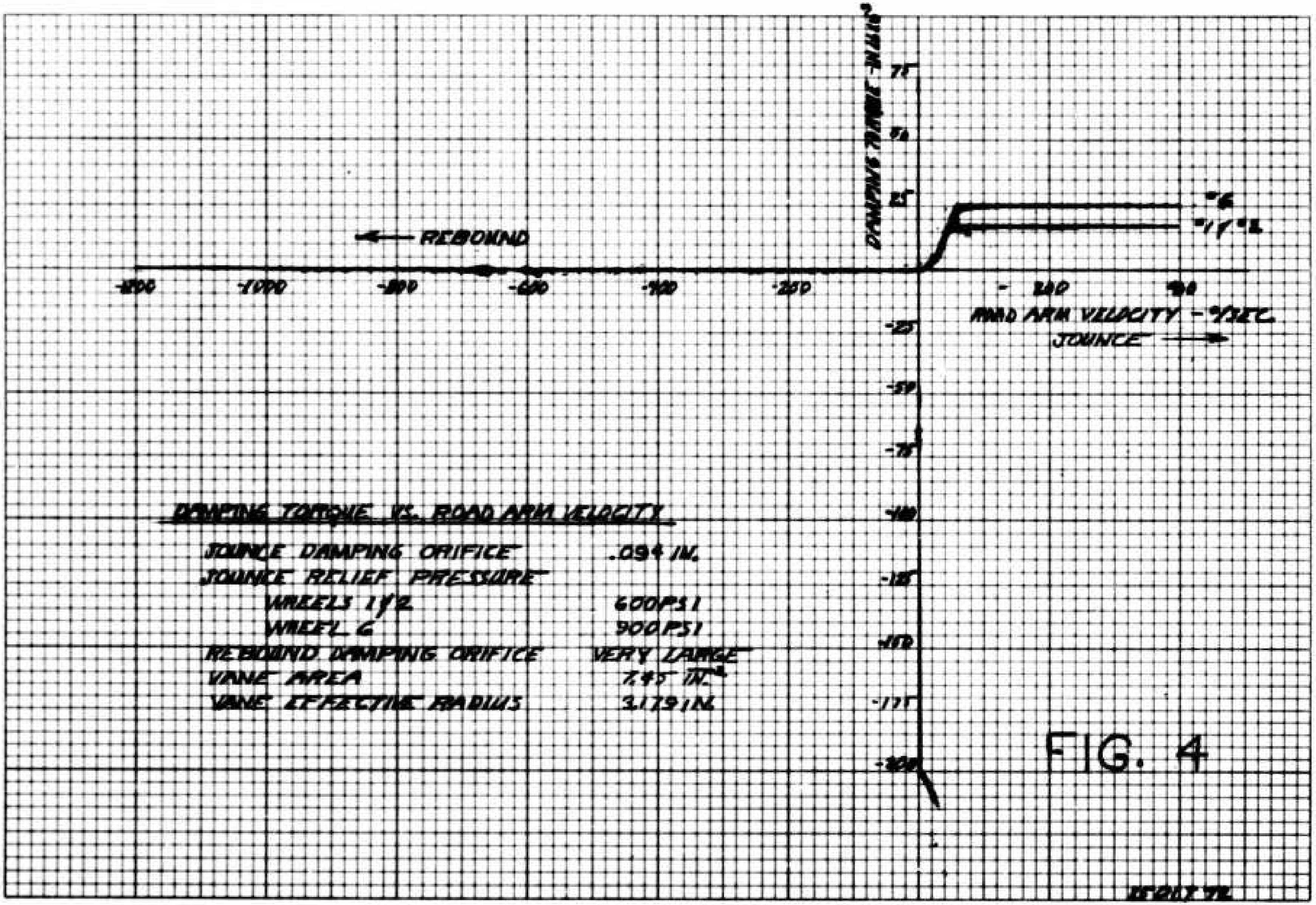
DAMPING TORQUE - IN. LB.
75
50
25
-25
-50
-75
-100
-125
-150
-175
-200
← REBOUND
-1200
-1000
-800
-600
-400
-200
200
400
ROAD ARM VELOCITY - °/SEC.
JOUNCE →
#6
#1 / #2
DAMPING TORQUE VS. ROAD ARM VELOCITY
JOUNCE DAMPING ORIFICE .094 IN.
JOUNCE RELIEF PRESSURE
WHEELS 1 / 2 600 PSI
WHEEL 6 900 PSI
REBOUND DAMPING ORIFICE VERY LARGE
VANE AREA 7.45 IN.²
VANE EFFECTIVE RADIUS 3.179 IN.

FIG. 4

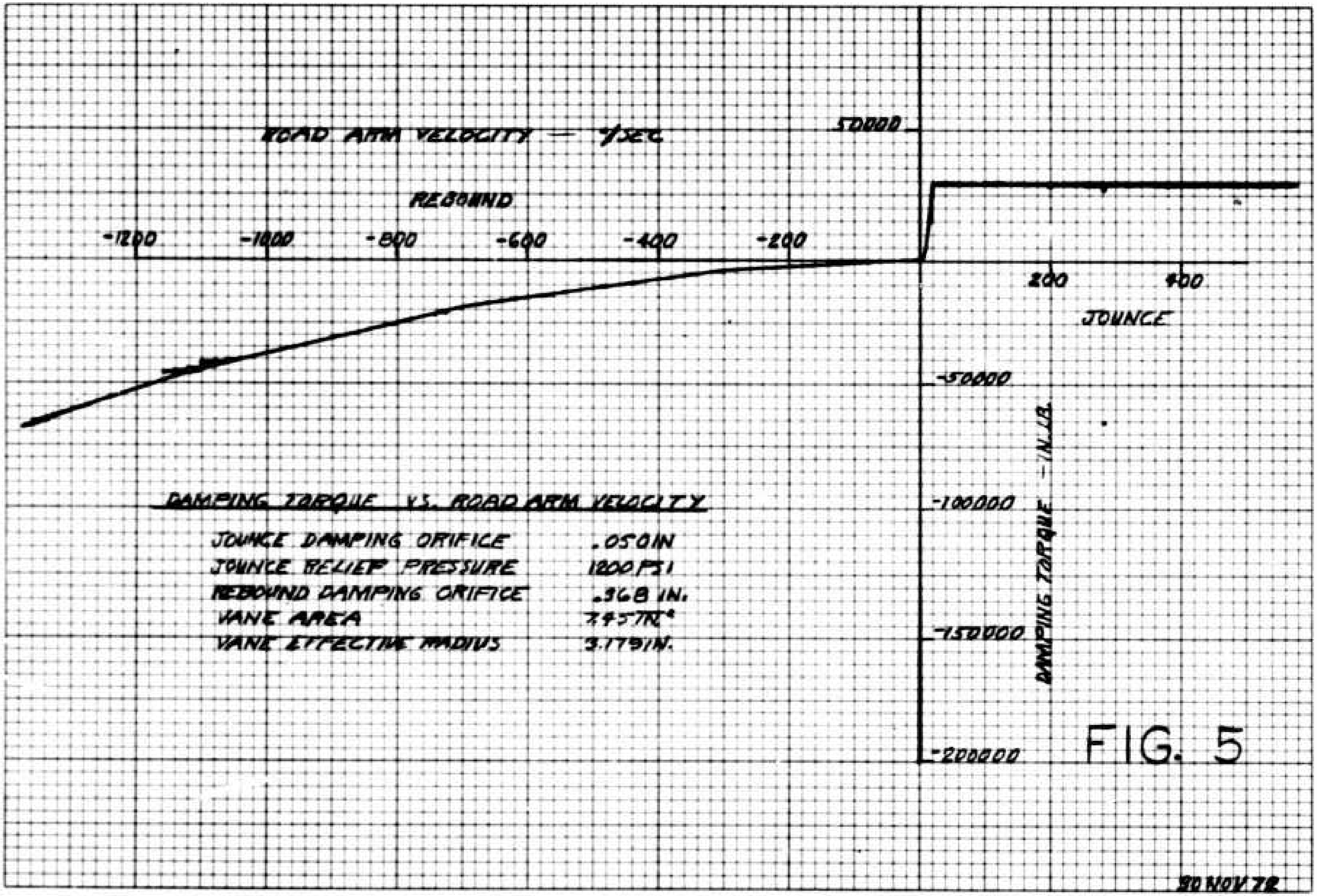

ROAD ARM VELOCITY — °/SEC
REBOUND
JOUNCE
-1200
-1000
-800
-600
-400
-200
200
400
50000
-50000
-100000
-150000
-200000
DAMPING TORQUE — IN.LB.
DAMPING TORQUE VS. ROAD ARM VELOCITY
JOUNCE DAMPING ORIFICE .050IN
JOUNCE RELIEF PRESSURE 1200PSI
REBOUND DAMPING ORIFICE .368 IN.
VANE AREA 7.457IN²
VANE EFFECTIVE RADIUS 3.779IN.
30 NOV 72

FIG. 5

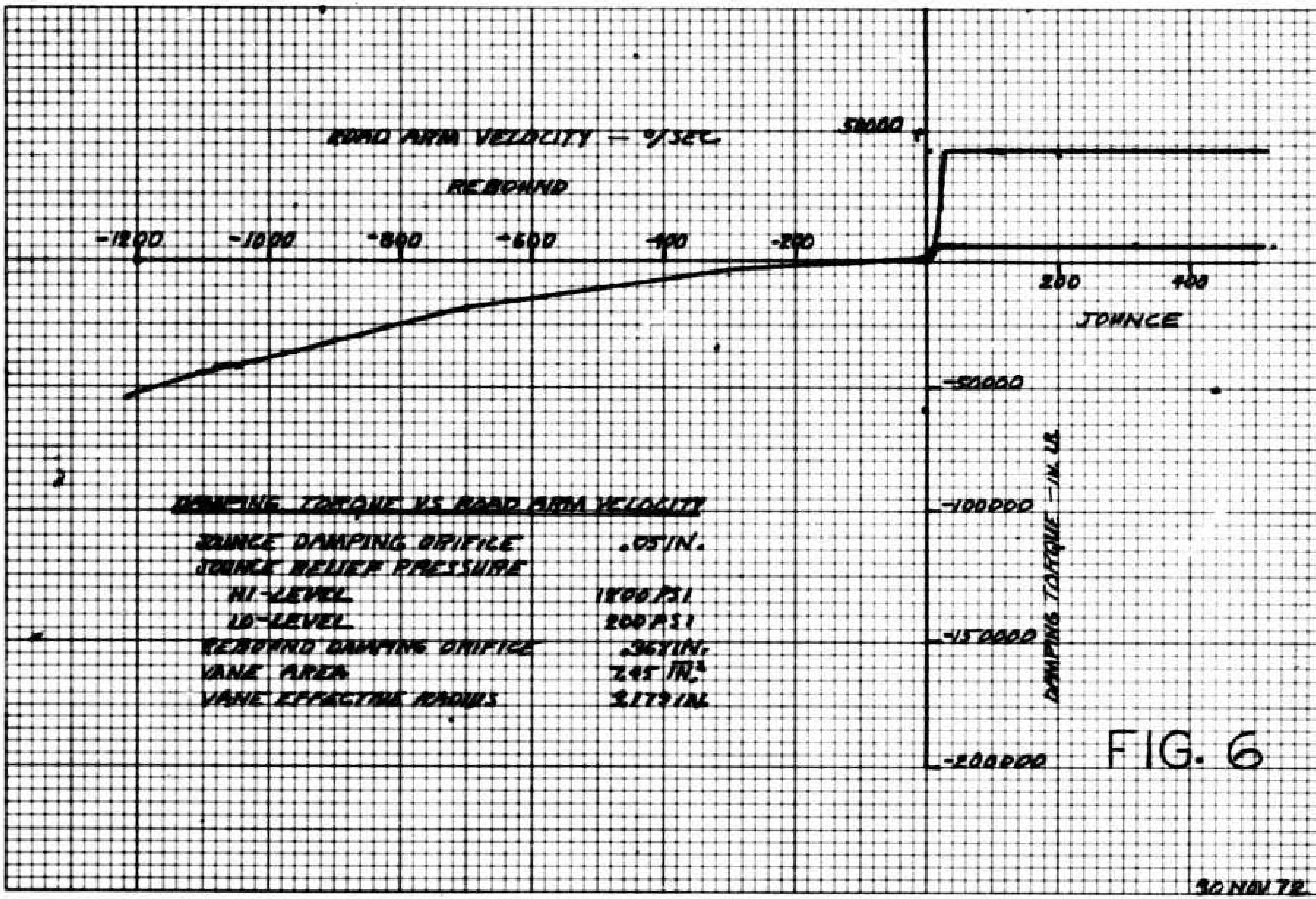
ROAD ARM VELOCITY — °/SEC
REBOUND
JOUNCE
-1200
-1000
-800
-600
-400
-200
200
400
50000
-50000
-100000
-150000
-200000
DAMPING TORQUE —IN. LB.
DAMPING TORQUE VS ROAD ARM VELOCITY
JOUNCE DAMPING ORIFICE .05 IN.
JOUNCE RELIEF PRESSURE
HI-LEVEL 1800 PSI
LO-LEVEL 200 PSI
REBOUND DAMPING ORIFICE .0367 IN.
VANE AREA 7.45 IN.^{2}
VANE EFFECTIVE RADIUS 3.179 IN.
30 NOV 72

FIG. 6

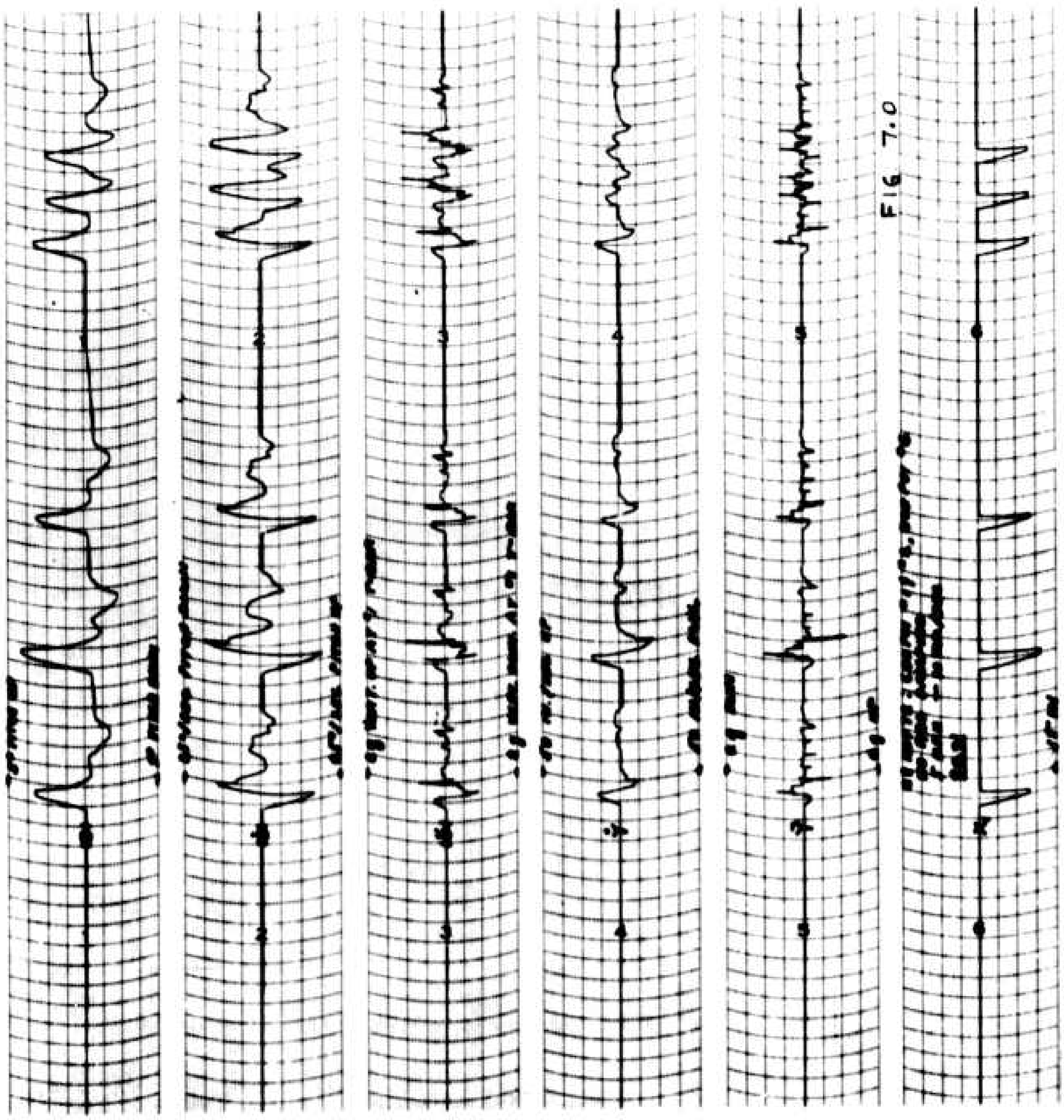

FIG 7.0

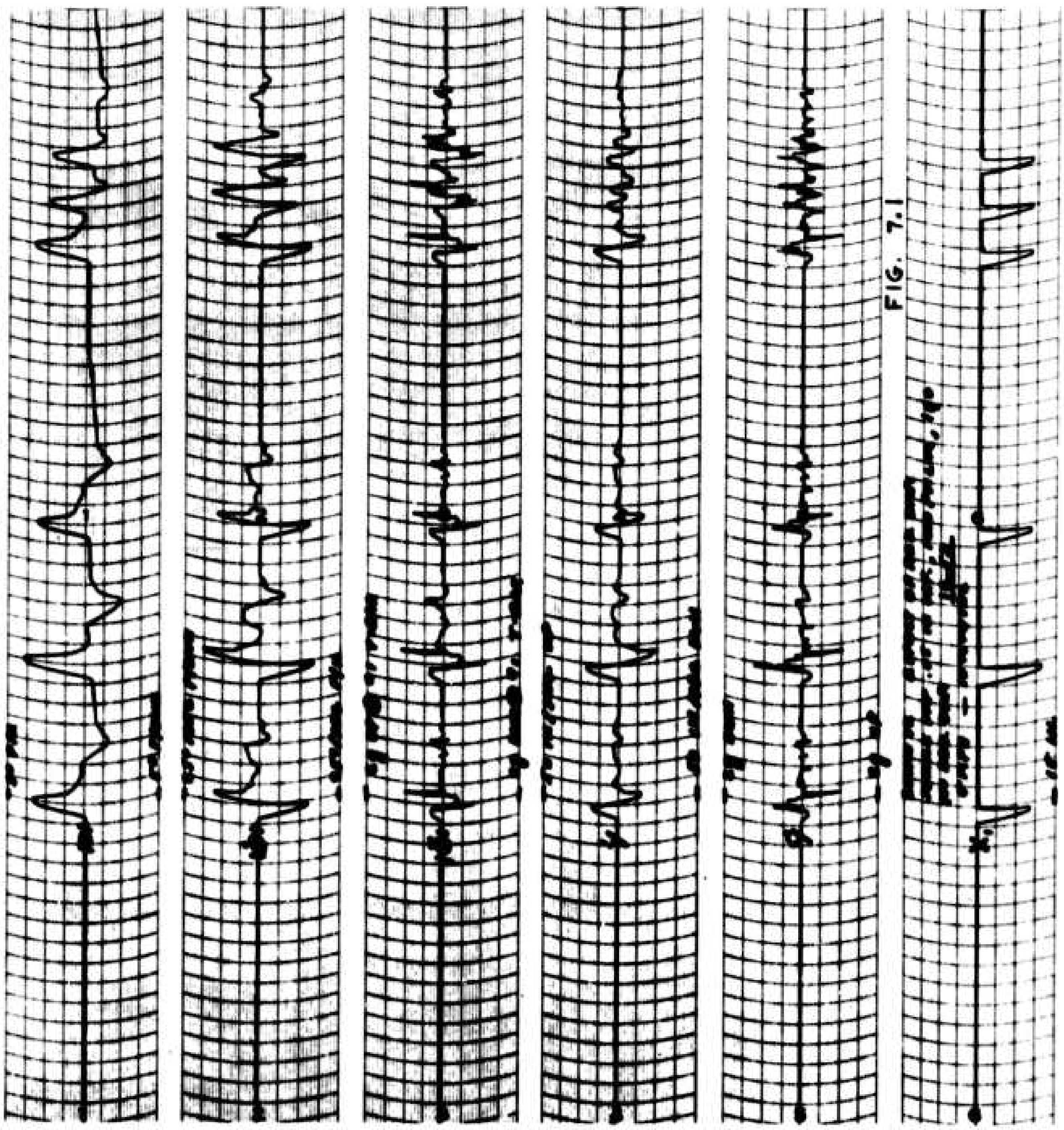

FIG. 7.1

FIG. 7.2

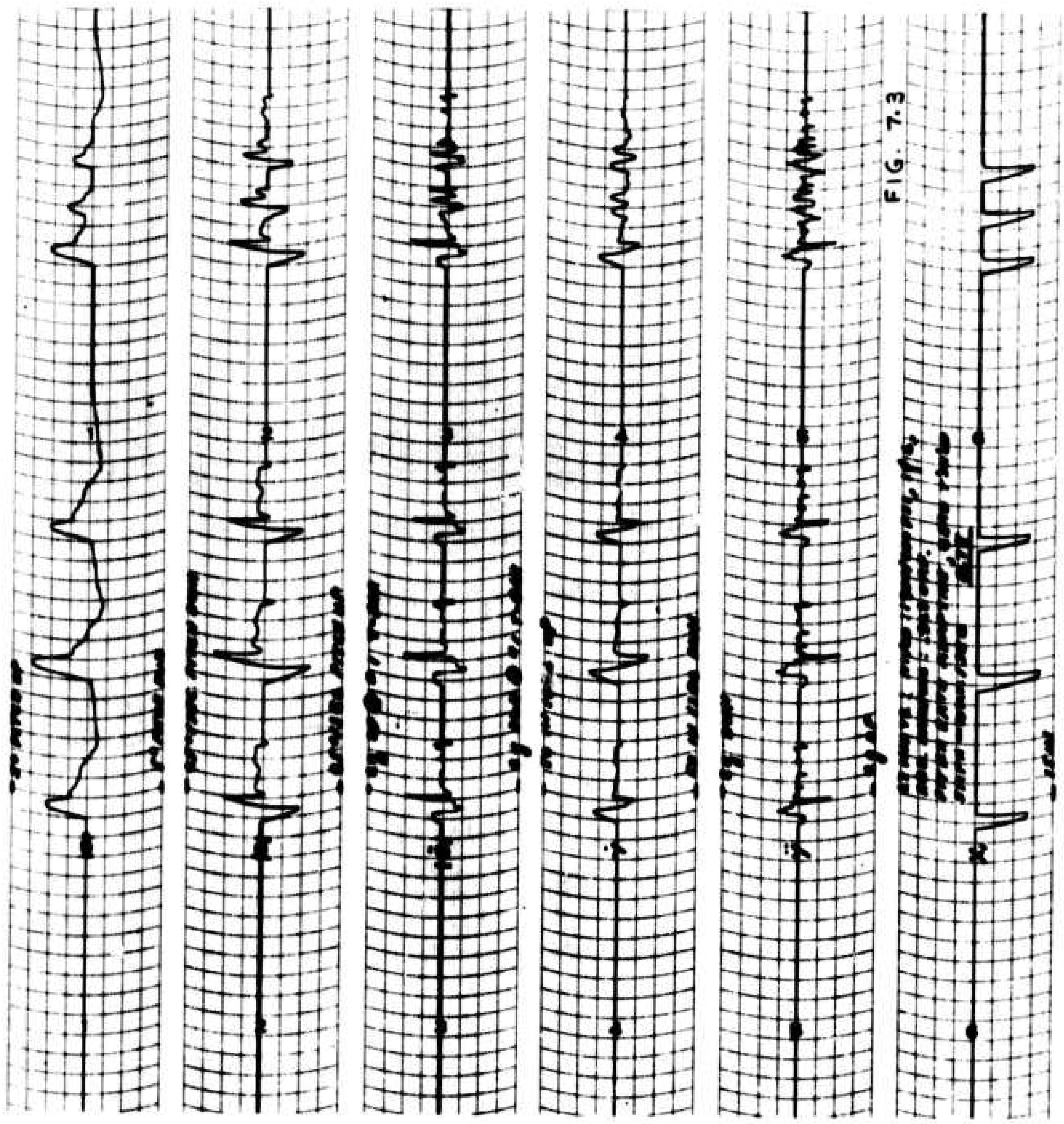

FIG. 7.3

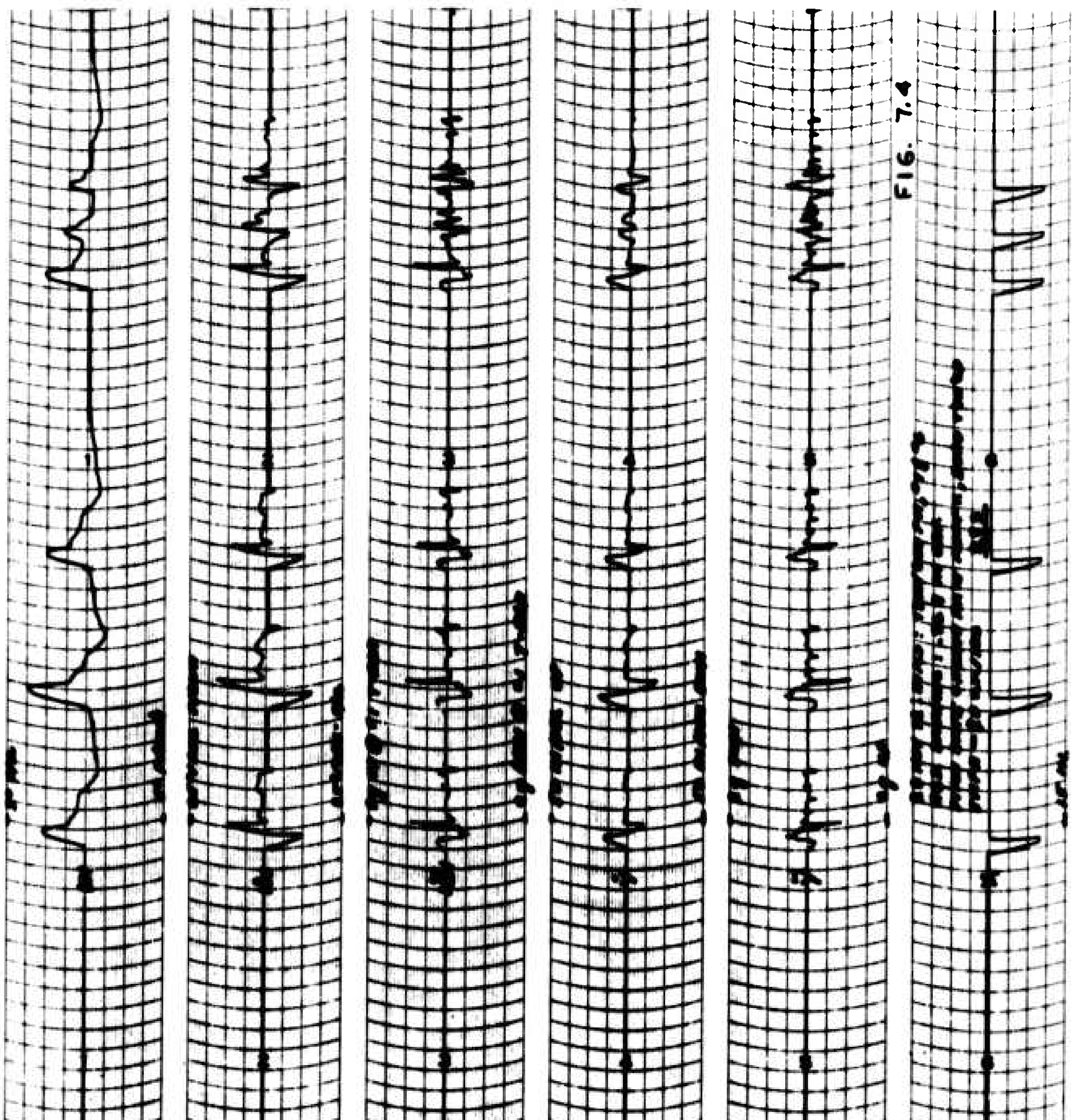

FIG. 7.4

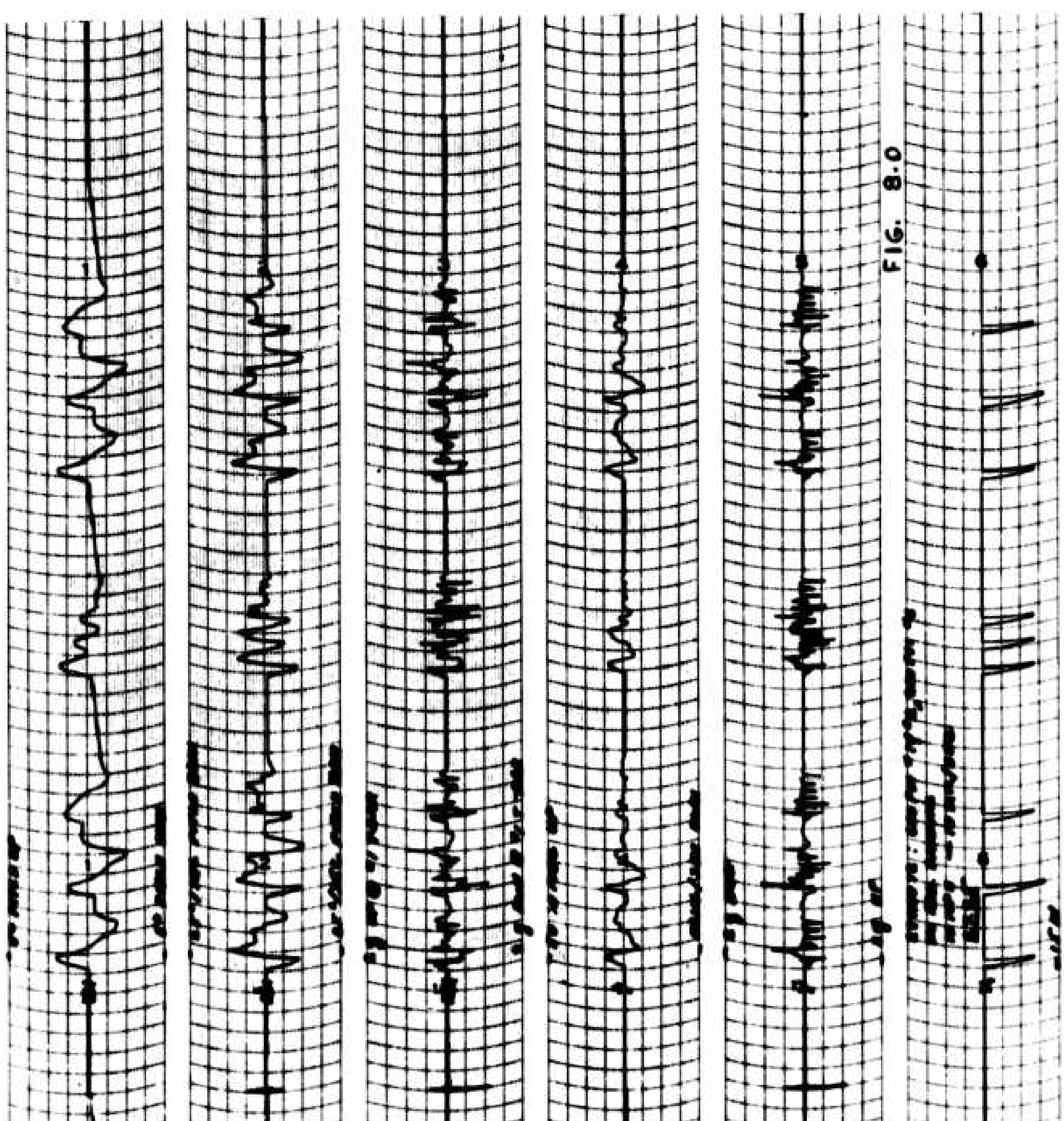

FIG. 8.0

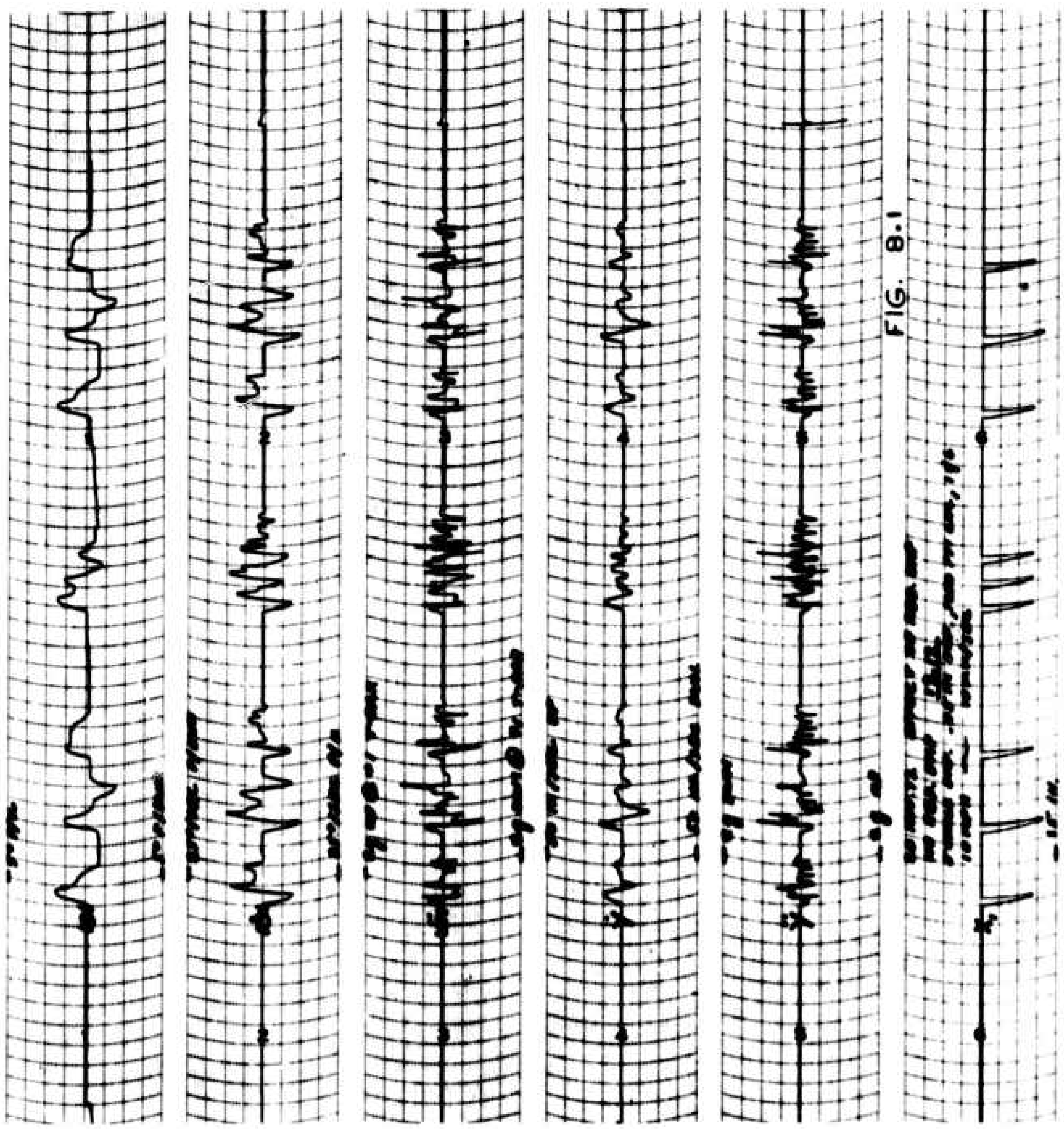

FIG. 8.1

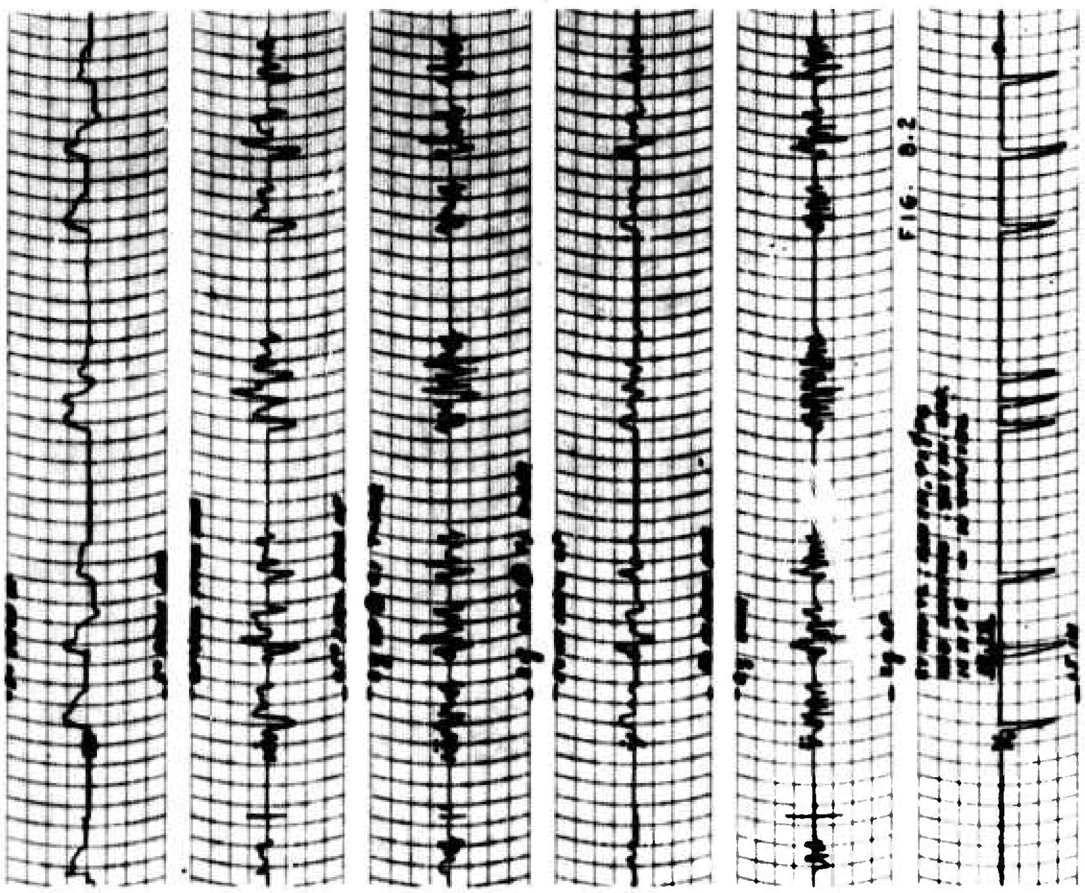

FIG. 8.2

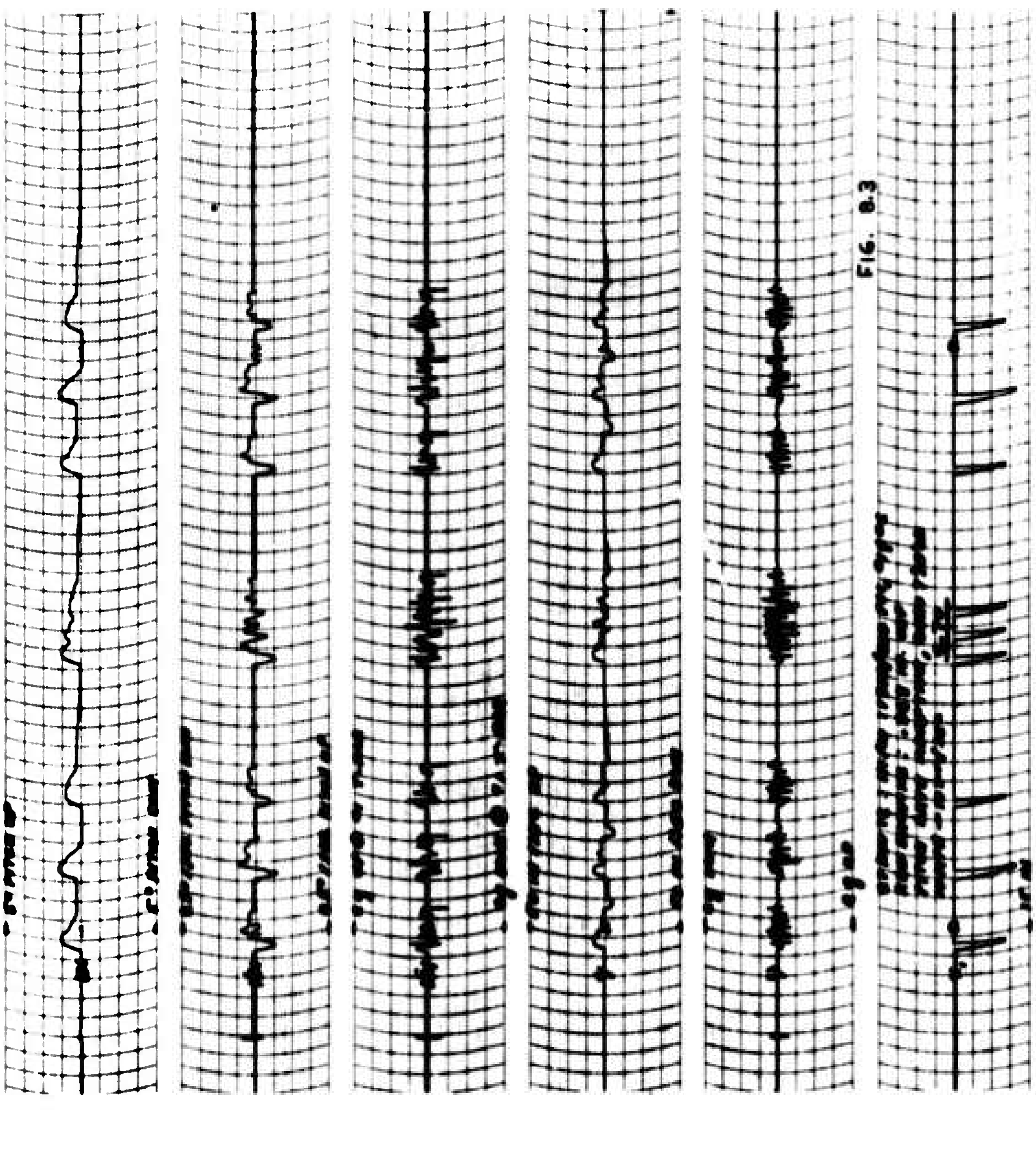

FIG. 8.3

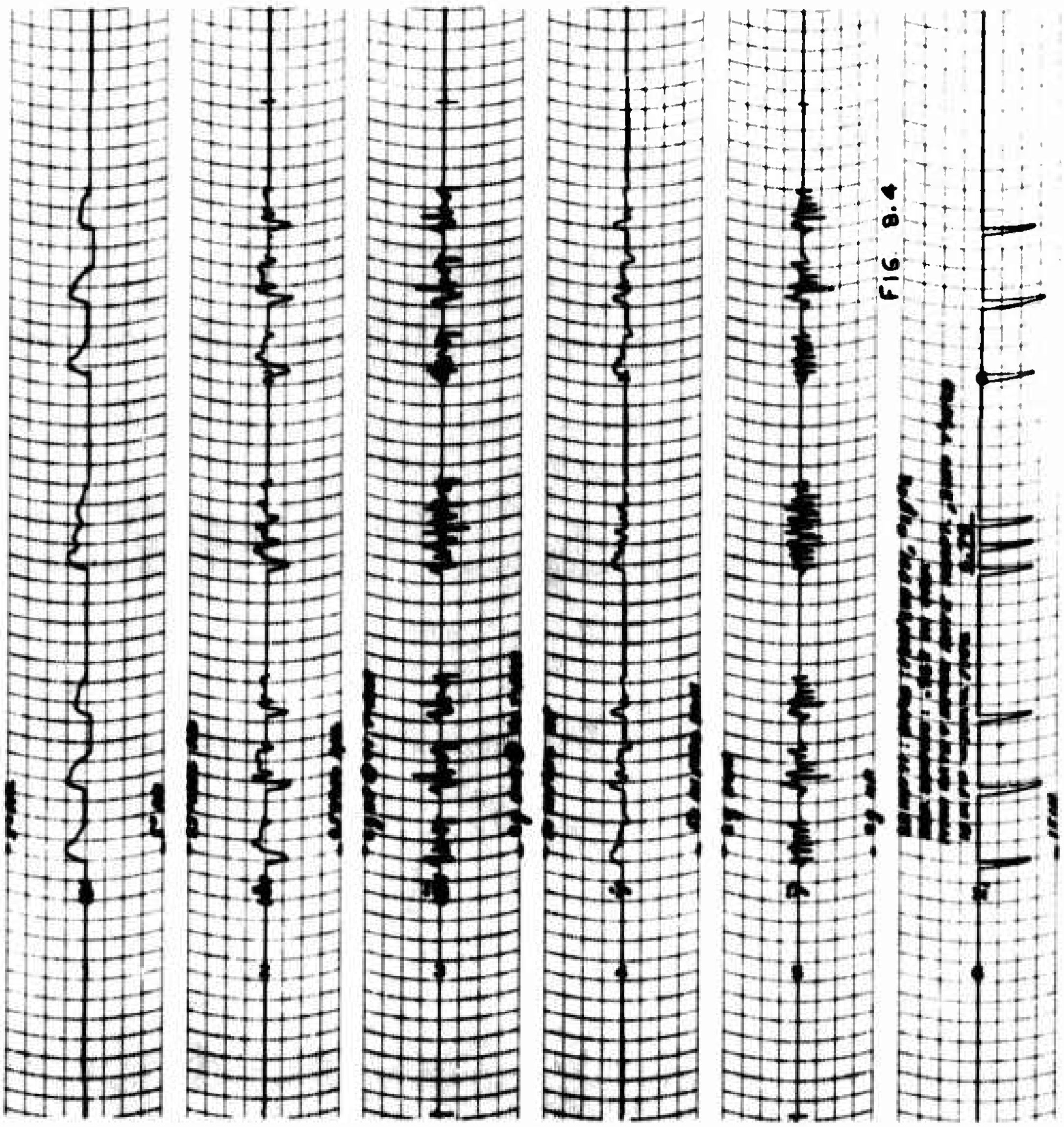

FIG. 8.4

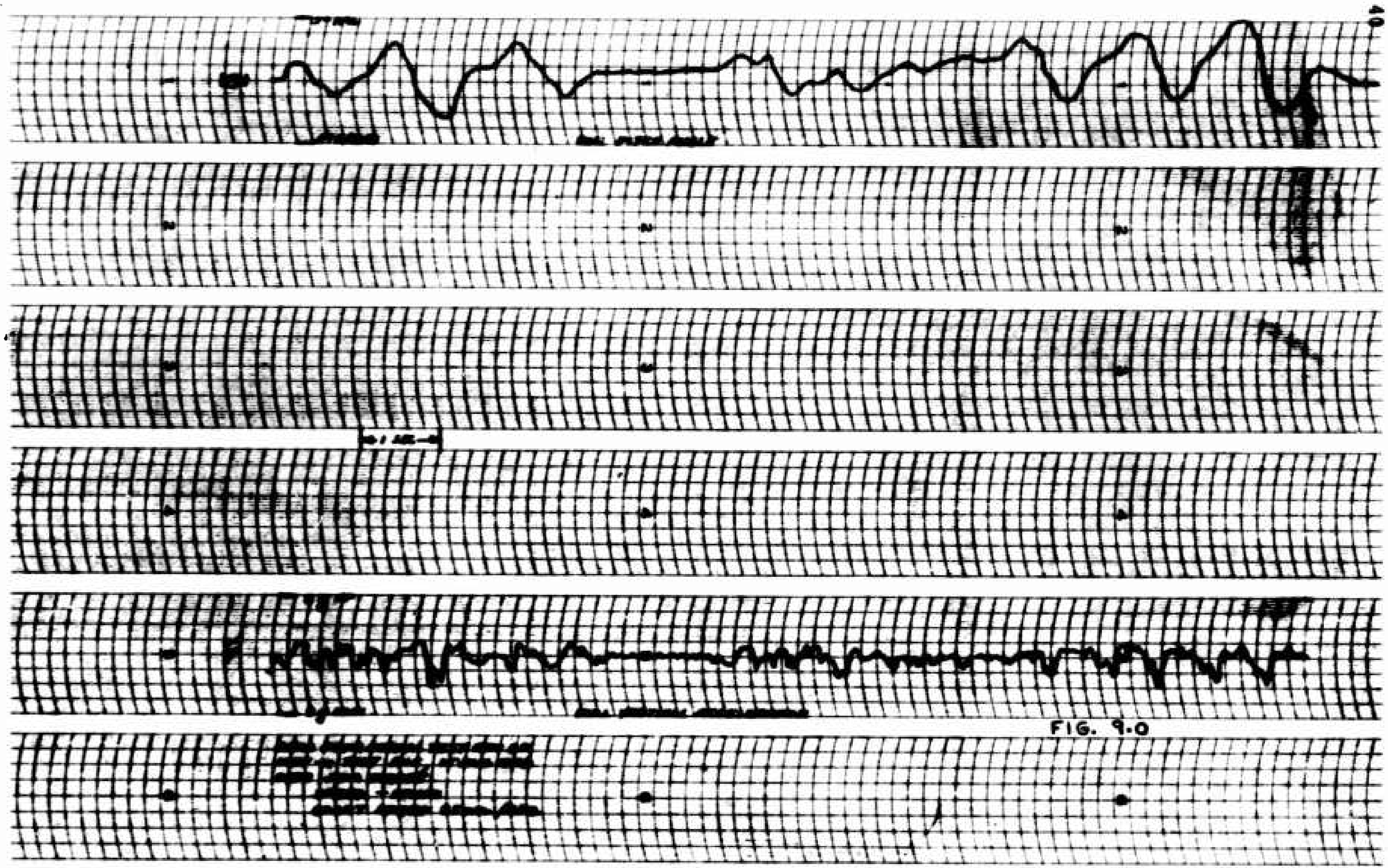

FIG. 9.0

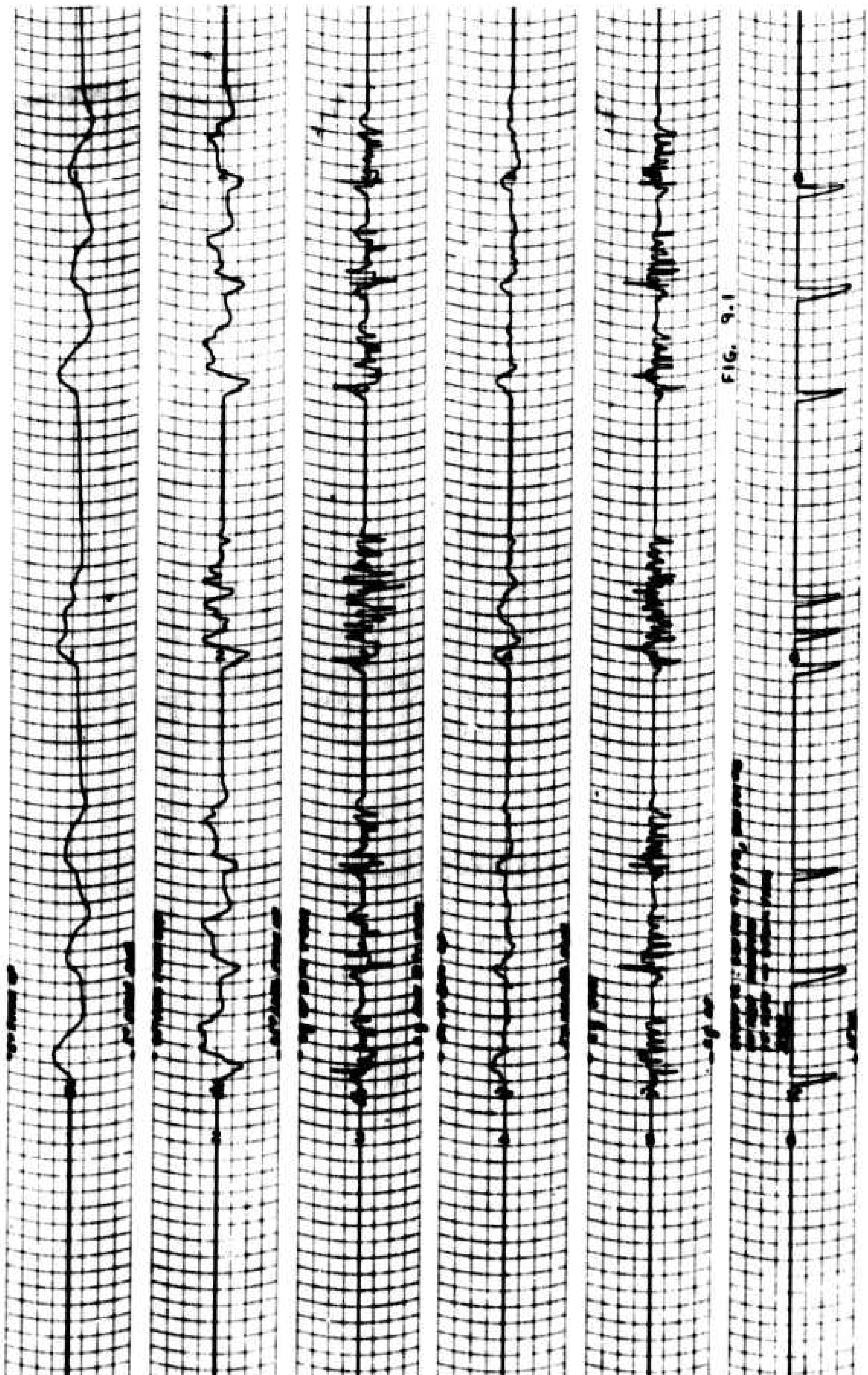

FIG. 9.1

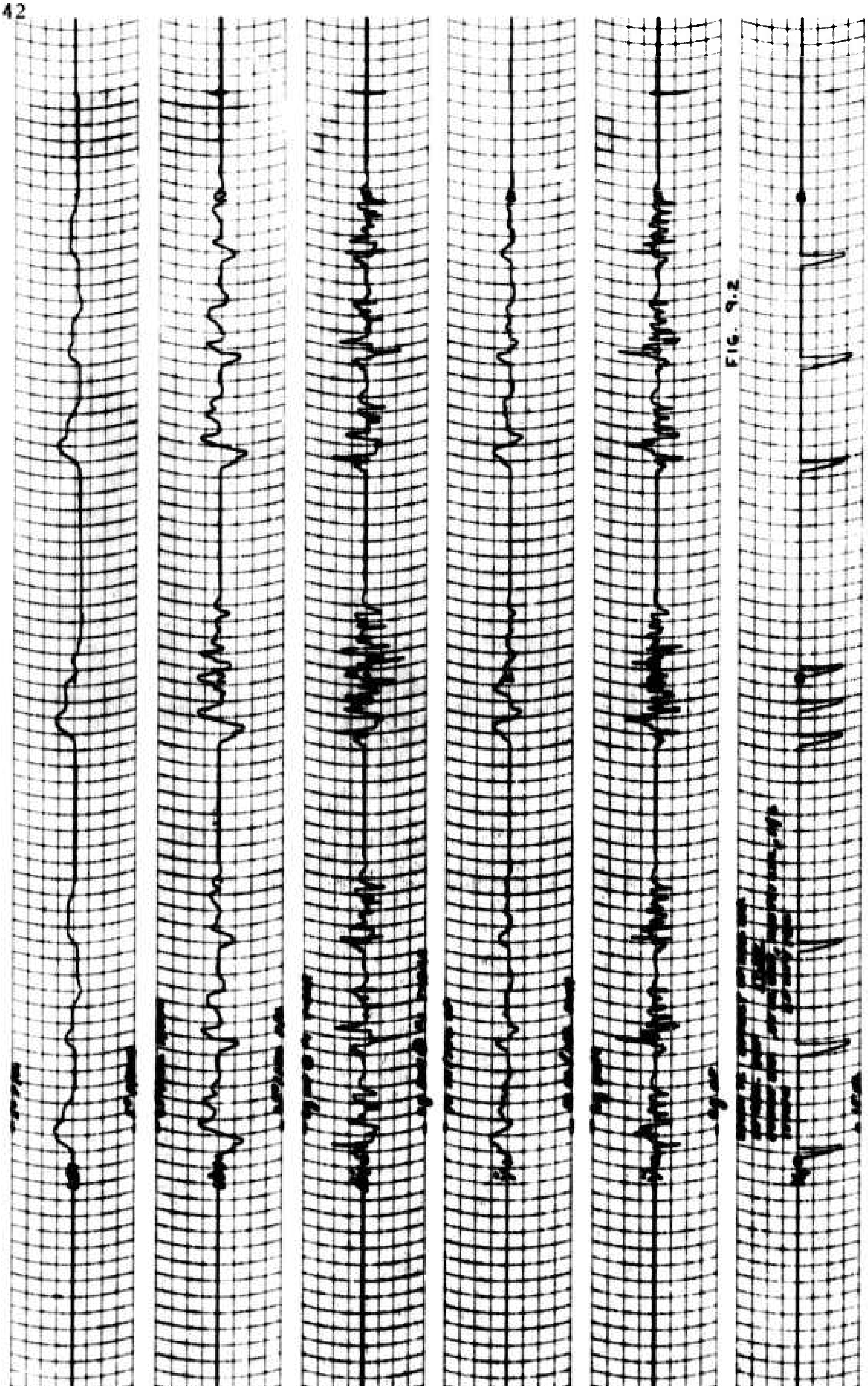

FIG. 9.2

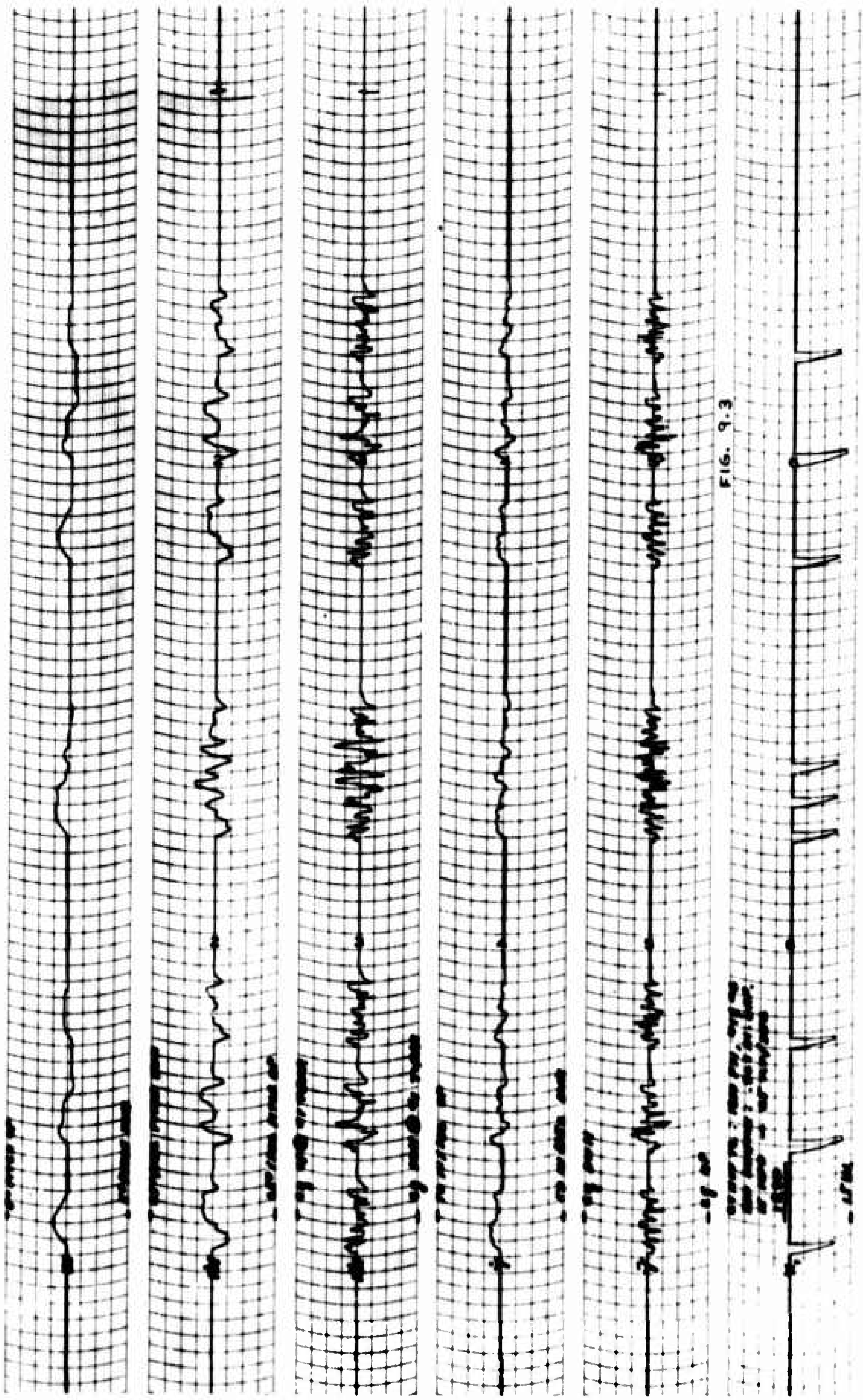

FIG. 9.3

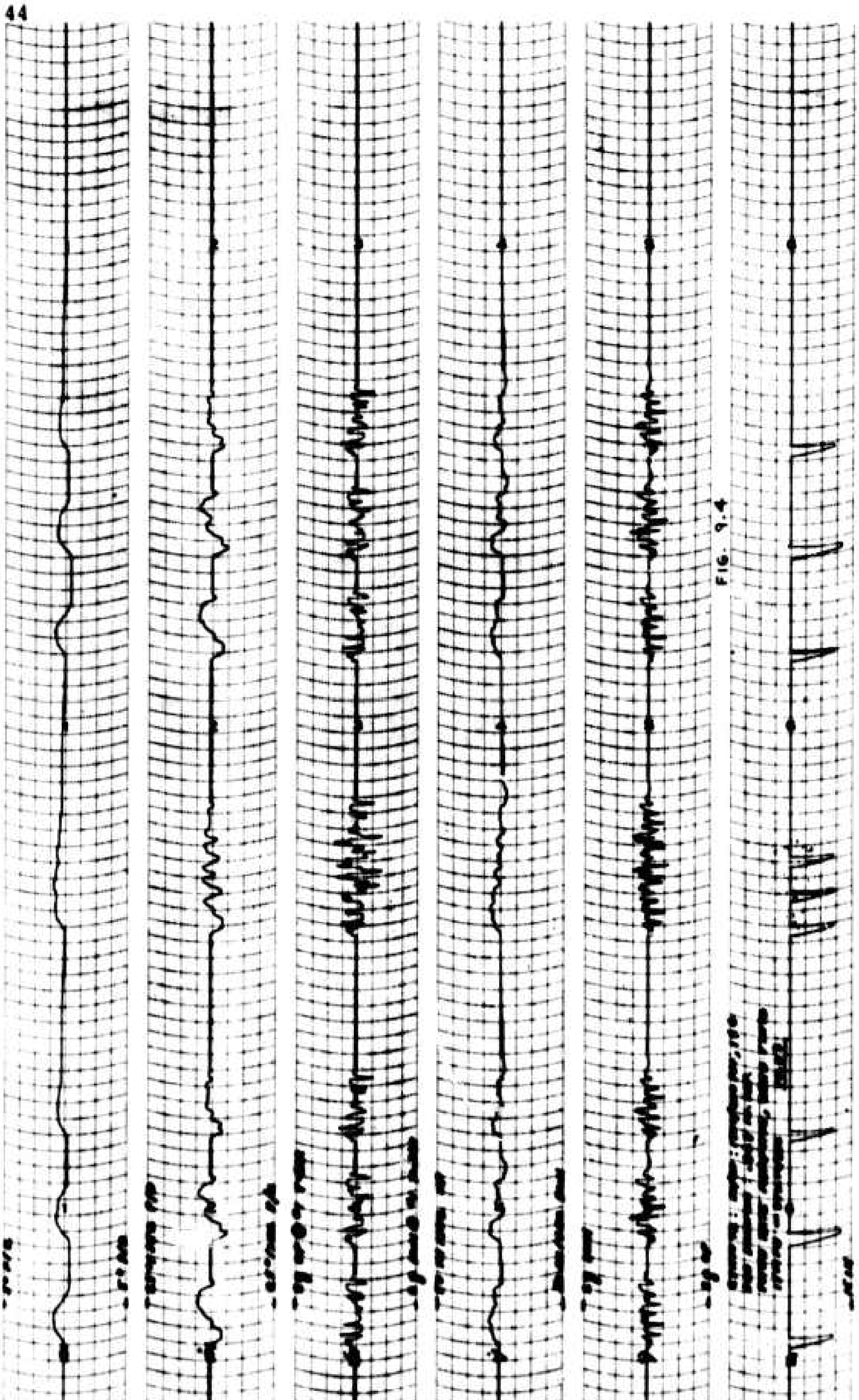

FIG. 9.4

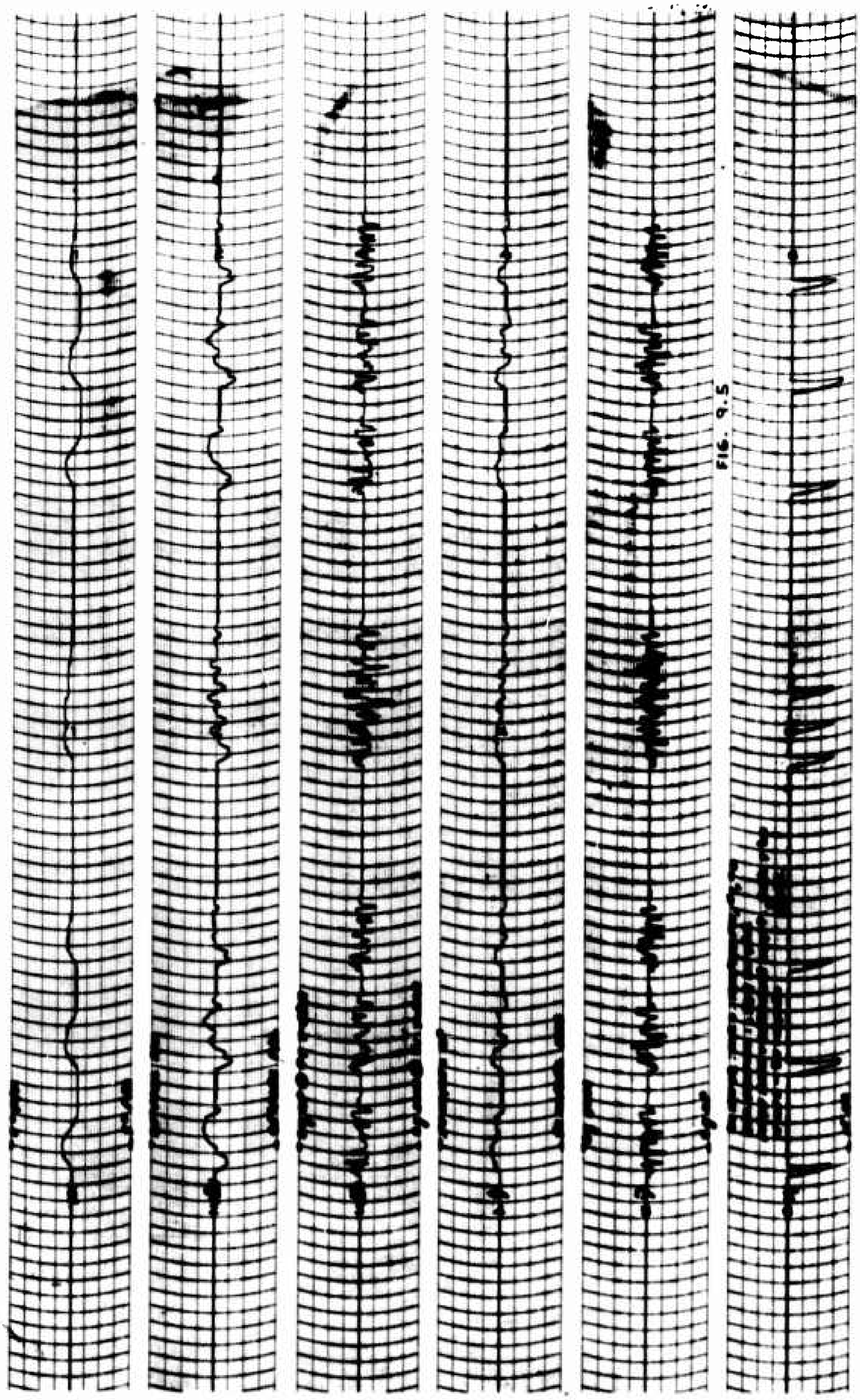

FIG. 9.5

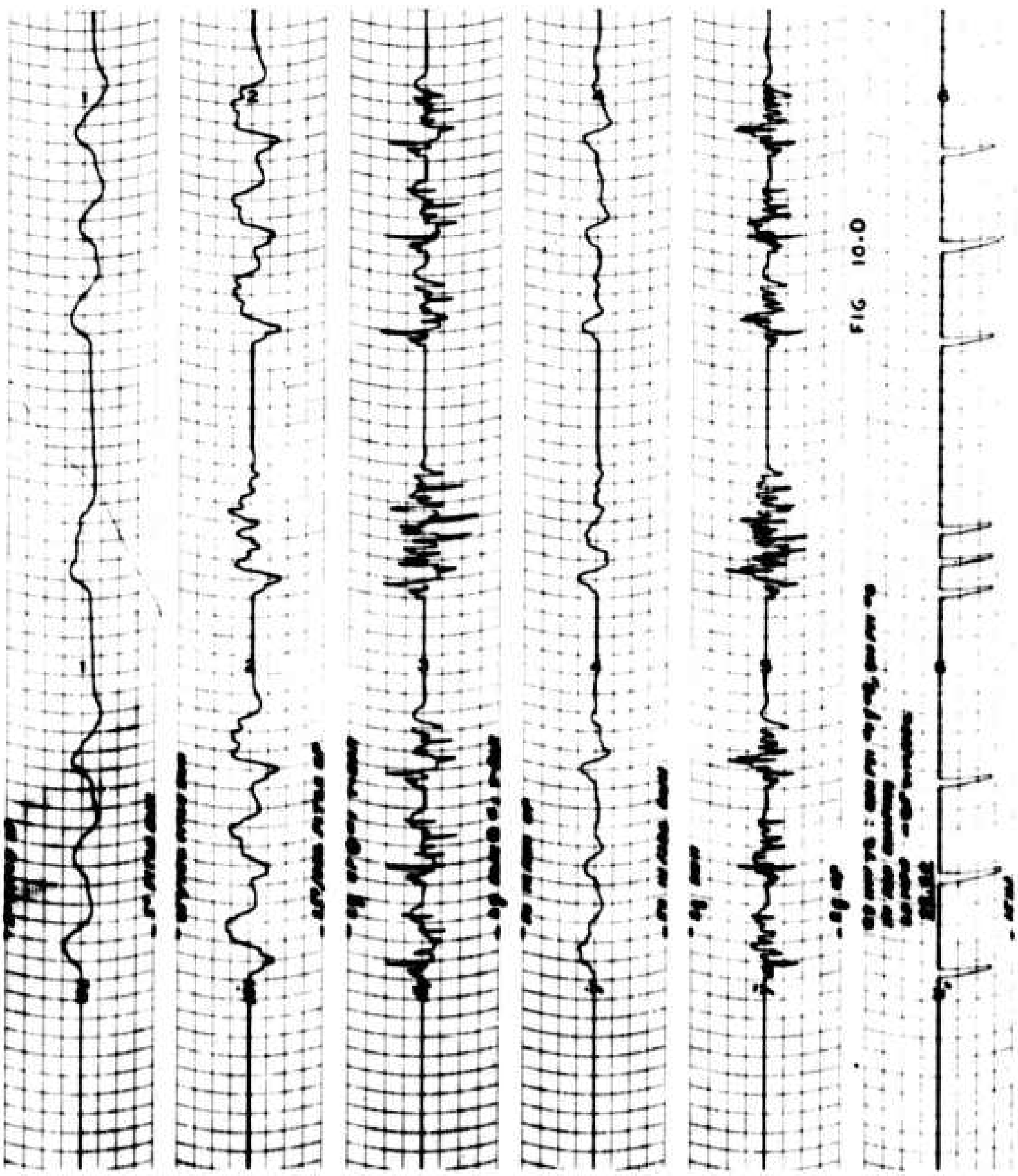

FIG 10.0

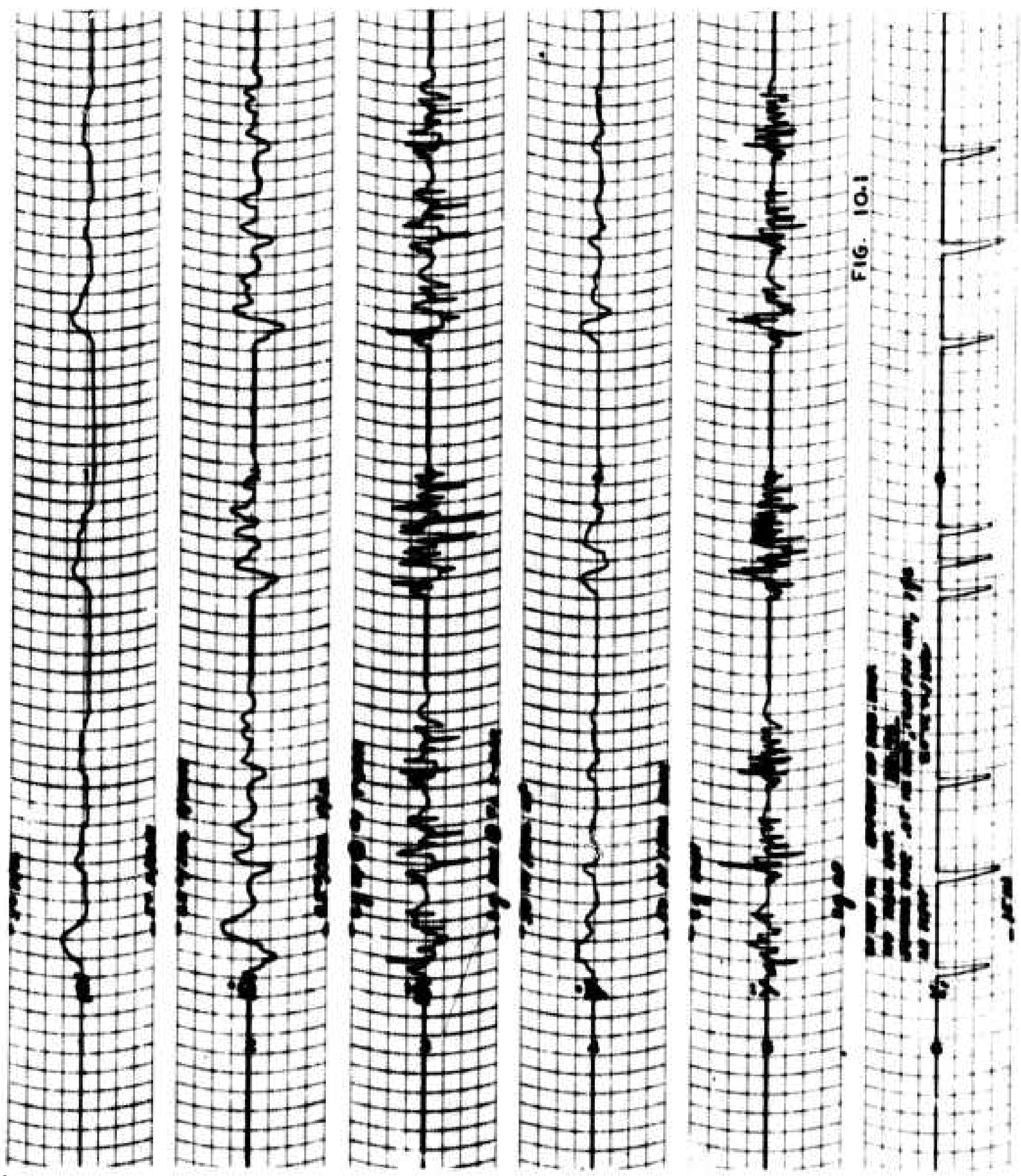

FIG. 10.1

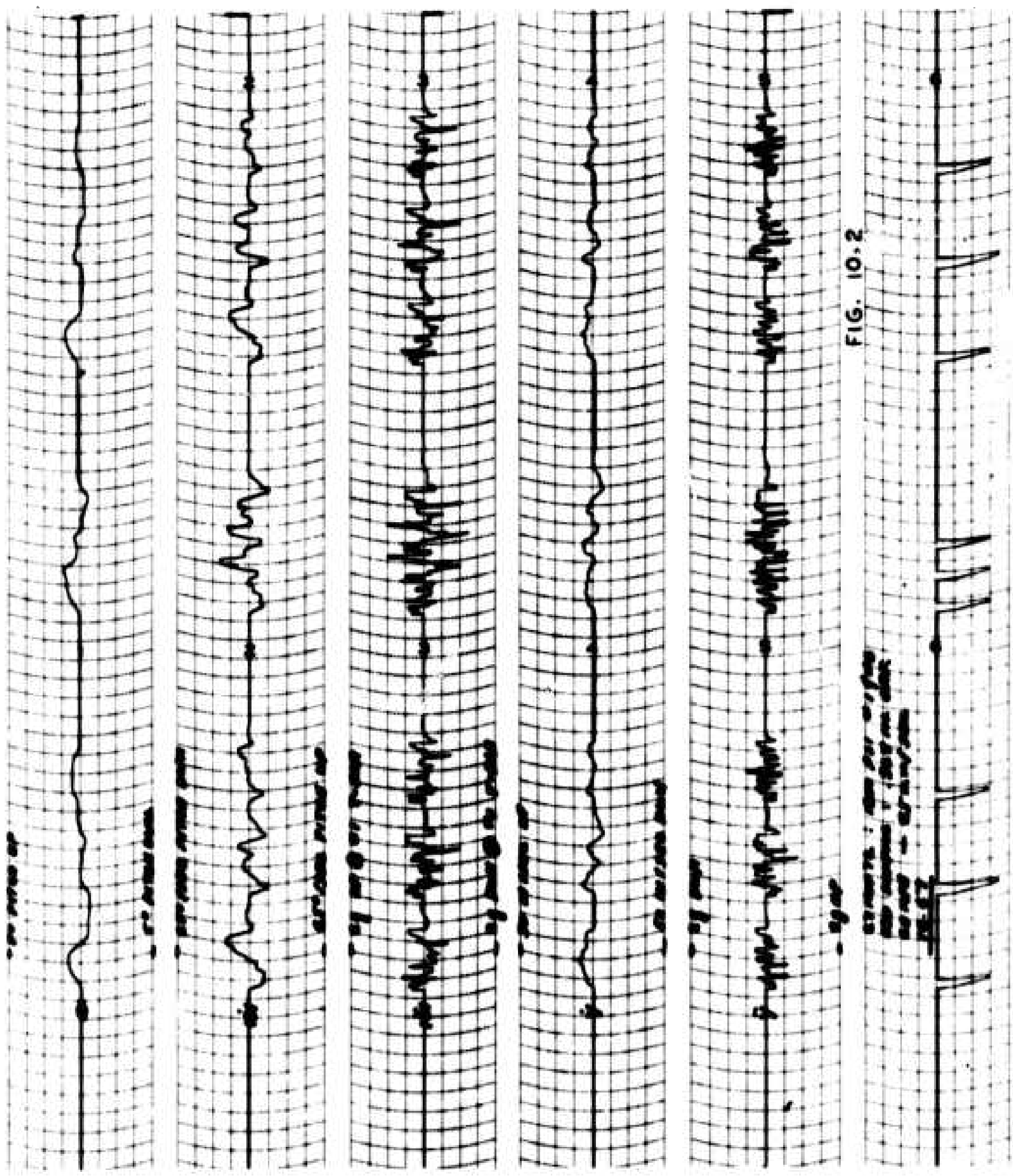

FIG. 10.2

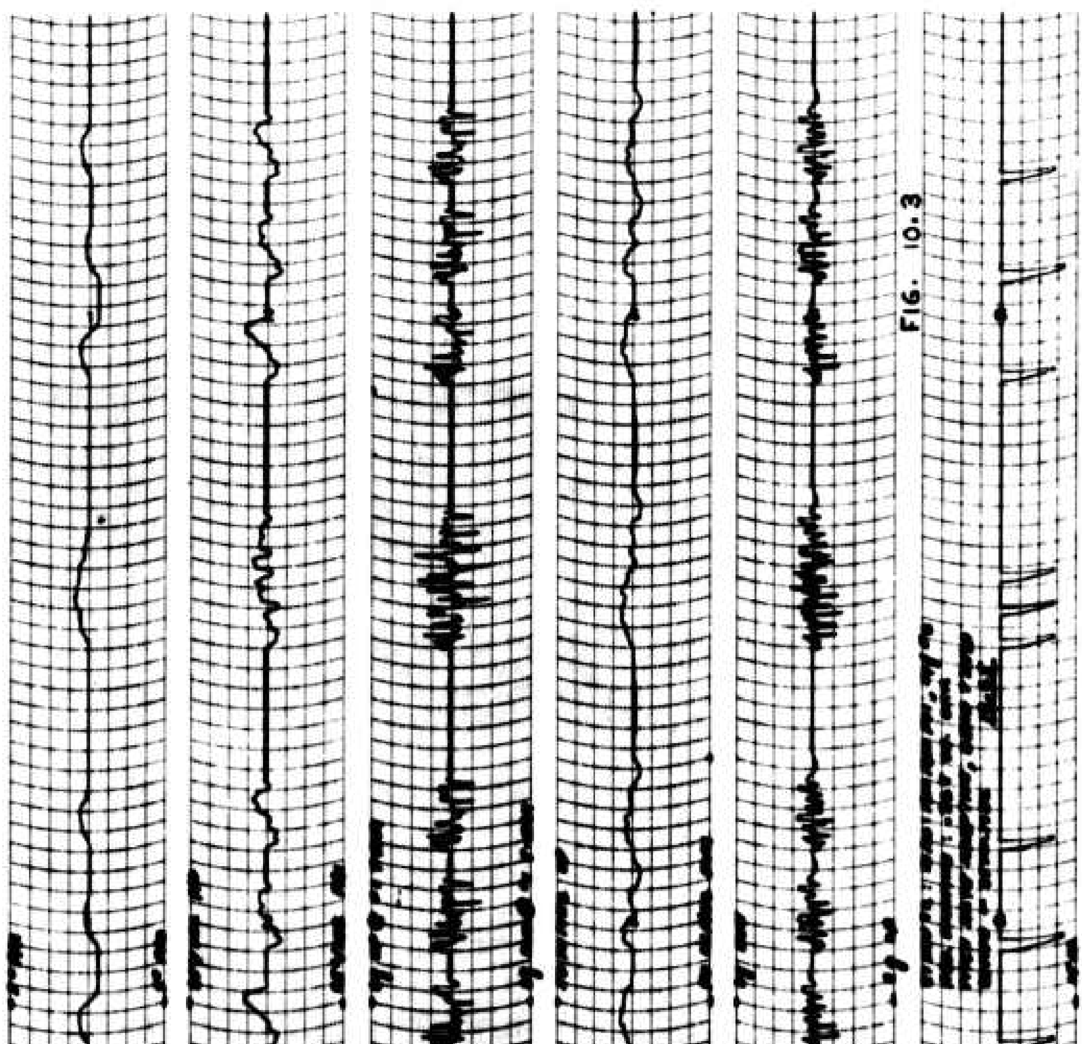

FIG. 10.3

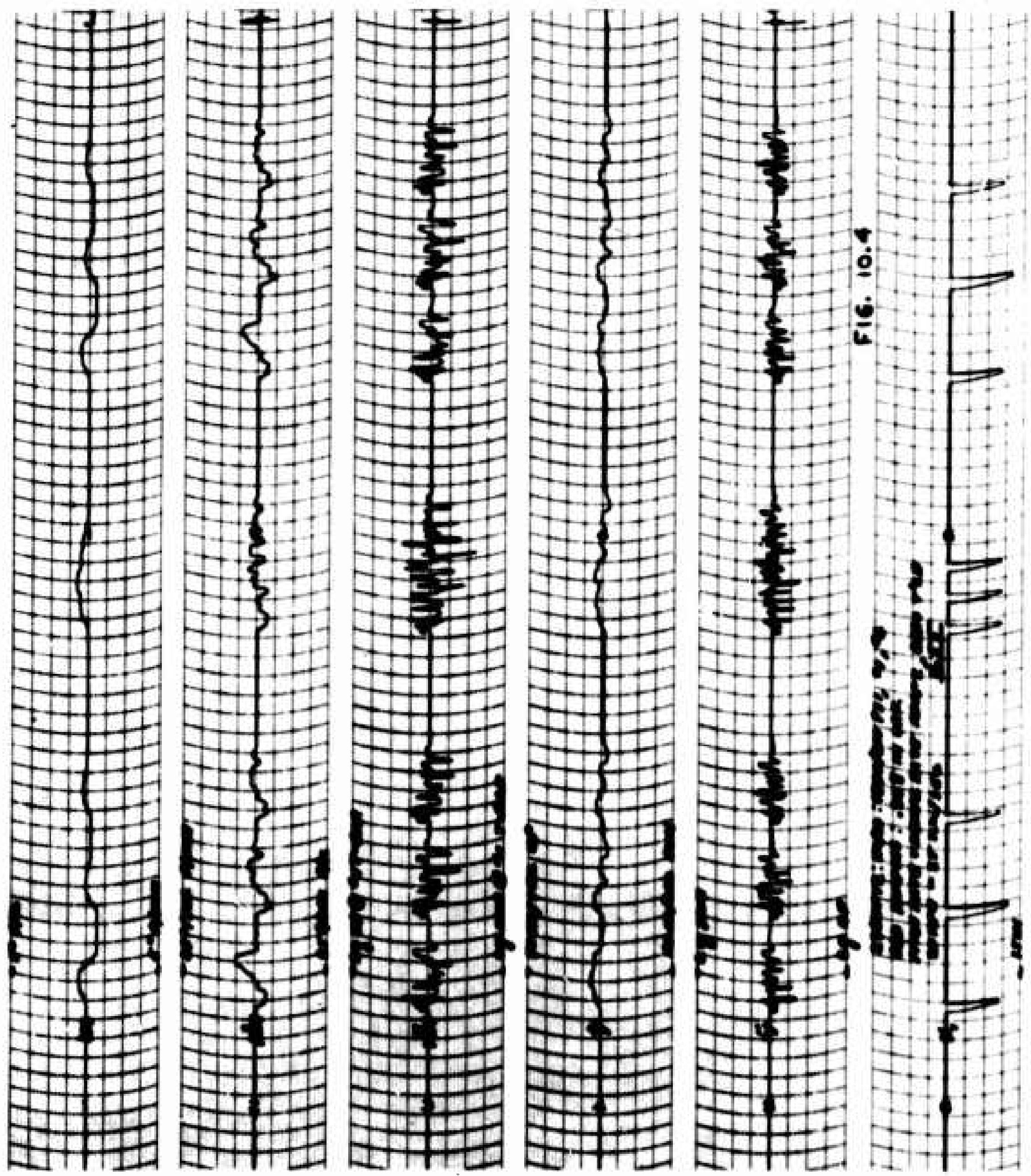

FIG. 10.4

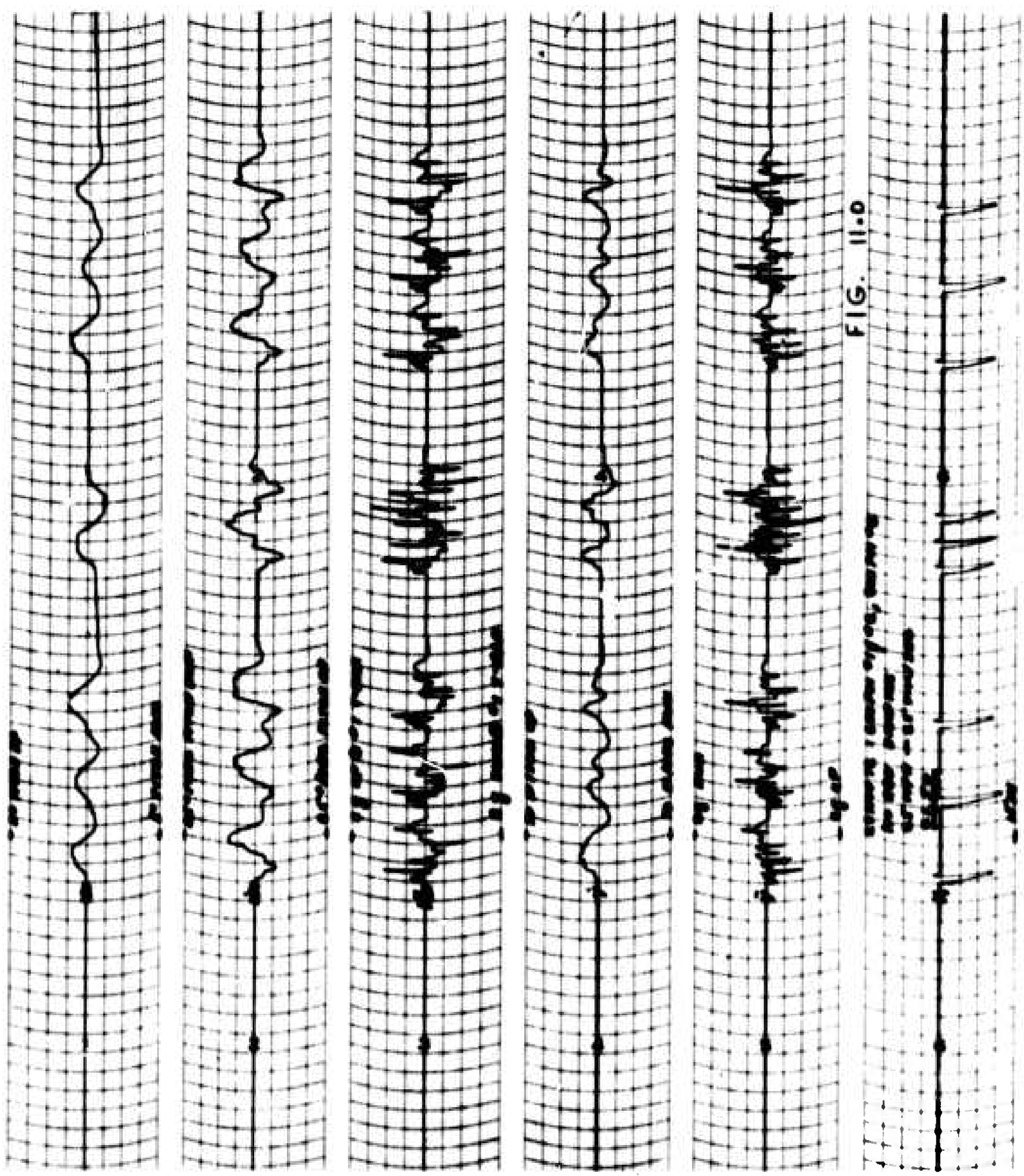

FIG. 11.0

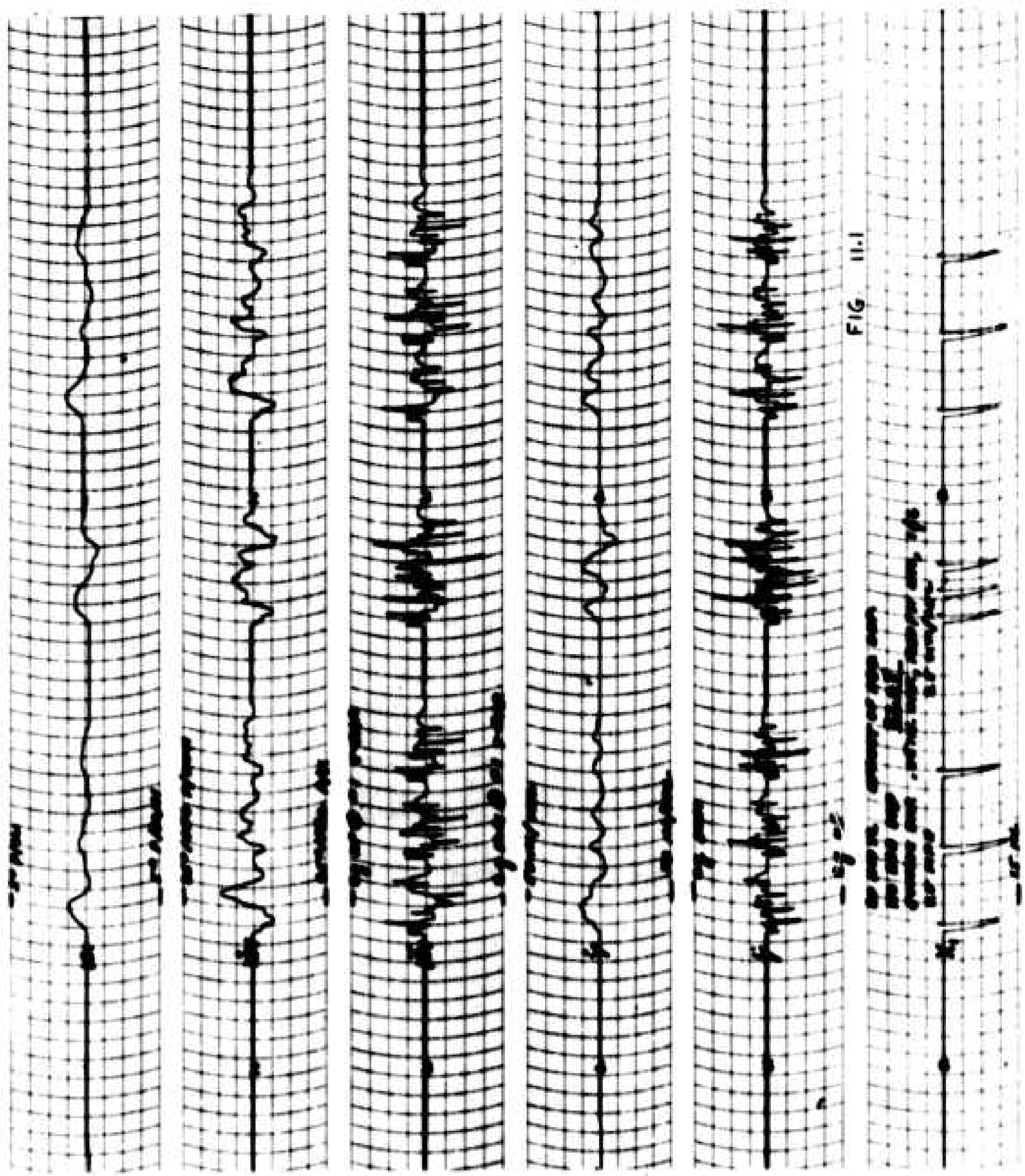

FIG 11.1

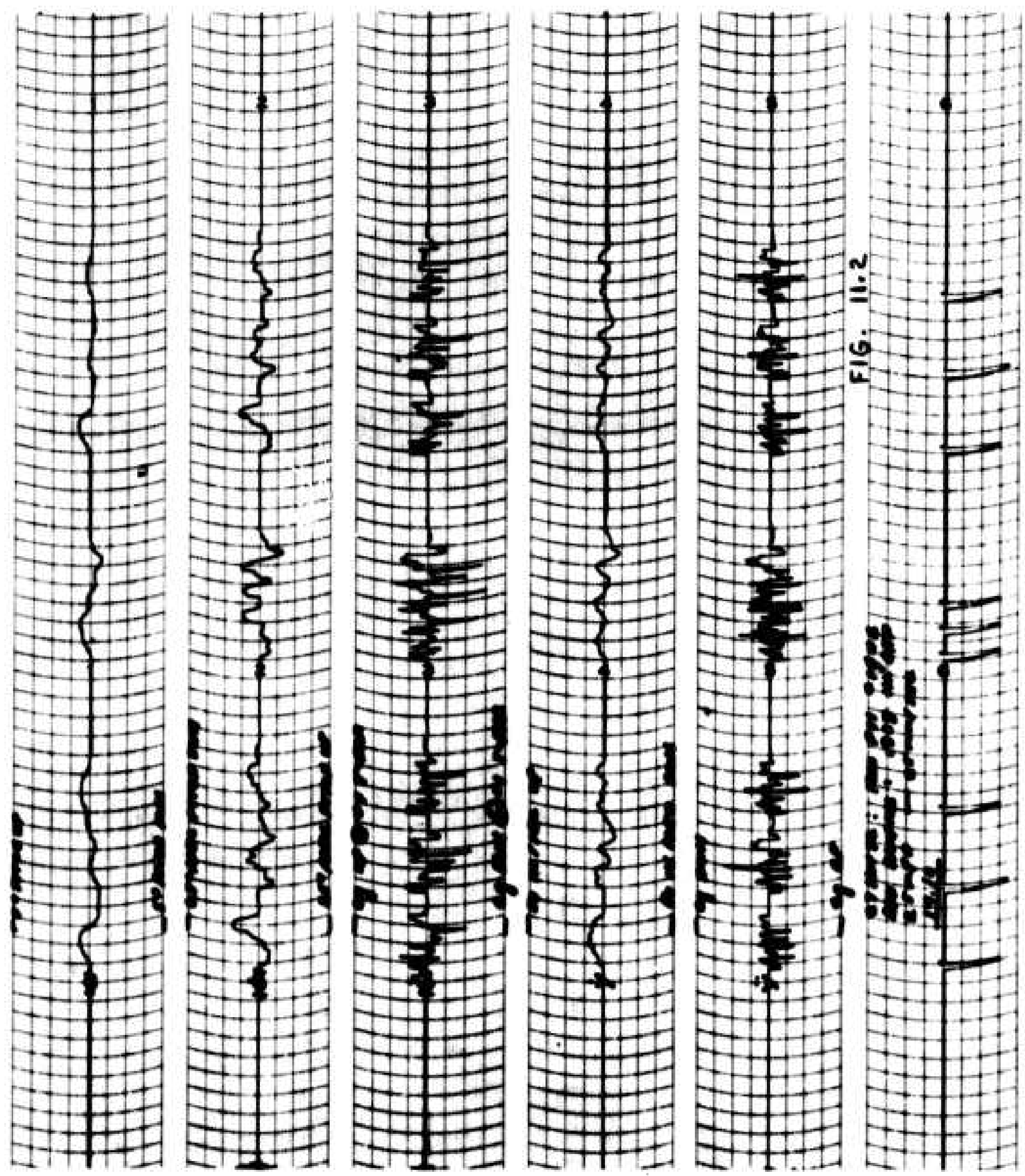

FIG. 11.2

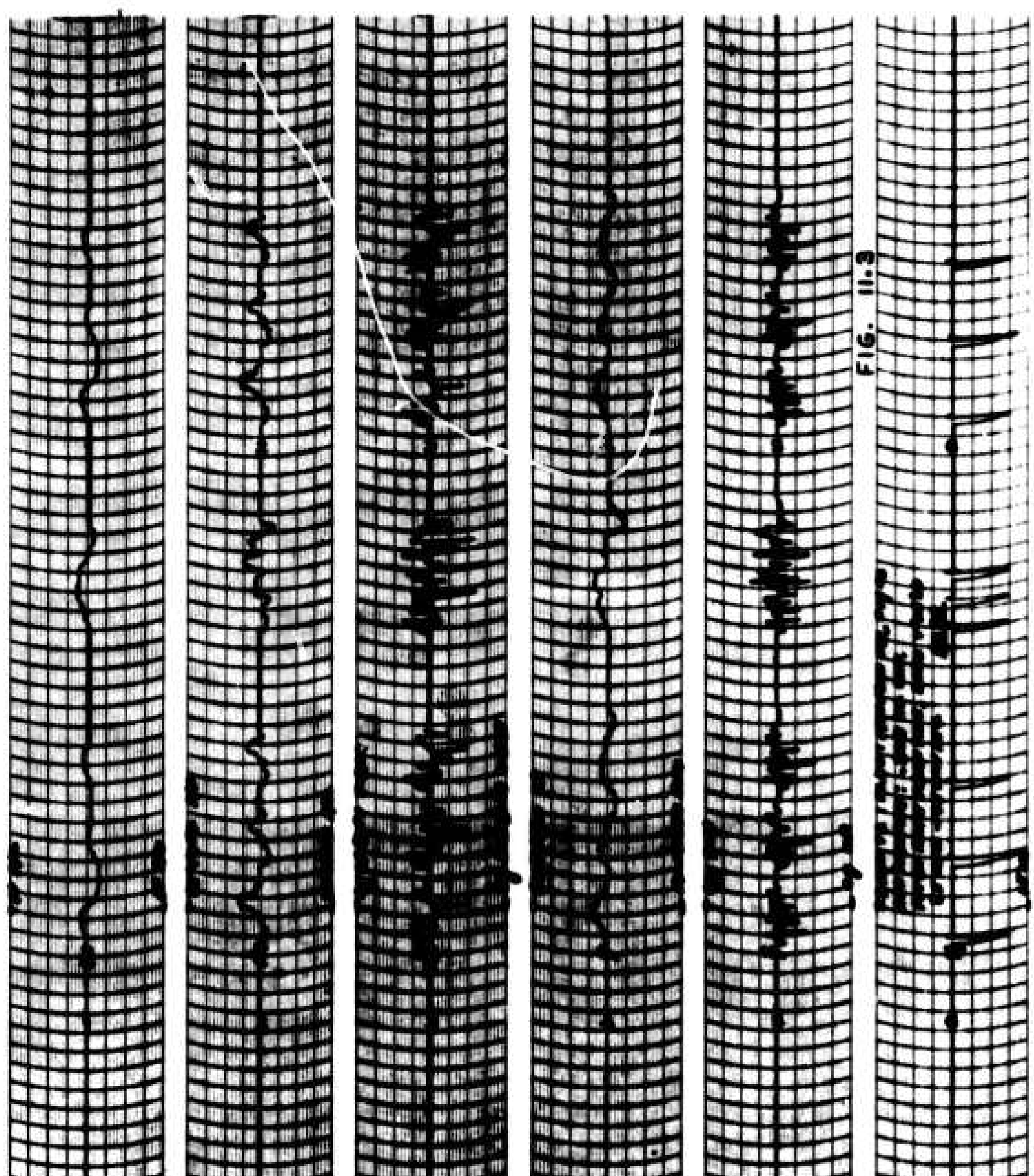

FIG. 11.3

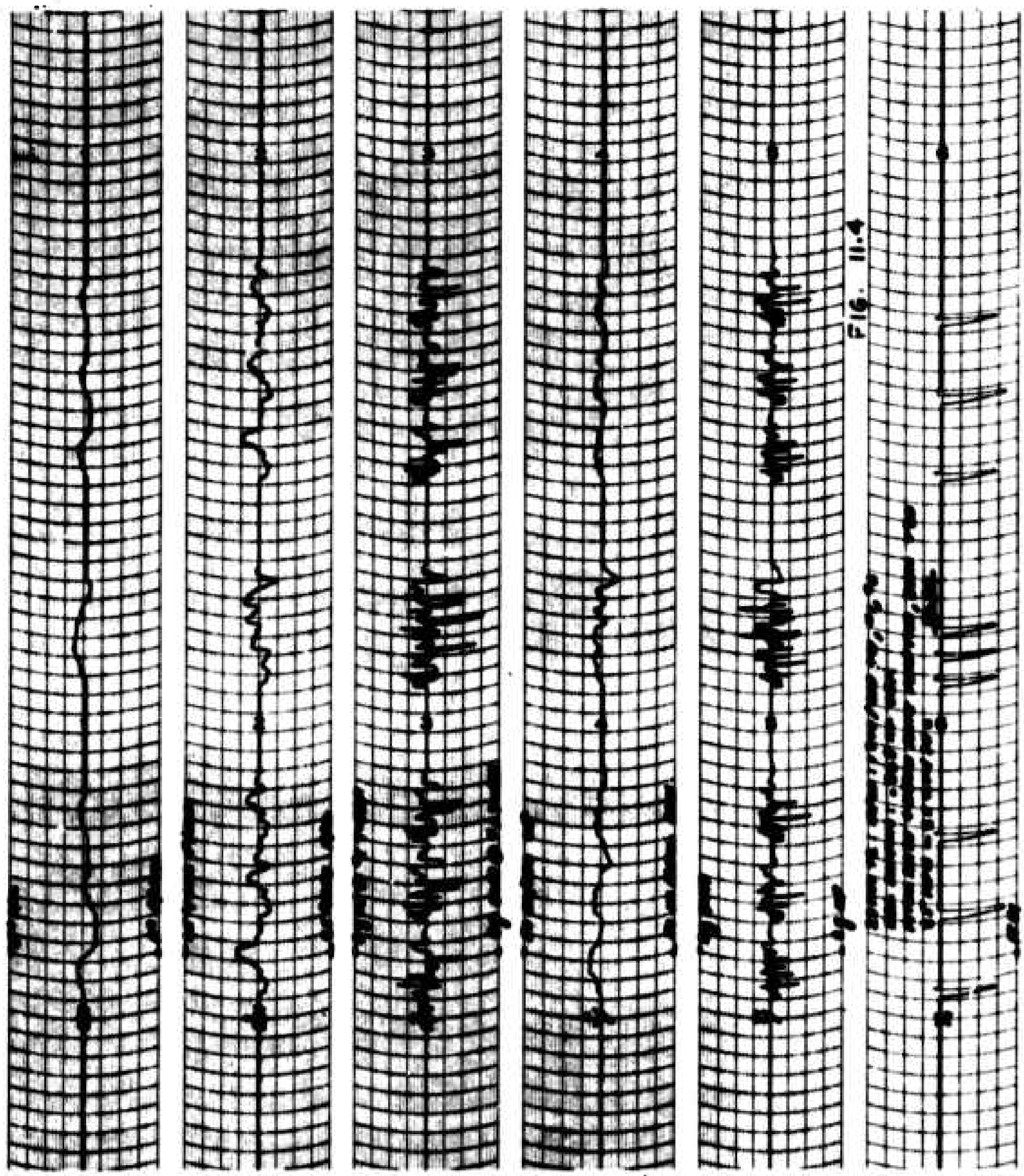

FIG. 11-4

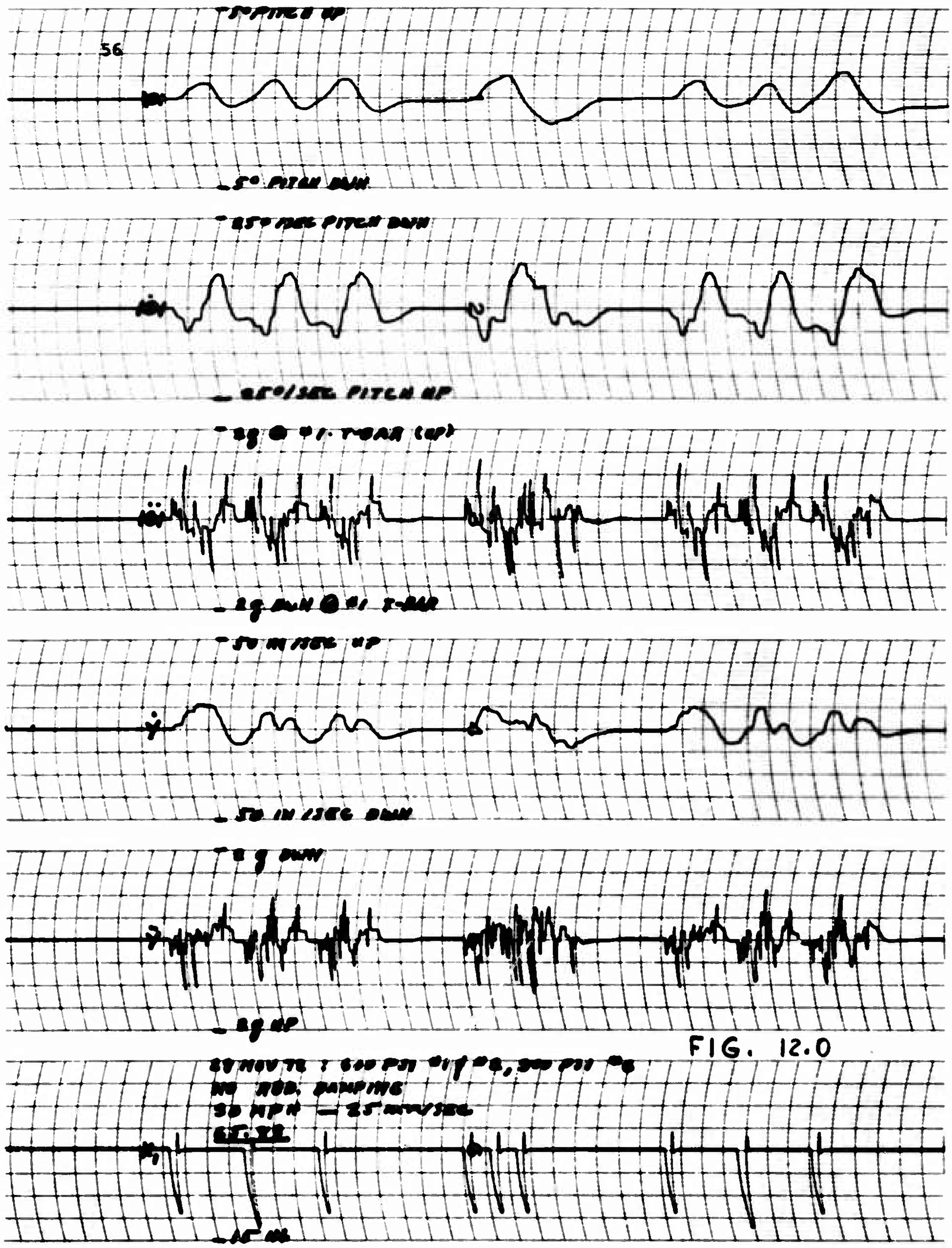

FIG. 12.0

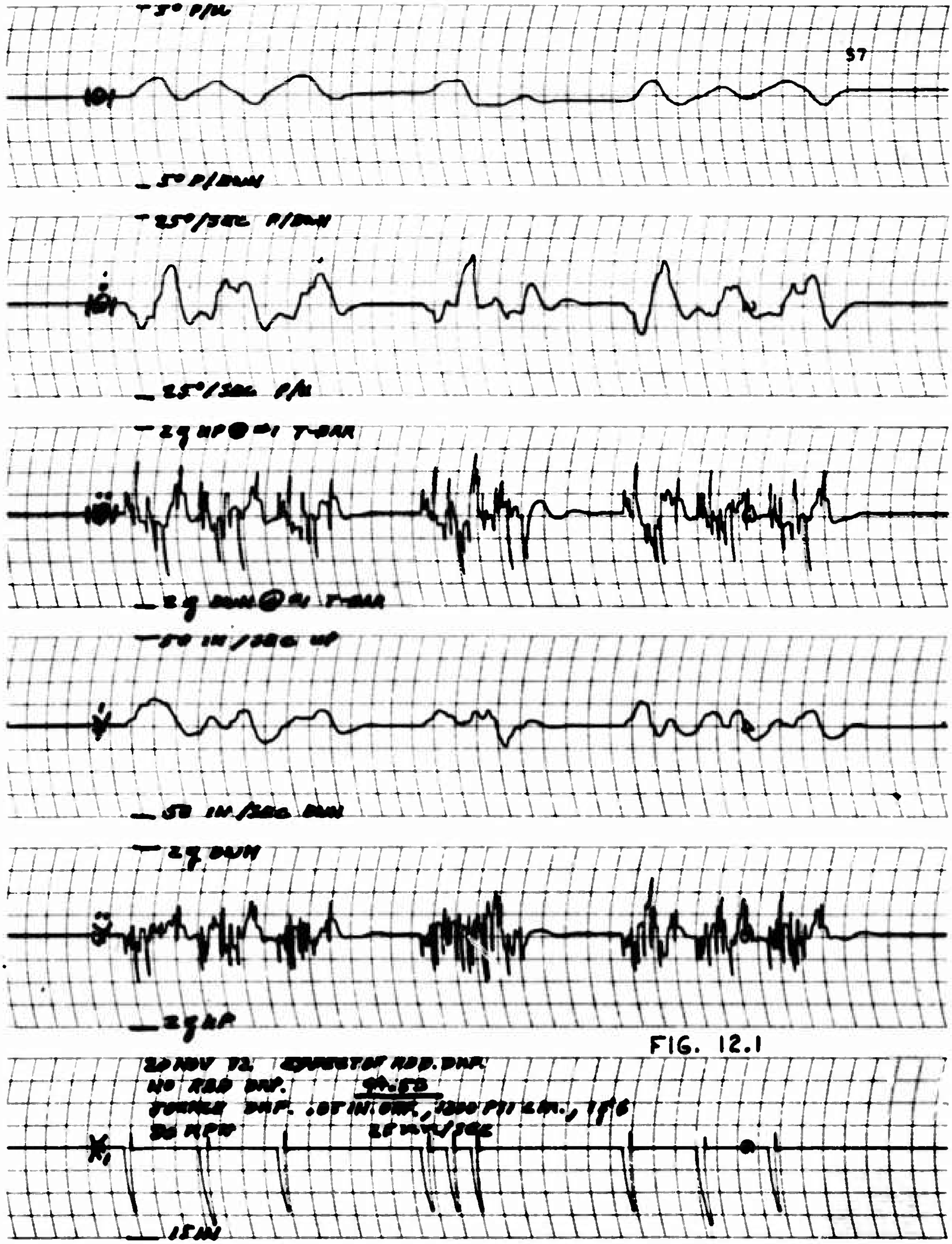

FIG. 12.1

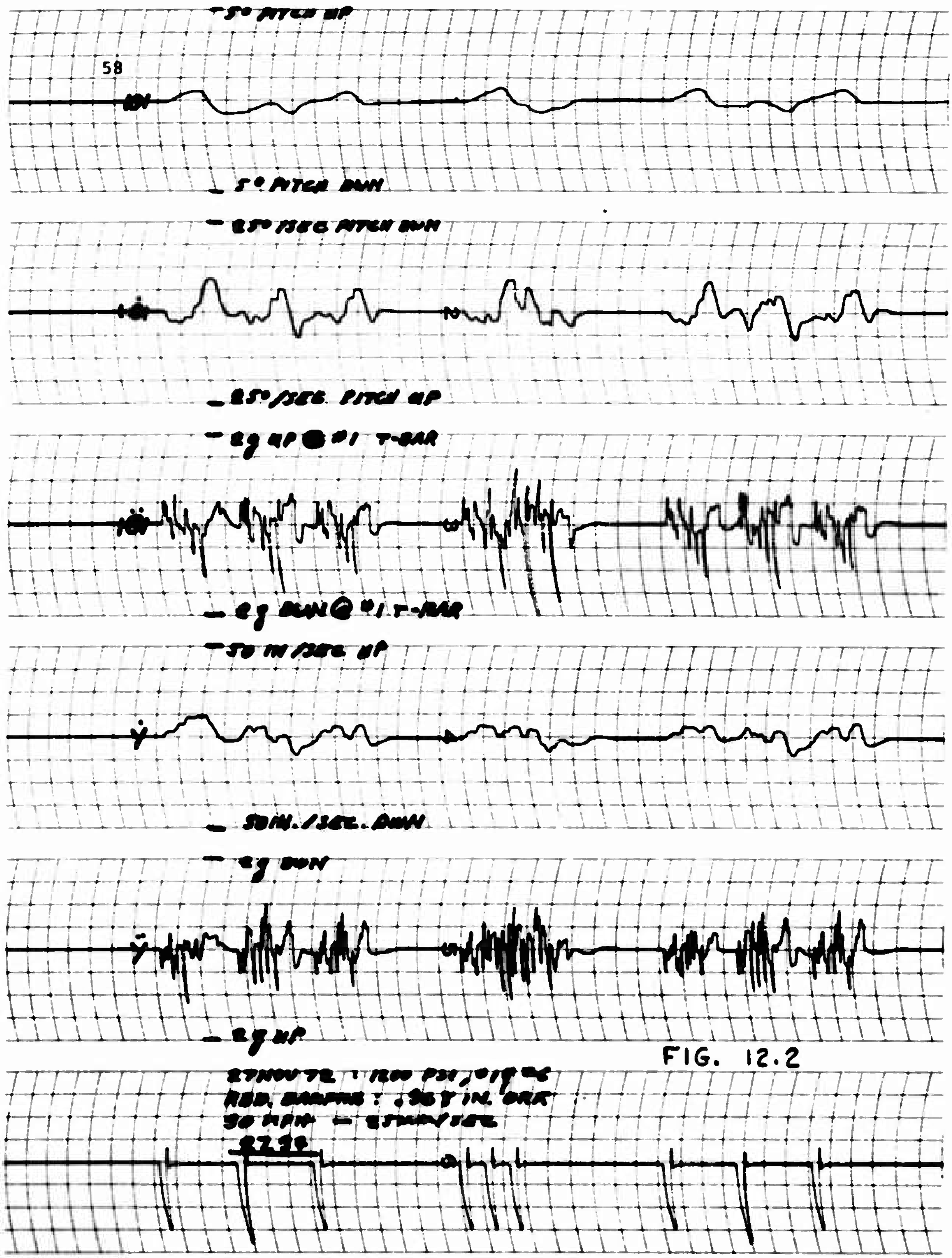
5° PITCH UP
5° PITCH DWN
25°/SEC PITCH DWN
25°/SEC. PITCH UP
2g UP @ #1 T-BAR
2g DWN @ #1 T-BAR
50 IN/SEC. UP
50IN./SEC. DWN
2g DWN
2g UP

FIG. 12.2

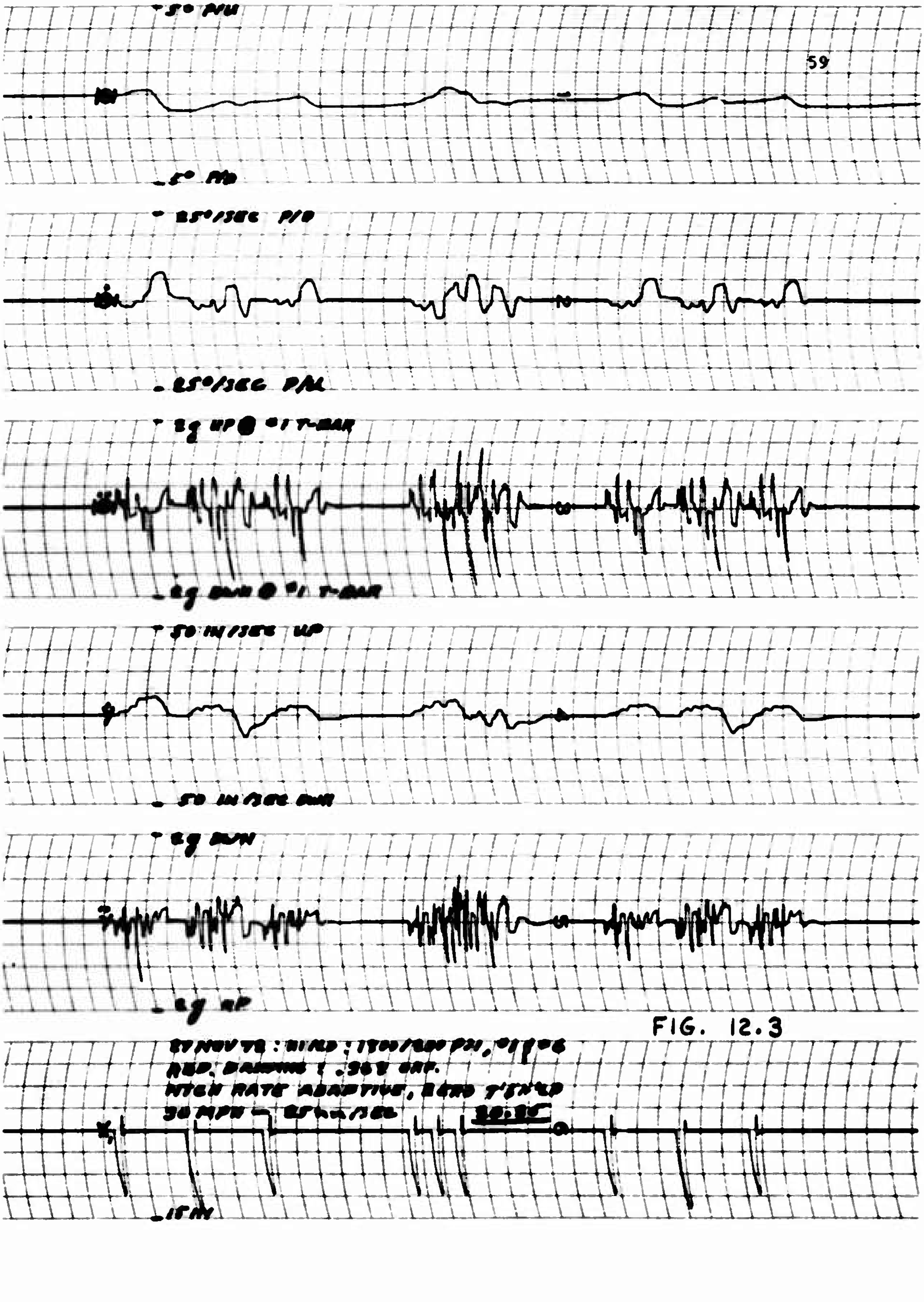

FIG. 12.3

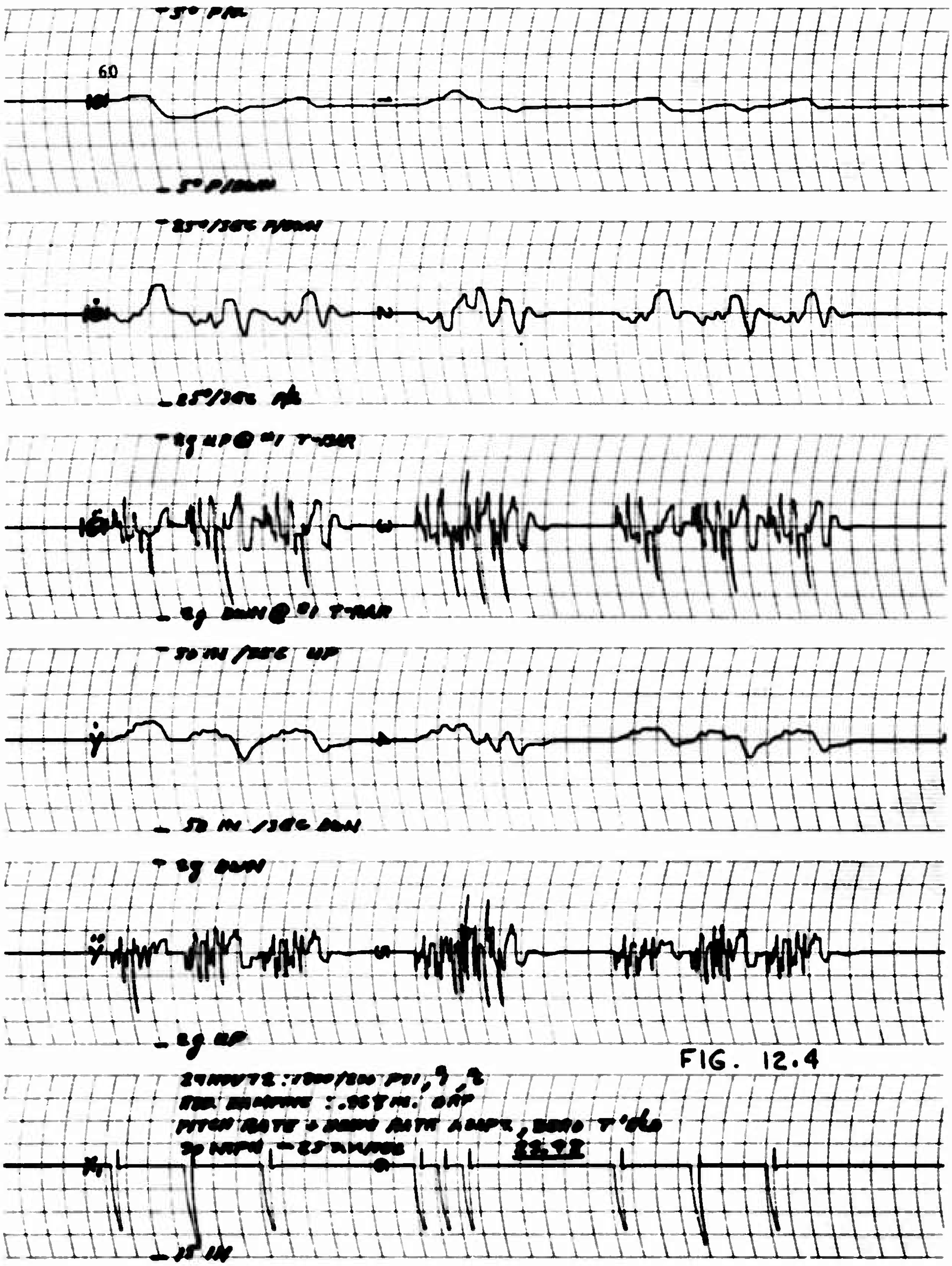

FIG. 12.4

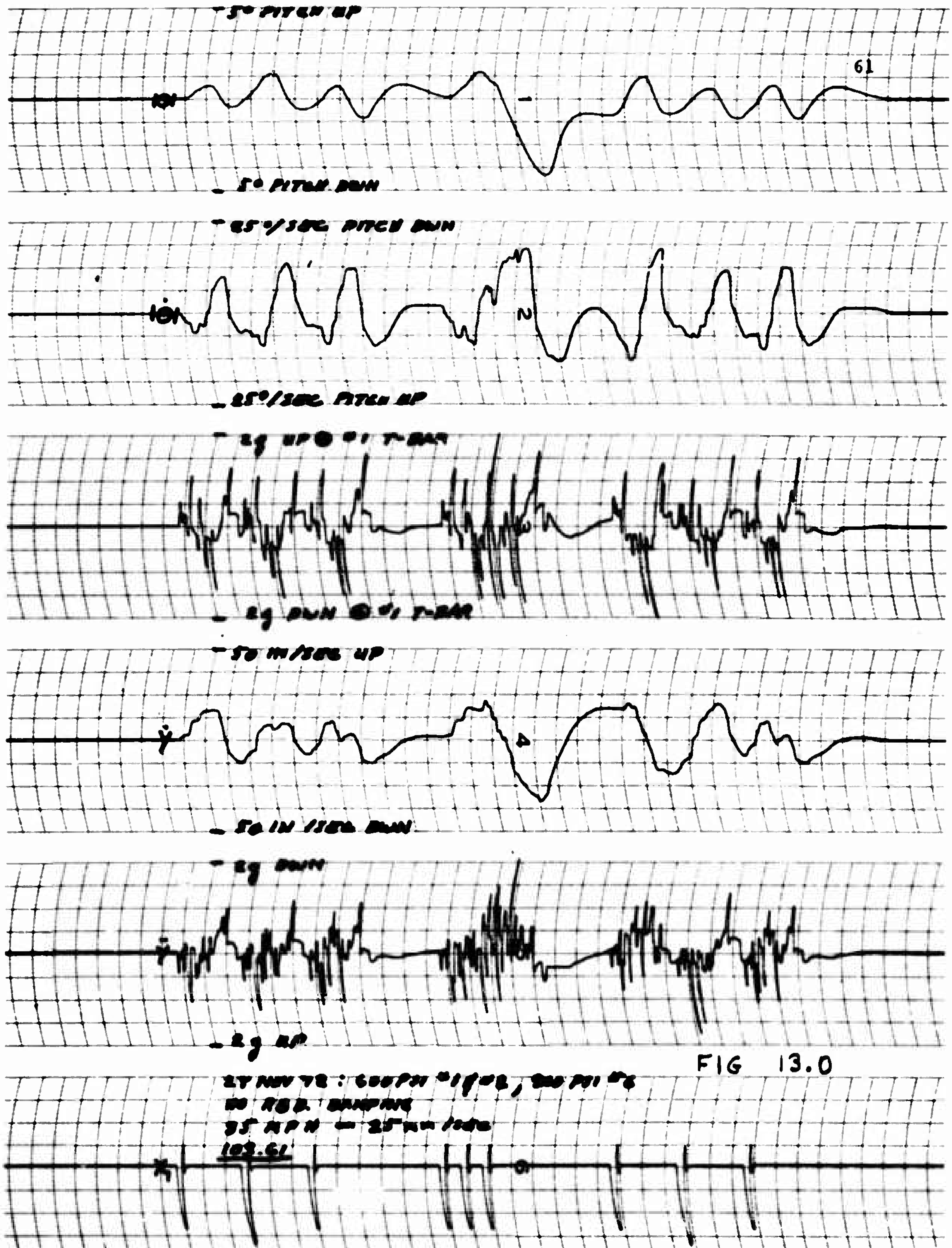
5° PITCH UP
5° PITCH DWN
25°/SEC PITCH DWN
25°/SEC PITCH UP
2g UP @ #1 T-BAR
2g DWN @ #1 T-BAR
50 IN/SEC UP
50 IN/SEC DWN
2g DWN
2g UP
35 MPH — 25mm/sec
103.61

FIG 13.0

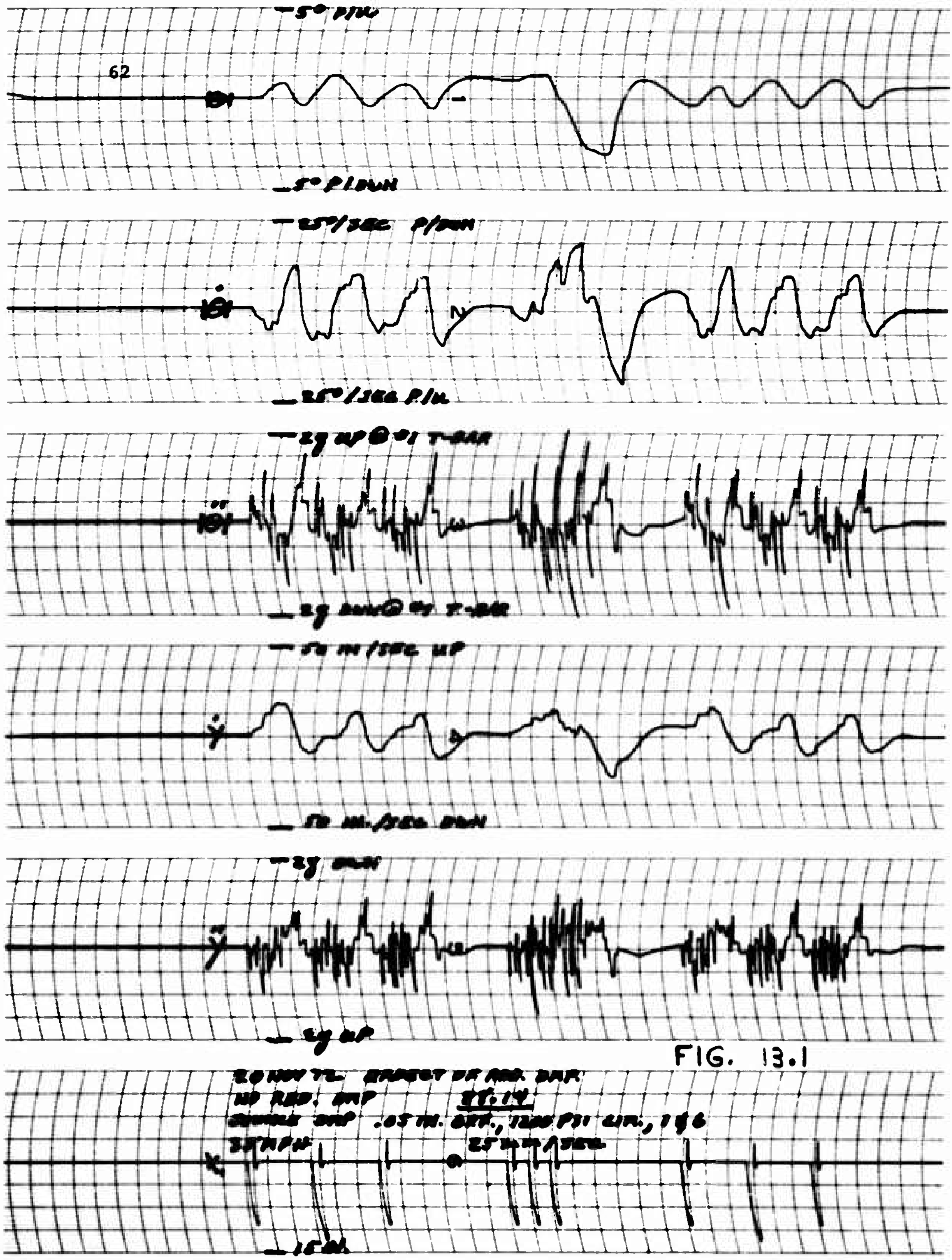

FIG. 13.1

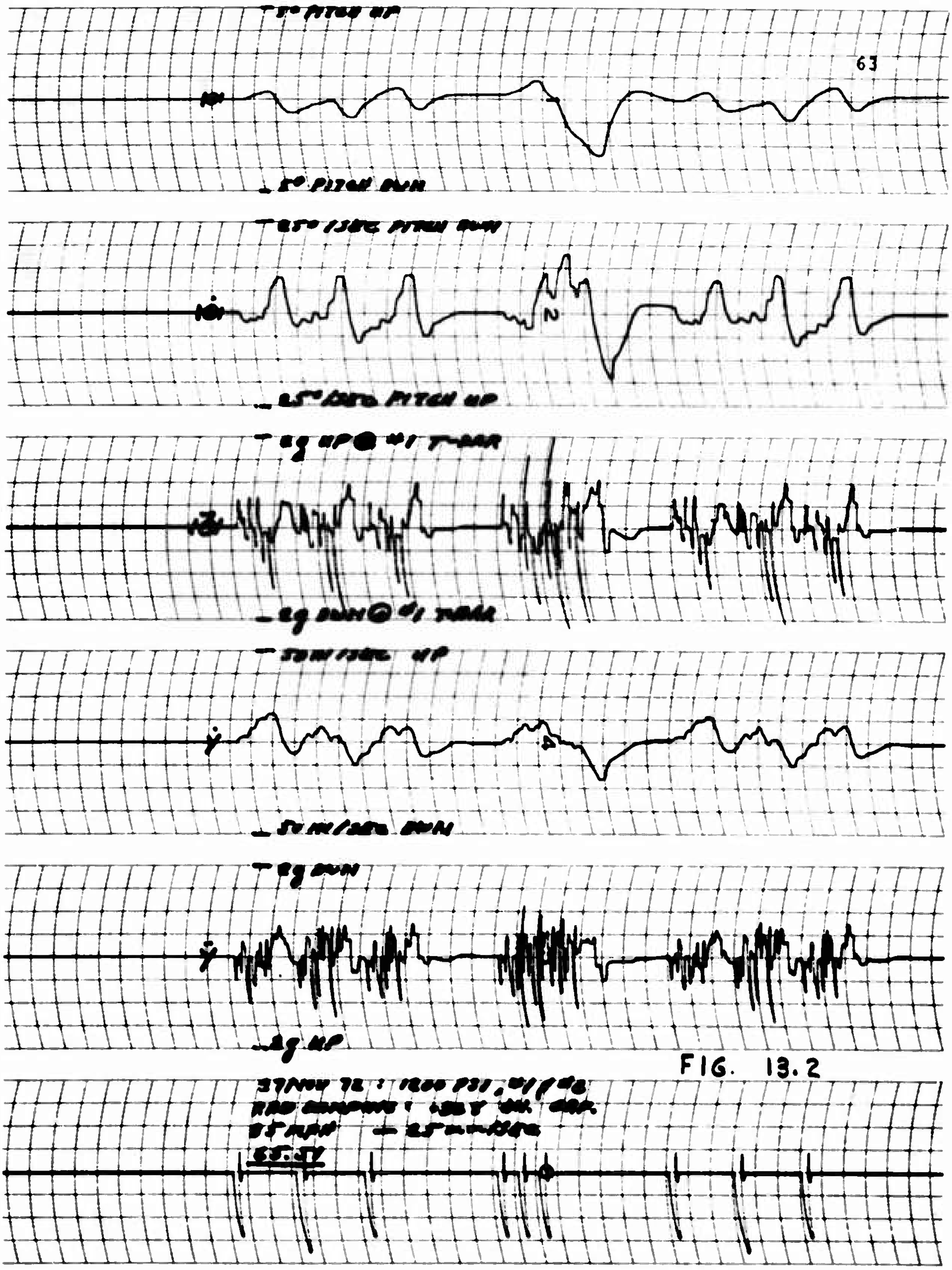

FIG. 13.2

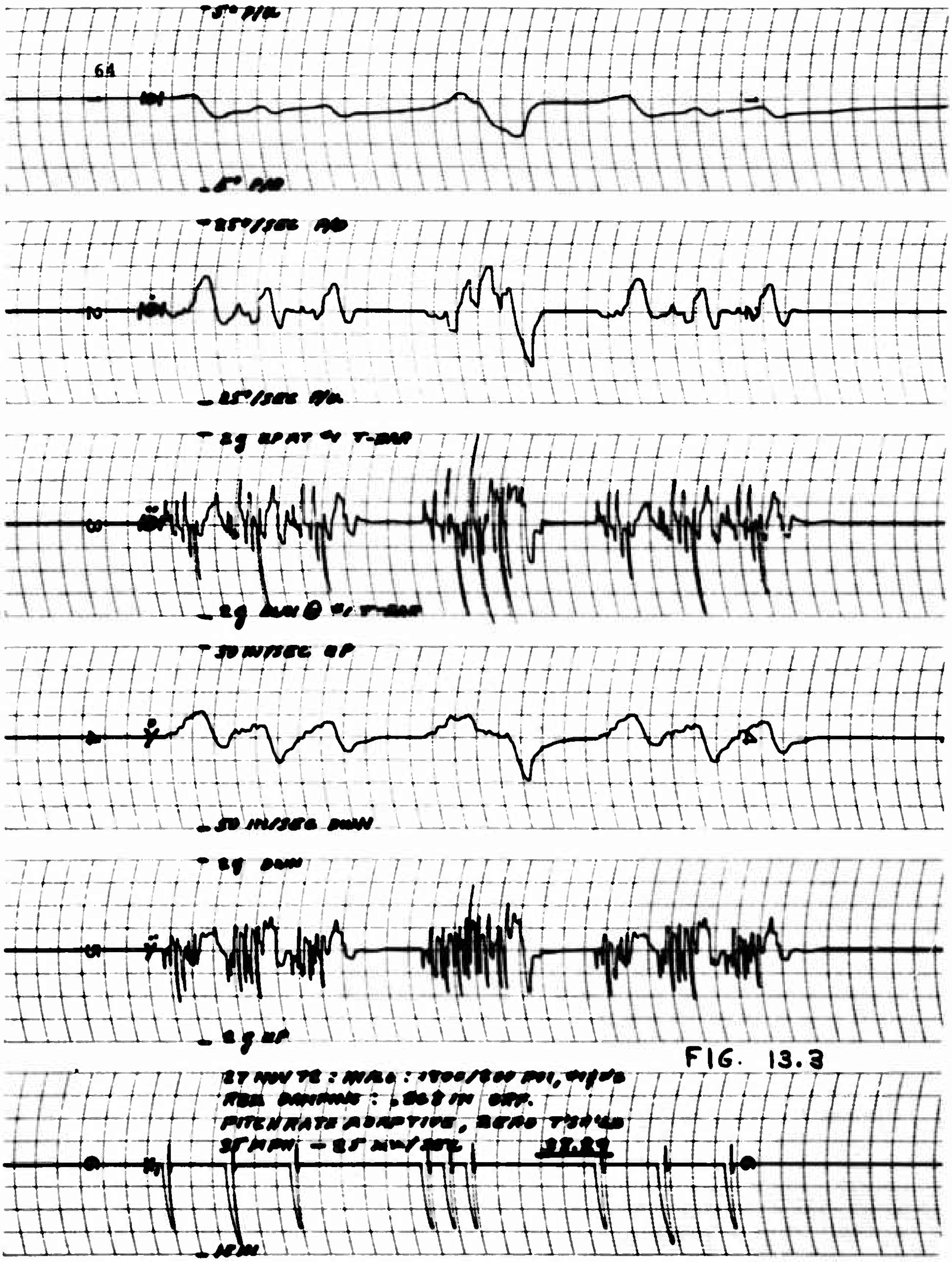

FIG. 13.3

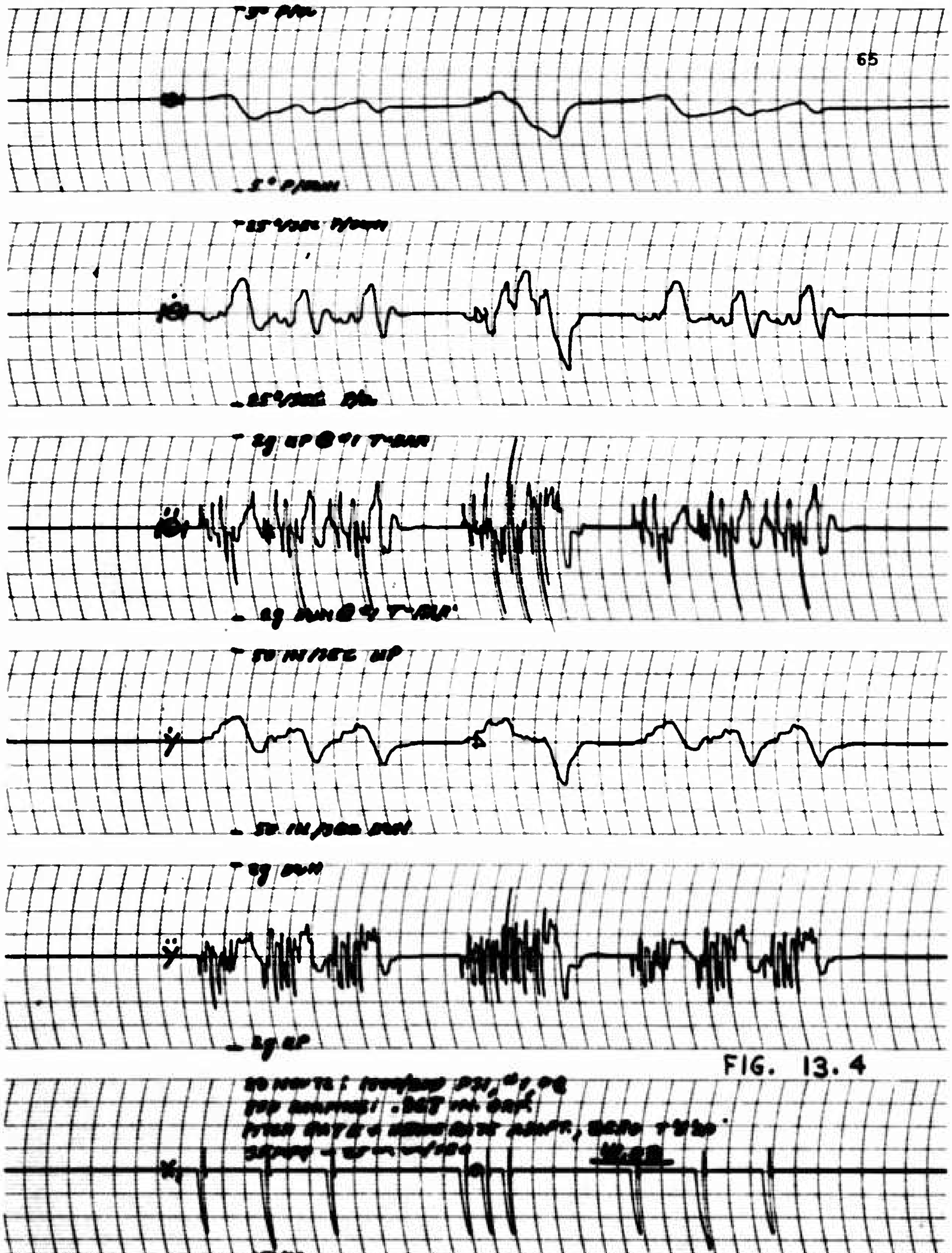

FIG. 13.4

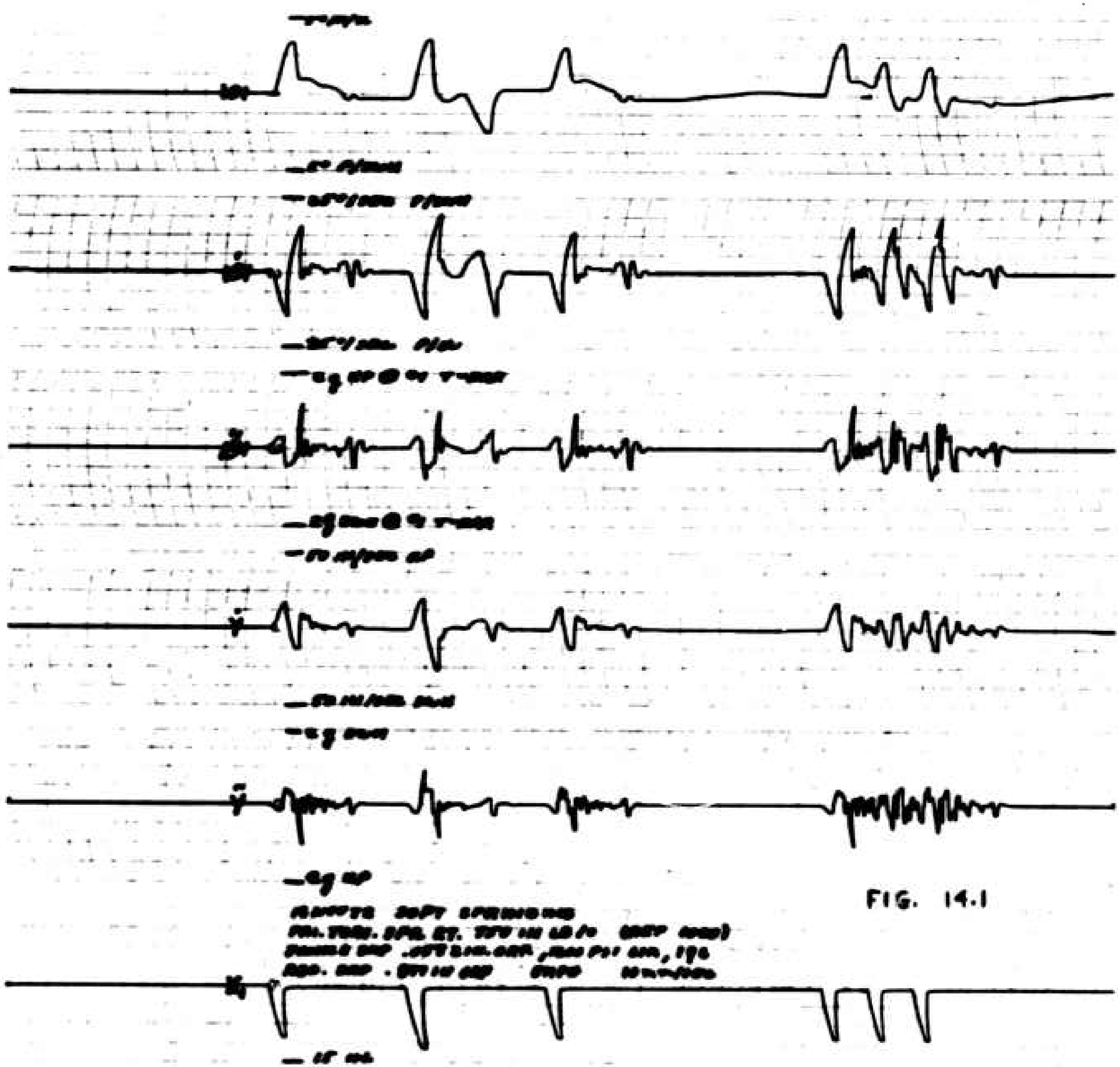

FIG. 14.1

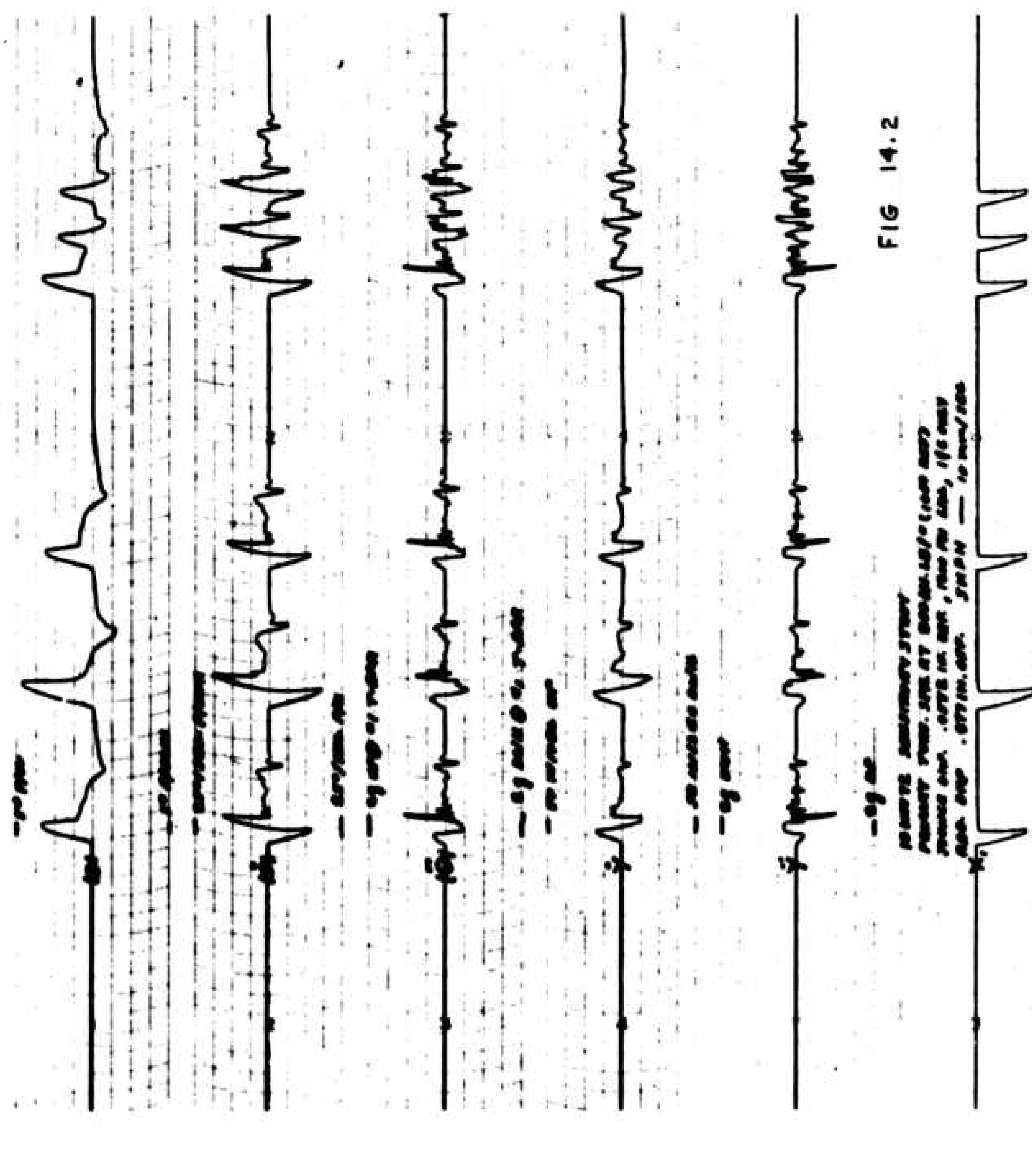

FIG 14.2

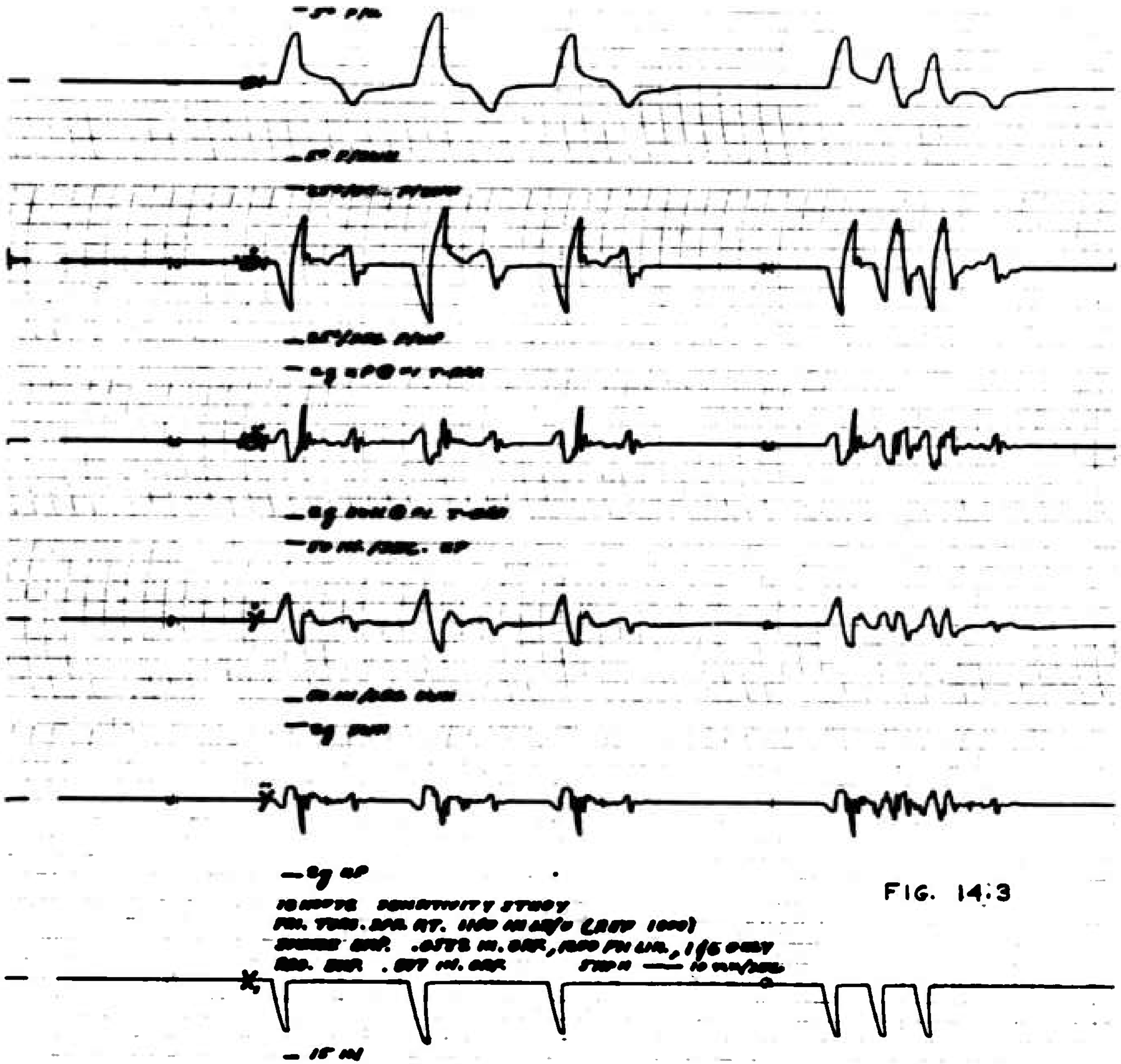

FIG. 14:3

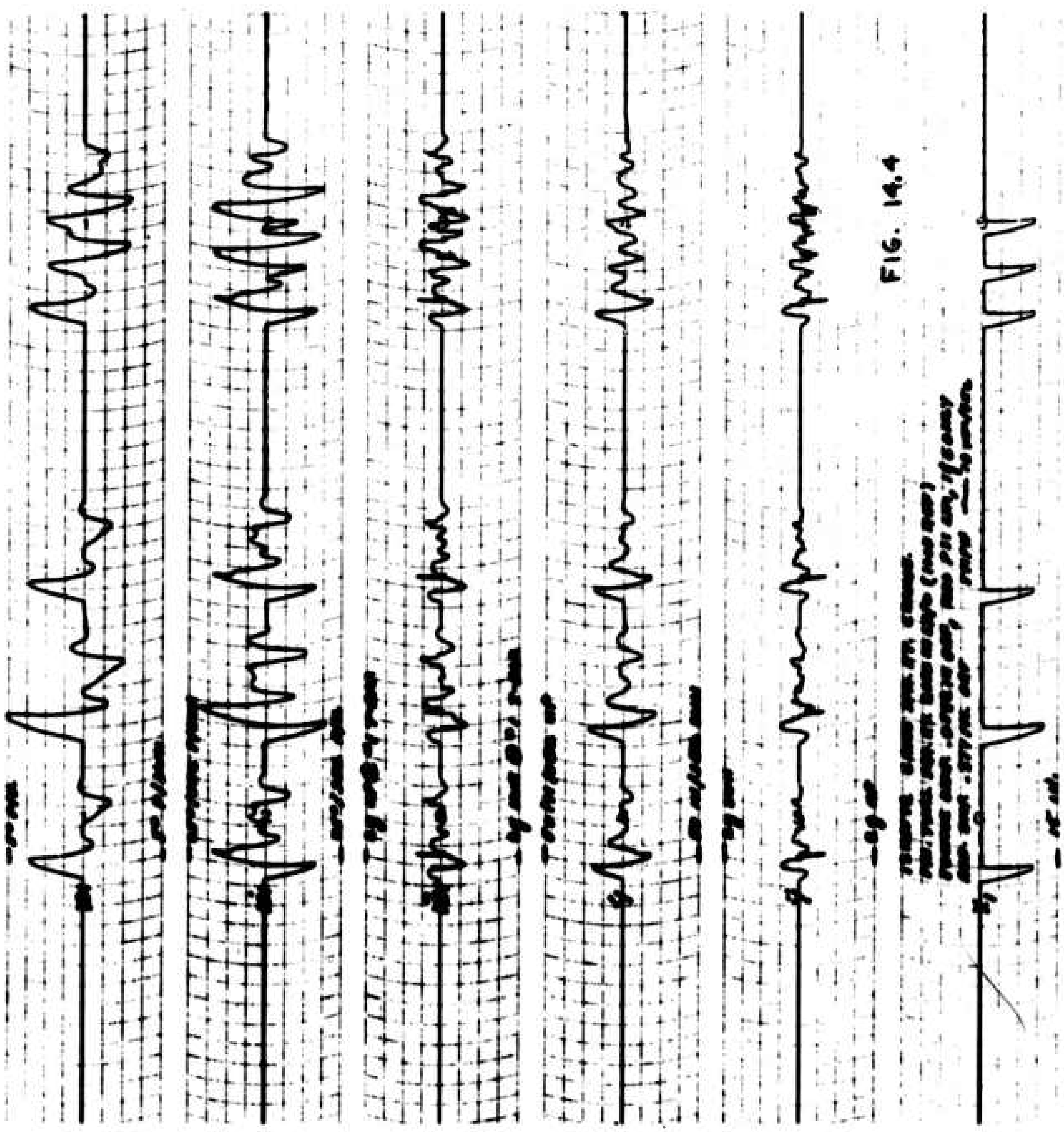

FIG. 14.4

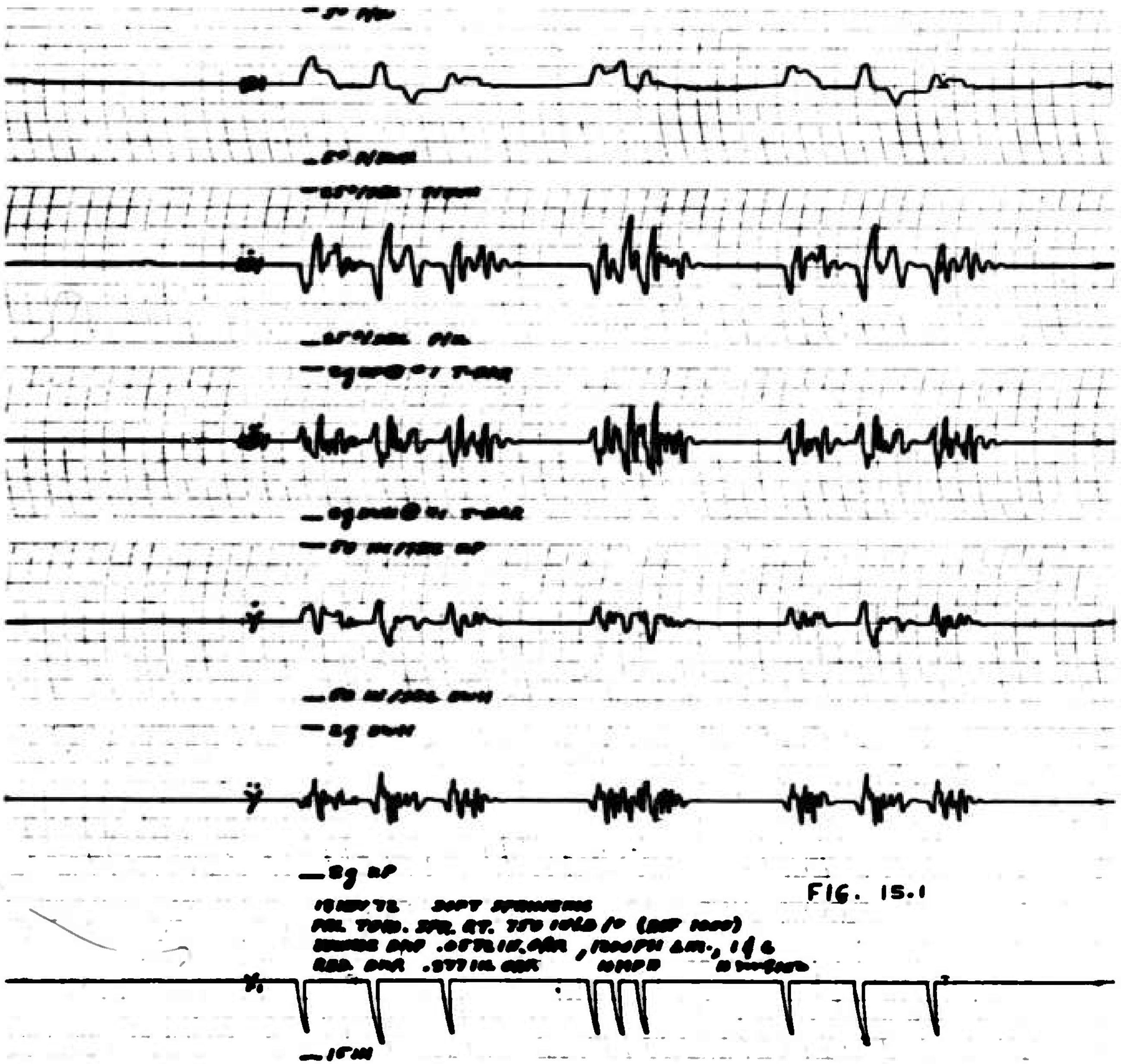

FIG. 15.1

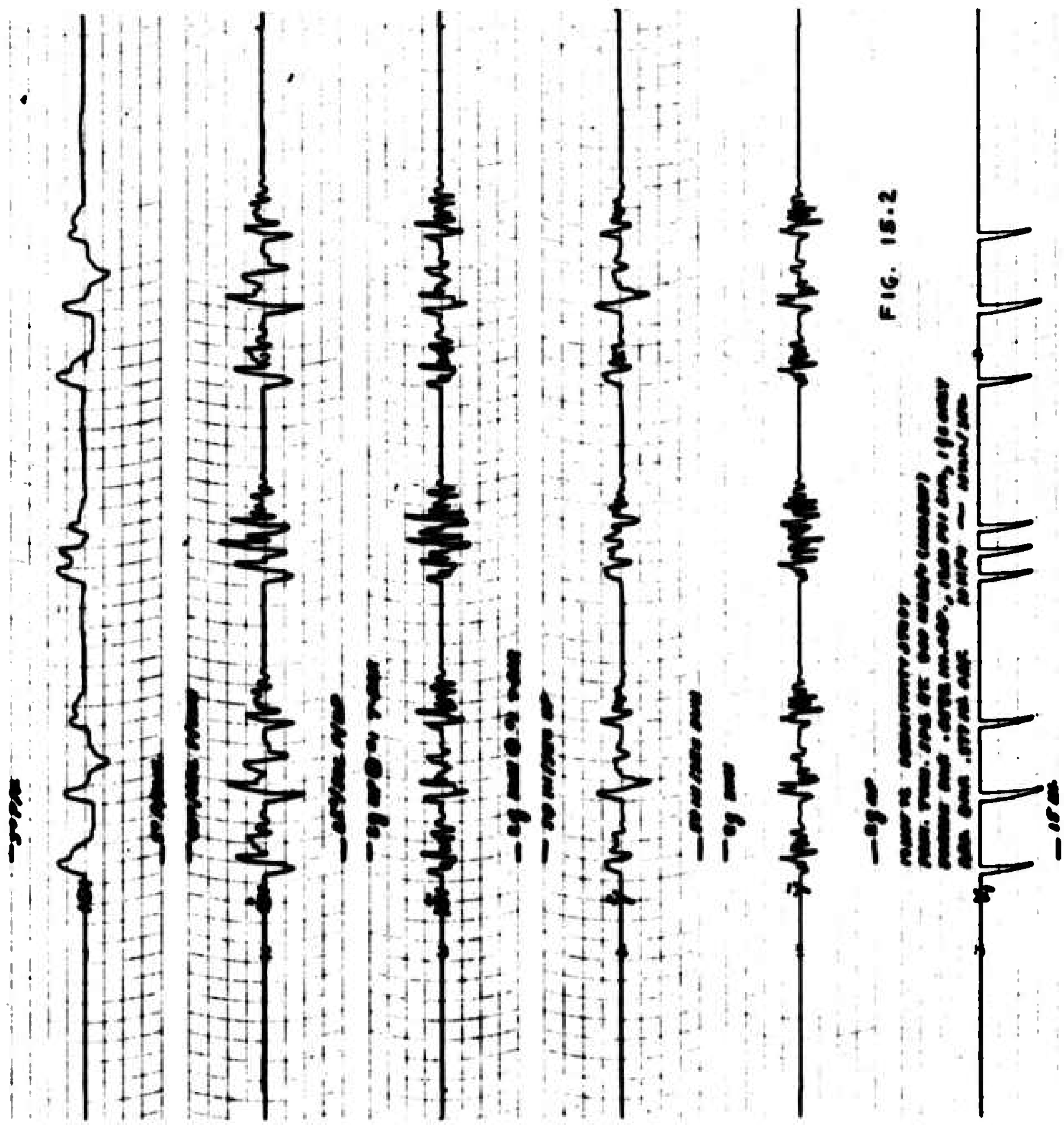

FIG. 15.2

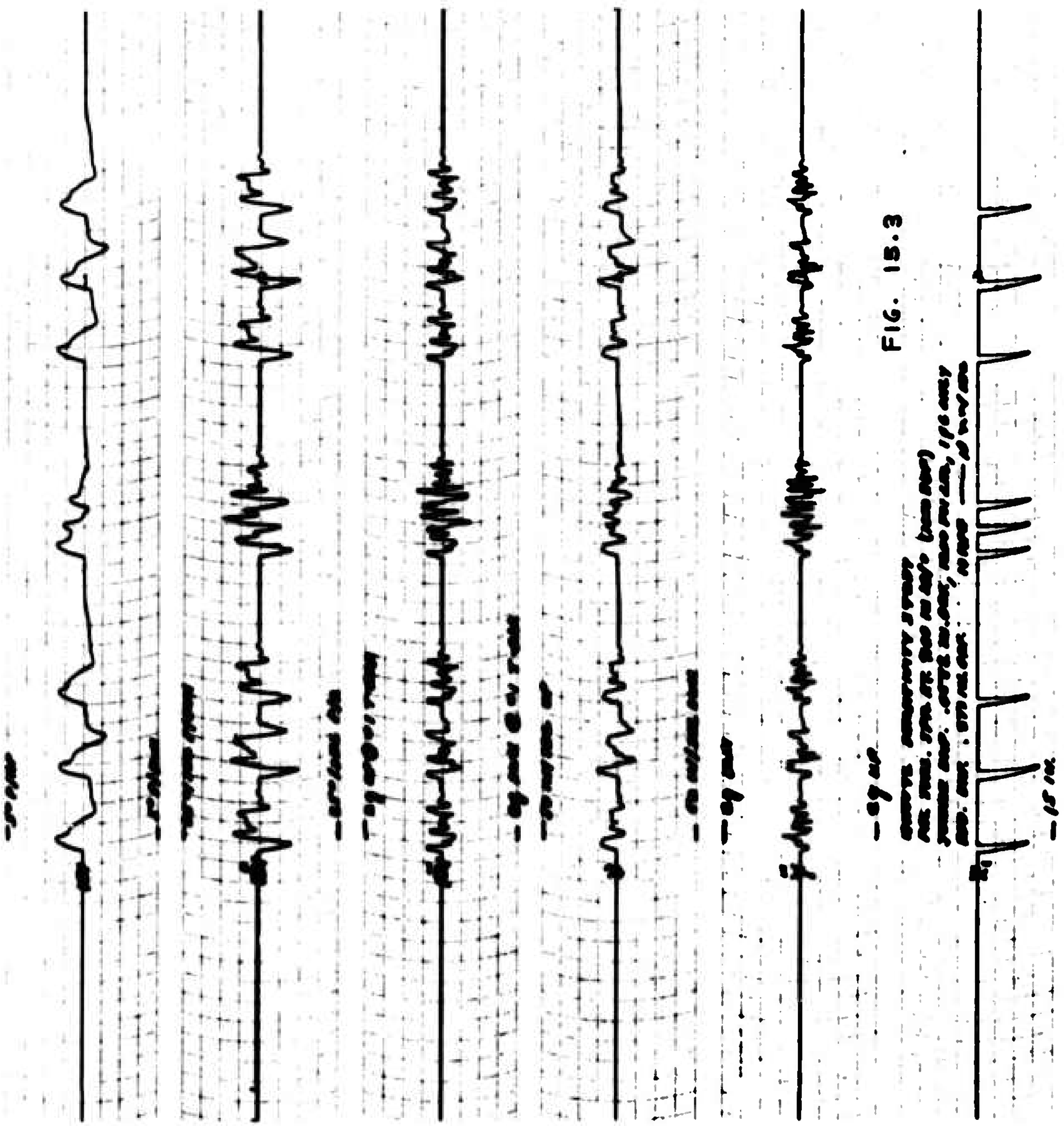

FIG. 15.3

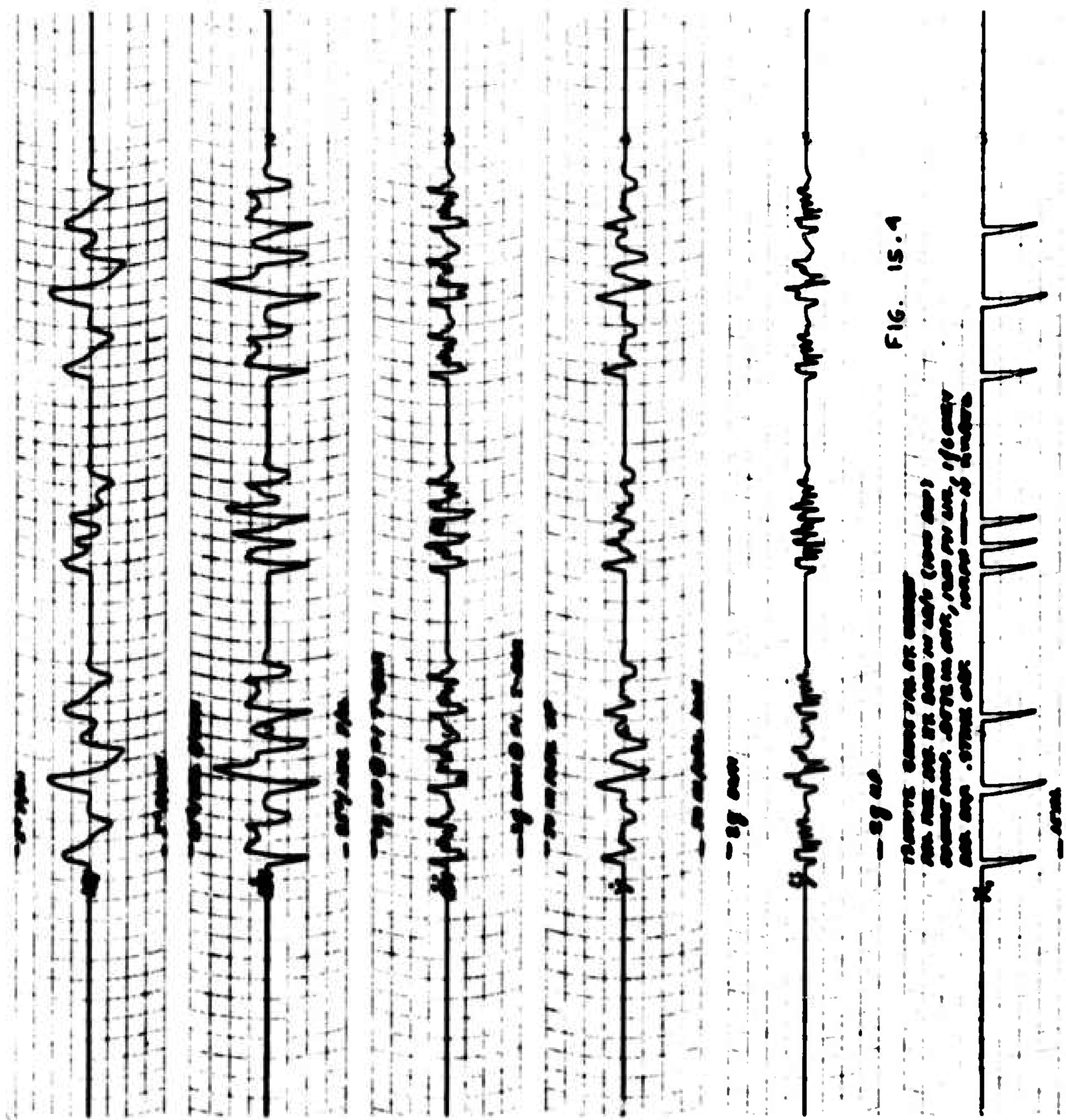

FIG. 15.4

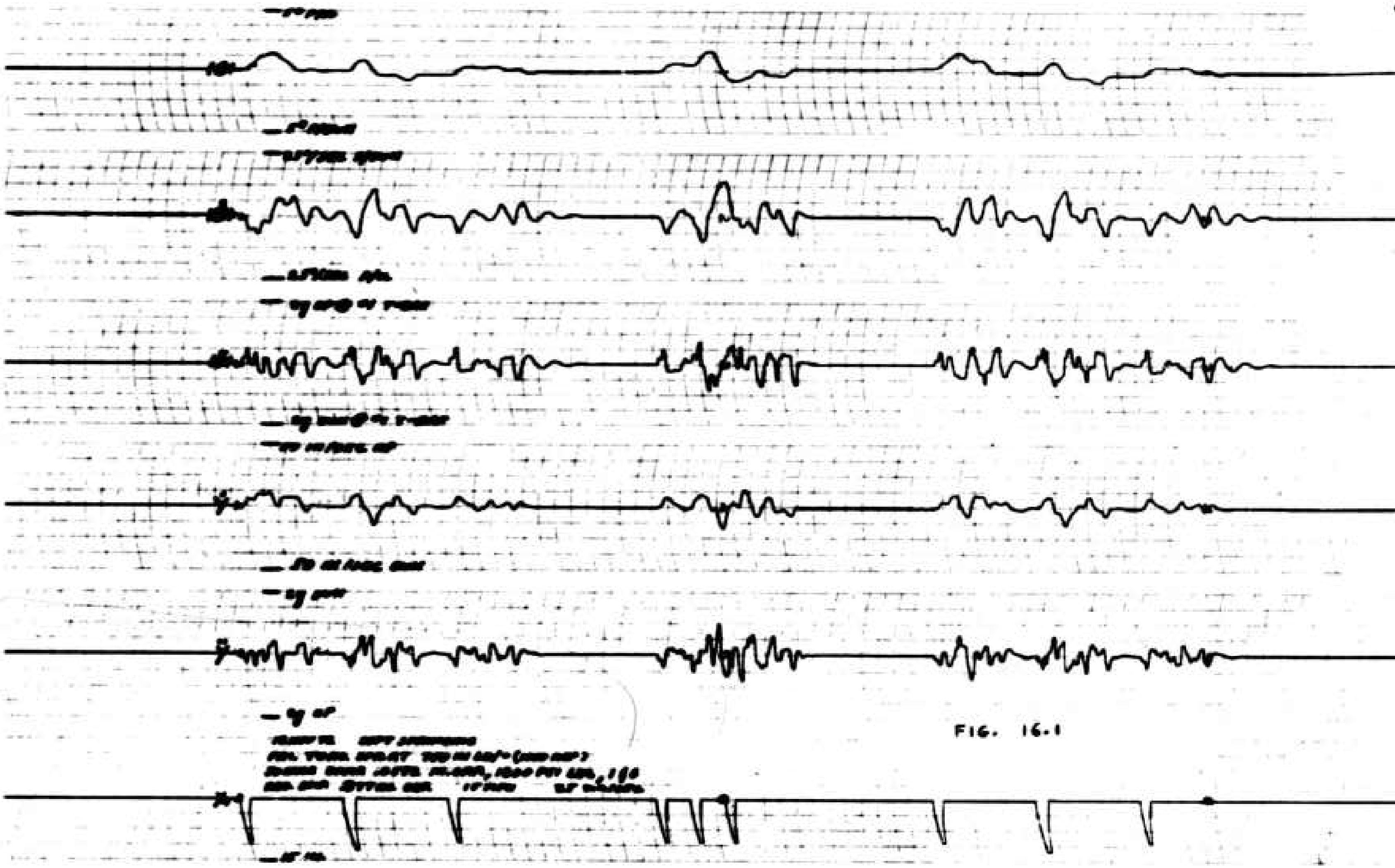

FIG. 16.1

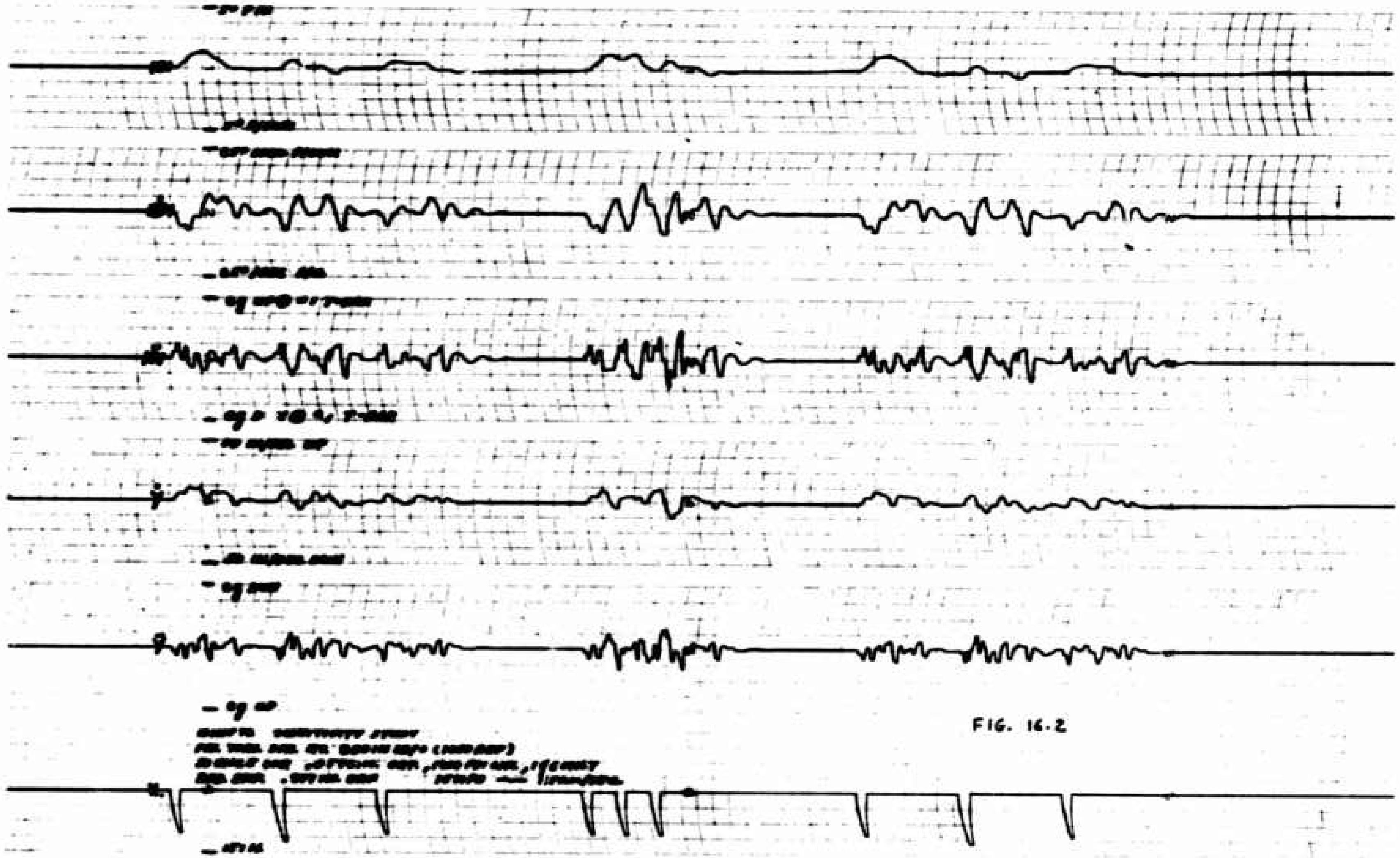

FIG. 16.2

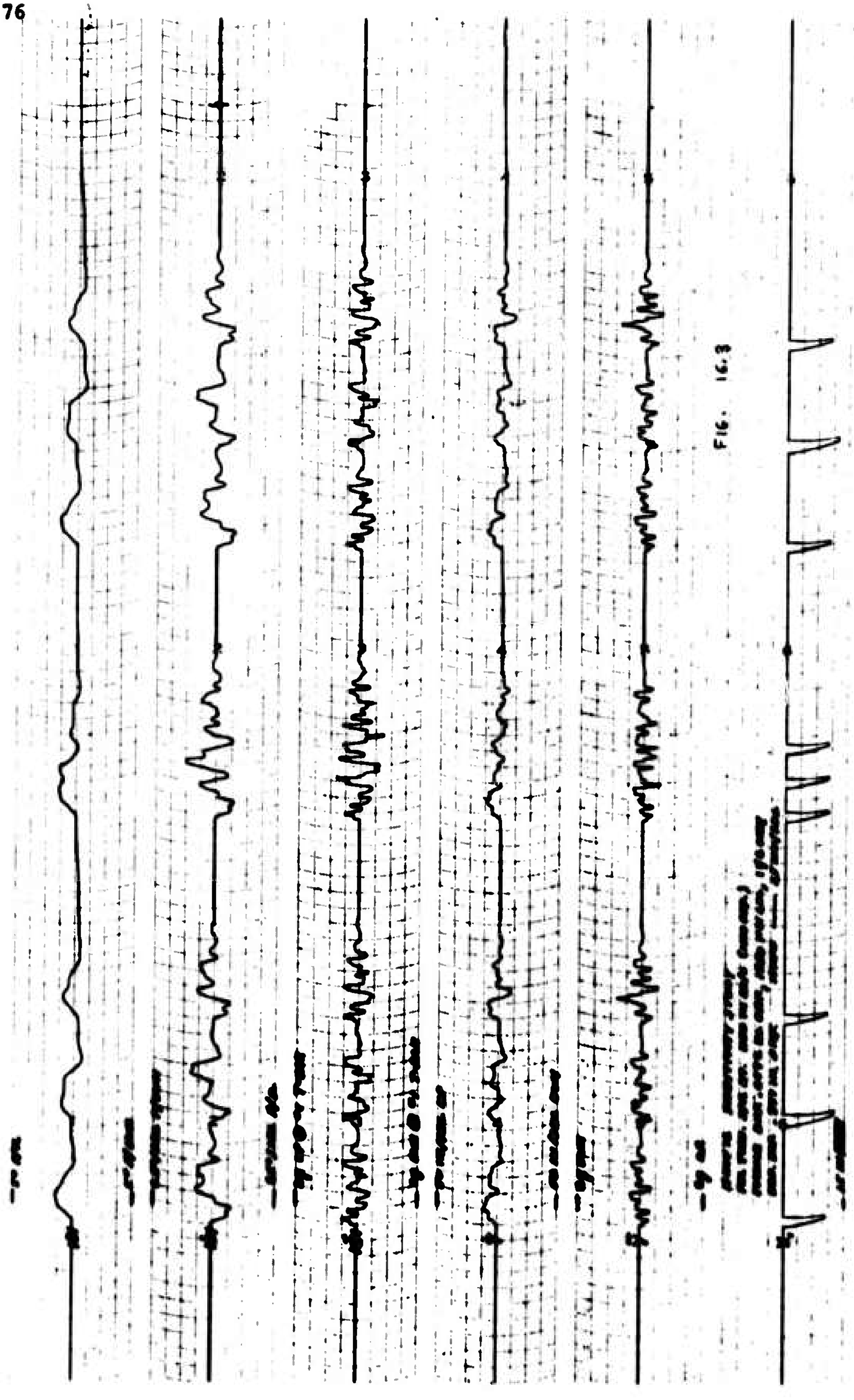

FIG. 16.3

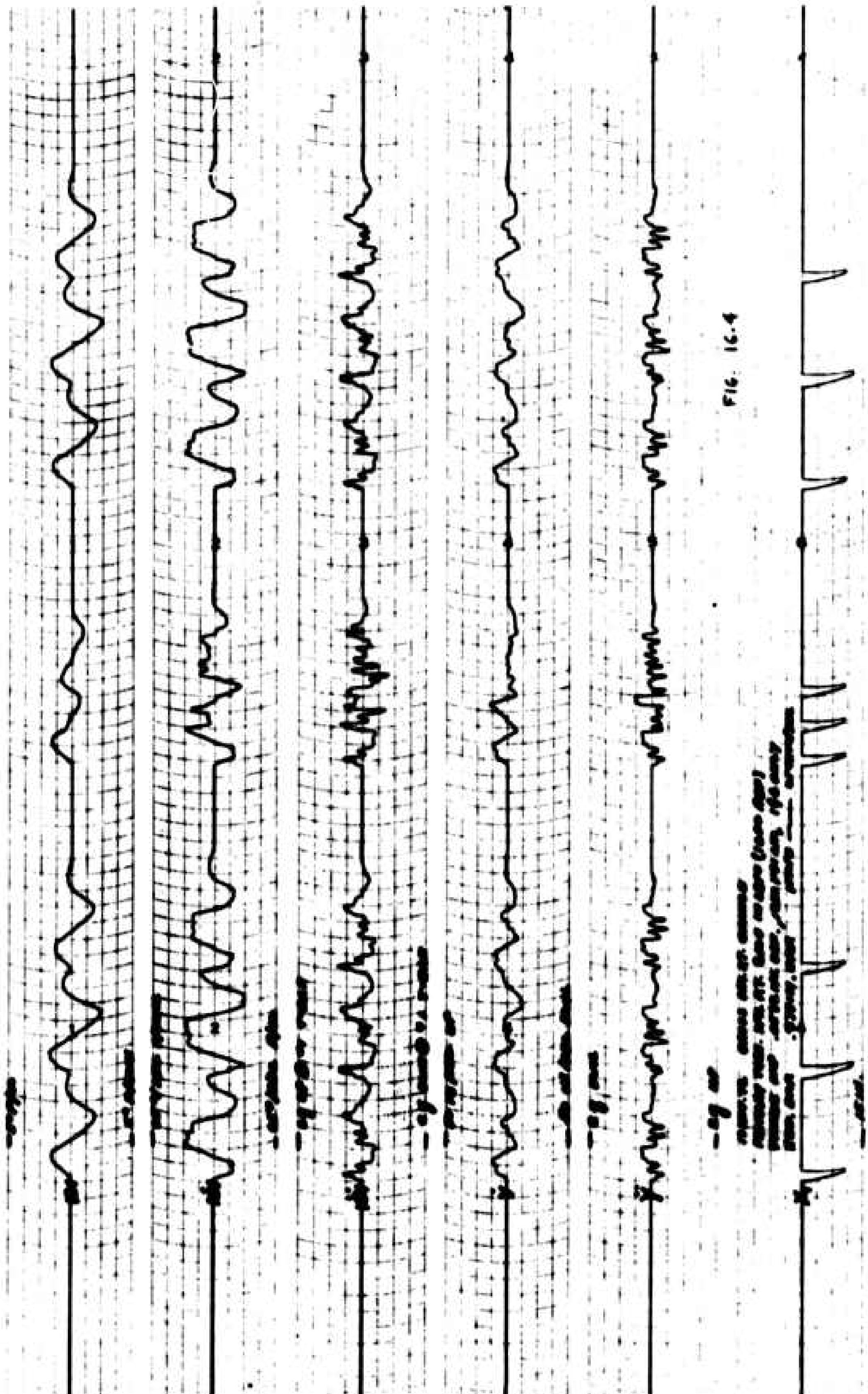

FIG. 16.4

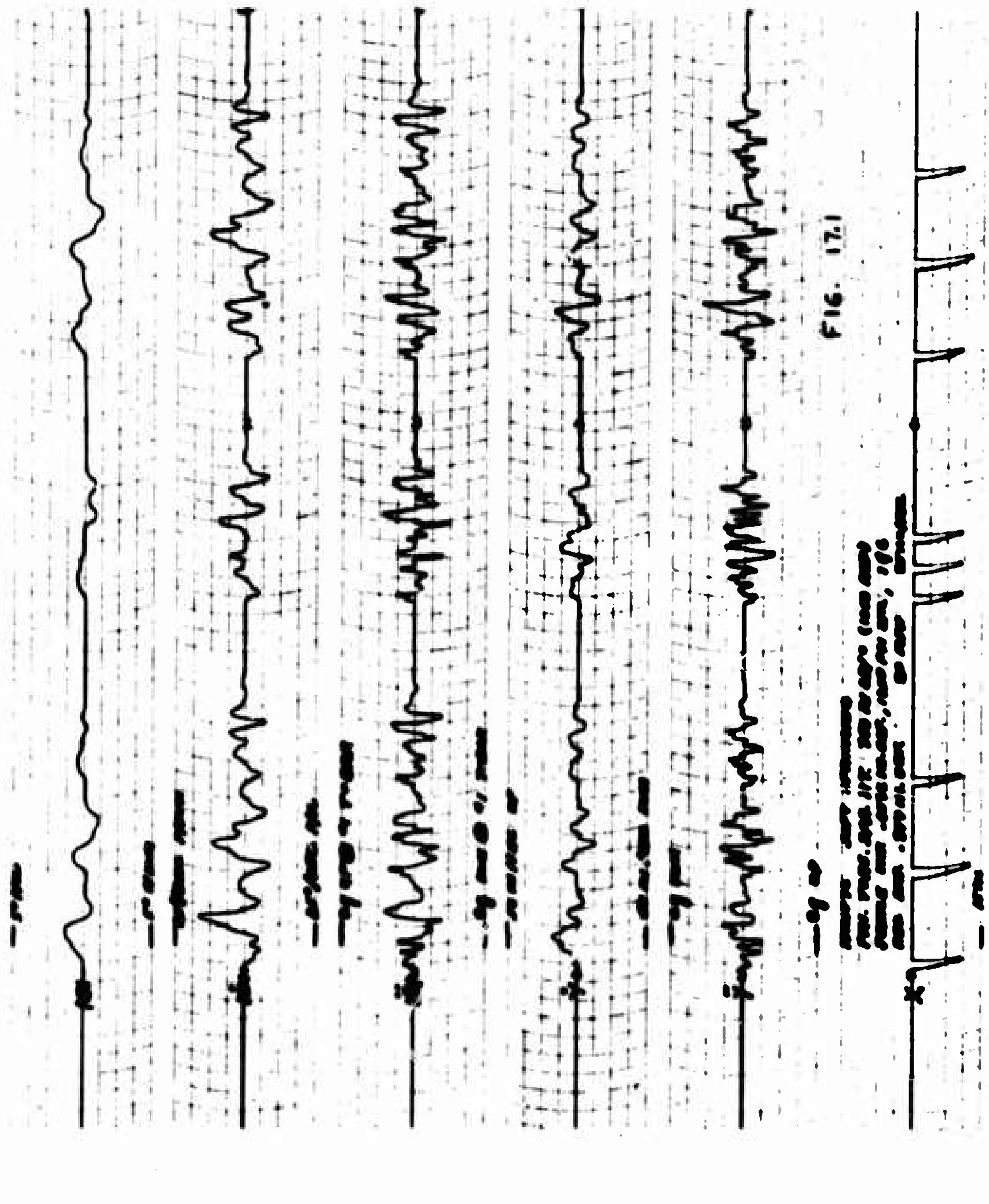

FIG. 17.1

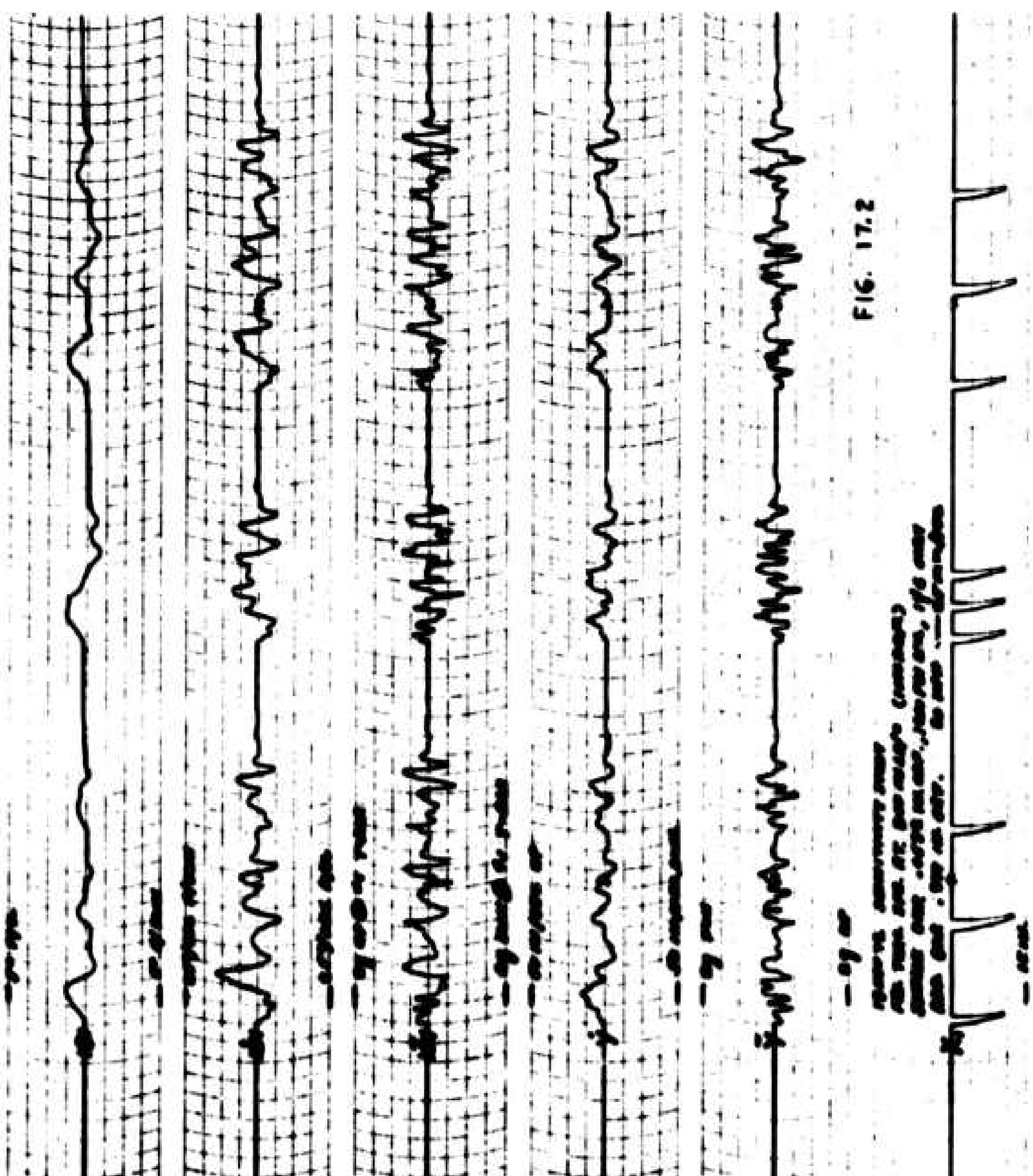

FIG. 17.2

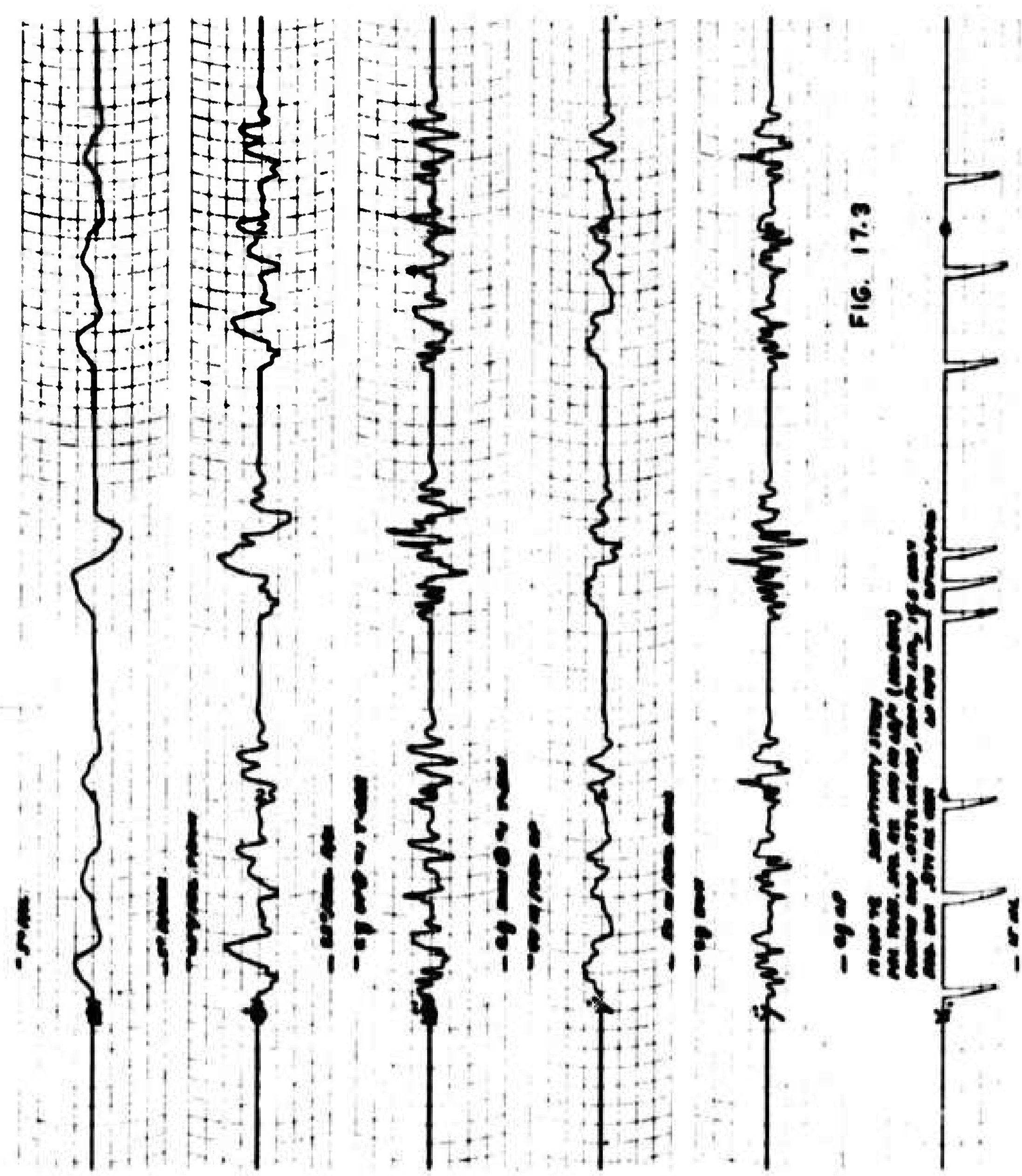

FIG. 17.3

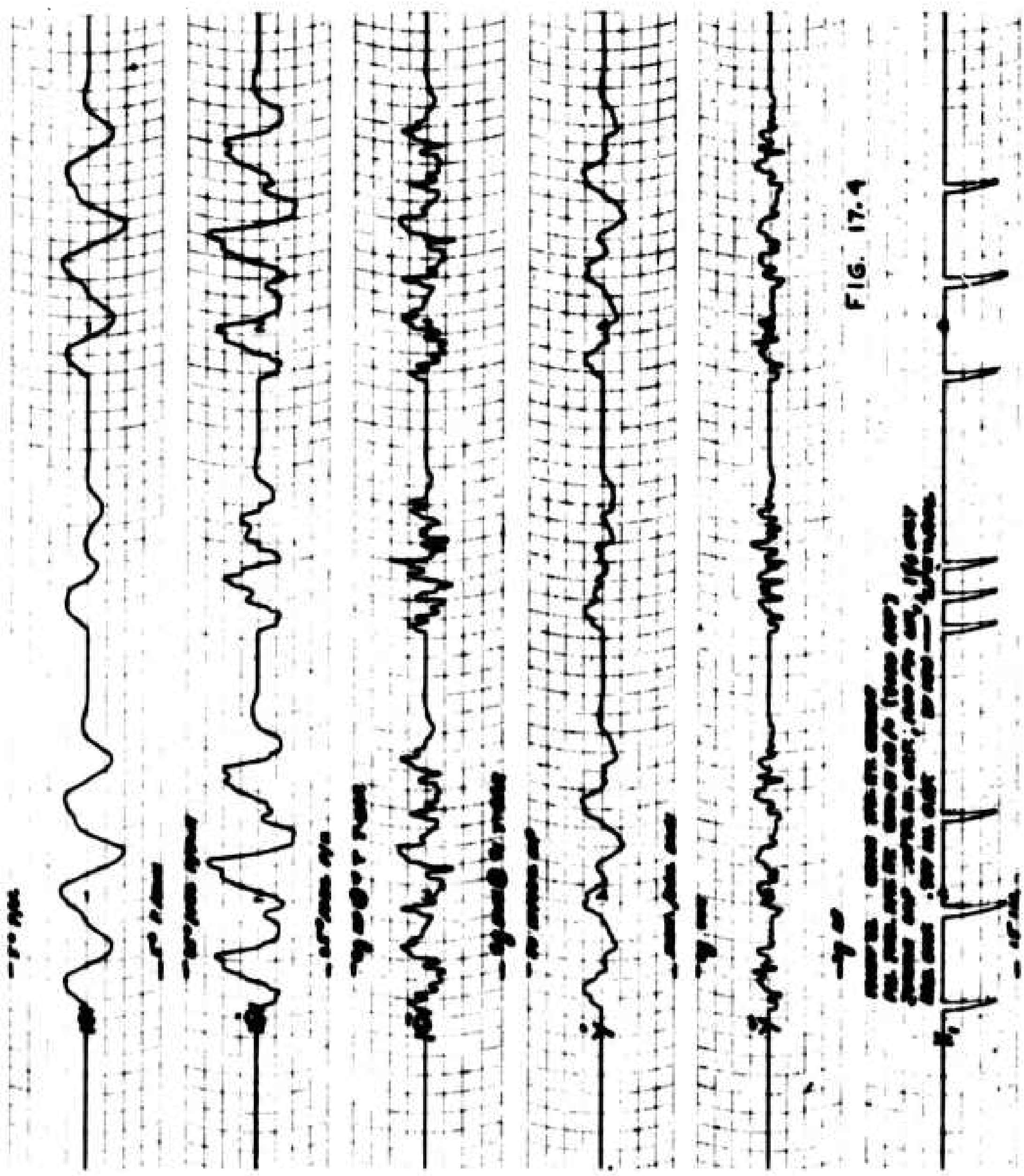

FIG. 17.4

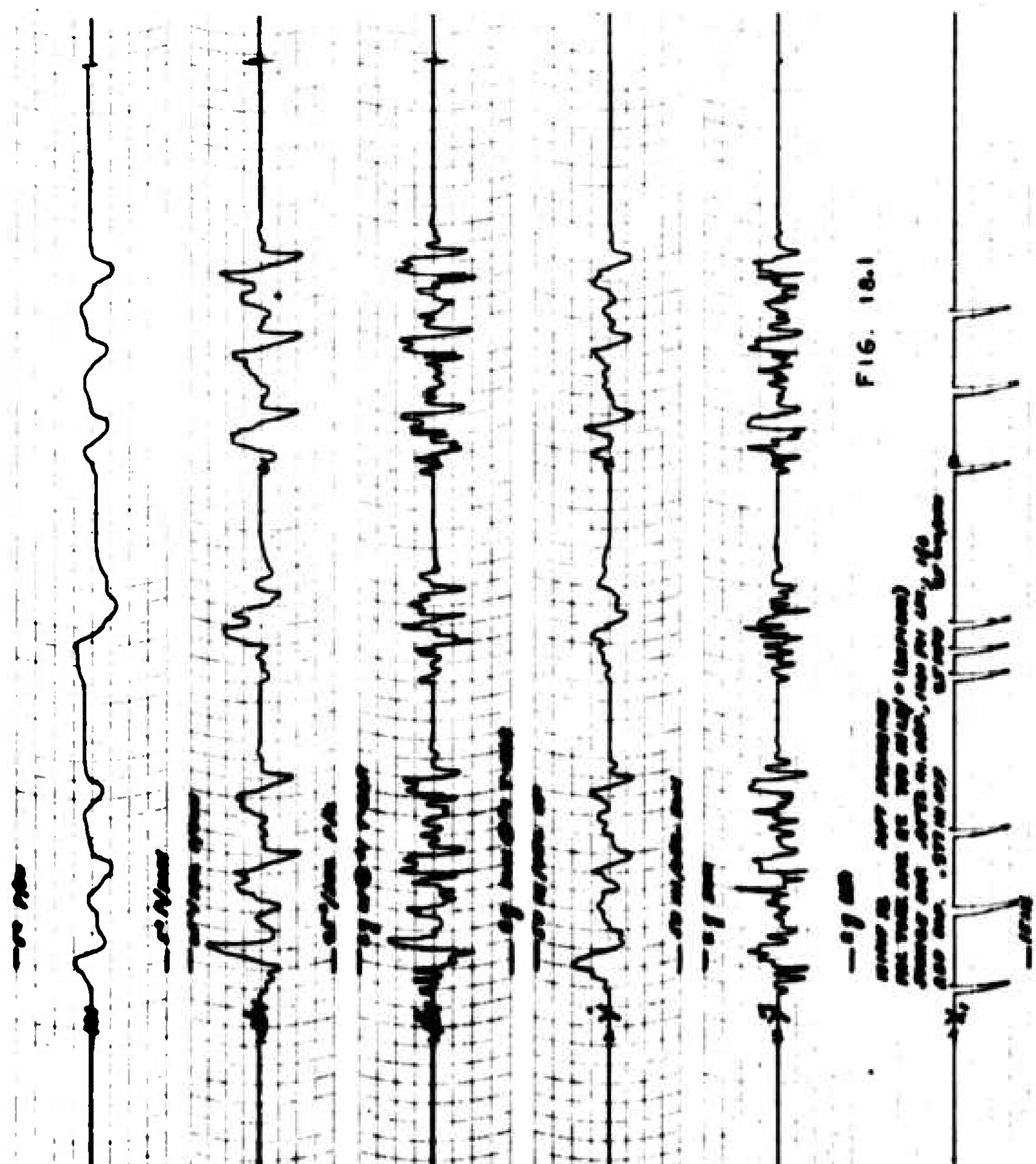

FIG. 18.1

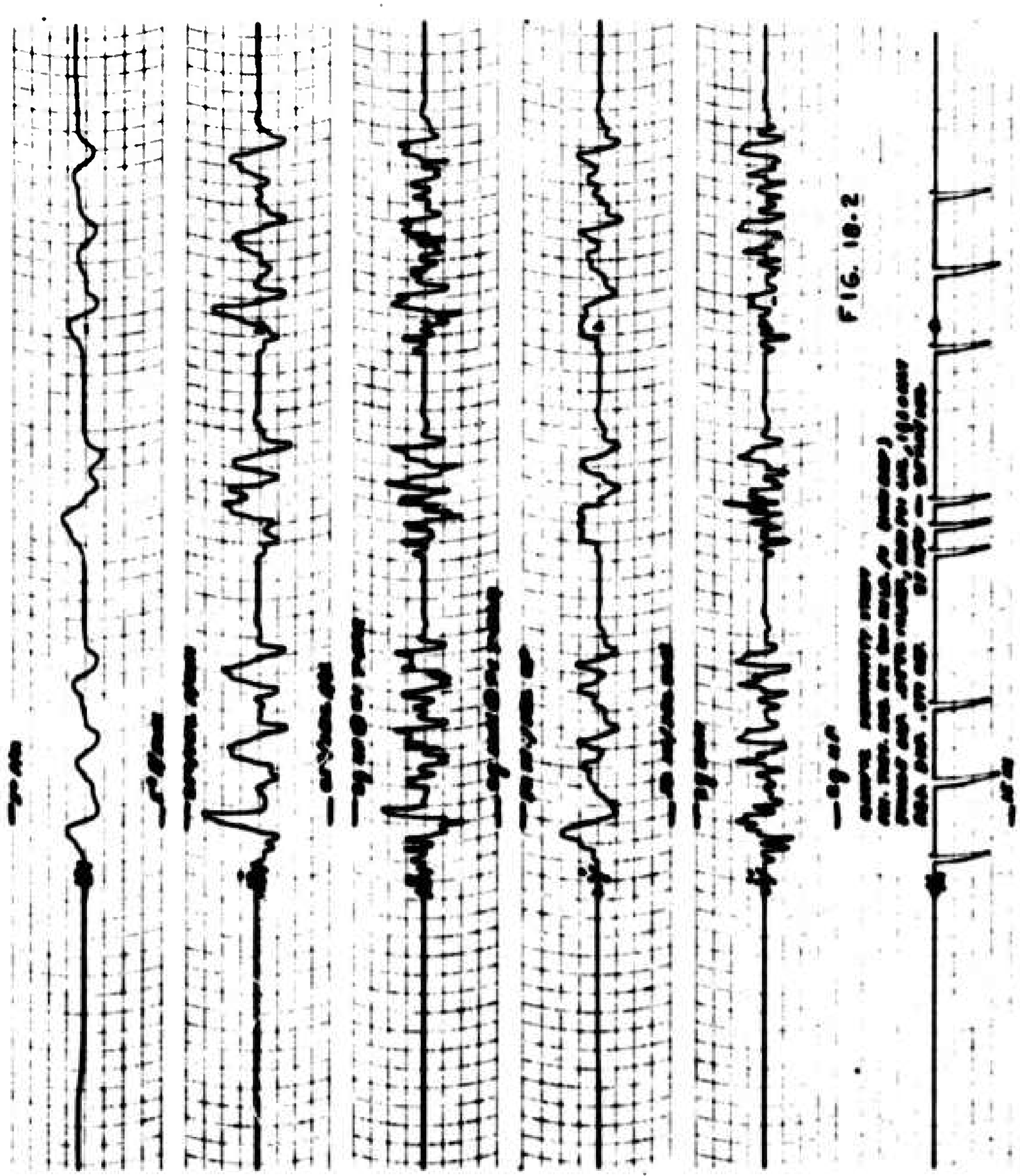

FIG. 10.2

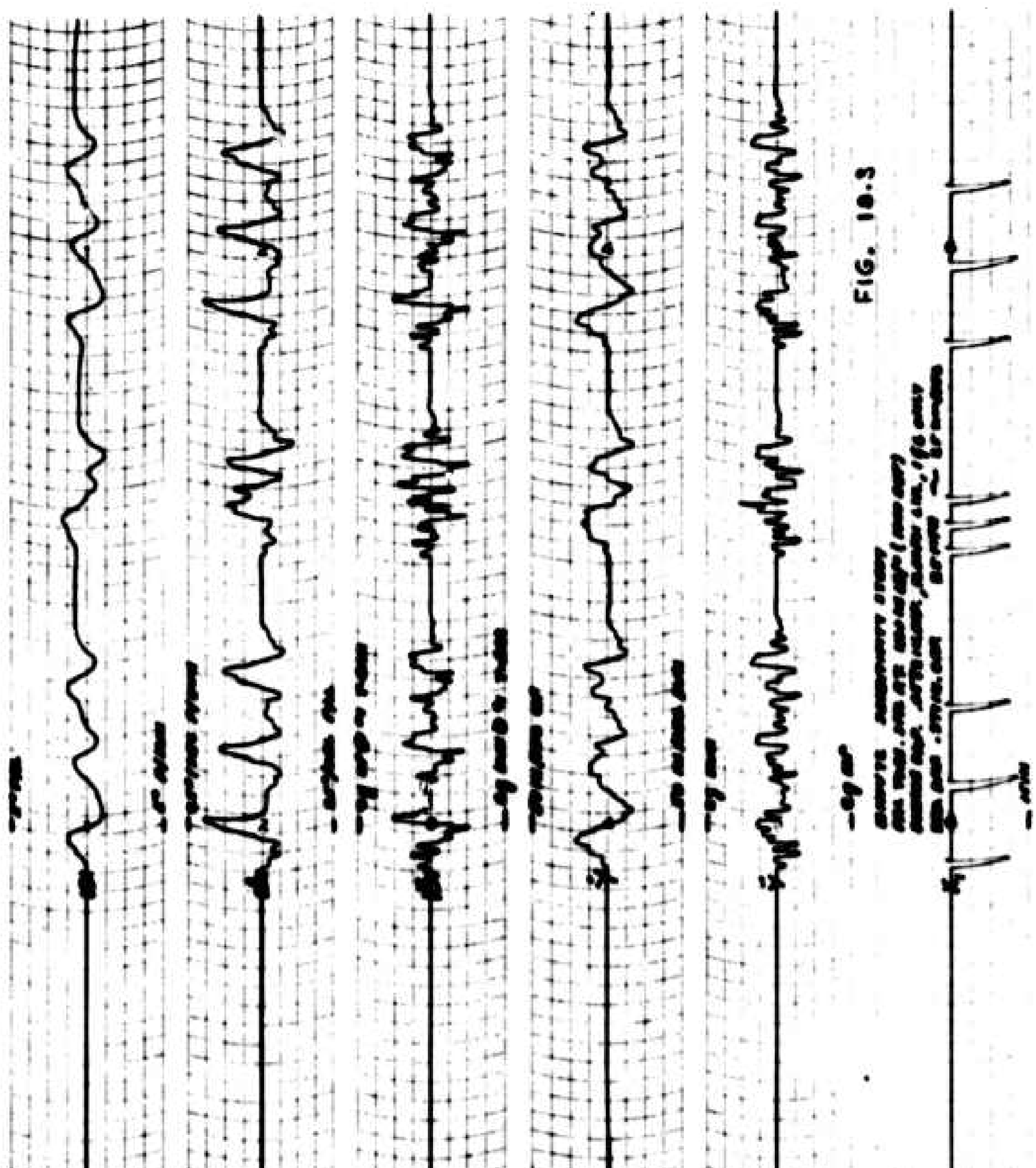

FIG. 10.3

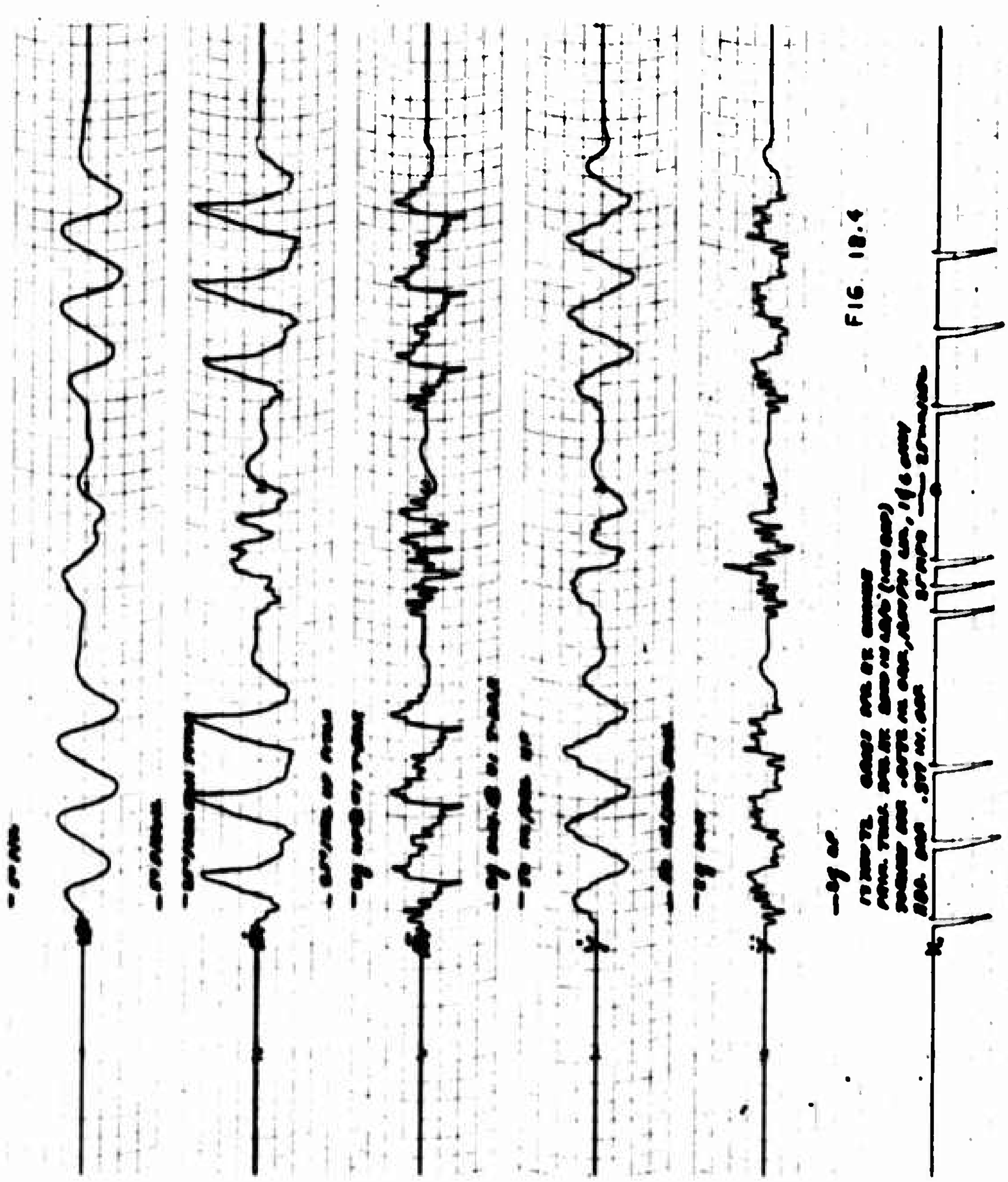

FIG. 18.4

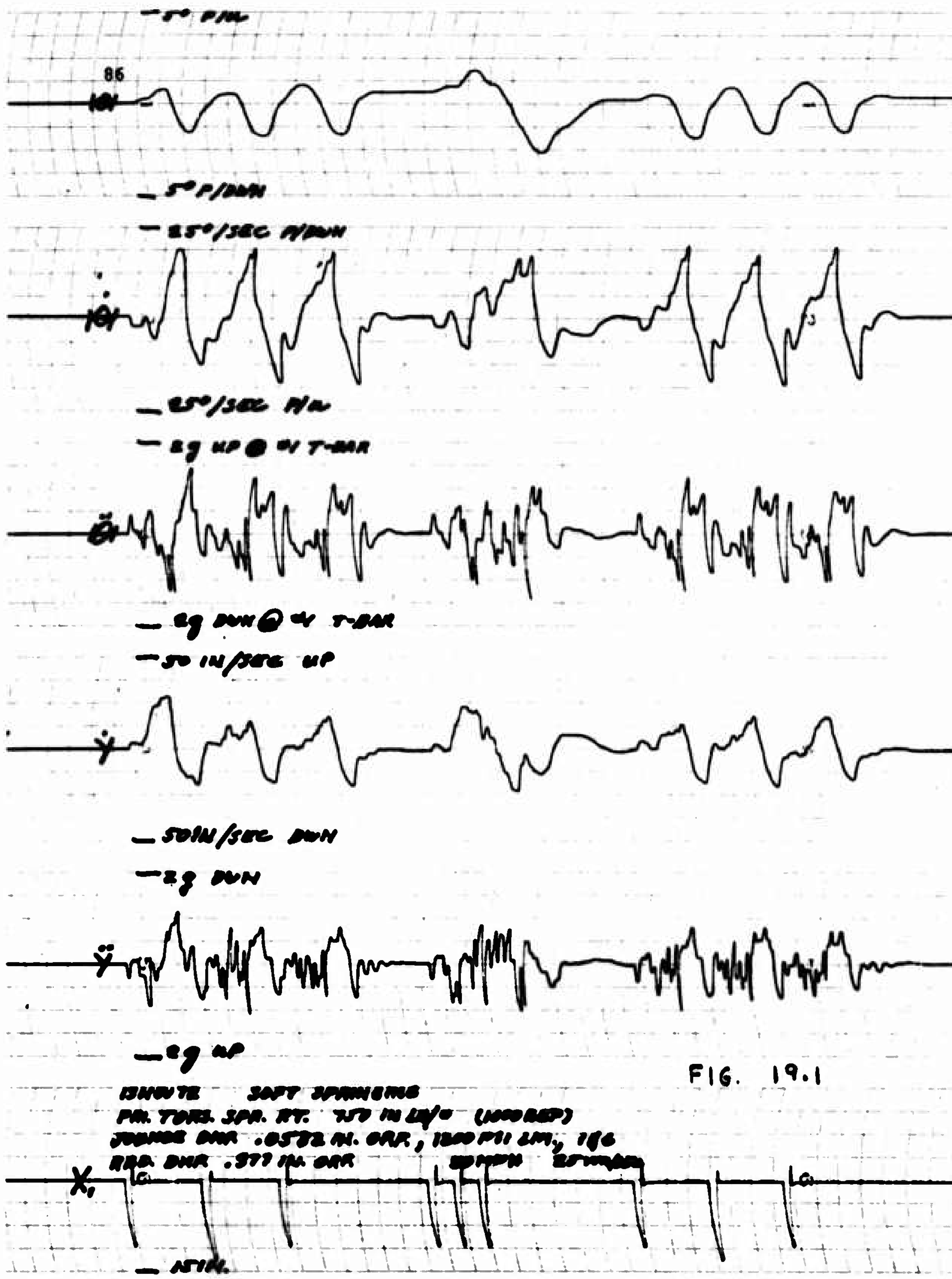

86
5° P/DWN
25°/SEC P/DWN
25°/SEC P/U
2g DWN @ 4 T-BAR
50 IN/SEC UP
50IN/SEC DWN
2g DWN
2g UP
SOFT SPRINGS

FIG. 19.1

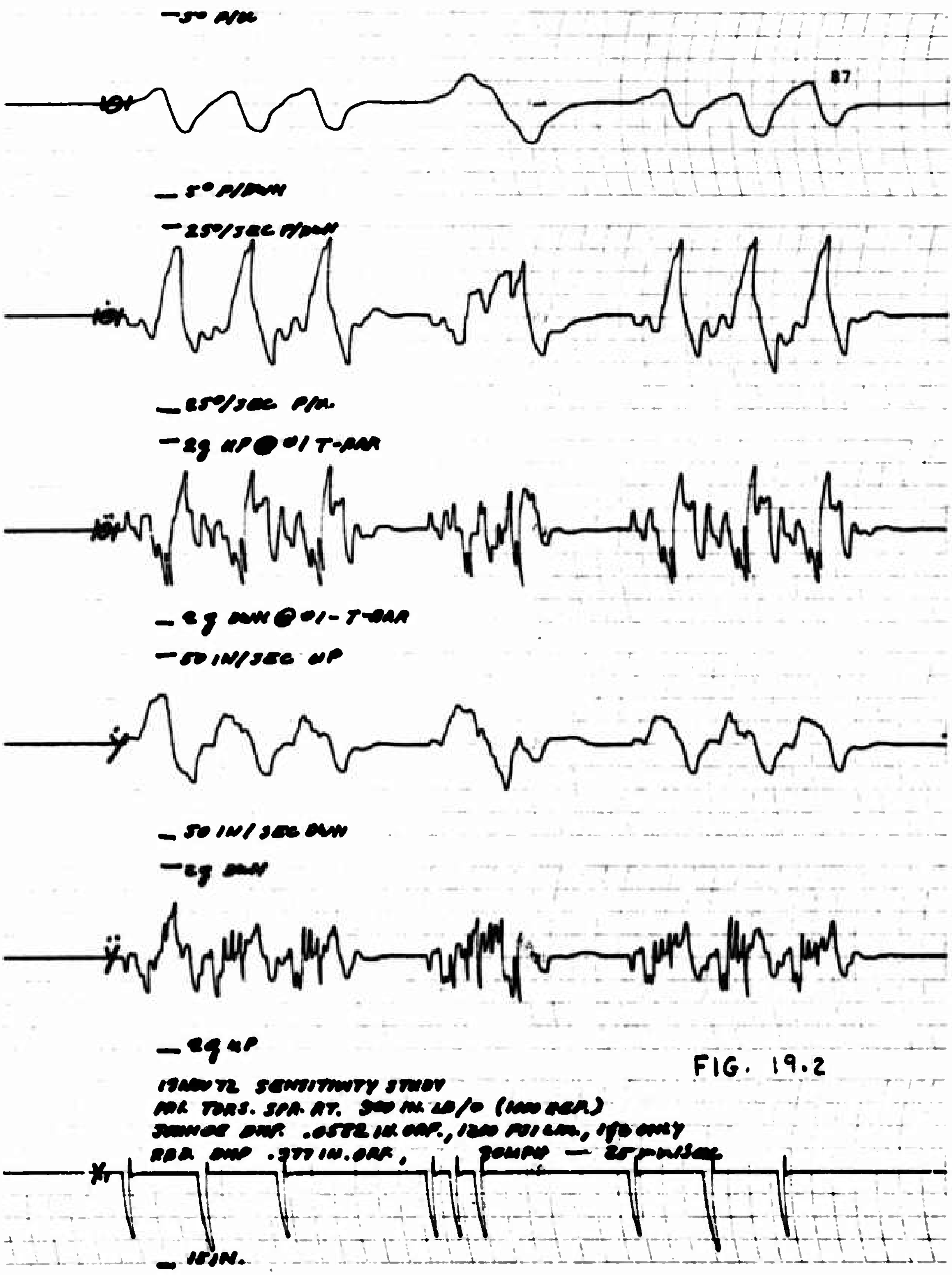
87
— 5° P/DWN
— 25°/SEC P/DWN
— 50 IN/SEC UP
— 50 IN/SEC DWN
— 2g DWN
— 2g UP
SENSITIVITY STUDY
— 15 IN.

FIG. 19.2

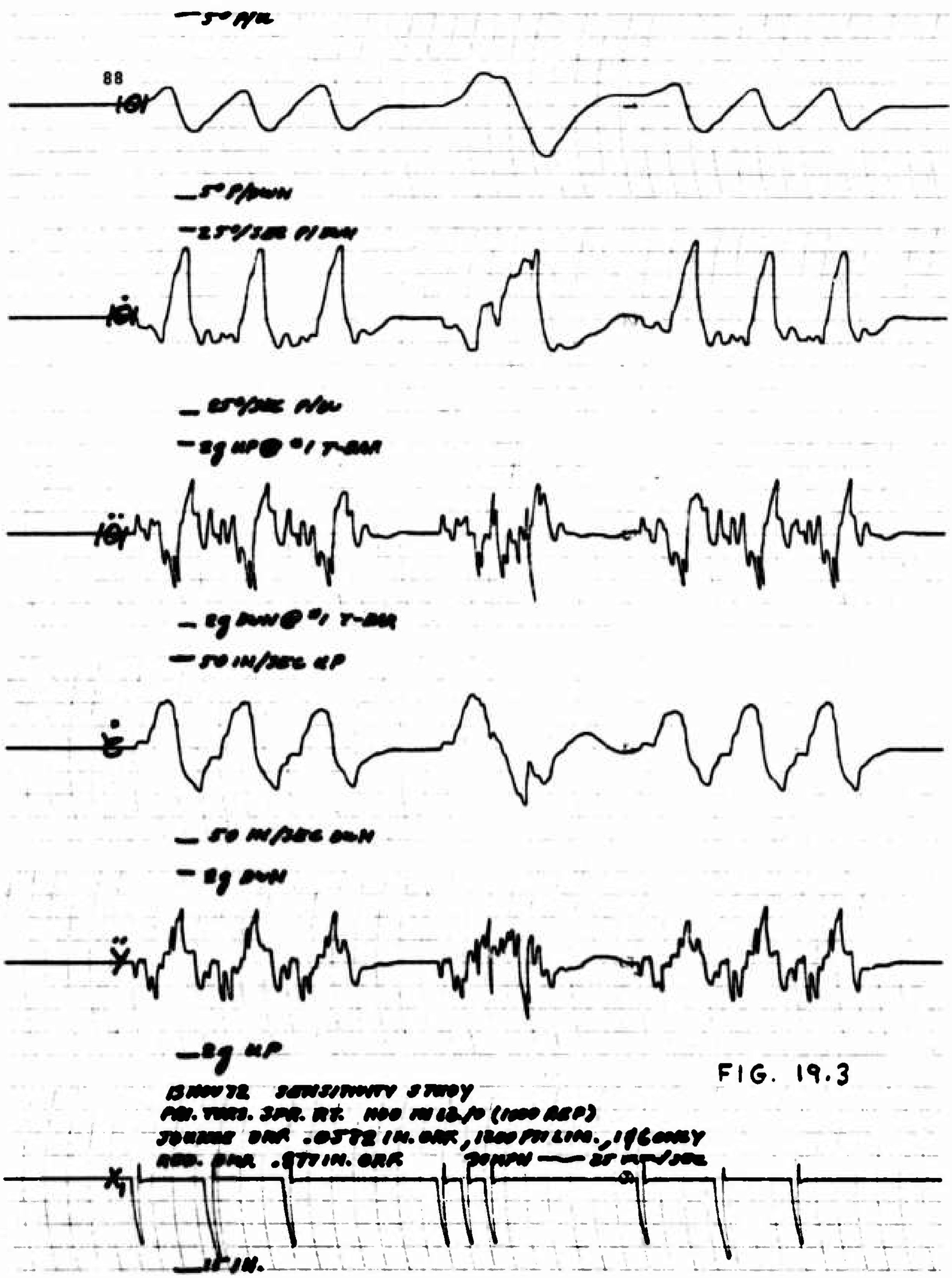

FIG. 19.3

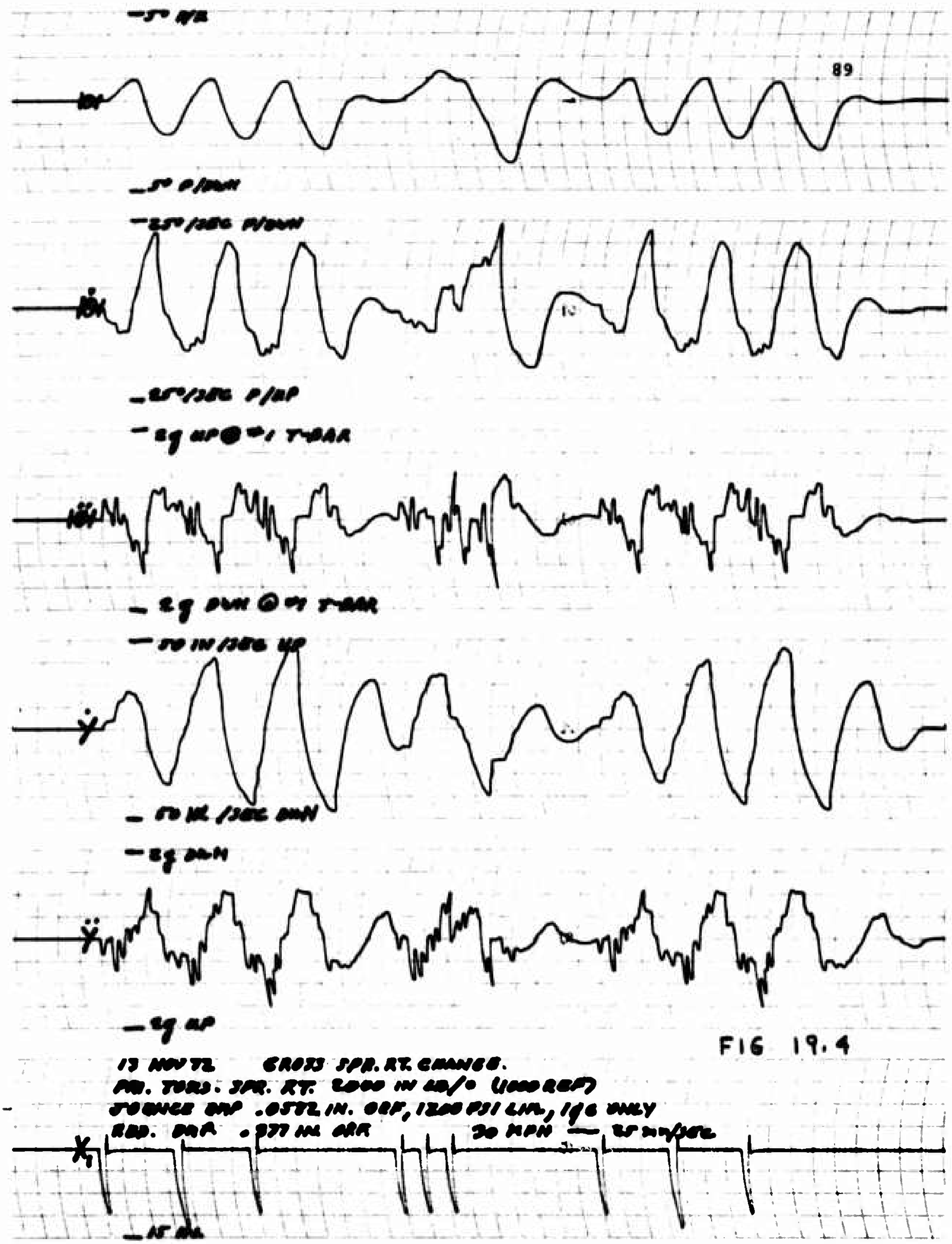
89
— 5° P/DWN
— 25°/SEC P/DWN
— 25°/SEC P/UP
— 2g UP @ #1 T-BAR
— 2g DWN @ #1 T-BAR
— 50 IN/SEC UP
— 50 IN./SEC DWN
— 2g DWN
— 2g UP
13 NOV 72 CROSS SPR. RT. CHANGE.
PRI. TORS. SPR. RT. 2000 IN LB/° (1000 REF)
BOUNCE DMP .0572 IN. ORF, 1200 PSI LIM., [illegible] ONLY
REB. DMP. .377 IN. ORF 30 MPH — 25 MM/SEC
— 15 IN.

FIG 19.4

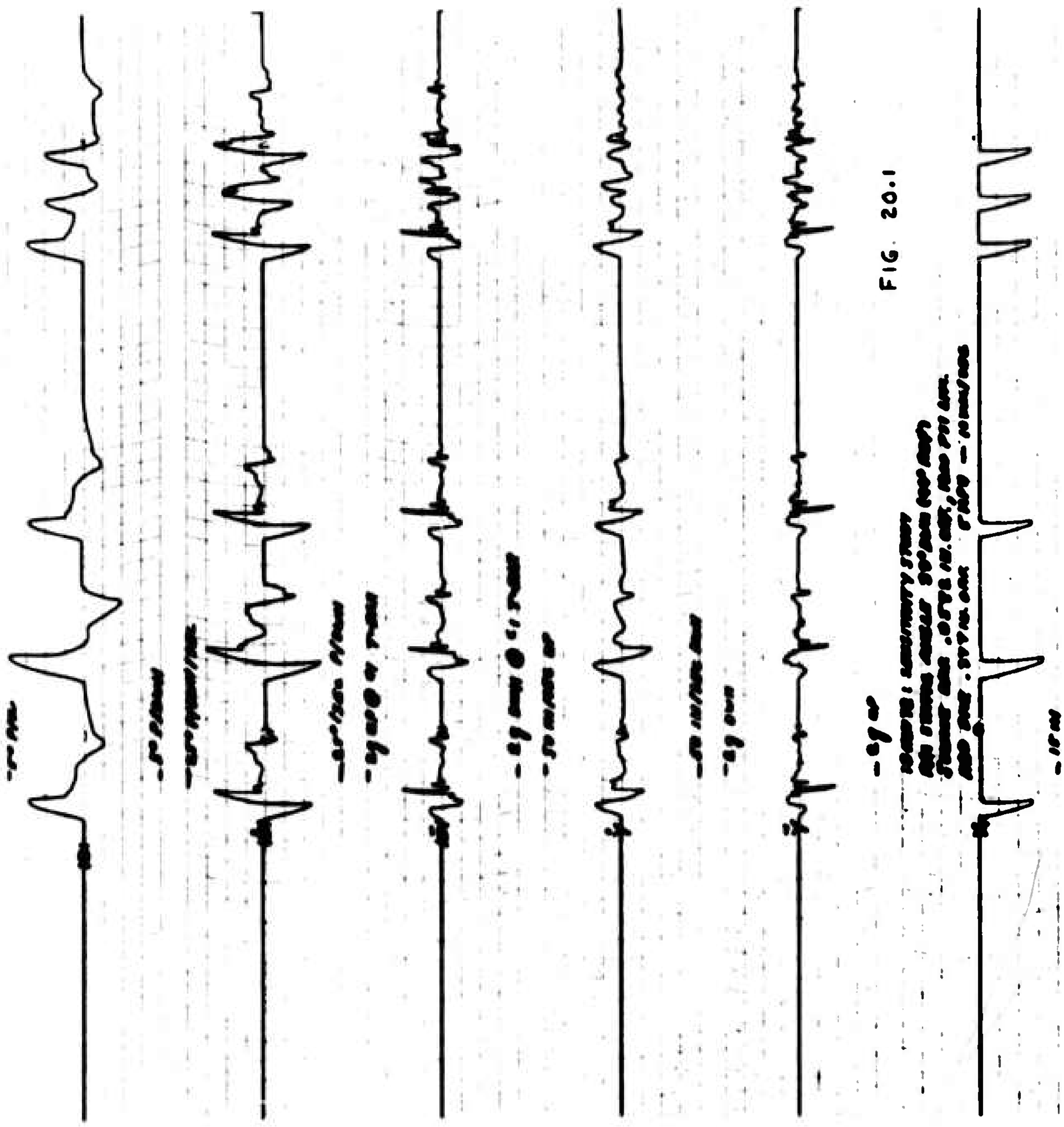

FIG. 20.1

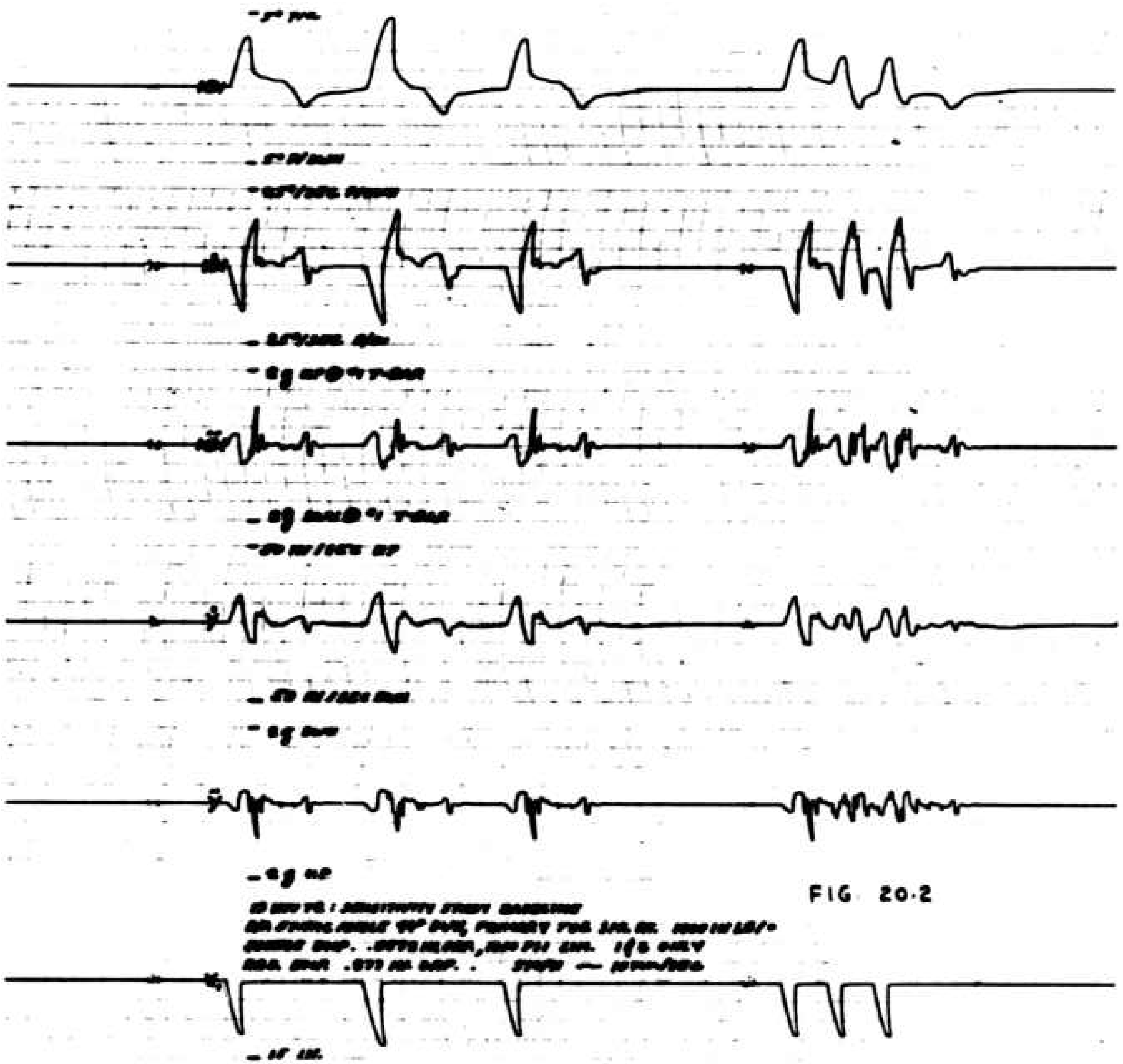

FIG. 20.2

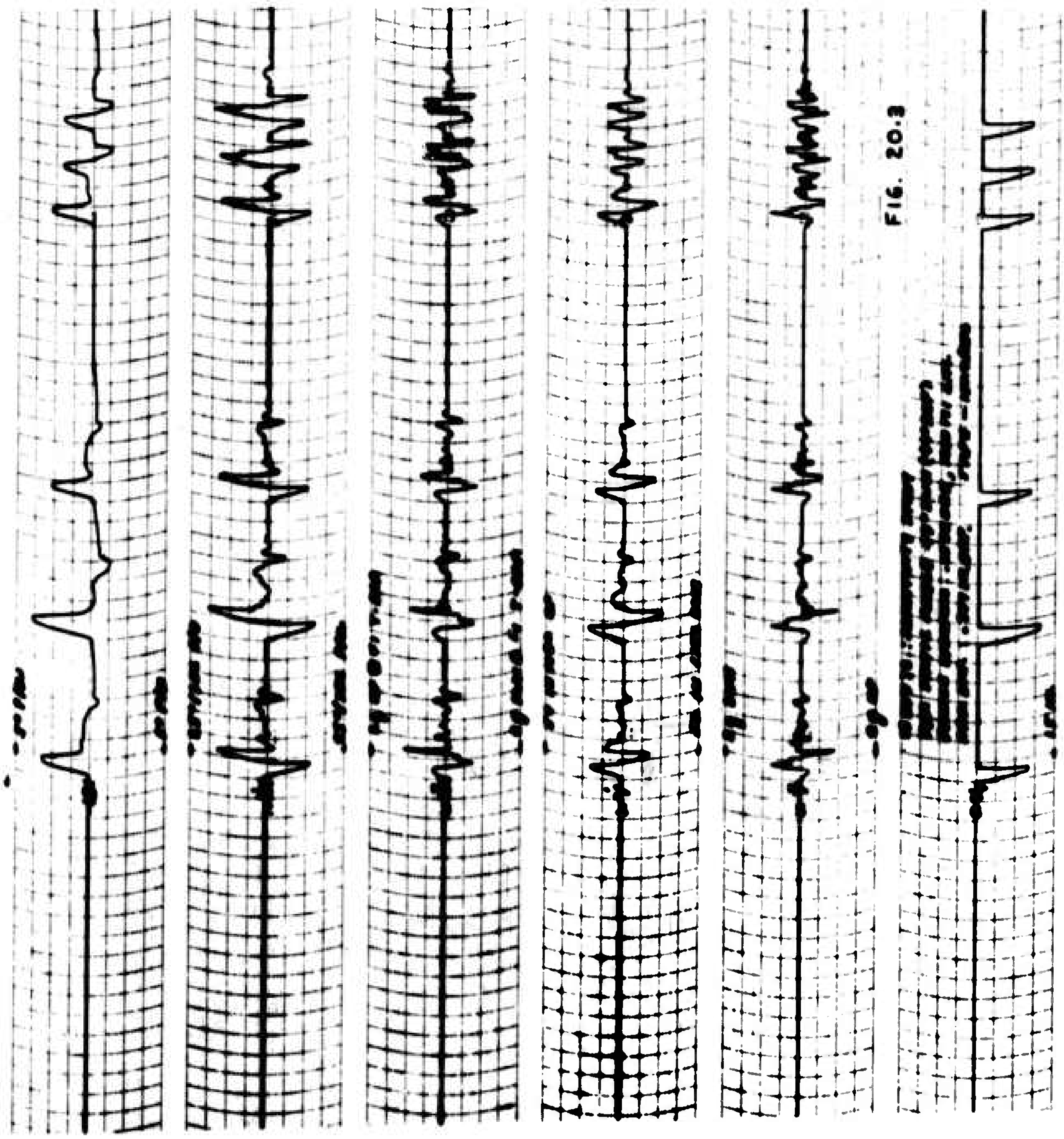

FIG. 20.3

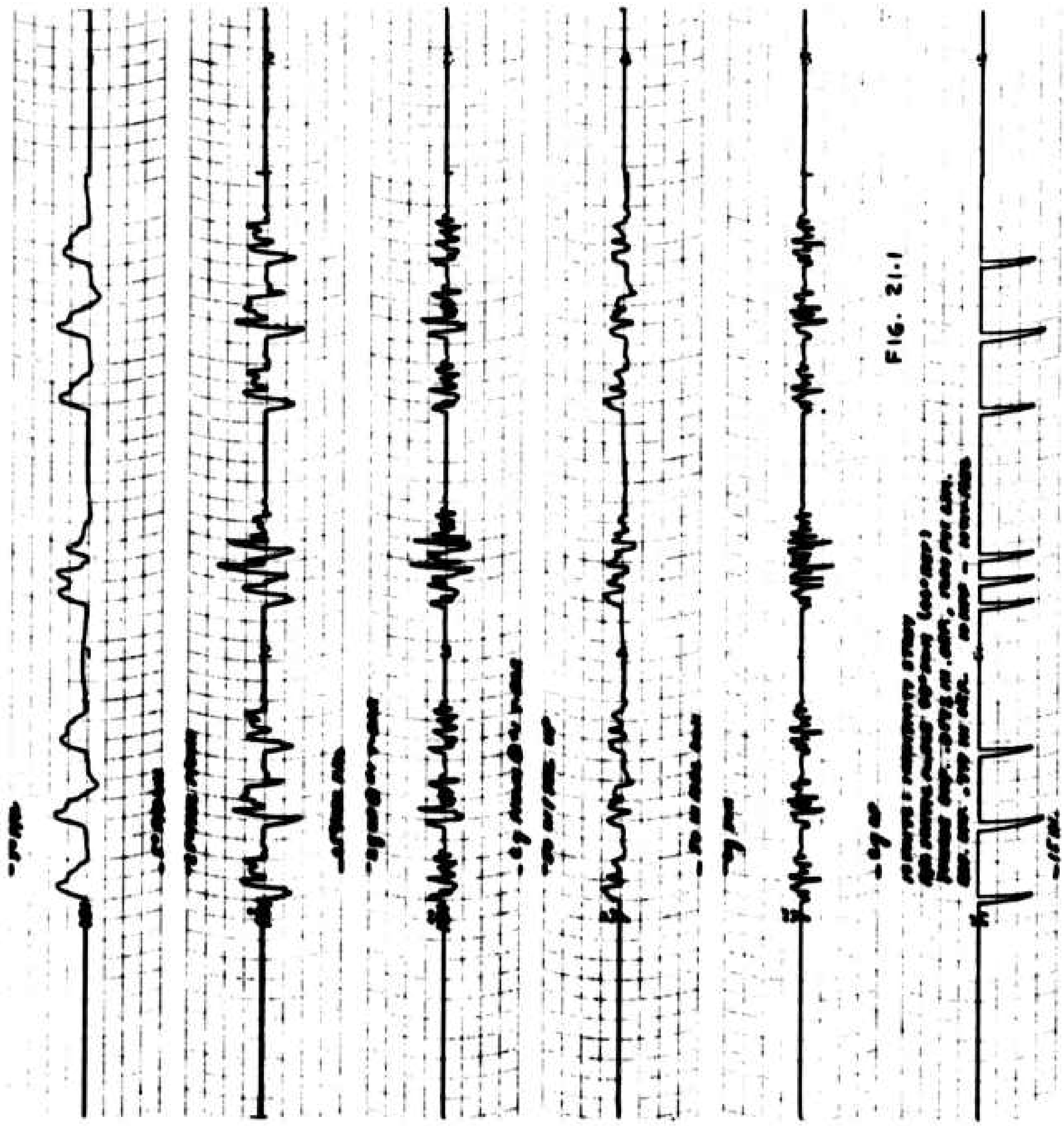

FIG. 21.1

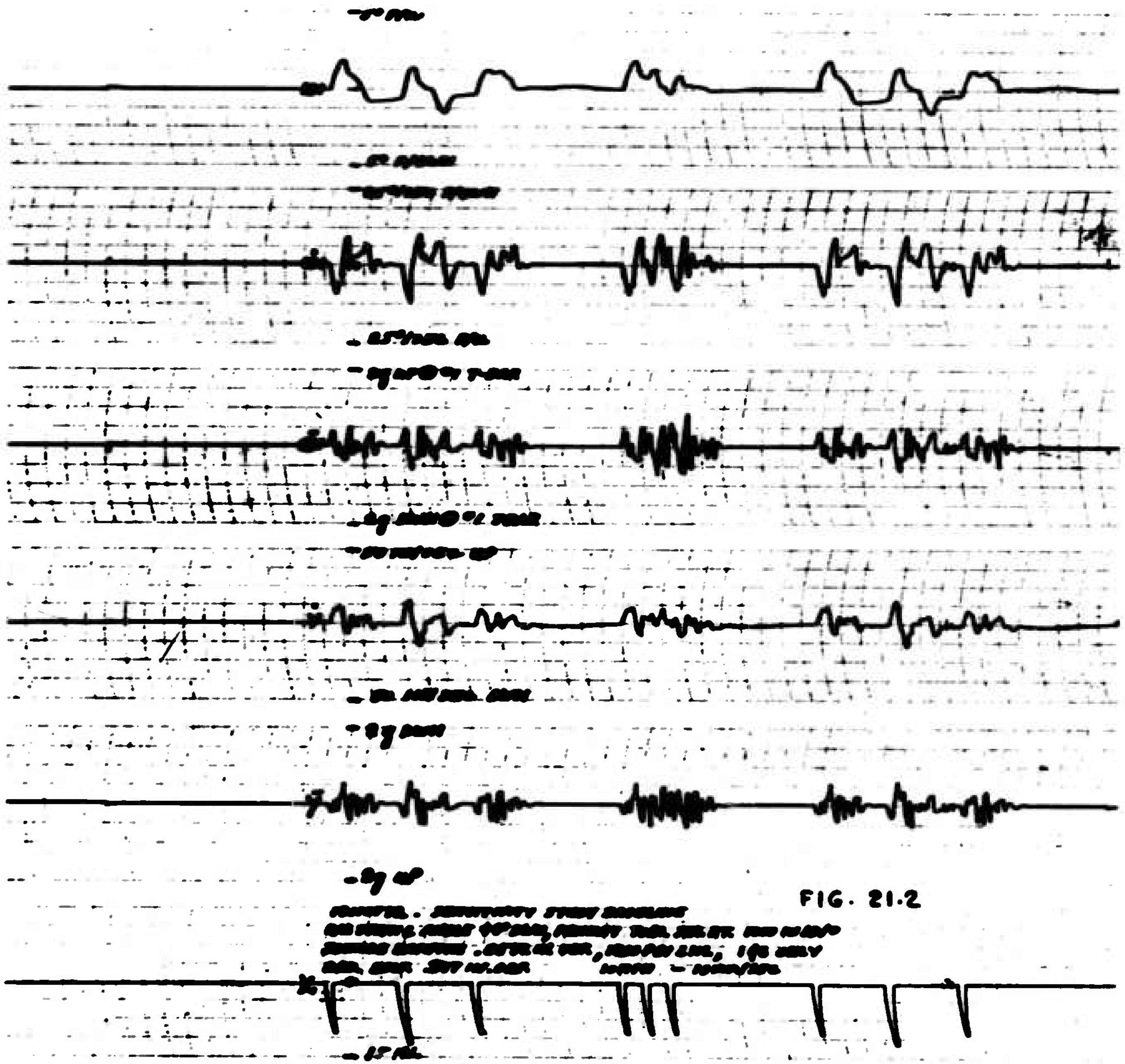

FIG. 21.2

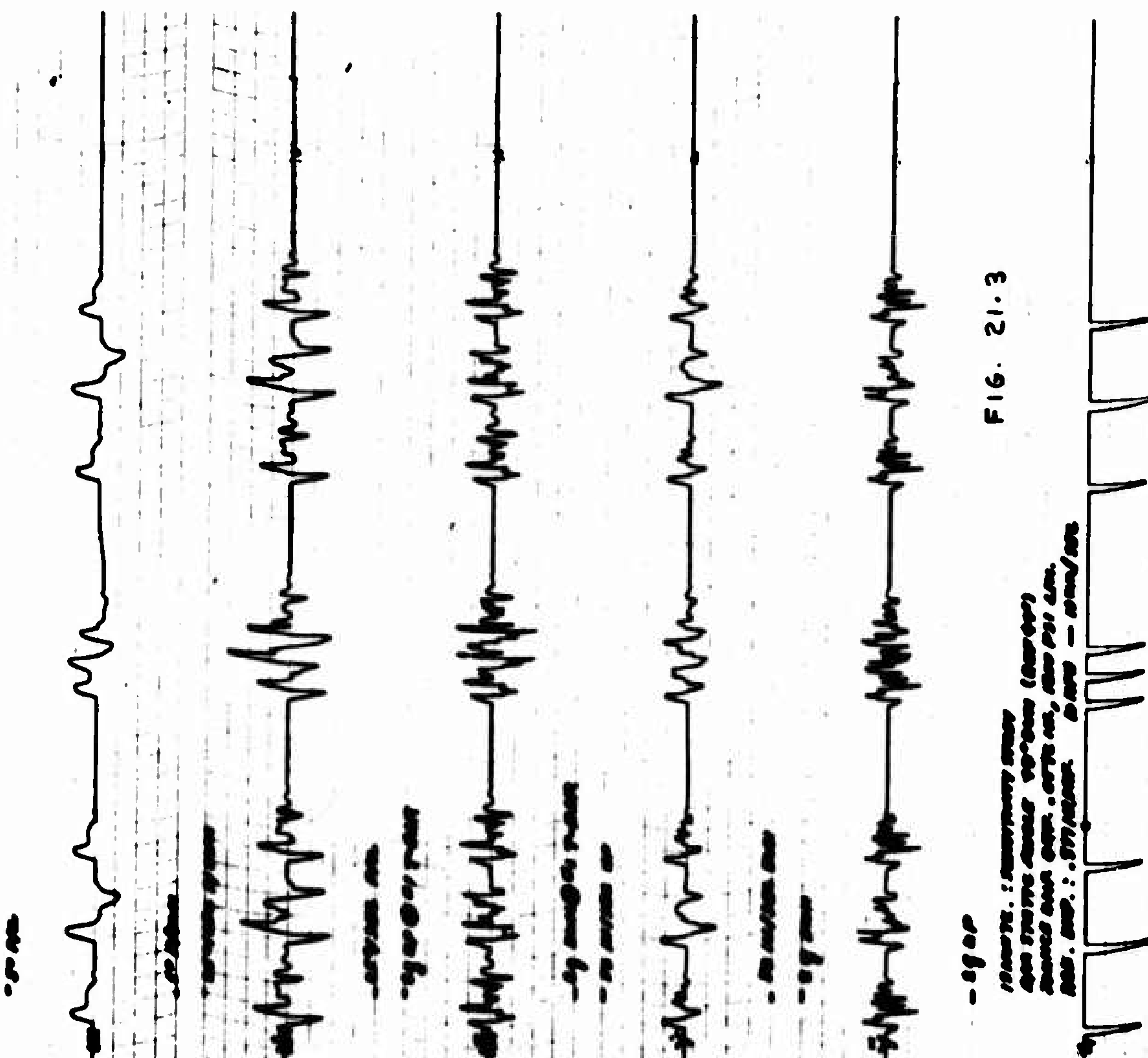

FIG. 21.3

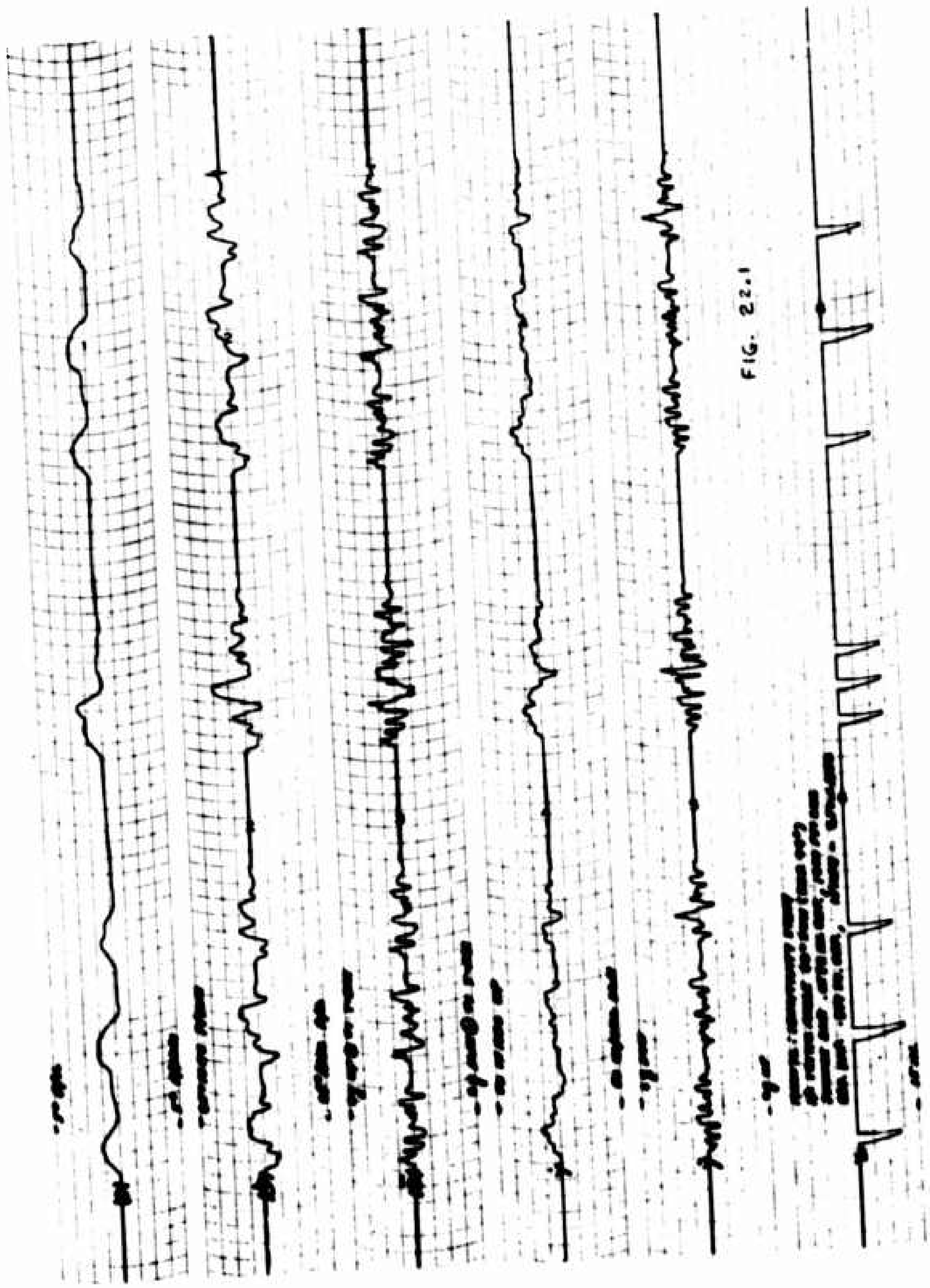

FIG. 22.1

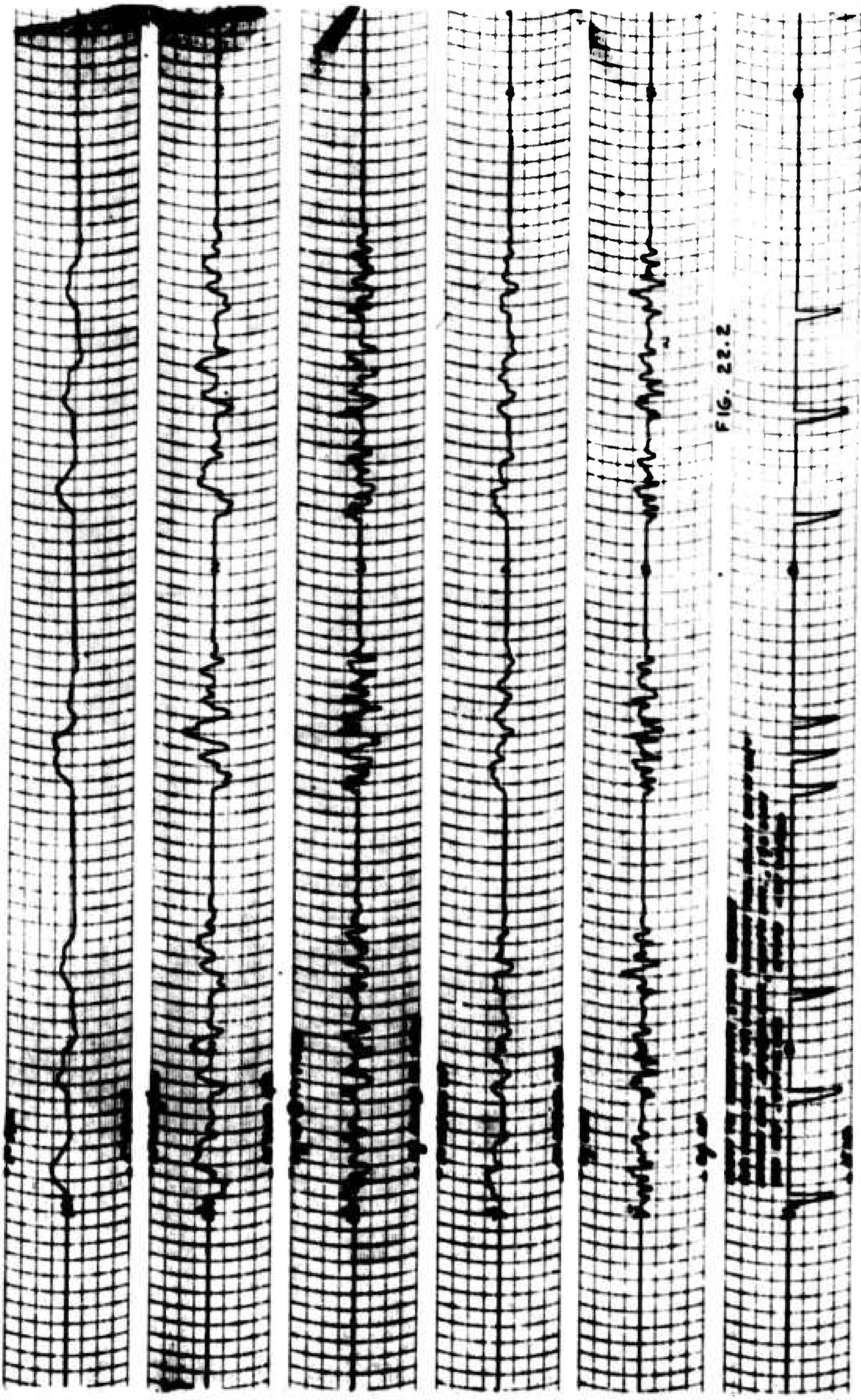

FIG. 22.2

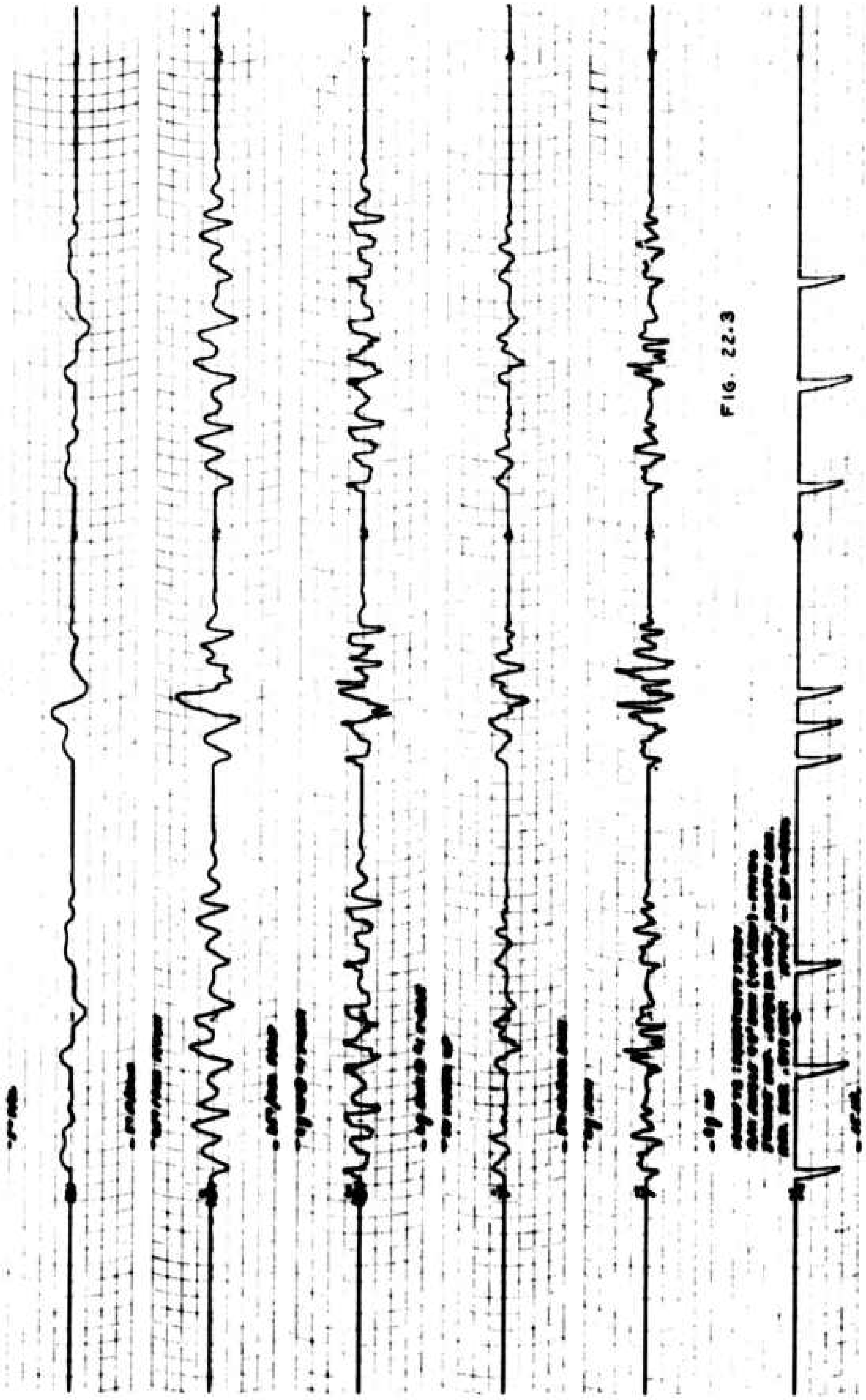

FIG. 22.3

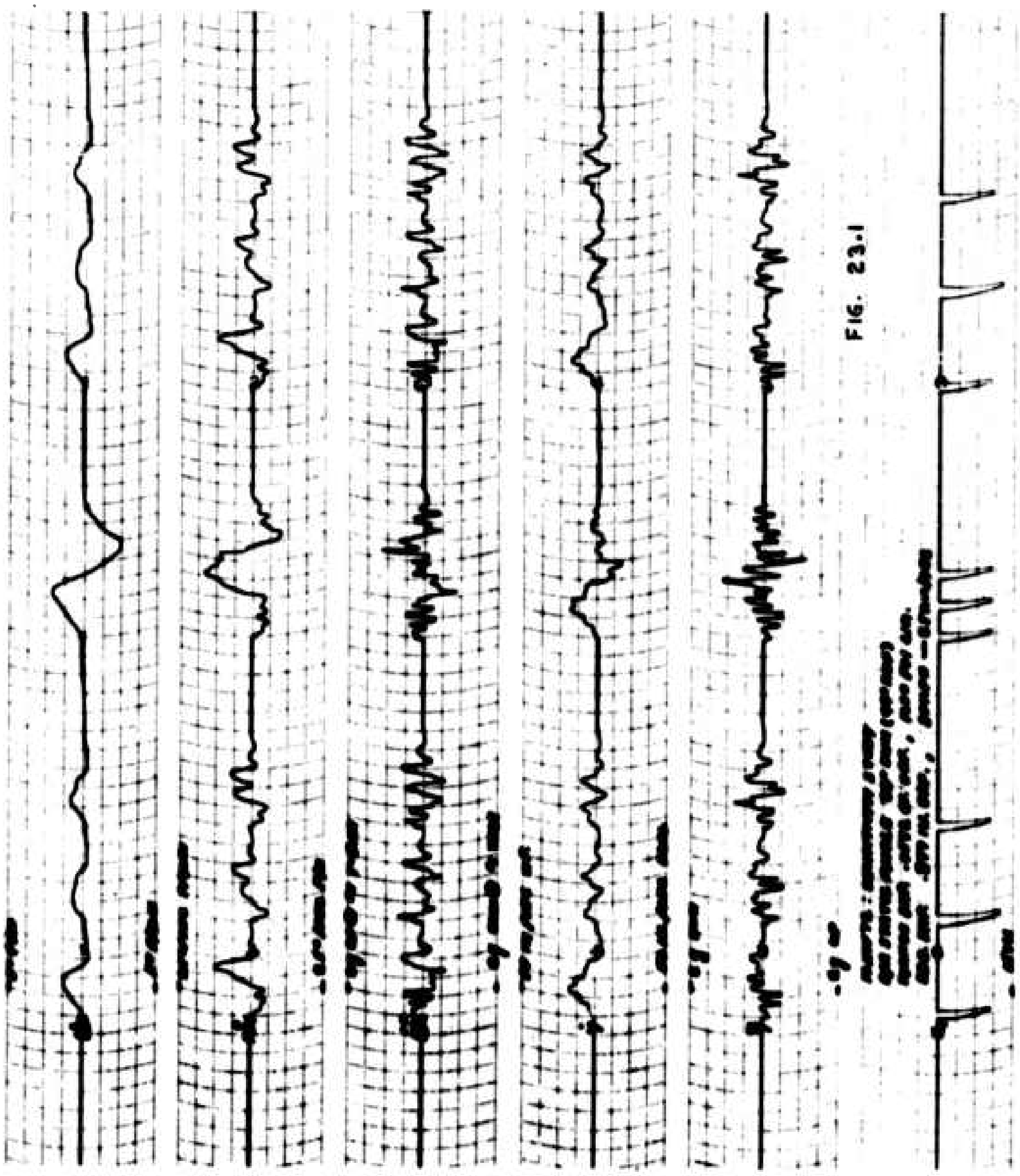

FIG. 23.1

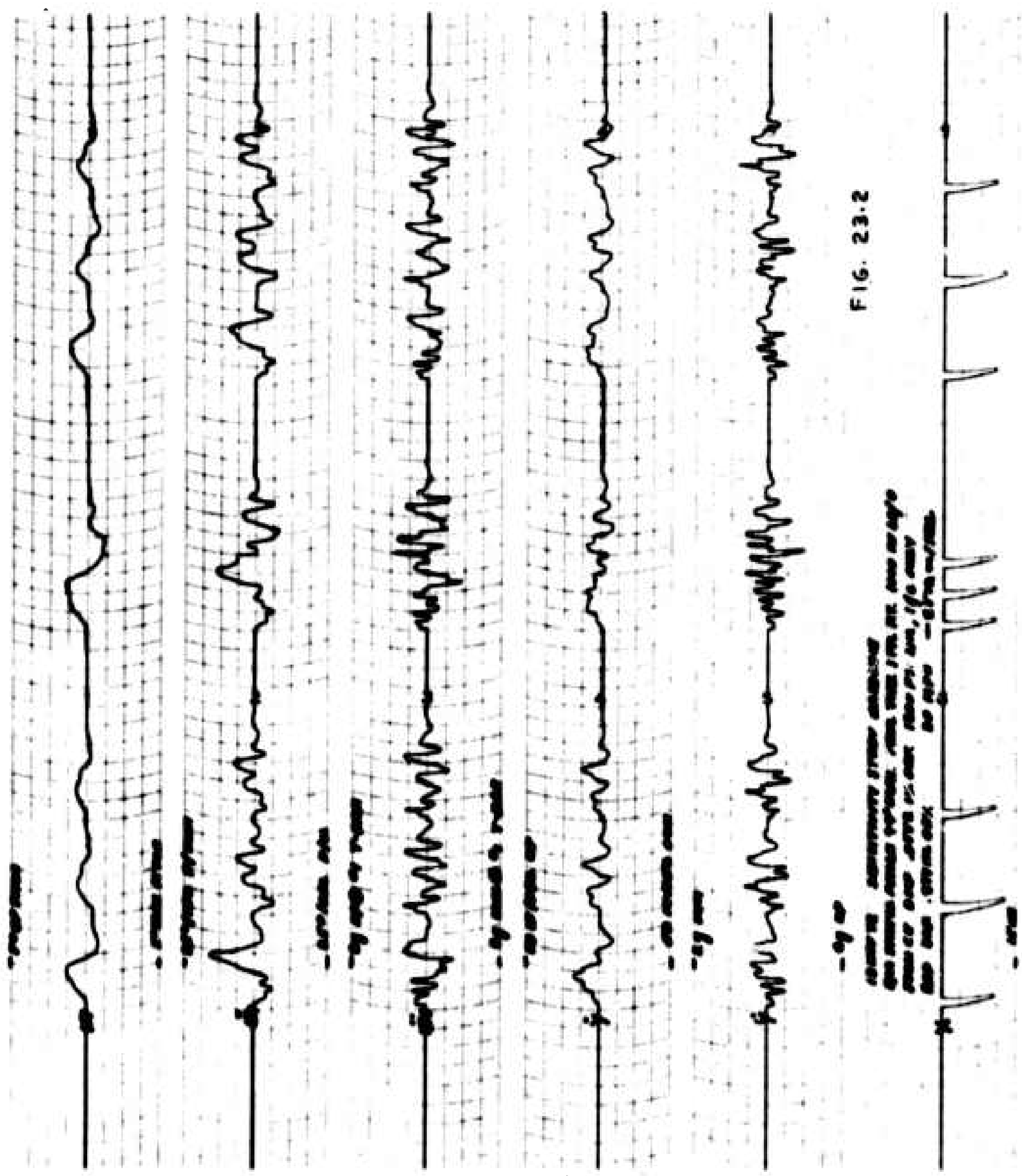

FIG. 23.2

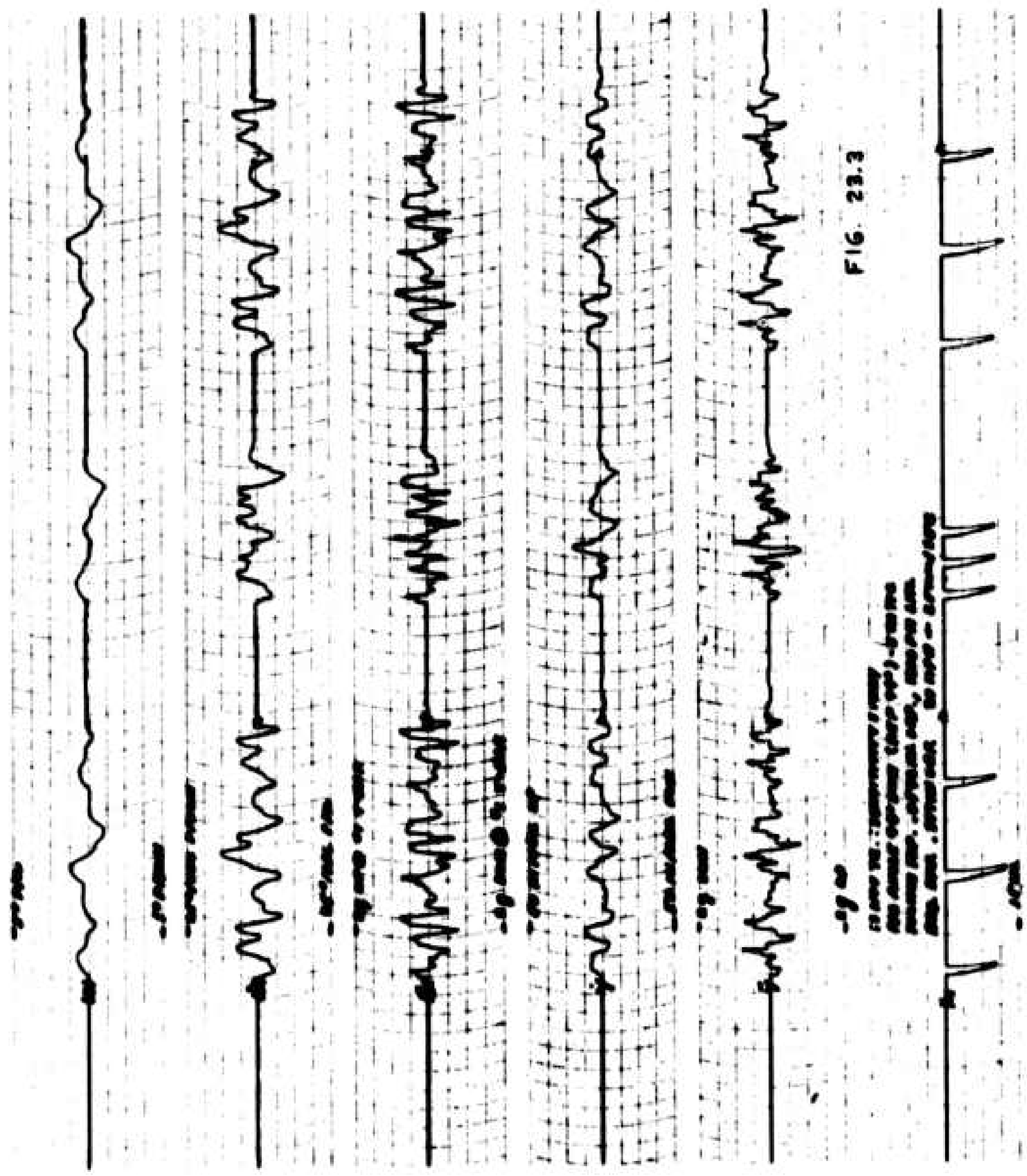

FIG. 23.3

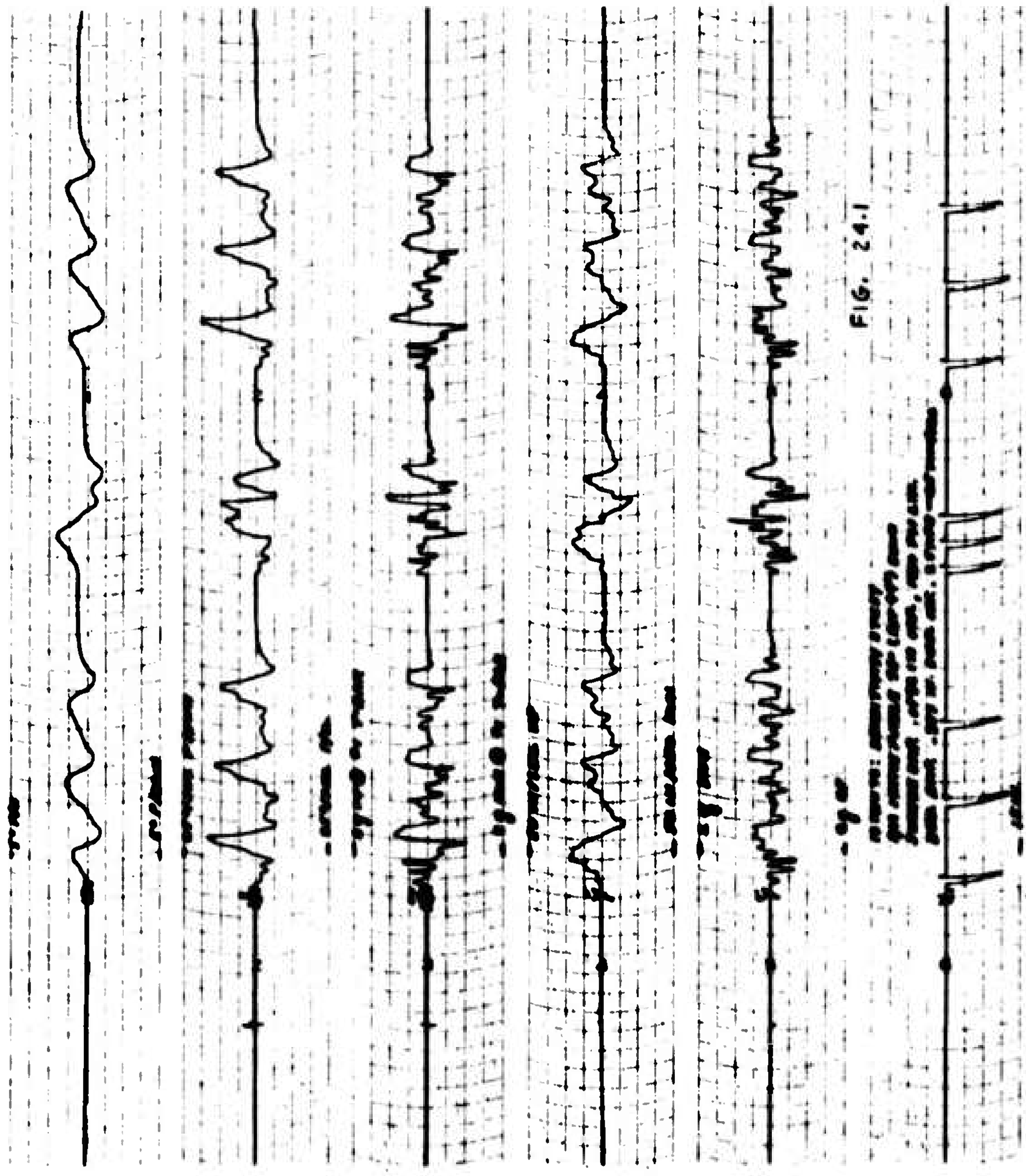

FIG. 24.1

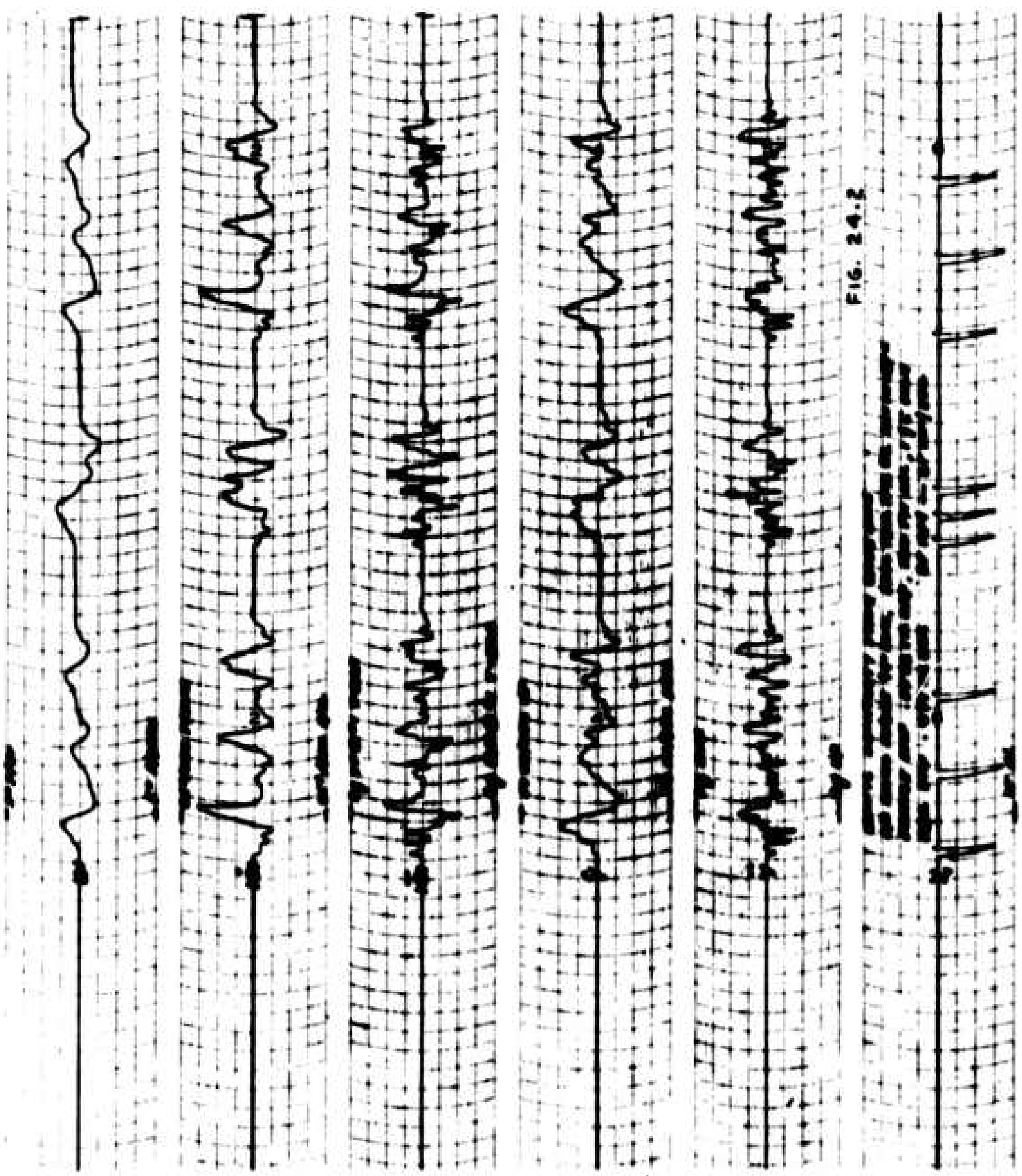

FIG. 24.2

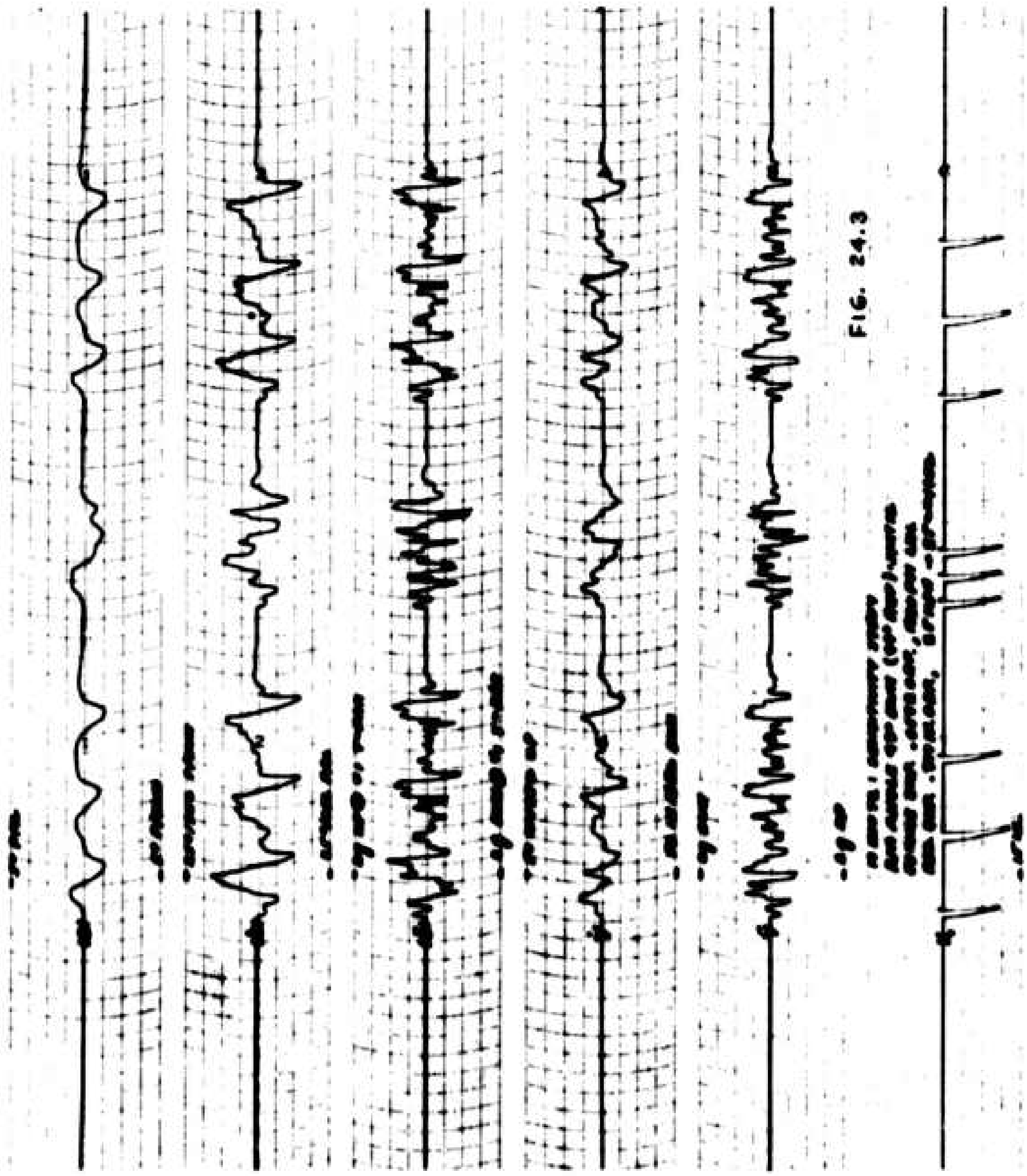

FIG. 24.3

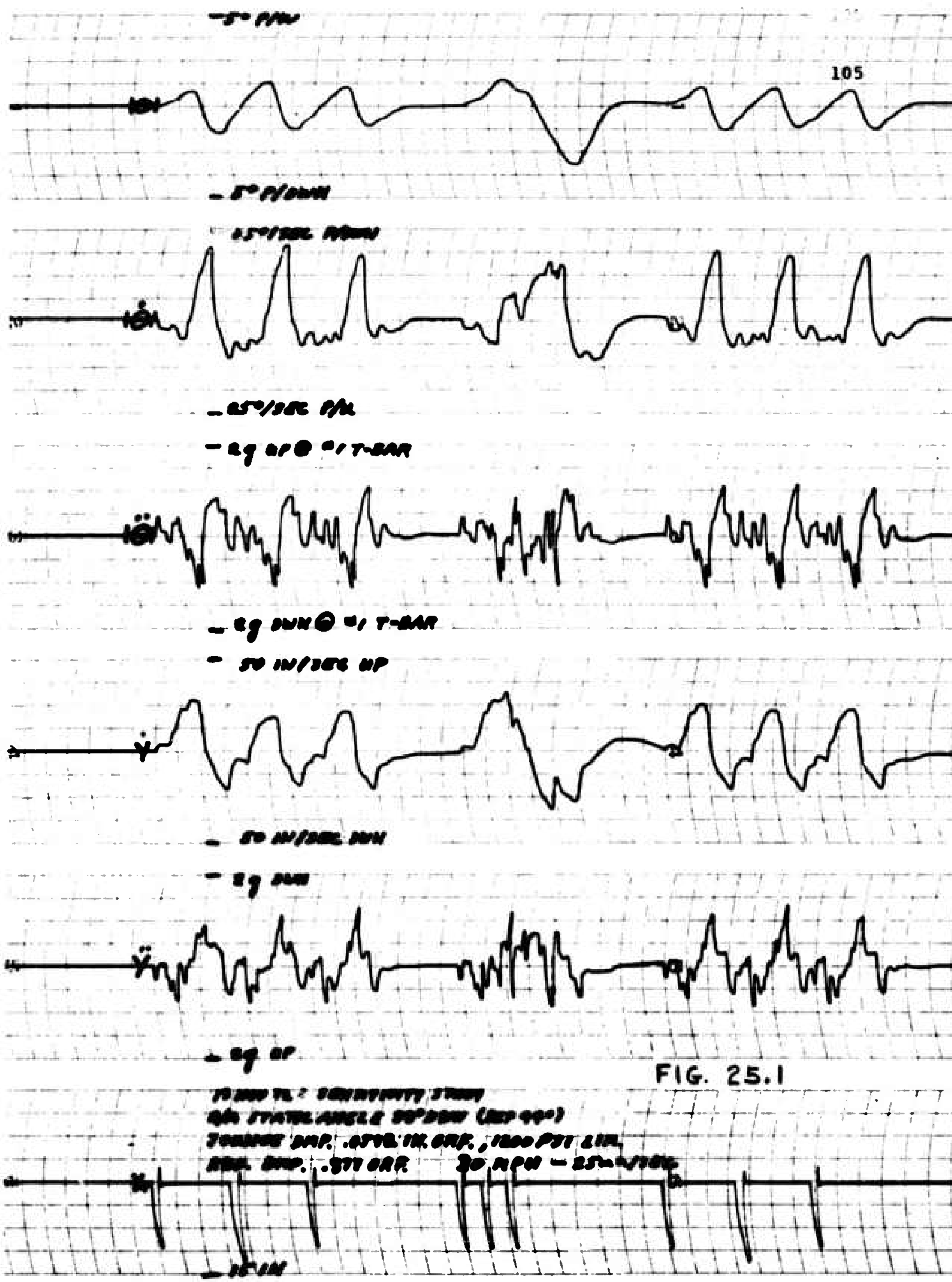

FIG. 25.1

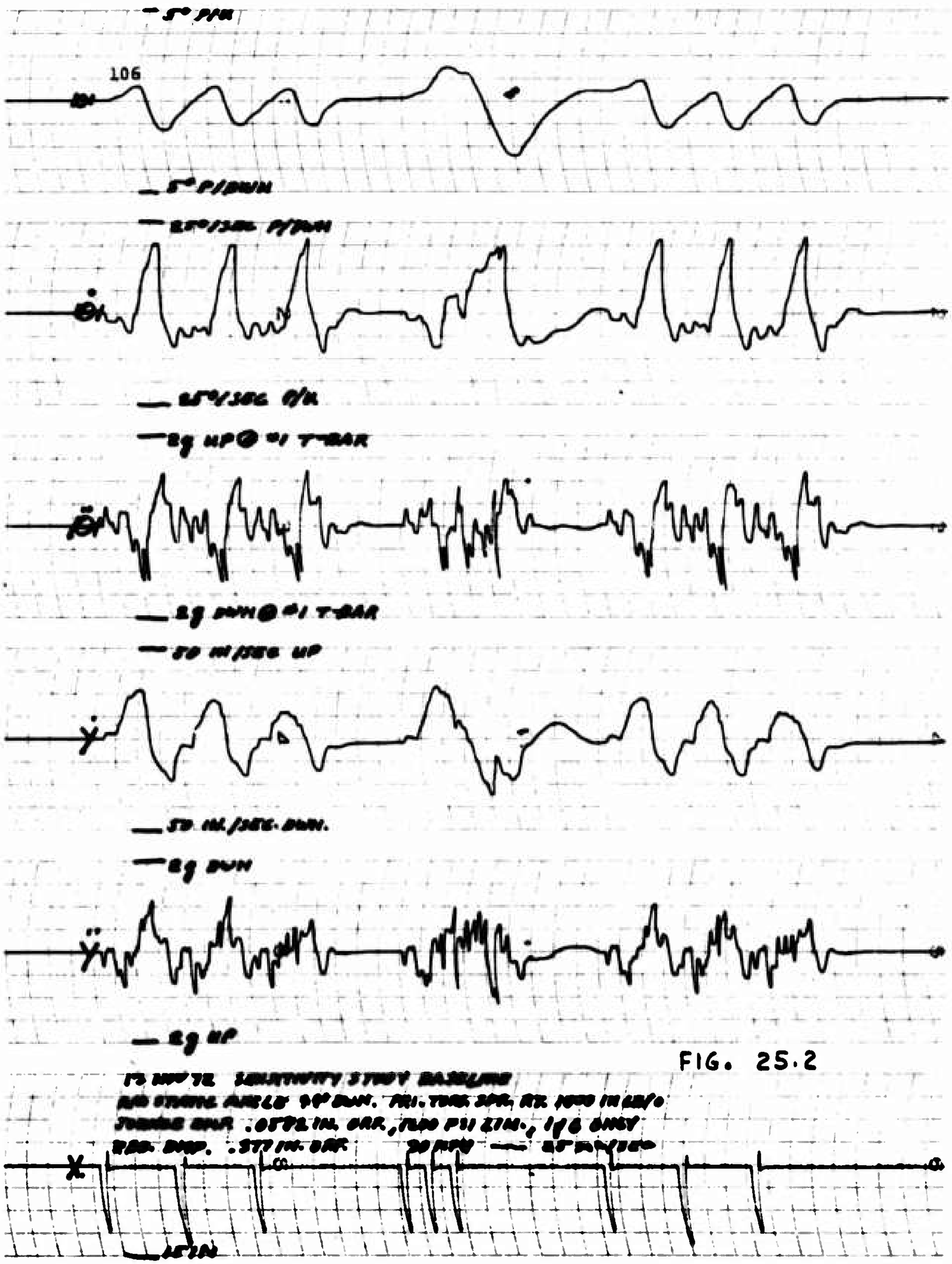
106
5° P/DWN
2g UP@ #1 T-BAR
2g DWN@ #1 T-BAR
50 IN/SEC UP
50 IN./SEC. DWN.
2g DWN
2g UP

FIG. 25.2

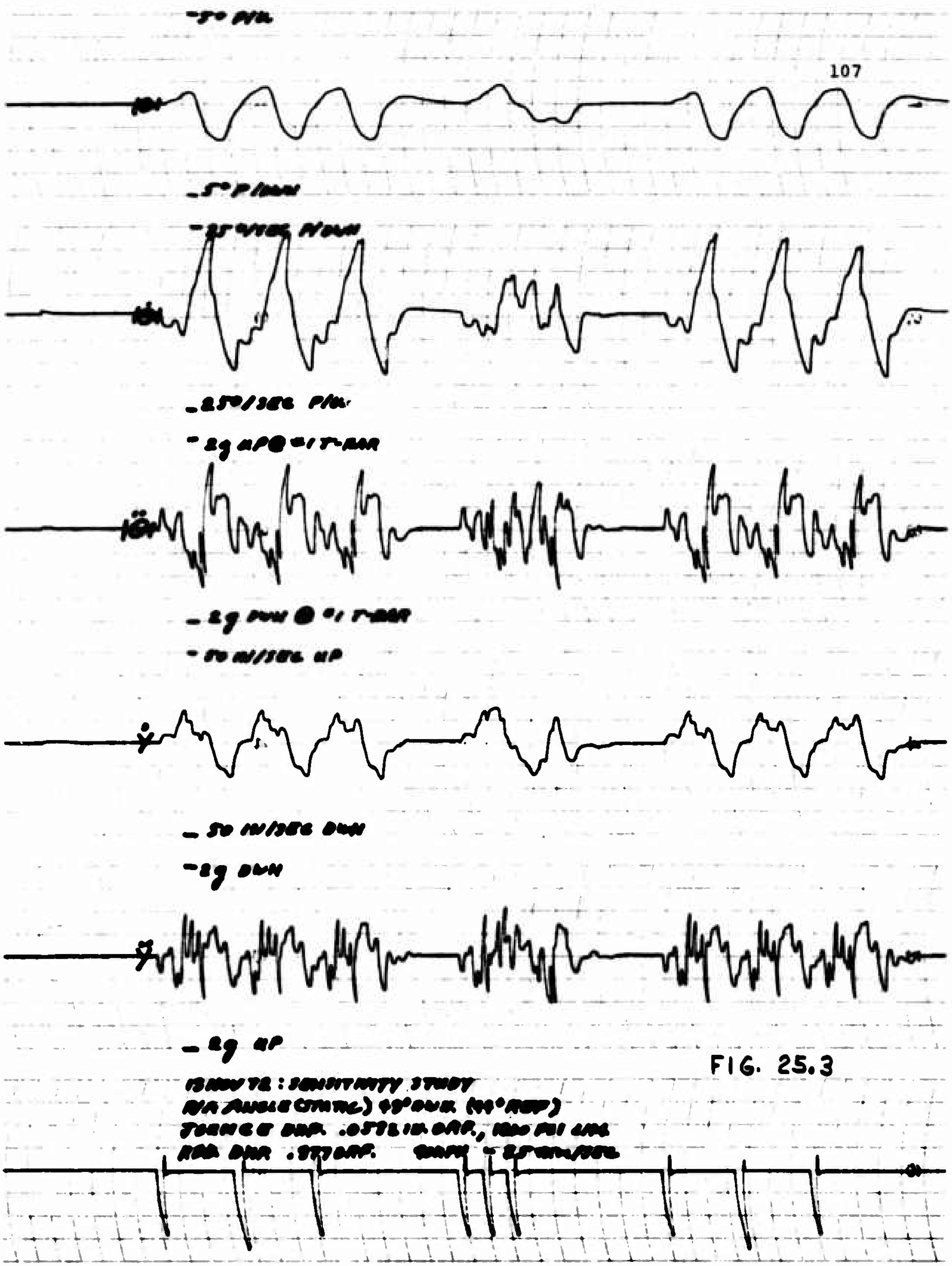

FIG. 25.3

OBSTACLE & COURSE DETAILS

SINE WAVE

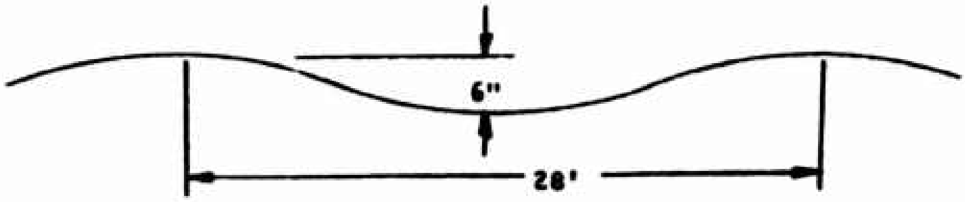

OBSTACLES

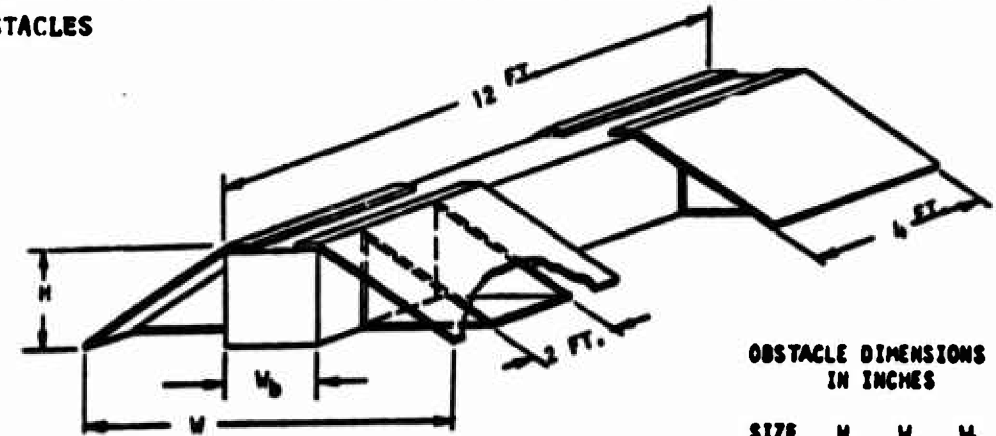

OBSTACLE DIMENSIONS IN INCHES

SIZE	H	W	W_b
6	6	24	6
8	8	32	8
10	10	40	8
12	12	48	10

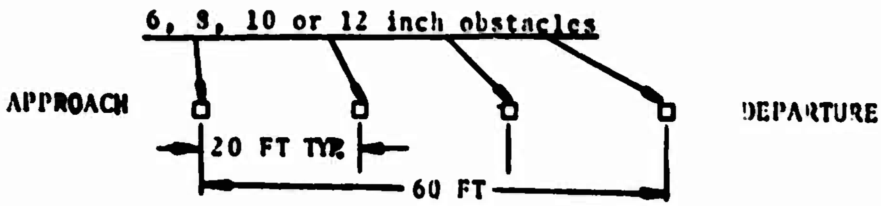

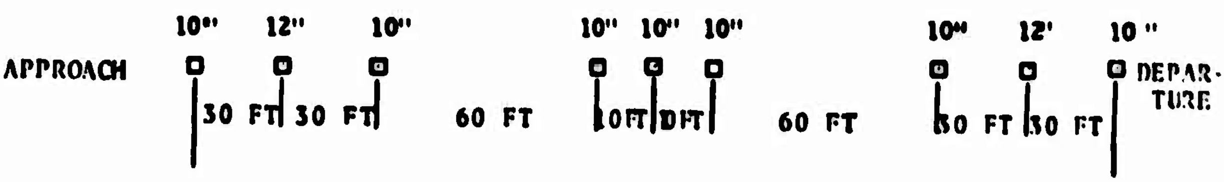

FIGURE 26

STANDARD HYDROPNEUMATIC SUSPENSION SYSTEM

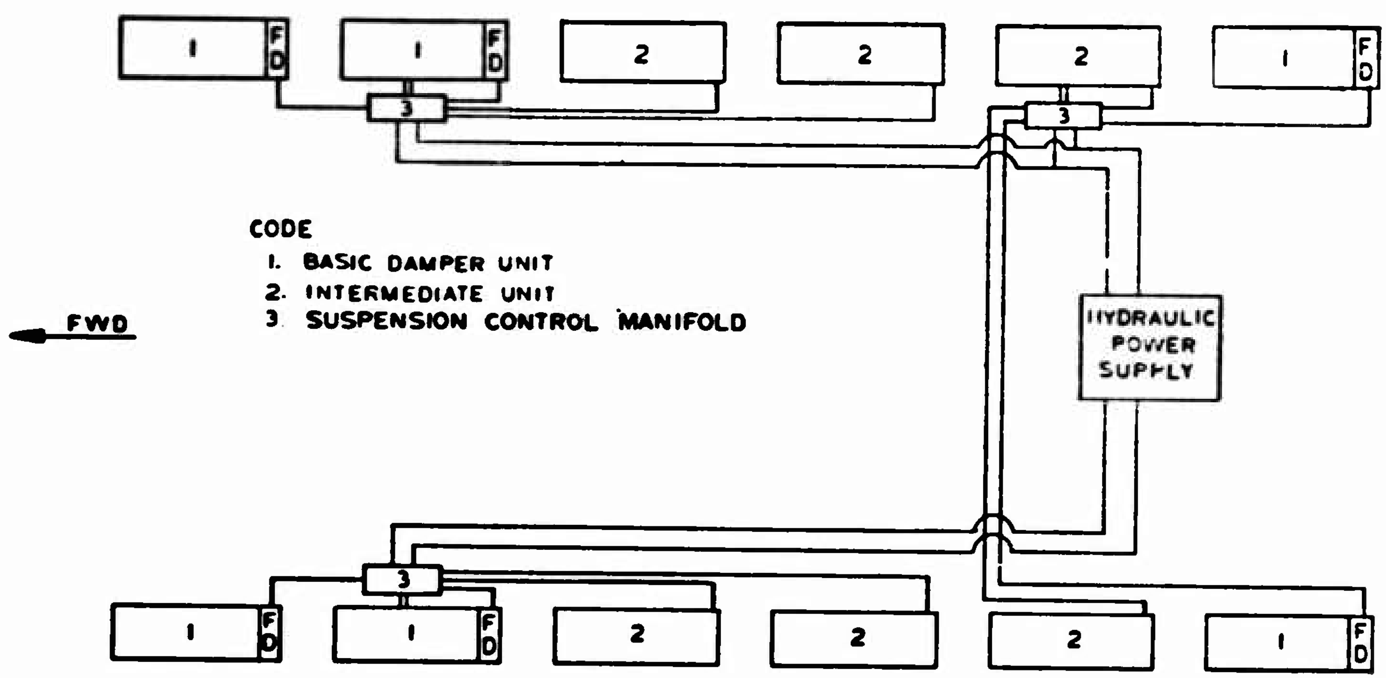

FIGURE 87.0

ADAPTIVE CONTROL SYSTEM

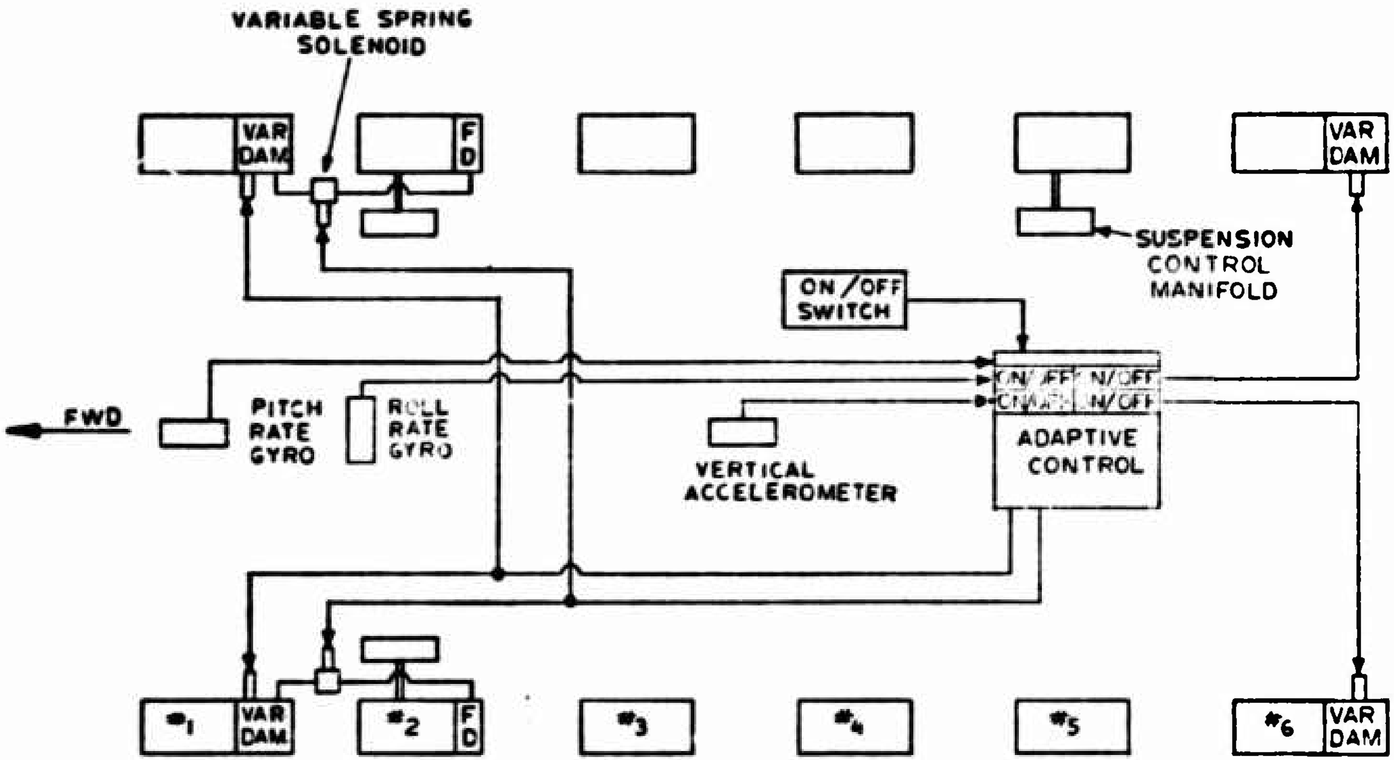

FIGURE 28.0

ADAPTIVE CONTROL SYSTEM - AUSTERE

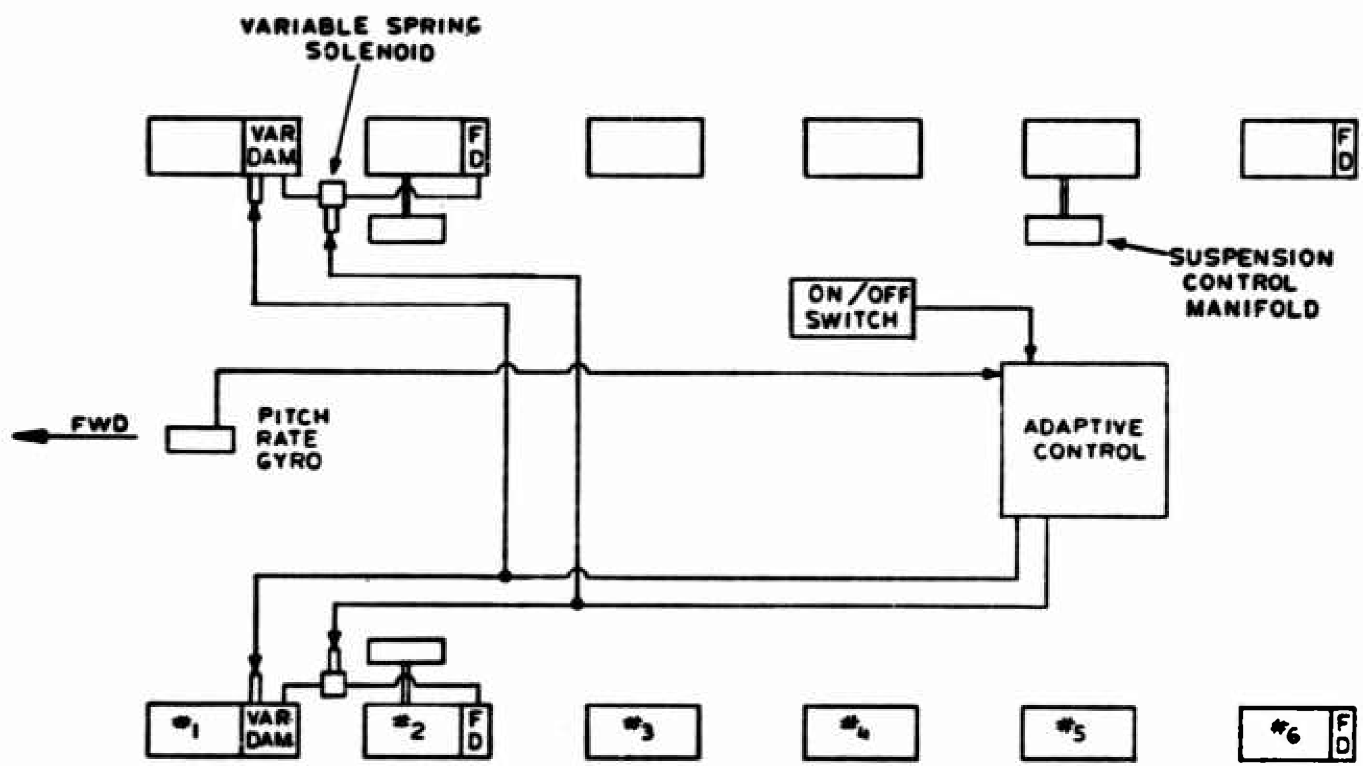

FIGURE 29.0

FIG. 30.0.

DAMPER VALVE-SOLENOID CONTROLLED

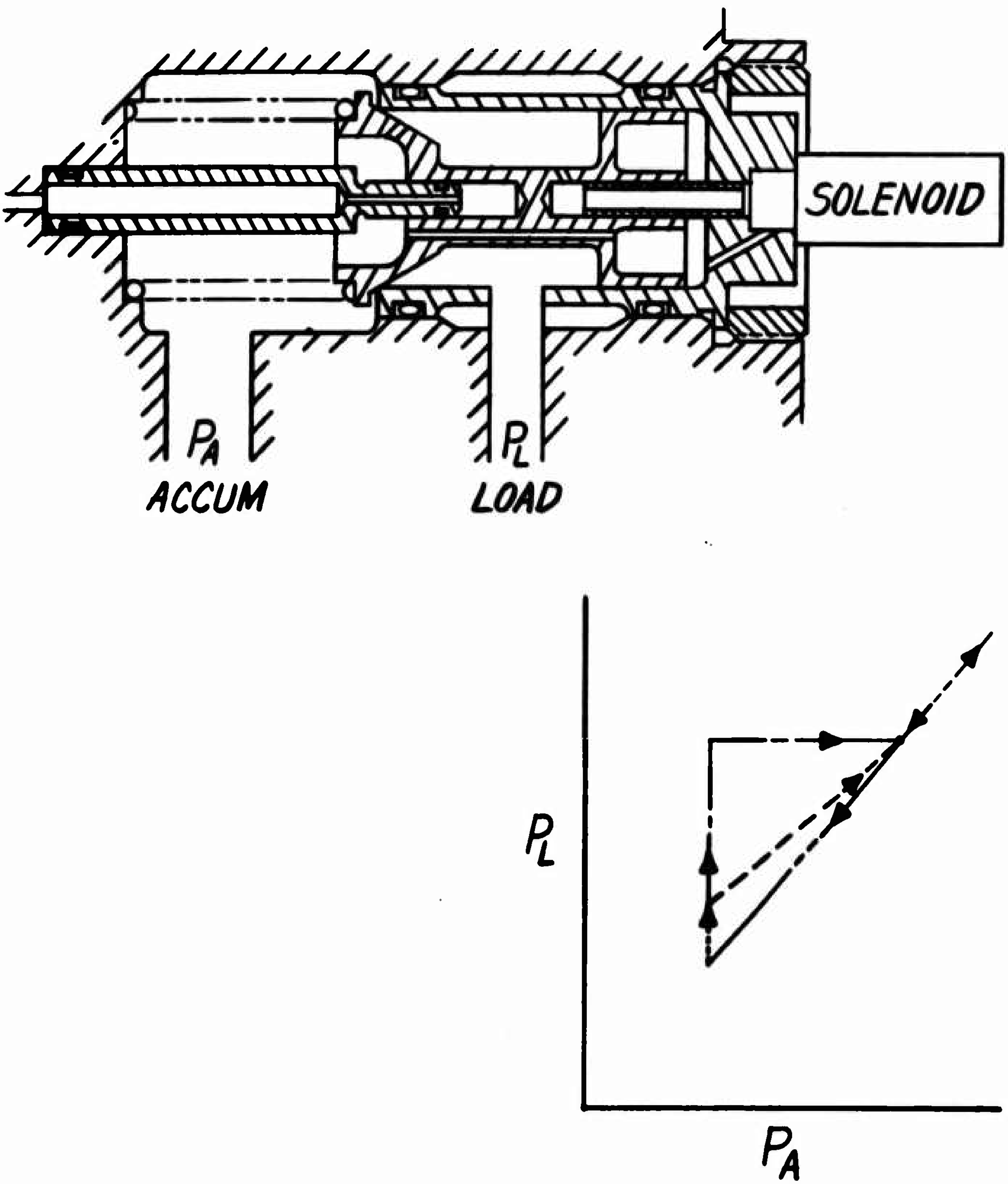

SWITCH LOGIC

FIGURE 31.0

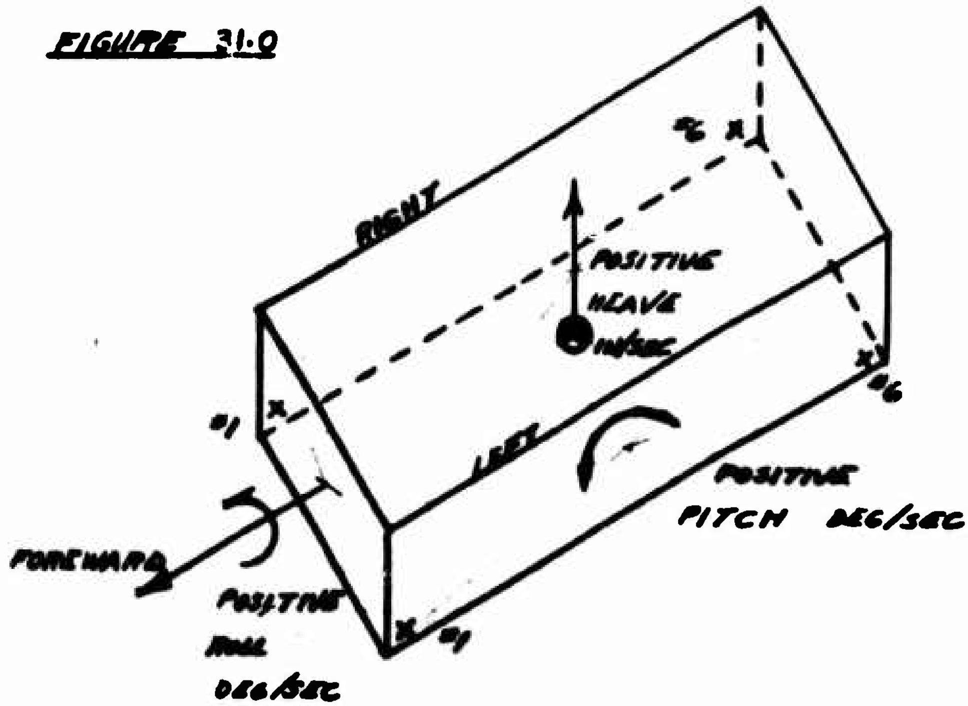

LEFT #1

HIGH DAMPING IF:
$\Sigma R+P-H>1.0$

LEFT #6

HIGH DAMPING IF:
$\Sigma R-P-H>1.0$

RIGHT #1

HIGH DAMPING IF:
$\Sigma -R+P-H>1.0$

RIGHT #6

HIGH DAMPING IF:
$\Sigma -R-P-H>1.0$

NOTE: POWER OFF RESULTS IN HIGH DAMPING LEVELS ON ALL DAMPED UNITS.
R, P, H ARE ROLL, PITCH, AND HEAVE RATES, RESP., REFERRED TO APPROPRIATE LOGIC SWITCHING LEVELS.

APPENDIX A

SYSTEM EQUATIONS

BASIC SYSTEM EQUATIONS

SYSTEM VARIABLES

x_i - GROUND CONTOUR HEIGHT INTERPRETED AS THE HEIGHT OF HUB OF UNDISTORTED i^{th} WHEEL IN CONTACT WITH GROUND. SEE FIG. #2

y_i - ACTUAL HEIGHT OF HUB OF i^{th} WHEEL WITH RESPECT TO ITS DATUM PLANE SEE FIG #2

ξ_i - HORIZONTAL POSITION OF HUB OF i^{th} WHEEL SEE FIG. #2

λ_i - ANGLE OF APPROACH OF TRACK TO i^{th} WHEEL WITH RESPECT TO TRUE HORIZONTAL, POSITIVE DOWNWARD

β_i - GROUND RISE ANGLE AHEAD OF i^{th} WHEEL RELATIVE TO TRUE HORIZONTAL SEE FIG #2

γ_i - ANGLE OF DEPARTURE OF TRACK FROM i^{th} WHEEL WITH RESPECT TO TRUE HORIZONTAL, POSITIVE ASCENDING

θ_i - ANGLE OF i^{th} ROAD ARM ABOVE HULL HORIZONTAL

τ_F - ANGLE OF DEPARTURE OF TRACK FROM FRONT IDLER/SPROCKET REFERRED TO PLANE $\perp$ TO PITCH PLANE AND CONTAINING C.G. AND FRONT IDLER/SPROCKET AXIS.

τ_R - ANGLE OF APPROACH OF TRACK TO REAR IDLER/SPROCKET REFERRED TO PLANE $\perp$ PITCH PLANE AND CONTAINING C.G. AND REAR IDLER SPROCKET AXIS.

ψ_i - ANGLE OF ROAD ARM BELOW TRUE HORIZONTAL (i^{th})

F_i - GROUND CONTACT NORMAL FORCE AT i^{th} WHEEL

F_{pi} - GROUND CONTACT TANGENTIAL FORCE AT i^{th} WHEEL

F_{Ri} - RADIAL COMPONENT OF FORCE BETWEEN HULL AND i^{th} ROAD ARM

F_{Ti} - PERPENDICULAR COMPONENT OF FORCE BETWEEN HULL AND i^{th} ROAD ARM

M_i - TORQUE BETWEEN HULL AND i^{th} SUSPENSION UNIT

Y - VERTICAL POSITION OF HULL C.G. WITH RESPECT TO DATUM

Z - HORIZONTAL POSITION OF HULL C.G.

Θ - Pitch Angle of HULL WITH RESPECT TO TRUE HORIZONTAL, POSITIVE DOWN IN FRONT.

BASIC SYSTEM EQUATIONS

SYSTEM VARIABLES

D_i - LENGTH OF TRACK BETWEEN i^{th} WHEEL AND $(i+1)^{th}$ WHEEL

D_F - LENGTH OF TRACK BETWEEN FRONT IDLER/SPROCKET AND FIRST WHEEL

D_R - LENGTH OF TRACK BETWEEN REAR WHEEL AND REAR IDLER/SPROCKET

H_i - AVERAGE HEIGHT OF GROUND CONTOUR BETWEEN i^{th} WHEEL AND THE $(i+1)^{th}$ WHEEL

S_i - DIFFERENCE BETWEEN D_i AND NOMINAL LENGTH OF TRACK BETWEEN i^{th} WHEEL AND $(i+1)^{th}$ WHEEL

T_{Ai} - TENSION FORCE IN TRACK APPROACHING i^{th} WHEEL

T_{Di} - TENSION FORCE IN TRACK DEPARTING i^{th} WHEEL

NOTE: C.G. USED IN ANY OF THE ABOVE REFERS TO THE CENTER OF GRAVITY OF THE SPRUNG MASS OF THE HULL

DATUM PLANES:

$Y = 0$ HULL LEVEL, ROAD ARMS IN NOMINAL STATIC POSITION (θ_0), ALL WHEELS UNDISTORTED AND JUST IN CONTACT WITH LEVEL GROUND: ALL x_i'S AND y_i'S ARE ZERO.

BASIC SYSTEM EQUATIONS

SYSTEM CONSTANTS AND PARAMETERS

C_D - SUSPENSION UNIT DAMPING COEFFICIENT. THIS MAY BE A FUNCTION OF VELOCITY AND DAMPING TORQUE LEVEL.

K_g - GROUND-TRACK-WHEEL INTERFACE SPRING RATE. NOT WELL DEFINED. USE MAXIMUM ACCEPTABLE VALUE, POSSIBLY INCLUDING SOME DAMPING

α - TORSIONAL SPRING RATE OF SUSPENSION SPRING MAY VARY WITH ROAD ARM ANGLE

m - LUMPED MASS OF WHEEL AND ROAD ARM AT WHEEL HUB

R - ROAD ARM LENGTH

θ_F - ANGLE OF ROAD ARM BELOW HULL HORIZONTAL AT WHICH SUSPENSION SPRING IS FULLY RELAXED

θ_0 - NOMINAL STATIC ANGLE OF ROAD ARM BELOW HULL HORIZONTAL

A_F - DISTANCE, MEASURED IN PITCH PLANE, OF C.G. FROM FRONT IDLER/SPROCKET AXIS

A_R - DISTANCE, MEASURED IN PITCH PLANE, OF C.G. FROM REAR IDLER/SPROCKET AXIS.

h - HEIGHT OF C.G. ABOVE PLANE OF SUSPENSION UNIT AXES

I - PITCH MOMENT OF INERTIA OF HULL ABOUT ITS C.G. (SPRUNG)

L_i - DISTANCE MEASURED IN HULL HORIZONTAL OF i^{th} SUSPENSION UNIT AXIS AHEAD OF HULL C.G.

M - SPRUNG MASS OF HULL

δ_i - ANGLE, MEASURED IN PITCH PLANE, BETWEEN LINE FROM C.G. TO i^{th} SUSPENSION UNIT AND HULL HORIZONTAL. SIGN SAME AS FOR L_i

ε_F - ANGLE, MEASURED IN PITCH PLANE, BETWEEN LINE FROM C.G. TO FRONT IDLER/SPROCKET AND HULL HORIZONTAL

ε_R - ANGLE, MEASURED IN PITCH PLANE, BETWEEN LINE FROM C.G. TO REAR IDLER/SPROCKET AND HULL HORIZONTAL

BASIC SYSTEM EQUATIONS

SYSTEM CONSTANTS AND PARAMETERS

C_{N_0} - WEIGHTING FACTOR FOR DETERMINING TRACK ANGLES

D_i - NOMINAL STATIC TRACK LENGTH BETWEEN i^{th} AND $(i+1)^{th}$ WHEEL

D_{F_0} - NOMINAL STATIC TRACK LENGTH BETWEEN FRONT IDLER SPROCKET AND FIRST WHEEL

D_{R_0} - NOMINAL STATIC TRACK LENGTH BETWEEN REAR IDLER/SPROCKET AND LAST WHEEL

K_T - TRACK EFFECTIVE SPRING RATE IN TENSION

T_0 - NOMINAL STATIC TRACK TENSION FORCE

h_F - HEIGHT OF FRONT SPROCKET OR IDLER ABOVE THE PLANE OF SUSPENSION UNIT AXES (TANK-VERTICAL DIR.)

h_R - HEIGHT OF REAR SPROCKET OR IDLER ABOVE THE PLANE OF SUSPENSION UNIT AXES (TANK VERTICAL DIR.)

L_F - DISTANCE OF FRONT IDLER OR SPROCKET AHEAD OF #1 SUSPENSION UNIT AXIS (TANK HORIZONTAL)

L_R - DISTANCE OF REAR SPROCKET OR IDLER BEHIND #6 SUSPENSION UNIT AXIS (TANK HORIZONTAL)

BASIC EQUATIONS

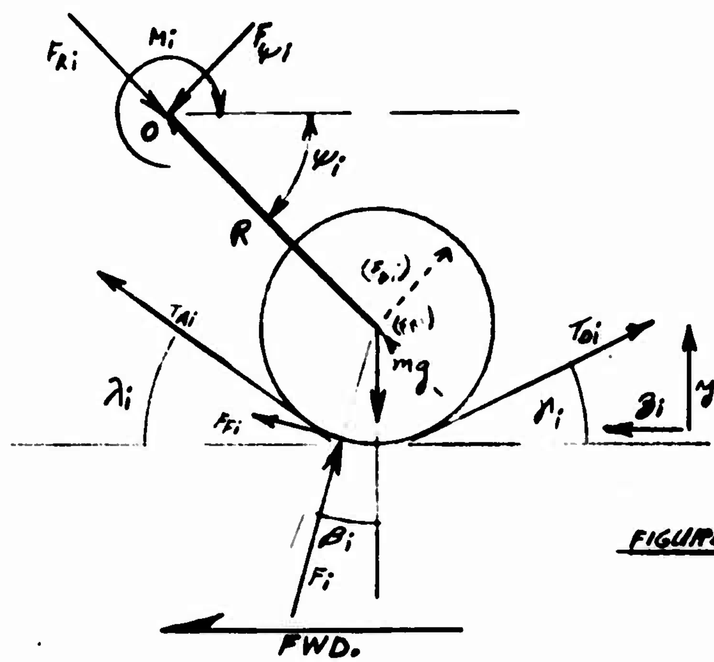

FIGURE # 1

SUSPENSION UNIT

SUMMATION OF VERTICAL FORCES

$$m\ddot{y}_i = F_i \cos\beta_i + T_{Ai} \sin\lambda_i + T_{Di} \sin\gamma_i + F_{Fi} \sin\beta_i$$

$$- F_{Ri} \sin\psi_i - F_{\psi i} \cos\psi_i - mg$$

SUMMATION OF HORIZONTAL FORCES

$$m\ddot{z}_i = F_{\psi i} \sin\psi_i + T_{Ai} \cos\lambda_i + F_{Fi} \cos\beta_i - F_{Ri} \cos\psi_i$$

$$- T_{Di} \cos\gamma_i - F_i \sin\beta_i$$

SUMMATION OF MOMENTS ABOUT "O"

$$M_i = RF_{\psi i} = \alpha(\theta_s + \theta_i) + C_D \dot{\theta}_i$$

BASIC EQUATIONS

SUSPENSION UNITS

CONSTRAINTS

$$-\psi_i = |\Theta| + \theta_i$$

$$F_{Fi} = T_{Di} - T_{Ai}$$

GROUND INTERFACE

$$F_i = \frac{K_g}{\cos\beta_i}\left[x_i - y_i\right]$$

BASIC EQUATIONS

HULL

SUMMATION OF VERTICAL FORCES (1/2 HULL)

$$\frac{M}{2}\ddot{Y} = \sum_{1}^{6} F_{\psi_i}\cos\psi_i + \sum_{1}^{6} F_{Ri}\sin\psi_i - T_{A1}\sin(\tau_F - \epsilon_F - \Theta)$$
$$- T_{DG}\sin(\tau_R - \epsilon_R + \Theta) - \frac{Mg}{2}$$

SUMMATION OF HORIZONTAL FORCES (1/2 HULL)

$$\frac{M}{2}\ddot{Z} = \sum_{1}^{6} F_{Ri}\cos\psi_i - \sum_{1}^{6} F_{\psi_i}\sin\psi_i + T_{DG}\cos(\tau_R - \epsilon_R + \Theta)$$
$$- T_{A1}\cos(\tau_F - \epsilon_F - \Theta)$$

SUMMATION OF MOMENTS ABOUT C.G.

$$\frac{I}{2}\ddot{\Theta} = \sum^{6} M_i + T_{A1}A_F\sin\tau_F - T_{DG}A_R\sin\tau_R$$
$$- \sum_{1}^{6}\sqrt{L_i^2+h^2}\left[F_{\psi_i}\cos(\psi_i+\Theta+\delta_i)\,\mathrm{sgn}L_i + F_{Ri}\sin(\psi_i+\Theta+\delta_i)\right]$$

CONSTRAINTS

$$\delta_i = \mathrm{TAN}^{-1}\left(\frac{h}{L_i}\right)$$

$$y = Y + R\left[\sin\theta_0 - \sin\psi_i\right] + h - \sqrt{L_i^2+h^2}\,\mathrm{SIGN}L_i\left[\sin(\delta_i+\Theta)\right]$$

$$z_i = Z - R\left[\cos\psi_i - \cos\theta_0\right] - L_i + \sqrt{L_i^2+h^2}\,\mathrm{SIGN}L_i\left[\cos(\delta_i+\Theta)\right]$$

$$\tau_F = \epsilon_F + \lambda_1 + \Theta$$

$$\tau_R = \epsilon_R + \gamma_6 - \Theta$$

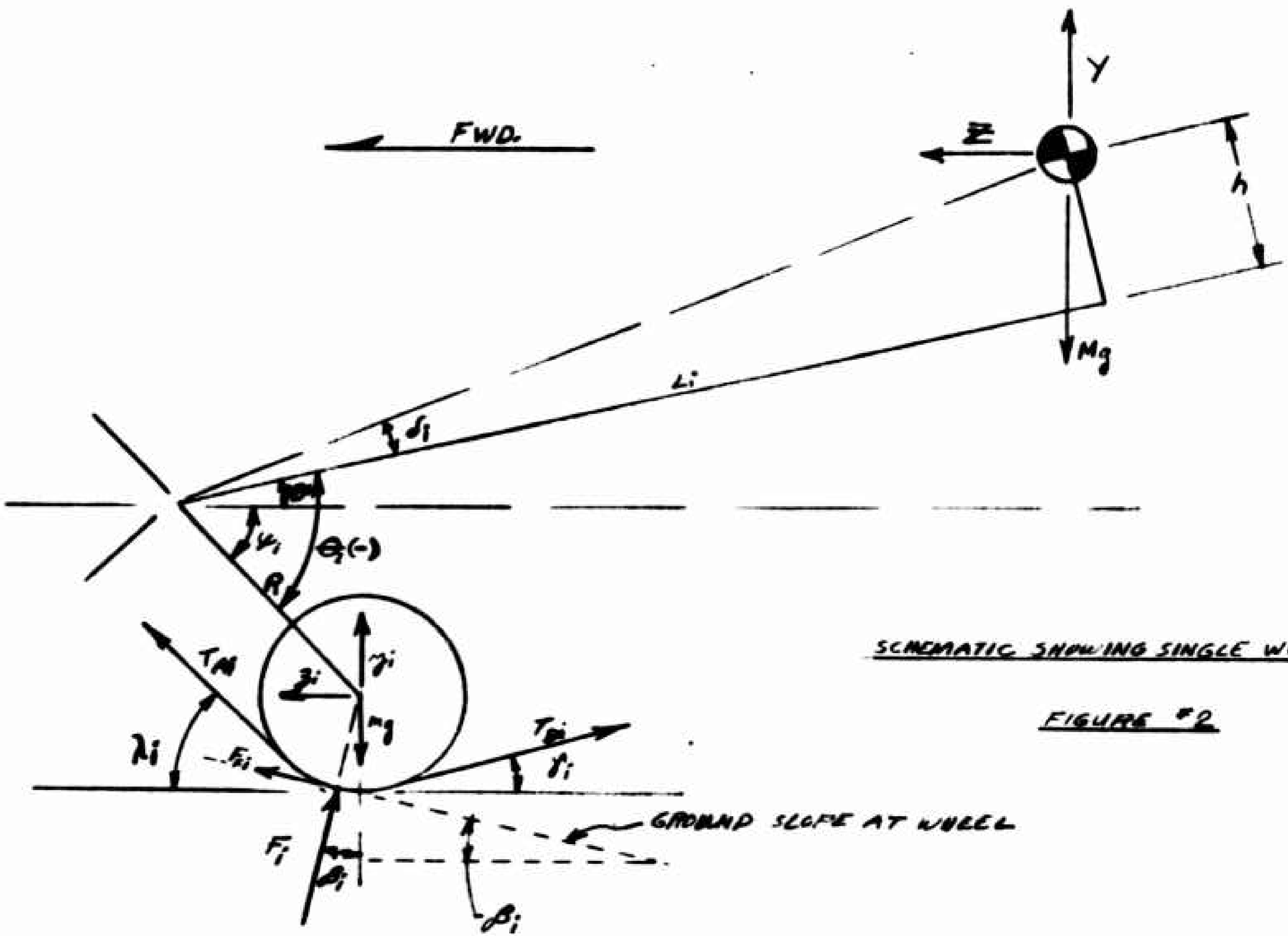

SCHEMATIC SHOWING SINGLE WHEEL

FIGURE #2

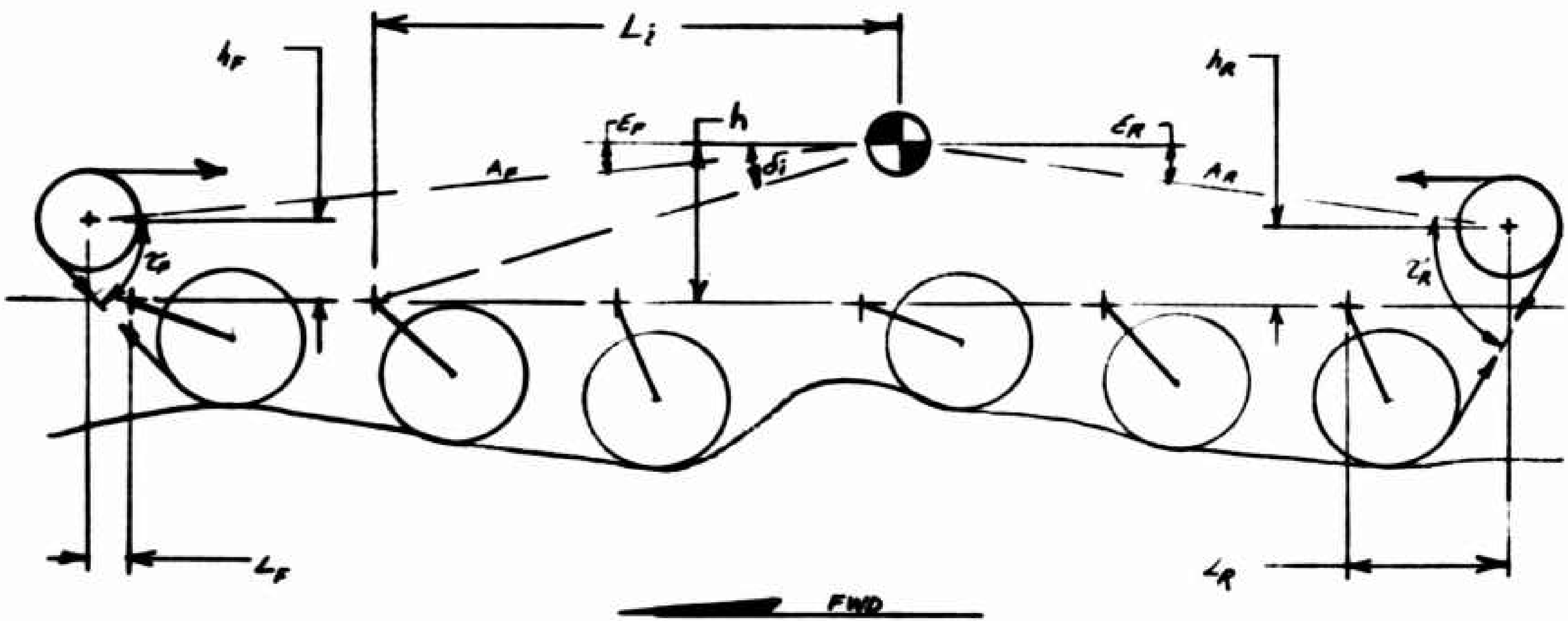

SCHEMATIC OF SUSPENSION SYSTEM

FIGURE #3

BASIC EQUATIONS

TRACK TENSION AND ITS APPLICATION

ASSUMPTIONS

1. TRACK IS ITSELF MASS-LESS
2. TRACK IS COMPLETELY FLEXIBLE IN BENDING
3. TRACK IS INFINITELY STIFF IN TENSION
4. TRACK SPANS DEPRESSIONS BETWEEN WHEELS, AND CONFORMS TO RISES BETWEEN WHEELS
5. BECAUSE OF ITEM #3, ABOVE, TRACK TENSION WILL MODIFY THE POSITION OF THE SUSPENSION UNITS IN ORDER TO MAINTAIN AN ESSENTIALLY CONSTANT LENGTH TRACK. TRACK LENGTH BETWEEN WHEELS ONE AND SIX WILL BE APPROXIMATE BASED ON ITEM #4 ABOVE.

CHANGE IN TRACK LENGTH BETWEEN ADJACENT WHEELS:

CONDITION #1 - GROUND LEVEL BETWEEN WHEELS IS COMPLETELY BELOW THE TWO WHEELS. FOR THIS CONDITION THE DESIRED LENGTH OF TRACK WILL BE TAKEN AS THE HYPOTENUSE OF THE RIGHT TRIANGLE FORMED BY THE WHEELS HORIZONTAL AND VERTICAL SEPARATIONS. THIS CAN BE WRITTEN AS

$$D_i = \left\{\left[(L_i - L_{i+1})\cos\phi_i - R(\cos\psi_i - \cos\psi_{i+1})\right]^2 + \left[y_i - y_{i+1}\right]^2\right\}^{1/2}$$

THE TRACK ANGLES RESULTING FROM THIS ARE

$$\gamma_i = -\lambda_{i+1} = \sin^{-1}\left(\frac{y_{i+1} - y_i}{D_i}\right)$$

TO DETERMINE IF THIS CONDITION EXISTS, THE CRITERION USED WILL BE THE SIGN OF THE DIFFERENCE OF THE AREAS UNDER THE GROUND CONTOUR CURVE AND THE TANGEANT LINE

TRACK TENSION AND ITS APPLICATION

CONDITION #1

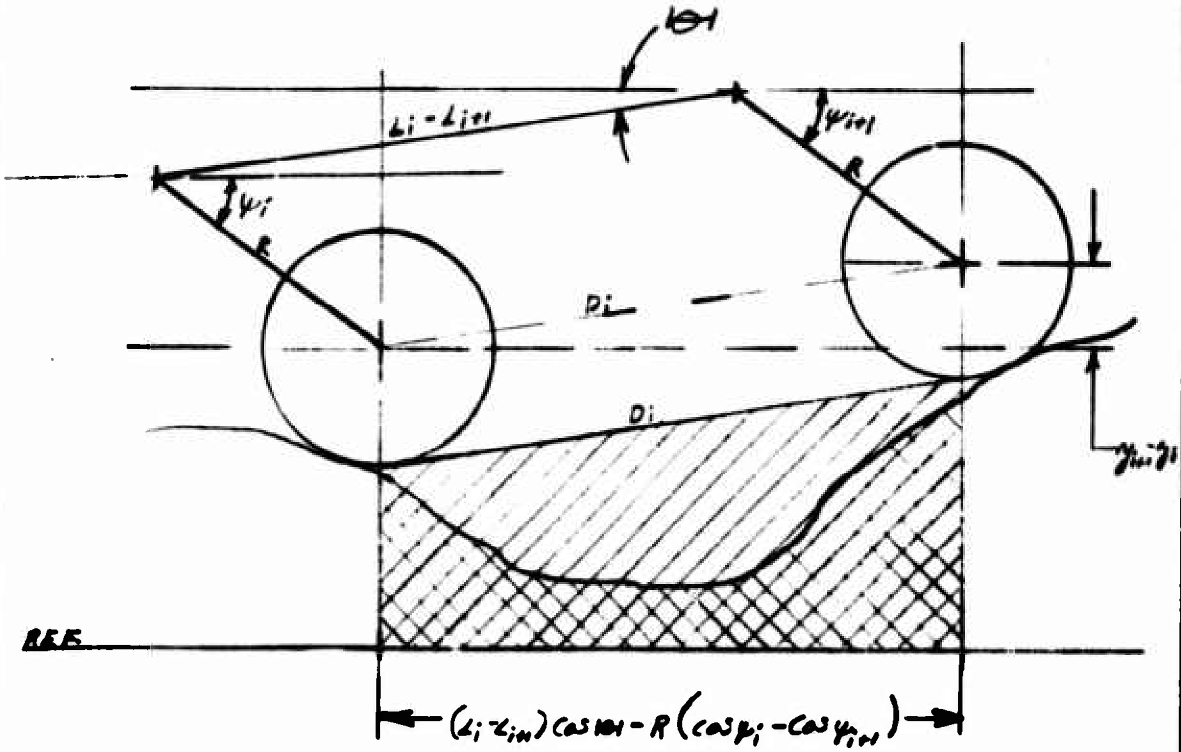

NOTE THAT THE AREA UNDER THE TANGEANT LINE IS GREATER THAN THE AREA UNDER THE GROUND CONTOUR LINE.

IF $\frac{y_1+y_2}{2}\left((L_i-L_{i+1})\cos\theta_i - R(\cos\psi_i - \cos\psi_{i+1})\right)$ AT TIME 't'

is GREATER-THAN-OR-EQUAL-TO $\int_0^t \dot{Z}(X_i - X_{i+1})\,dt$

USE CONDITION #1.

THE POSSIBILITY THAT THE ABOVE CRITERION BE SATISFIED WITH SOME OF GROUND CONTOUR ABOVE TANGEANT LINE WILL BE IGNORED.

TRACK TENSION AND ITS APPLICATION

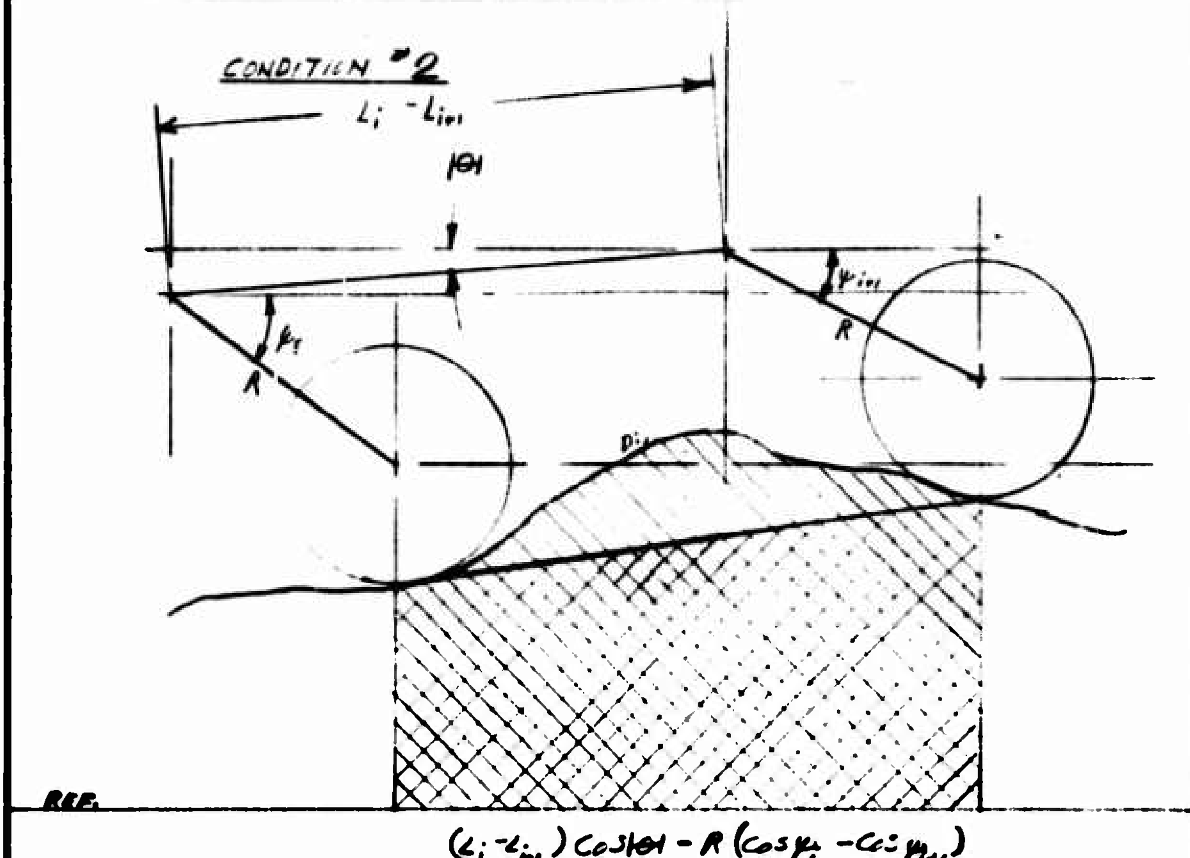

NOTE THAT THE AREA UNDER THE TANGEANT LINE IS LESS THAN THE AREA UNDER THE GROUND CONTOUR LINE.

IF $\frac{Z_i + Z_{i+1}}{2}\left[(L_i - L_{i+1})\cos\Theta - R(\cos\psi_i - \cos\psi_{i+1})\right]$ AT TIME 't' IS LESS THAN $\int_0^t \dot{Z}(x_i - x_{i+1})\,dt$ USE CONDITION #2

AGAIN, CONDITIONS SATISFYING THE ABOVE CRITERION BUT WITH SOME CONTOUR BELOW TANGEANT WILL BE IGNORED

TRACK TENSION AND ITS APPLICATION

CONDITION #2 - GROUND LEVEL BETWEEN WHEELS IS ABOVE TANGEANT BETWEEN WHEELS. FOR THIS CONDITION THE DESIRED LENGTH OF TRACK WILL BE TAKEN AS THE LENGTH OF THE GROUND CONTOUR BETWEEN WHEELS. THE VEHICLE IS ASSUMED TO HAVE STARTED FROM A NOMINAL STATIC POSITION.

$$D_i = L_i - L_{i+1} + \int_0^{t_0} (\dot{s}_i - \dot{s}_{i+1})\,dt$$

$$\dot{s}_i = \sqrt{\dot{x}_i^2 + \dot{z}^2} = \dot{z}\sqrt{\tan^2\beta_i + 1} = \frac{\dot{z}}{\cos\beta_i}$$

$$D_i = L_i - L_{i+1} + \int_0^{t_0} \dot{z}\left(\frac{1}{\cos\beta_i} - \frac{1}{\cos\beta_{i+1}}\right)dt$$

THE TRACK ANGLES TO BE USED FOR THIS CONDITION DO NOT LEND THEMSELVES TO READY CALCULATION. ASSUME THE RISE BETWEEN WHEELS TO HAVE AN EFFECTIVE HEIGHT

$$H_i = \left[\frac{y_i + y_{i+1}}{2} + \frac{\text{AREA UNDER CURVE} - \text{AREA UNDER TANGENT}}{(L_i - L_{i+1})\cos|\theta| - R(\cos\psi_i - \cos\psi_{i+1})}\right]$$

$$\tan^{-1}\gamma_i = \frac{2(H_i - y_i)C_H}{(L_i - L_{i+1})\cos|\theta| - R(\cos\psi_i - \cos\psi_{i+1})}$$

$$\tan^{-1}\lambda_{i+1} = \frac{2(H_i - y_{i+1})C_H}{(L_i - L_{i+1})\cos|\theta| - R(\cos\psi_i - \cos\psi_{i+1})}$$

C_H IS A FACTOR DEPENDANT ON THE FORM OF THE GROUND CONTOUR BETWEEN WHEELS. A VALUE OF 3 TO 4 SEEMS REASONABLE.

TRACK TENSION AND ITS APPLICATION

GROUND CONTOUR FORM FACTOR 'C_N'.

FOR CONVENIENCE, LET $y_i = y_{i+1} = 0$ = ~~[illegible]~~, STATIC

1. TRIANGULAR CONTOUR, MIDWAY BETWEEN WHEELS

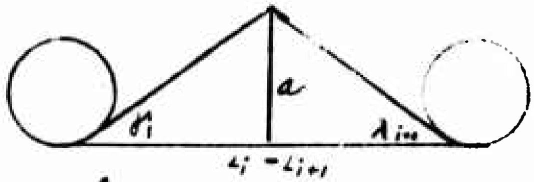

$$H = \frac{A}{L_i - L_{i+1}} = \frac{a}{2}$$

$$\tan^{-1}\gamma_1 = \tan^{-1}\lambda_{i+1} = \frac{h}{L_i - L_{i+1}} = \frac{2H}{L_i - L_{i+1}}$$

$$C_N = 2$$

2. PARABOLIC CONTOUR, MIDWAY BETWEEN WHEELS

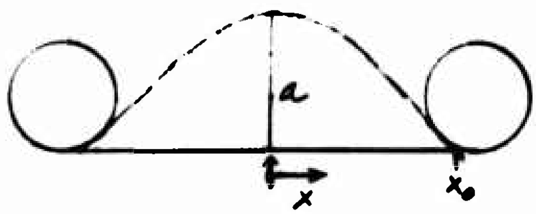

$$H_i = \frac{A}{L_i - L_{i+1}}$$

$$A = 2\int_0^{x_0}\left(a - \frac{ax^2}{x_0^2}\right)dx \; 2\left[ax - \frac{ax^3}{3x_0^2}\right]_0^{x_0} = \frac{4ax_0}{3}$$

$$L_i - L_{i+1} \approx 2x_0$$

$$H_i \approx \frac{2a}{3}$$

$$\tan^{-1}\gamma_i = \tan^{-1}\lambda_{i+1} \approx -\text{SLOPE OF PARABOLA AT } x_0$$
$$= \frac{2h}{x_0} = \frac{3H}{x_0} \approx \frac{6H_i}{L_i - L_{i+1}}$$

$$C_N = 6$$

TRACK TENSION AND ITS APPLICATION

IGNORING THE CHANGES IN THE LENGTH OF TRACK WRAPPED AROUND WHEELS, IDLERS, AND SPROCKET, AND THE DIFFERENCE IN RADII BETWEEN THESE, THE REMAINING LENGTH CHANGES MAY BE REPRESENTED BY THE CHANGE IN CENTER DISTANCES BETWEEN #1 WHEEL AND THE FRONT IDLER/SPROCKET AND BETWEEN #6 WHEEL AND THE REAR IDLER/SPROCKET.

FRONT

$$D_F = \left[(h_F - R\sin\theta_1)^2 + (L_F + R\cos\theta_1)^2\right]^{1/2}$$

$$= \left[h_F^2 + L_F^2 + R^2 + 2R(L_F\cos\theta_1 - h_F\sin\theta_1)\right]^{1/2}$$

REAR

$$D_R = \left[(h_R - R\sin\theta_6)^2 + (L_R - R\cos\theta_6)^2\right]^{1/2}$$

$$= \left[h_R^2 + L_R^2 + R^2 - 2R(L_R\cos\theta_6 + h_R\sin\theta_6)\right]^{1/2}$$

NOTICE THAT SIGN θ_1 IS (-) FOR ROAD ARM ANGLES BELOW HORIZONTAL. θ_6 IS (+)

THE CHANGES IN THESE LENGTHS ARE THE DIFFERENCES FROM NOMINAL STATIC VALUES:

$$D_{F_0} = \left[h_F^2 + L_F^2 + R^2 + 2R(L_F\cos\theta_0 + h_F\sin\theta_0)\right]^{1/2}$$

$$D_{R_0} = \left[h_R^2 + L_R^2 + R^2 - 2R(L_R\cos\theta_0 - h_R\sin\theta_0)\right]^{1/2}$$

TRACK TENSION AND ITS APPLICATION

TOTAL "CHANGE" IN TRACK LENGTH

$$\Delta L = (D_F - D_{F_0}) + (D_R - D_{R_0}) + \sum_0^5 (D_i - D_i^\circ)$$

WHERE $D_i^\circ = L_i - L_{i+1}$

NOMINAL TRACK TENSION

$$T_{BASIC} = T_0 + K_T \Delta L$$

WHERE T_0 IS STATIC NOMINAL TRACK TENSION

IT IS POSSIBLE TO APPLY AN APPROACH SIMILAR TO THAT USED IN CONSIDERING THE GROUND BETWEEN WHEELS TO BEGIN TO PICK UP TRACK LOADING AHEAD OF WHEEL #1, AND TO CARRY IT BEYOND WHEEL #6. THIS WOULD PROVIDE FORCES KNOWN TO EXIST AS WHEEL #1 APPROACHES SHARPLY RISING GROUND OR AS WHEEL #6 LEAVES SHARPLY FALLING GROUND. EQUATIONS DESCRIBING THIS ARE NOT INCLUDED.

APPENDIX B

SYSTEM EQUATIONS AND COMPUTER DIAGRAMS

BASIC EQUATIONS for i^{th} WHEEL

Ground/Wheel Interface (See Fig 1)

$i = 1, (n - c_o)$
where n = wheels/side

1 $$F_i = \frac{K_g}{\cos\beta_i}(x_i - y_i)$$ $F_i \geq 0$

F_i = Force generated at wheel/ground contact
K_g = Effective Ground/Wheel "spring rate"
β_i = Angle of ground with horizontal
x_i = Position of hub of undistorted wheel above its datum
y_i = Actual position of wheel hub above its datum

Actual Wheel Hub Position (See Fig 2)

2 $$y_i = Y - L_i \sin(\cancel{\Theta} + \delta_i) + R \sin\theta_0 - R \sin\psi_i$$

Y = Vertical Position of vehicle C.G. above its datum, $Y = h$ when road arms of wheels are in static position and wheels are just in ground contact but unloaded (zero pitch of hull; $h/L_i = \sin\delta_i$)
L_i = Distance of Road Arm pivot from vehicle C.G. (+ for those ahead of C.G., − for those behind)
$\cancel{\Theta}$ = Vehicle pitch angle measured from horizontal, positive with front end low.
R = Length of Road Arm
θ_0 = Static Road Arm angle below plane of Road Arm pivots
ψ_i = Actual angle of Road Arm below true horizontal
δ_i = Angle in pitch plane between line drawn from C.G. to road arm pivots and plane of road arm pivots, sign same as L_i
h = Height of C.G. above plane of roadarm pivot points.

Sketch for Equation 4

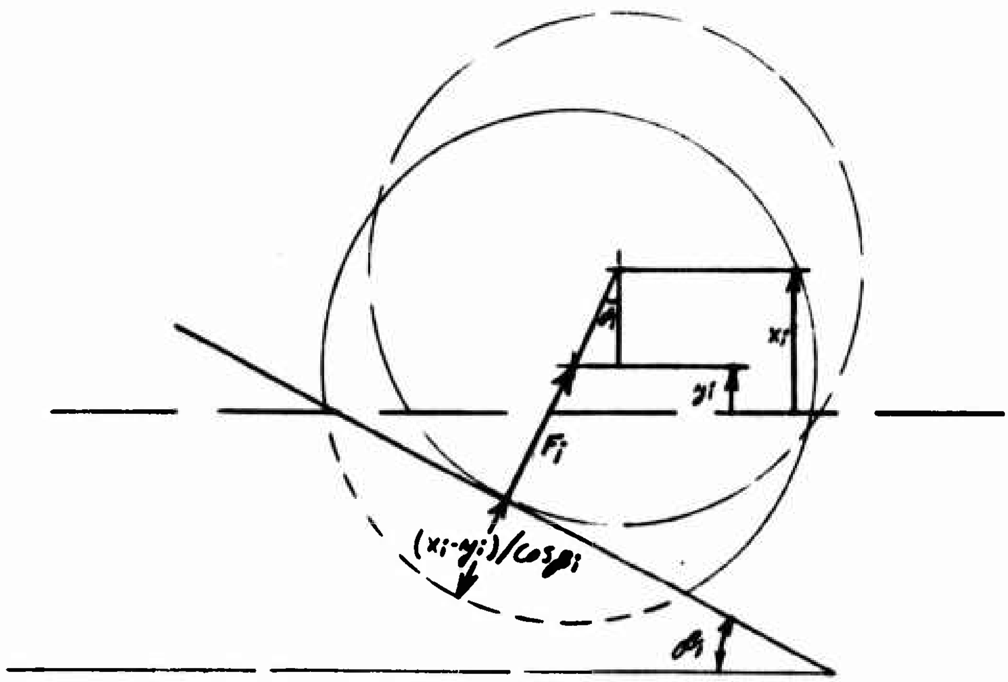

FIGURE 1

Sketch for Equation 2

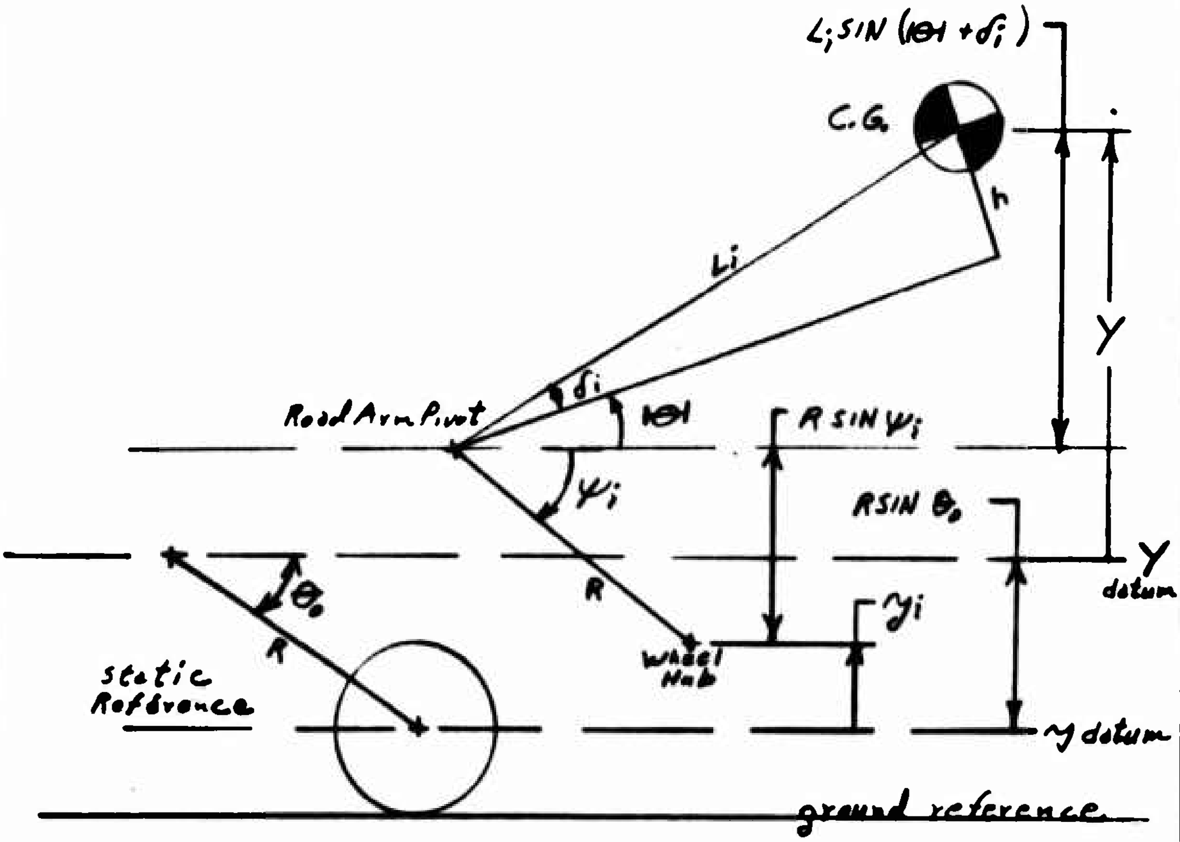

Static Conditions, Wheel on Ground Reference

$\Theta = 0$

$\psi_i = \theta_o$

$Y = h$

$y = 0$

FIGURE 2

BASIC EQUATIONS for i^{th} WHEEL, CONT'D

Road Arm Angle

3 $$\psi_i = -\theta_i - \cancel{\Theta}$$

θ_i = Road Arm angle above plane of vehicle Road Arm pivots

Torque Balance

4 $$m\ddot{\theta}_i R = -mg\cos\psi_i + F_i\cos(\psi_i - \beta_i) - \frac{1}{R}(M_{i1} + M_{i2}) + \frac{F_T R_i}{R}$$

(Note: θ_i is actually relative to the vehicle hull, so the angle ψ_i would appear to be preferred. Since the velocity $\dot{\theta}_i$ is a desired quantity elsewhere in the simulation, and since $\ddot{\Theta}$ and $\dot{\Theta}$ are of much lower magnitude, this is felt to be a reasonable approximation)

g = gravitational constant

m = Lumped (effective) mass of wheel and road arm

R_i = Effective Radius for track tension force

M_{i1} = Torque due to suspension springs and stops

M_{i2} = Torque due to damping forces

F_T = Track Tension Force

Spring Torque

5 $$M_{i1} = \alpha(\theta_R + \theta_i) + \alpha_B(\widetilde{\theta_i - \theta_B}) + K_\infty(\widetilde{\theta_i - \theta_j} + \underset{\sim}{\theta_i + \theta_3})$$

α = Primary torsional spring rate of suspension unit

θ_R = Road Arm angle below plane of road arm pivots at which spring torque vanishes.

BASIC EQUATIONS, CONT'D, i^{th} WHEEL

Spring Torque, Cont'd

α_B = Secondary torsional spring rate of suspension unit

θ_B = Angle above plane of vehicle road arm pivots at which secondary spring is engaged.

K_α = Large value used here to simulate stops.

θ_J = Angle above road arm pivot plane at which jounce stop is encountered.

θ_R = Angle below road arm pivot plane at which rebound stop is encountered.

$\tilde{a}$ = a for $a \geq 0$, = 0 for $a < 0$. $\underset{\sim}{a}$ = a for $a \leq 0$, = 0 for $a > 0$.

Damper Torque

6 $$M_{i2} = F_S R \cos\theta_0 |\dot{\theta}_i| \left(\frac{\tilde{\dot{\theta}}_i}{\dot{\theta}_0} + \frac{\underset{\sim}{\dot{\theta}_i}}{\dot{\theta}_0'} \right); \quad |M_{i2}| \leq F_D R \cos\theta_0, \; C = 0$$
$$|M_{i2}| \leq F_D' R \cos\theta_0, \; C = 1$$

F_S = Static Ground Force

$F_D R \cos\theta_0$ = Damping torque limit in jounce due to Damper valve operation (normal)

$F_D' R \cos\theta_0$ = Switched Damping torque limit (Note: This representation allows the 'Damping Force' F_D or F_D' to be compared directly with the wheel nominal static load)

$\dot{\theta}_0$ = Jounce velocity which will develop rated damping pressure across bleed orifice (1g)

$\dot{\theta}_0'$ = Rebound velocity required to develop rated rebound damping torque (1g)

C = 0 or 1; Logic signal from adaptive damping control.

Effective Track Tension Radius

7 $$R_1 = -9.5\left(.45 - \frac{\theta_2}{80^\circ}\right)\left(1 - \frac{\widetilde{\theta_1 + 13^\circ}}{40^\circ} + \frac{\theta_2 + 13^\circ}{68^\circ}\right), \text{ wheel \#1}$$

θ_1 = wheel #1 road arm angle relative to hull

θ_2 = wheel #2 road arm angle relative to hull

BASIC EQUATIONS, CONT'D, i^{th} WHEEL

Effective Track Tension Radius

8 $$R_i = +R\left(\frac{y_{i-1} - 2y_i + y_{i+1}}{\ell}\right), \quad i = 2, 3, 4, 5 \;\; R_i \leq 0$$

ℓ = Distance Between Road Arm Pivots, Ave

$$R_6 = +4.5\left(2 + \frac{\theta_5}{44} - \frac{\theta_6 + 32^\circ}{32^\circ} + \frac{\theta_6 + 32}{52^\circ}\right) \quad \text{wheel \#6}$$

$R_6 \leq 0$

Track Tension Force

9 $$F_T = K_T\left(s_0 + s_1 + s_6\right) - \rho V_s^2, \quad F_T \geq 0$$

K_T = Spring Rate of Track
s_0 = Initial Stretch of track
s_1 = Stretch of Track due to wheel #1
s_6 = stretch of Track due to wheel #6
ρ = Track Density (mass / unit length)
V_s = Vehicle Speed.

Track Stretch

10 $$s_1 = 7.0\left(1 + \frac{\theta_1}{78}\right)\left(1 - .75\,\frac{44^\circ + \theta_2}{67.5^\circ}\right)$$

11 $$s_6 = -3.6\left(1 + \frac{\theta_6}{78^\circ}\right)\left(1 + 2\,\frac{44^\circ + \theta_5}{68^\circ}\right)$$

Note: Equations 7, 8, 10, 11 are based on curves shown on succeeding two pages. These curves in turn are based on geometry of the MICV-70 Test Rig. (Fig. 3 & Fig 4)

FIGURE 3

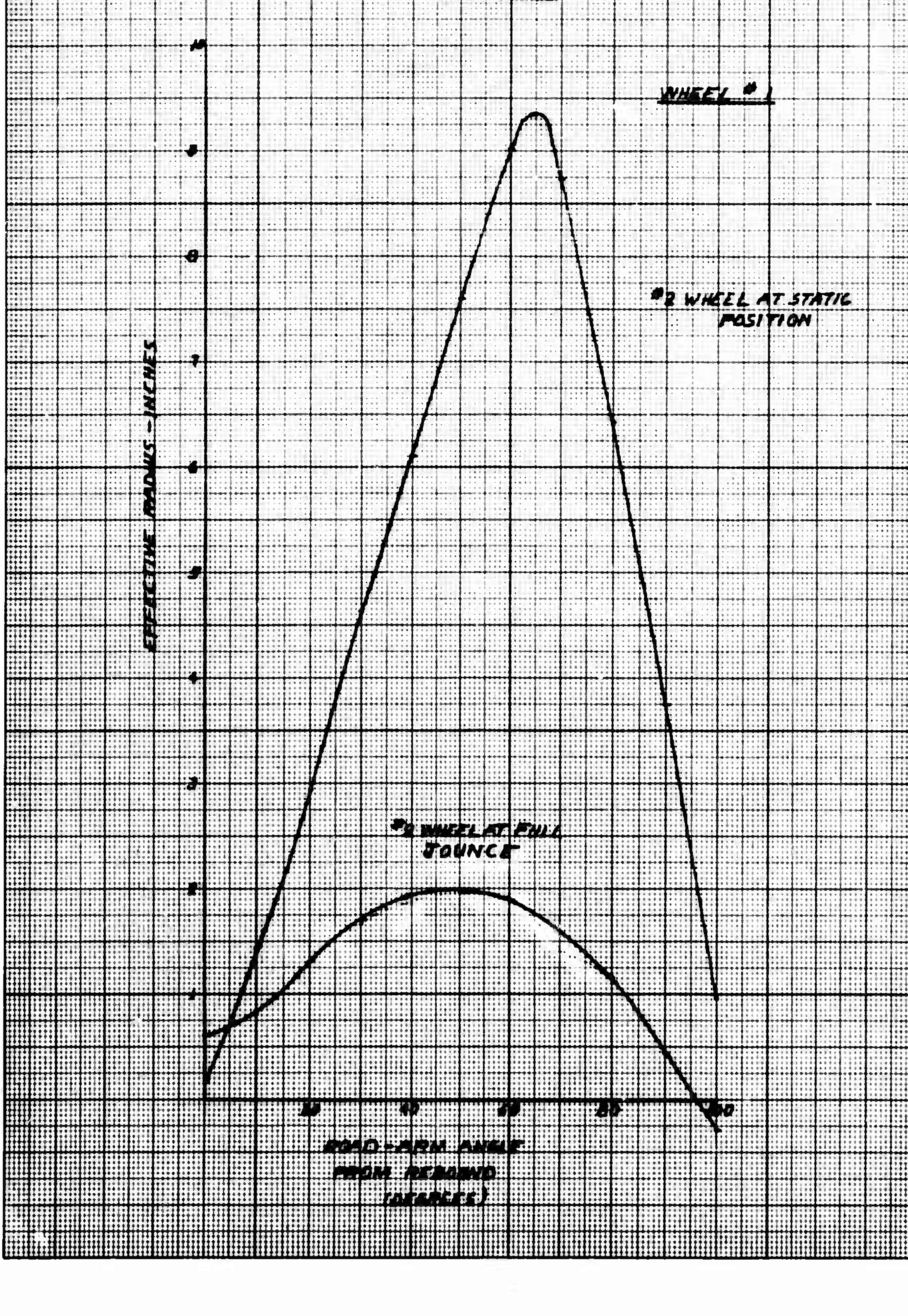
WHEEL # 1
#2 WHEEL AT STATIC POSITION
#2 WHEEL AT FULL JOUNCE
EFFECTIVE RADIUS - INCHES
ROAD-ARM ANGLE FROM REBOUND (DEGREES)
20
40
60
80
100

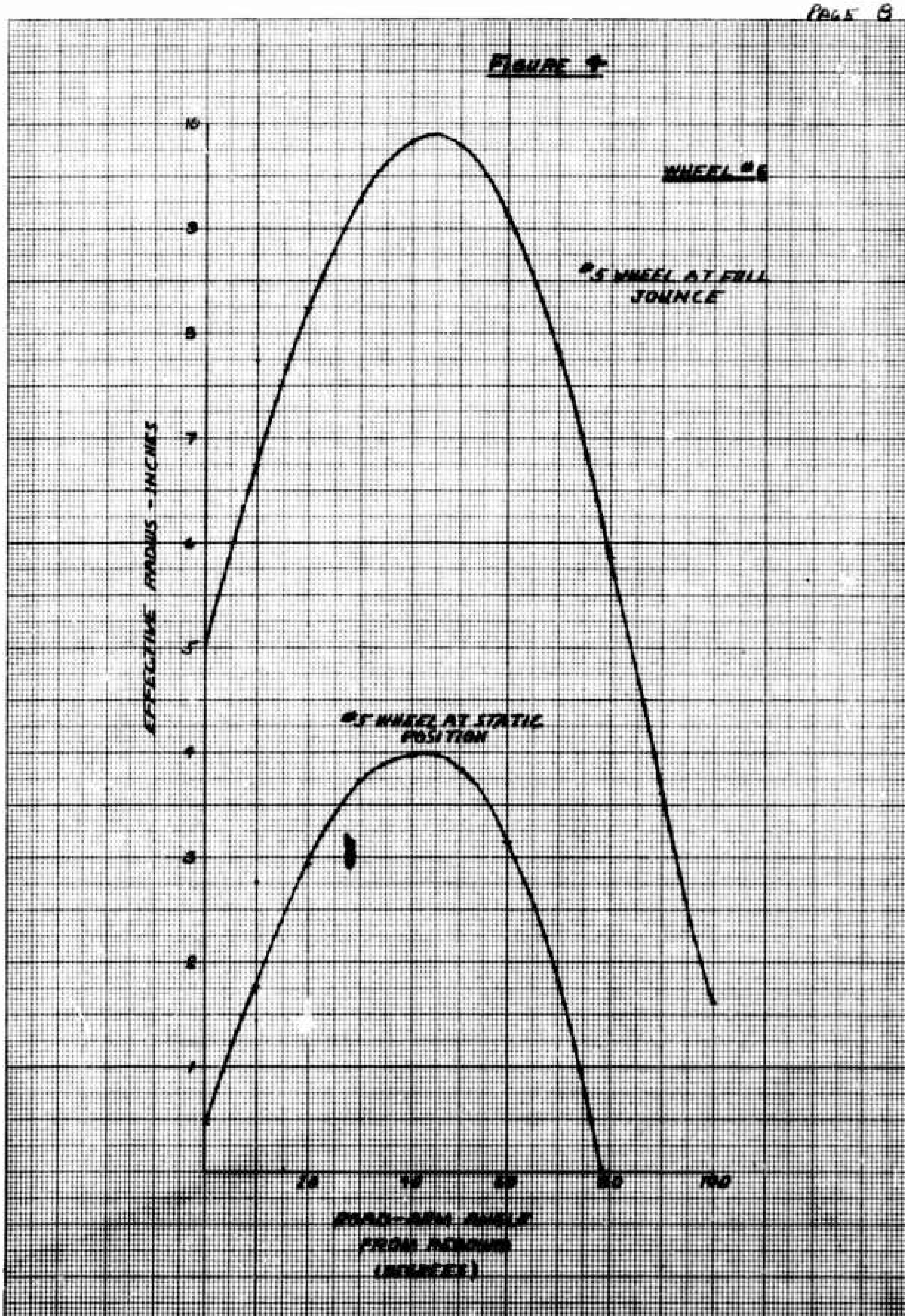
FIGURE 4
WHEEL #6
#5 WHEEL AT FULL JOUNCE
#5 WHEEL AT STATIC POSITION
EFFECTIVE RADIUS - INCHES
ROAD-ARM ANGLE FROM REBOUND (DEGREES)

BASIC EQUATIONS, HULL DYNAMICS

Pitch

12 $$\frac{I}{2}\ddot{\Theta} = \sum_{i=1}^{6}\Big\{-F_i\left[L_i\cos(\beta_i+\delta_i+\Theta) - R\cos(\psi_i-\beta_i)\right]$$
$$+ mR\ddot{\theta}_i\left[L_i\cos(\psi_i+\delta_i+\Theta) - R\right]$$
$$+ mR\dot{\theta}_i^2\left[L_i\sin(\psi_i+\delta_i+\Theta)\right]$$
$$+ mg\left[L_i\cos(\delta_i+\Theta) - R\cos\psi_i\right]\Big\}$$

I = Sprung Moment of Inertia about C.G.

Heave

13 $$\frac{M}{2}\ddot{Y} = \sum_{i=1}^{6}\left\{F_i\cos\beta_i - mR\ddot{\theta}_i\cos\psi_i - mR\dot{\theta}_i^2\sin\psi_i\right\}$$
$$-6mg - \frac{Mg}{2}$$

M = Vehicle Sprung Mass

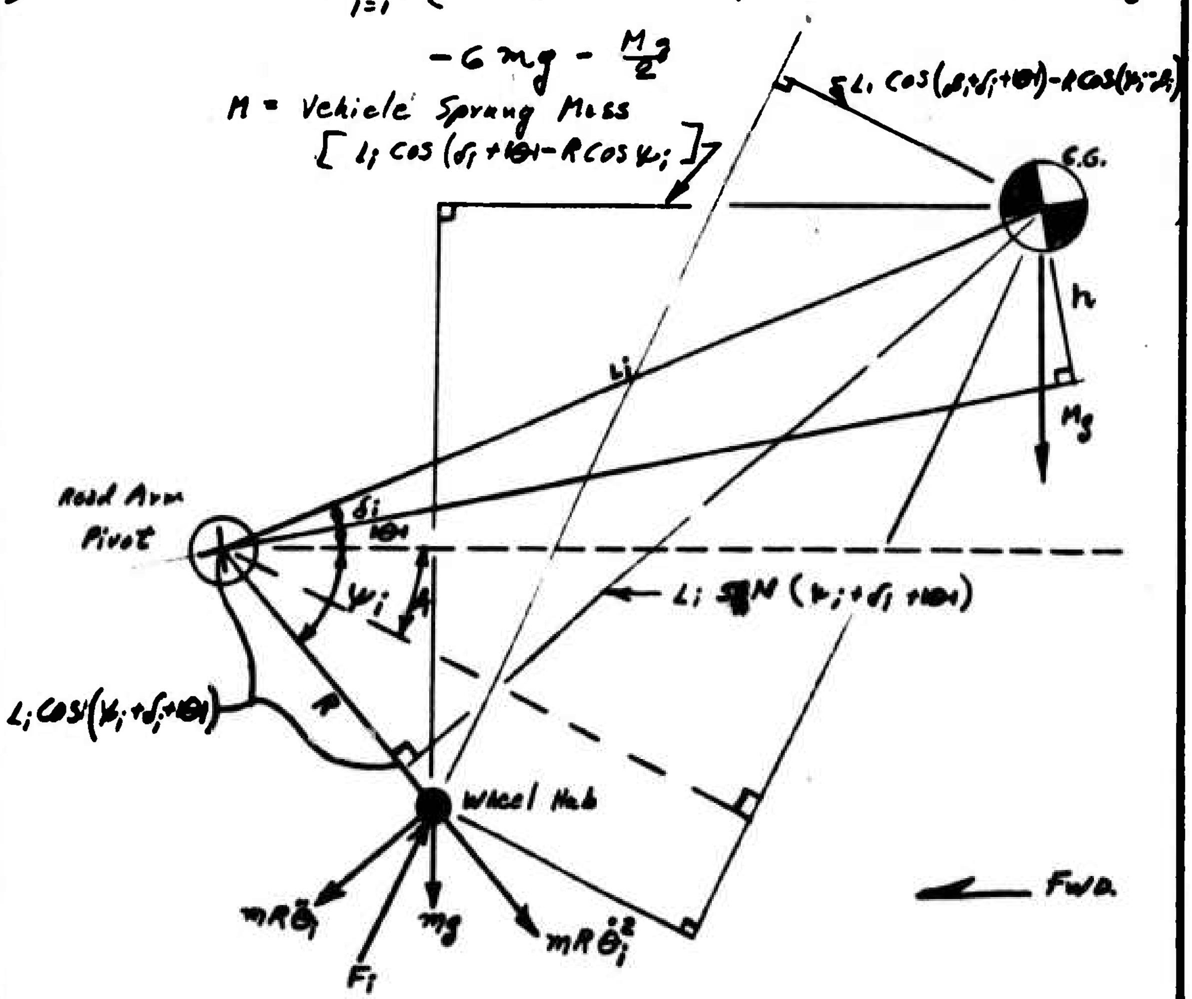

COMPUTER EQUATIONS

$\cos\beta_i$ in the ground force equation can be ignored in the simulation, since the value of K_g will make the wheel/ground loop very fast with respect to the other loops in the problem so that the range of $\cos\beta_i$ will have negligible effect at this point in the simulation. Use $\cos\beta_i = 1$

1] $$\frac{20F_m}{K_g R}\left[\frac{F_i}{2F_m}\right] = 100\left[\frac{X_i}{10R}\right] - 10\left[\frac{y_i'}{R}\right] - 10(\sin\theta_0)[1]$$

F_m = Normalizing Factor = M_g = 90000 Lb.

Using $\sin(|\Theta| + \delta_i) = \sin|\Theta|\cos\delta_i + \cos|\Theta|\sin\delta_i$, and noting that $|\Theta|$ is small: $\sin|\Theta| \approx |\Theta|$, $\cos|\Theta| \approx 1$,
$\sin(|\Theta| + \delta_i) \approx |\Theta|\cos\delta_i + \sin\delta_i$.

Define $y_i' = y_i - R\sin\theta_0$, $\qquad Y' = Y - L_i \sin\delta_i = Y - h$

2] $$\left[\frac{y_i'}{R}\right] = \left[\frac{Y'}{R}\right] - \operatorname{sgn} L_i\left(\frac{|L_i|\cos\delta_i\,\theta_m}{10R}\right)\left[\frac{|\Theta|}{.1\theta_m}\right] - [\sin\psi_i]$$

θ_m = Normalizing Factor = 90° or $\pi/2$ radians

3] $$10\left[\frac{\psi_i}{\theta_m}\right] = -10\left[\frac{\theta_i}{\theta_m}\right] - \left[\frac{|\Theta|}{.1\theta_m}\right]$$ and

$$\left[\frac{\psi_i - \beta_i}{\theta_m}\right] = -\left[\frac{\theta_i}{\theta_m}\right] - .1\left[\frac{|\Theta|}{.1\theta_m}\right] - 3\tfrac{1}{3}\left[\frac{\beta_i}{3\frac{1}{3}\theta_m}\right]$$

4] $$k\left[\frac{m\ddot{\theta}_i R}{k F_m}\right] = 2\left[\frac{F_i\cos(\psi_i - \beta_i)}{2F_m}\right] + k\left[\frac{R_i}{R}\right]\cdot\left[\frac{F_T}{kF_m}\right]$$
$$- \left(\frac{\alpha\,\theta_R}{F_m R}\right)[1] - \left(\frac{\alpha\,\theta_m}{F_m R}\right)\left[\frac{\theta_i}{\theta_m}\right] - \left(\frac{\alpha_B\,\theta_m}{F_m R}\right)\left[\frac{\widetilde{\theta_i - \theta_g}}{\theta_m}\right]$$
$$- k\sqrt{\frac{M_{iz}}{kF_m R}}\cdot\left|\sqrt{\frac{M_{iz}}{kF_m R}}\right| - K_\omega\left[\frac{\widetilde{\theta_i - \theta_j} + \widetilde{\theta_i - \theta_k}}{\theta_m}\right]$$

k = multiplier gain factor = 5.586 = 1/.1789

5] $$\left(\sqrt{\frac{F_m k}{F_G\cos\theta_0}}\,\frac{\dot{\theta}_g}{\theta_m}\right)\sqrt{\frac{M_{iz}}{kF_m R}} + \left(\sqrt{\frac{kF_m}{F_G\cos\theta_0}}\,\frac{\dot{\theta}_g' - \dot{\theta}_g}{\theta_m}\right)\sqrt{\frac{M_{iz}}{kF_m R}} = \frac{\dot{\theta}_i}{\theta_m},$$

$$\left|\sqrt{\frac{M_{iz}}{kF_m R}}\right| \le \sqrt{\frac{F_G\cos\theta_0}{kF_m}} \qquad c = 0$$

$$\le \sqrt{\frac{F_G'\cos\theta_0}{kF_m}} \qquad c = 1$$

COMPUTER EQUATIONS, CONT'D

6] $$.1\frac{d}{d\tau}\left[\frac{\dot\theta_i}{\dot\theta_n}\right] = 20\left[\frac{m\ddot\theta_i R}{k F_n}\right], \text{ Setting } \dot\theta_n = \frac{.01\, k F_n t_o}{2 m R}$$

Note $t_o \tau = t$ — time scale

7] $$.1\frac{d}{d\tau}\left[\frac{\theta_i}{\theta_n}\right] = 10\left(\frac{\dot\theta_n t_o}{10^2\,\theta_n}\right)\left[\frac{\dot\theta_i}{\dot\theta_n}\right]$$

8] $$\left(\frac{F_n k}{K_T R}\right)\left[\frac{F_T}{k F_n}\right] = \left(\frac{S_o}{R}\right)[1] + \left[\frac{S_1}{R}\right] + \left(\frac{11.35}{R}\right)\left[\frac{S_6}{11.35}\right] - \left(\frac{\rho V_s^2}{K_T R}\right)[1]$$
$$- K_s \underline{F_T}$$

9] $$k\left(\frac{R}{K\cdot 15}\right)\left[\frac{S_1}{R}\right] = k\left(.967 + \frac{\theta_i}{\theta_n}\right)\cdot\left[.256 - \frac{1}{2}\frac{\theta_2}{\theta_n}\right]$$

10] $$k\left[\frac{S_6}{1.083}\right] = -k\left[.967 + \frac{\theta_6}{\theta_n}\right]\cdot\left[.867 + \frac{\theta_5}{\theta_n}\right]$$

11] $$10\left(\frac{k}{10R}\right)\left[\frac{y_{i-1} - 2y_i + y_{i+1}}{2}\right] = \frac{y_{i-1}}{R} - 2\frac{y_i}{R} + \frac{y_{i+1}}{R}$$

or

$$10\left(\frac{.1k}{R\cos\theta_o}\right)\left[\frac{R_i}{R}\right] = \frac{y_{i-1}}{R} - 2\frac{y_i}{R} + \frac{y_{i+1}}{R} \qquad i = 2,3,4,5$$

where $R_i = R\cos\theta_o\left[\frac{y_{i-1}}{2} - \frac{2y_i}{2} + \frac{y_{i+1}}{2}\right]$

12] $$k\left(\frac{R}{9.5}\cdot\frac{64}{90}\cdot\frac{90}{90}\right)\left[\frac{R_1}{R}\right] = -k\left[.4 - \frac{\theta_2}{\theta_n}\right]\cdot\left[.9 + \frac{\theta_1}{\theta_n} - 2.7\,\frac{\theta_i + 13}{\theta_n}\right]$$

13] $$*\left(\frac{52R}{4.5 F_n}\right)\left[\frac{R_6}{R}\right] = 10\left(\frac{136}{900}\right)[1] + 10\left(\frac{52}{900}\right)\left[\frac{\theta_5}{\theta_n}\right] + \frac{\theta_6}{\theta_n} - 10\left(\frac{84}{320}\right)\left[\frac{\theta_6 + 38}{\theta_n}\right]$$

*NOTE: In equation 13 the term involving wheel weight has been dropped. This is a minor effect.

In equation 11 the simulation approximates the track tension radius by using the vertical component of static road-arm angle.

COMPUTER EQUATIONS, HULL DYNAMICS

The term $\cos(\beta_i + \delta_i + \Theta)$ in equation 17 can be expanded and then simplified using the approximations $\sin\Theta = \Theta$ and $\cos\Theta = 1$ for small values of Θ. This expression becomes $\cos(\beta_i + \delta_i) - \Theta \sin(\beta_i + \delta_i)$. The angle β_i is $0°$ on the level and $\approx +30°$ on an up ramp and $\approx -30°$ on a down ramp, so the angle functions can be switchable gains in the simulation. The presence of Θ would normally require a multiplication, since F_i appears as a multiplier. $|\Theta|$, however is less than .1, and on wheels #1 and #6 (and possibly #2) where F_i can be large due to damping forces the angle $(\beta_i + \delta_i)$ is of magnitude less than 45°, so that the term with the factor Θ represents less than 10% of the other. We can further simplify by using $\cos(\beta_i + \delta_i + \Theta) \approx \cos(\beta_i + \delta_i) - \Theta \sin(\beta_i + \delta_i) \approx \cos(\beta_i + \delta_i)$

$$\left[\frac{F_i}{2F_m}\cos(\beta_i + \delta_i + \Theta)\frac{L_i}{L_m}\right] \cong \left(\frac{L_i}{L_m}\cos\delta_i\right)\left[\frac{F_i}{2F_m}\right] - \left(\frac{L_i}{L_m}\left(\cos\delta_i - \cos(\beta_o + \delta_i)\right)\widetilde{\operatorname{sgn}\beta_i}\right)\left[\frac{F_i}{2F_m}\right] + \left(\frac{L_i}{L_m}\left(\cos\delta_i - \cos(-\beta_o + \delta_i)\right)\widetilde{\operatorname{sgn}\beta_i}\right)\left[\frac{F_i}{2F_m}\right] \tag{18}$$

where $\beta_i = \beta_o$ when $\operatorname{sgn}\beta_i$ (+)

$\beta_i = -\beta_o$ when $\operatorname{sgn}\beta_i$ (−)

$\beta_o = 30°$

L_m = Normalizing factor − use max. value of $|L_i|$

COMPUTER EQUATIONS, HULL DYNAMICS, CONT'D

By the use of a simulation of the behavior of a single suspension unit it has been determined that the two terms in equation 12 which contain Θ_i derivatives and angle functions may be replaced by a single term containing $\ddot{\Theta}_i$ with no changes in effect due to hull or road-arm angles.

The term involving the weight of wheel and roadarm is of little significance, Dynamically.

15] $$\left[\frac{I\ddot{\Theta}_1}{4F_nL_m}\right] = \sum_1^6 \left[\frac{F_i}{2F_n}\cos(\beta_i+\psi_i+\Theta_1)\frac{L_i}{L_m}\right] + \sum_1^6\left(\frac{R}{L_m}\right)\left[\frac{F_i}{2F_n}\cos(\psi_i+\beta_i)\right] + \sum_1^6\left(\frac{kC_iD_i}{4L_m}\right)\frac{mR\ddot{\Theta}_i}{kF_n}$$

16] $$\left[\frac{F_i}{2F_n}\cos(\psi_i-\beta_i)\right] = \left[\frac{F_i}{2F_n}\right]\cdot\left[\cos(\psi_i-\beta_i)\right]$$

17] $$.1\frac{d}{dt}\left[\frac{4\dot{\Theta}_1}{.1\,\dot{\Theta}_n}\right] = \left(\frac{16F_nL_mt_0}{\dot{\Theta}_nI}\right)\left[\frac{I\ddot{\Theta}_1}{4F_nL_m}\right]$$

18] $$.1\frac{d}{dt}\left[\frac{\Theta_1}{.1\,\Theta_n}\right] = 2\left(\frac{.1\,\dot{\Theta}_nt_0}{8\,\Theta_n}\right)\left[\frac{4\dot{\Theta}_1}{.1\,\dot{\Theta}_n}\right]$$

Similarly, the $\ddot{\Theta}_i$ and $\dot{\Theta}_i^2$ terms in the equation for vertical motion of the hull may be replaced with a single term involving $\ddot{\Theta}_i$ with constant coefficients in the simulation.

19] $$\frac{F_i\cos\beta_i}{2F_n\cos\beta_0} = \frac{F_i}{2F_n} + \left(\frac{1-\cos\beta_0}{\cos\beta_0}\right)\frac{F_i}{2F_n}\left(1-\frac{|\beta_i|}{\beta_0}\right)$$

COMPUTER EQUATIONS, HULL DYNAMICS, CONT'D

20] $$10\left(\frac{.1}{\cos\beta_0}\right)\left[\frac{M\ddot{Y}'}{4F_n}\right] = \sum_1^6 \left[\frac{F_i\cos\beta_i}{2F_n\cos\beta_0}\right] - \sum_1^6 \left(\frac{\ell\cos\beta}{4\cos\beta_0}\right)\left[\frac{m\ddot{\theta}R}{\ell F_n}\right] - \left(\frac{6\,mg}{2F_n\cos\beta_0}\right)[1] - \left(\frac{Mg}{4F_n\cos\beta_0}\right)[1]$$

21] $$\frac{d}{d\tau}\left[\frac{\dot{Y}'}{.2R\dot{\theta}_n}\right] = 10\left(\frac{2F_n t_0}{MR\dot{\theta}_n}\right)\left[\frac{M\ddot{Y}}{4F_n}\right]$$

22] $$\frac{d}{d\tau}\left[\frac{Y'}{R}\right] = 20\left(\frac{.2\dot{\theta}_n t_0}{20}\right)\left[\frac{\dot{Y}'}{.2R\dot{\theta}_n}\right]$$

TORQUES PRODUCED BY TRACK TENSION ON SUSPENSION UNITS #1 AND #6

The track tension force puts a load on the individual wheels which can be translated into a torque about the road-arm pivot points. Thus there can be said to be an effective radius, dependent upon wheel position and track angle which when multiplied by track tension will produce this torque as a product. Figures 3 and 4 contain plots of this radius against road-arm position (referred to full rebound) for wheels 1 and 6, respectively. Curves are shown for two positions of the adjacent wheels. The geometry used in deriving these curves was a mean between nominals for right and left hand suspension systems for the MICV-70 test rig.

Consider figure 3. The effective radius shown here includes the effect of the track tension on the front idler acting through the linkage to the front suspension unit. The appearance of the two curves shown suggests that the variation in track angle between wheels 1 and 2 due to the position of wheel 2 may be simulated by using wheel 2 position in a factor which decreases in size with increase in the wheel 2 road-arm angle.

The basic curve form on figure 3 was taken in the approximation for simulation to be triangular. The apex occurs at approximately 65° above the rebound stop, which corresponds to −13° in the simulation. A value of 9.5 was used as an apex value for #2 wheel in static position. The factor involving #2 wheel position was given a value of 1.0 at static position and approximately 0.2 at full jounce. The slopes were chosen to approximate those of the curve for #2 wheel, in static position. We have

$$R_1 = 9.5\left(.45 - \frac{\theta_2}{80}\right)\left(1 - \frac{\theta_1 + 13^\circ}{40^\circ} + \frac{\theta_1 + 13^\circ}{68^\circ}\right)$$

TORQUES PRODUCED BY TRACK TENSION ON SUSPENSION UNITS #1 AND #6.

Now consider figure 4. These curves suggest that the effect of the track angle between wheels 5 and 6 is to shift the vertical location of the curve as a whole. For the simulation this shift was assumed to be linear with the position of #5 road-arm. As with wheel #1 the approximation substitutes a triangular form for the curves. The vertical location of the triangle is determined by the position of wheel #5. The apex of these triangles was set at 44° above the rebound stop or −32° in the simulation. A value of 4.5 for R_6 was taken at this location with wheel #5 at static position, and a value of 11 with wheel #5 at full jounce. Approximating the slopes, we have

$$R_6 = 4.5\left(2 + \frac{\theta_5}{44} - \frac{\theta_6 + 32}{32} + \frac{\theta_6 + 32}{52}\right)$$

For the simulation a sign must be associated with these Radii to give the correct sense to the torque.

TRACK STRETCH DUE TO MOTION OF WHEELS 1 AND 6

The same curves used to determine the effective radius for the track tension at wheels 1 and 6 may be used to develop a relationship between track stretch and the wheel positions. At any point (θ, R) on the curves, with θ now expressed in radians, the amount the track has stretched from the θ_0 position may be expressed as

$$\Delta S = \frac{1}{\theta - \theta_0} \int_{\theta_0}^{\theta} R \, d\theta$$

This gives the average ordinate over the interval

The equations developed to linearize this relation for the simulation are

$$s_1 = 7.0 \left(1 + \frac{\theta_1}{78}\right)\left(1 - .75 \, \frac{44 + \theta_2}{67.5}\right)$$

$$s_6 = -3.6 \left(1 + \frac{\theta_6}{78}\right)\left(1 + 2 \, \frac{44 + \theta_5}{68}\right)$$

where s_1 and s_6 changes in length from static conditions.

INERTIA FORCES ON A TRACK FREE OF GROUND CONTACT

Consider for this derivation an interior (that is neither a front nor a back) wheel of a tracked vehicle. Assume a vehicle forward speed V_s. Assume also a no-slip condition between ground and track, so that V_s is also the track speed relative to the hull.

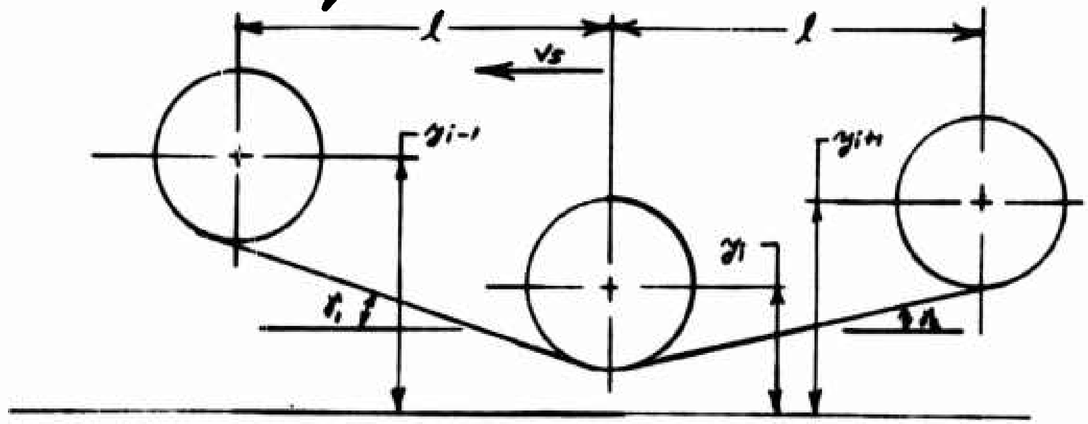

The downward velocity of points on the track ahead of the i^{th} wheel and out of wheel contact is $V_s \sin\theta_1$. The upward velocity of points just behind the i^{th} wheel and out of wheel contact is $V_s \sin\theta_2$. The change in vertical velocity is then $V_s(\sin\theta_2 + \sin\theta_1)$. The rate of momentum change going around the i^{th} wheel is therefore $\dot{m} V_s (\sin\theta_2 + \sin\theta_1)$ where $\dot{m}$ is equal to ρV_s and ρ is the mass density / unit length of track. This gives $\rho V_s^2(\sin\theta_2 + \sin\theta_1)$ as the force required to effect this change of momentum.

$$\sin\theta_1 = \frac{y_{i-1} - y_i}{\sqrt{l^2 + (y_{i-1} - y_i)^2}} \quad , \quad \sin\theta_2 = \frac{y_{i+1} - y_i}{\sqrt{l^2 + (y_{i+1} - y_i)^2}}$$

If $y_{i-1} - y_i$ & $y_{i+1} - y_i$ are small with respect to l, we can approximate this by substituting the tangent and write for the momentum force:

$$F_I = \rho V_s^2 \left[\frac{y_{i-1} - 2y_i + y_{i+1}}{l} \right]$$

TRACK TENSION FORCES ON INTERIOR WHEELS

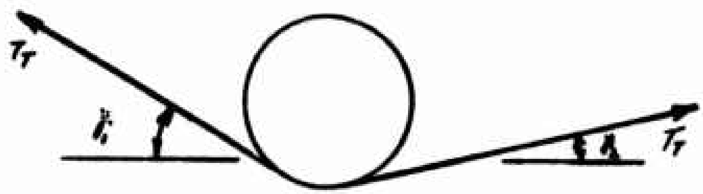

For the configuration shown above, the vertical component of the track tension force 'T_T' acting on the wheel can be seen to be

$$F_T = T_T \left(\sin \beta_2 + \sin \beta_1 \right)$$

This can be seen to be of the same form as that for the track momentum (inertia) force, so that the momentum force can be interpreted as a modification of the effect of the track tension on any wheel.

For the interior wheels for $y_{i-1} - y_i$ and $y_{i+1} - y_i$ small with respect to ℓ (Ref. previous page), we can substitute the tangent for the sine.

$$F_T \approx T_T \left(\frac{y_{i-1} - 2y_i + y_{i+1}}{\ell} \right)$$

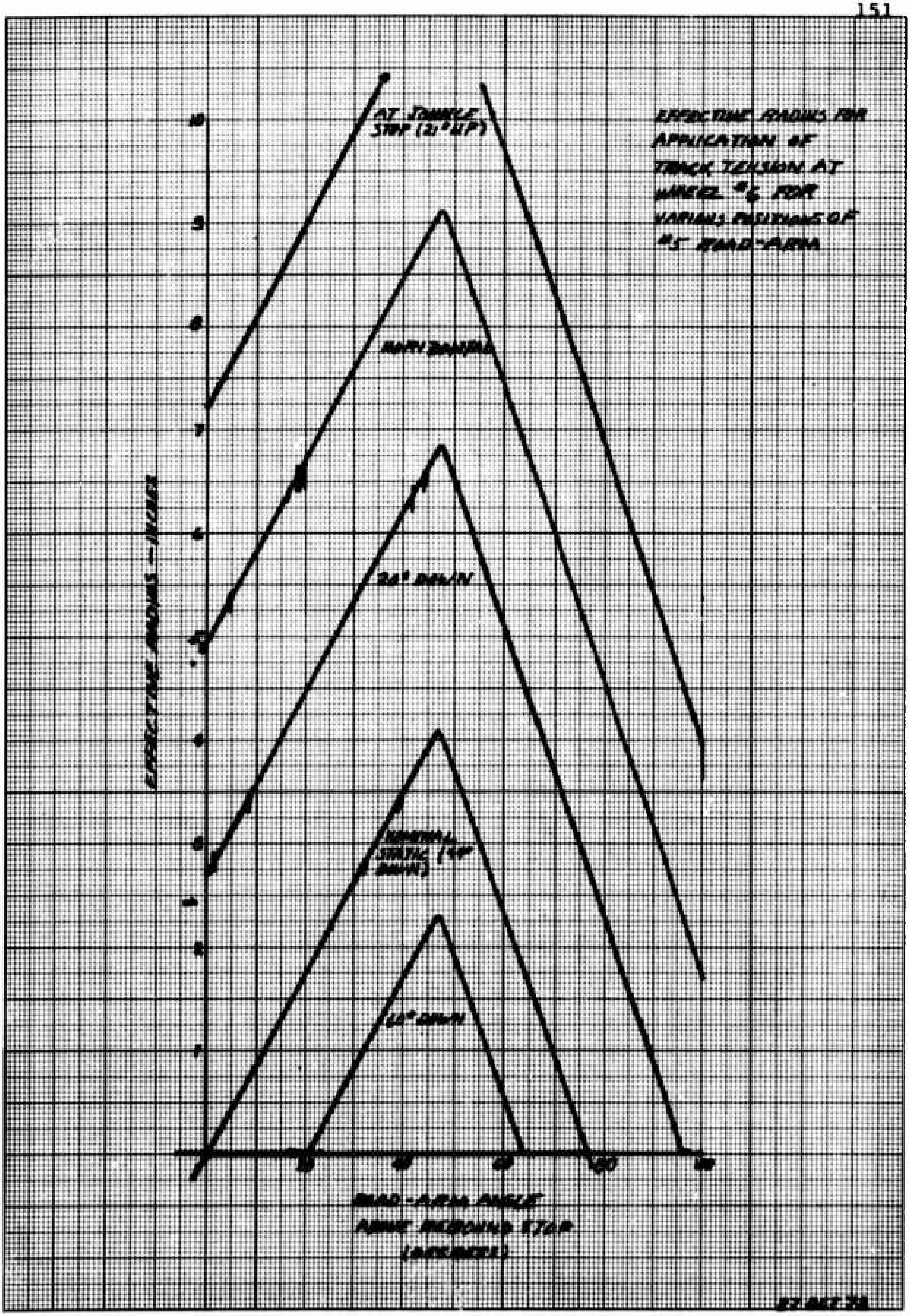
EFFECTIVE RADIUS FOR APPLICATION OF TRACK TENSION AT WHEEL #6 FOR VARIOUS POSITIONS OF #5 ROAD-ARM
AT JOUNCE STOP (21° UP)
HORIZONTAL
20° DOWN
NOMINAL STATIC (4° DOWN)
ROAD-ARM ANGLE ABOVE REBOUND STOP (DEGREES)

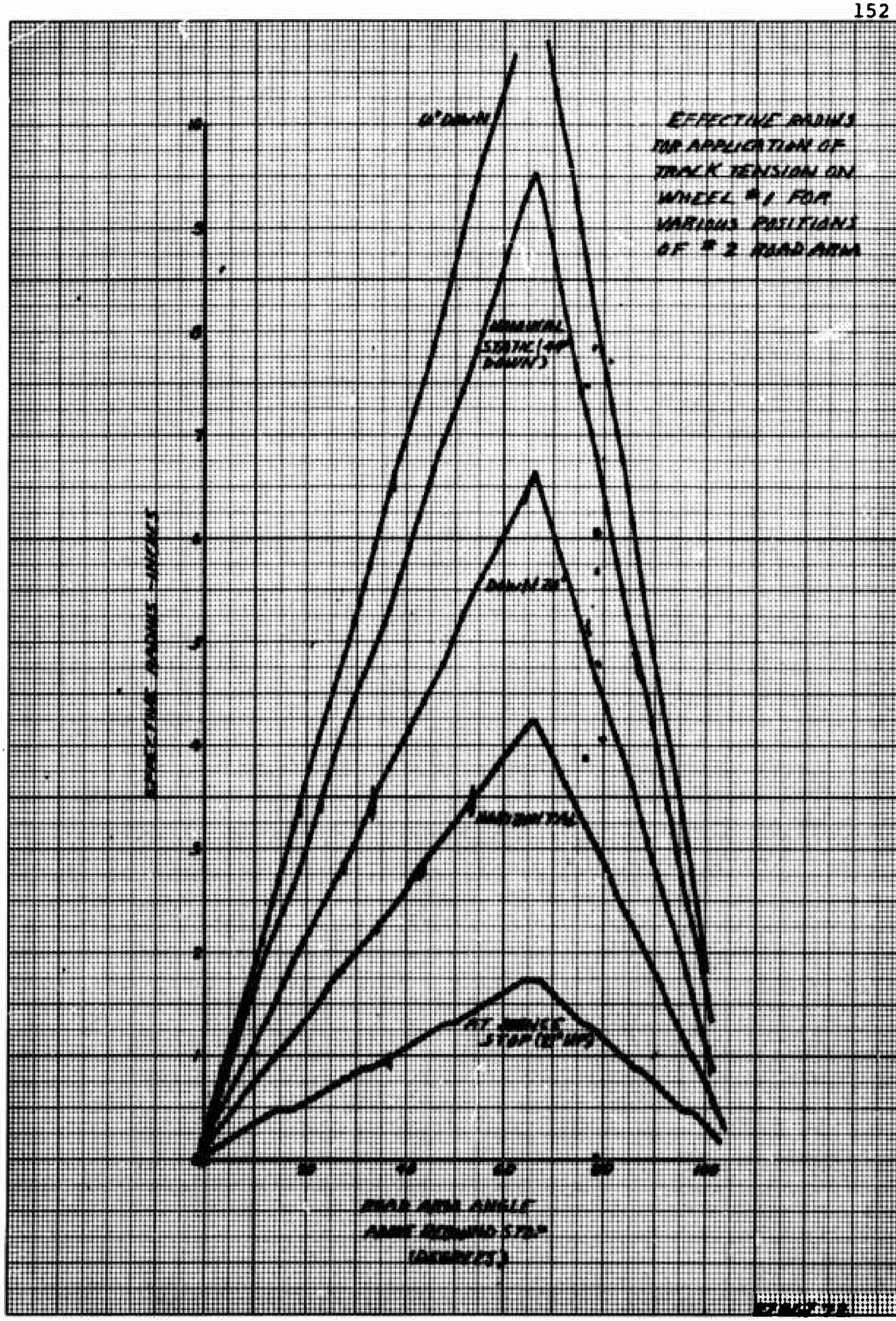
EFFECTIVE RADIUS FOR APPLICATION OF TRACK TENSION ON WHEEL #1 FOR VARIOUS POSITIONS OF #2 ROAD ARM
EFFECTIVE RADIUS - INCHES
20
40
60
80
100
ROAD ARM ANGLE
ABOVE REBOUND STOP
(DEGREES)

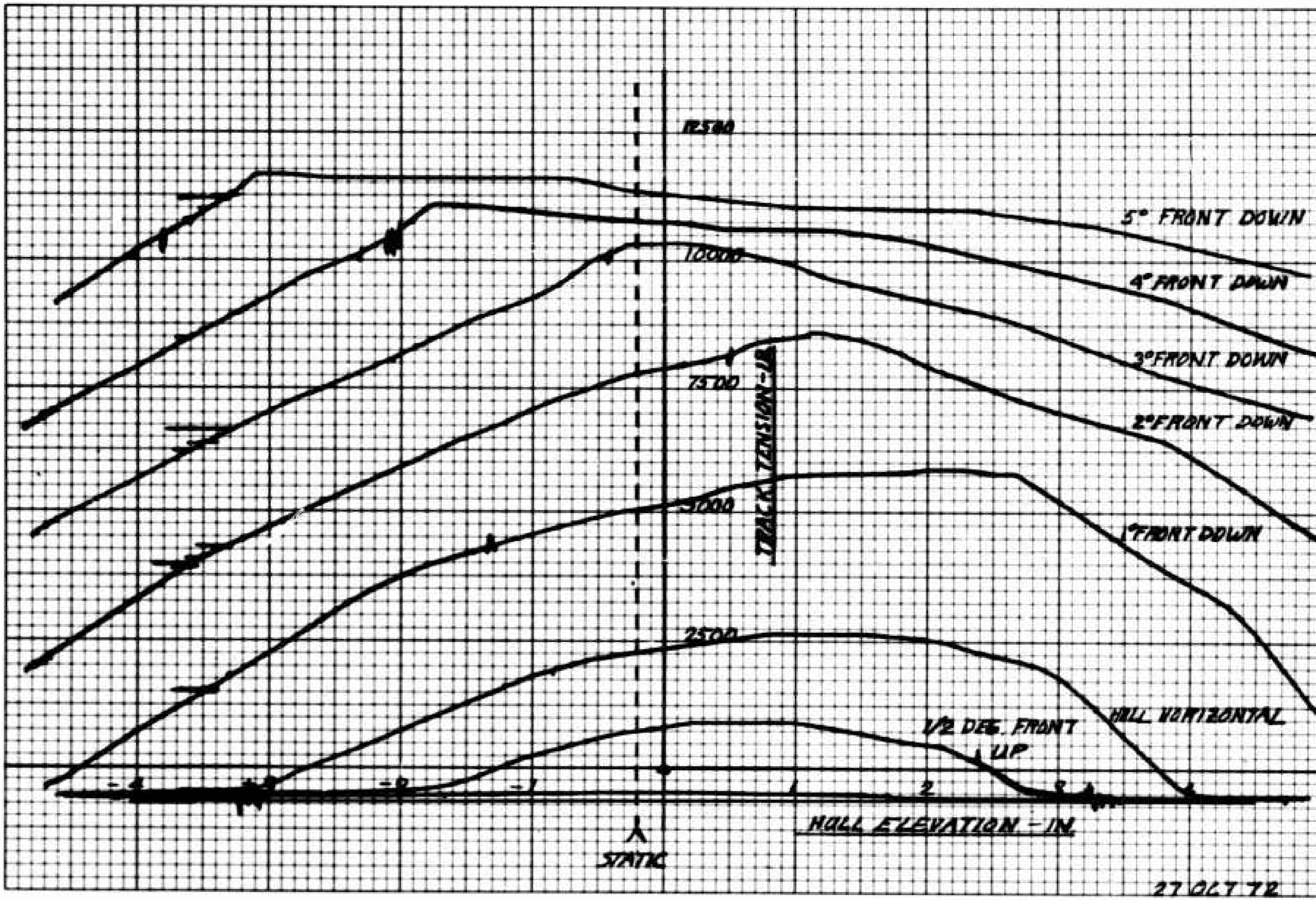
12500
10000
7500
5000
2500
TRACK TENSION - LB
5° FRONT DOWN
4° FRONT DOWN
3° FRONT DOWN
2° FRONT DOWN
1° FRONT DOWN
HULL HORIZONTAL
1/2 DEG. FRONT UP
-4
-3
-2
-1
1
2
3
4
STATIC
HULL ELEVATION - IN.
27 OCT 72

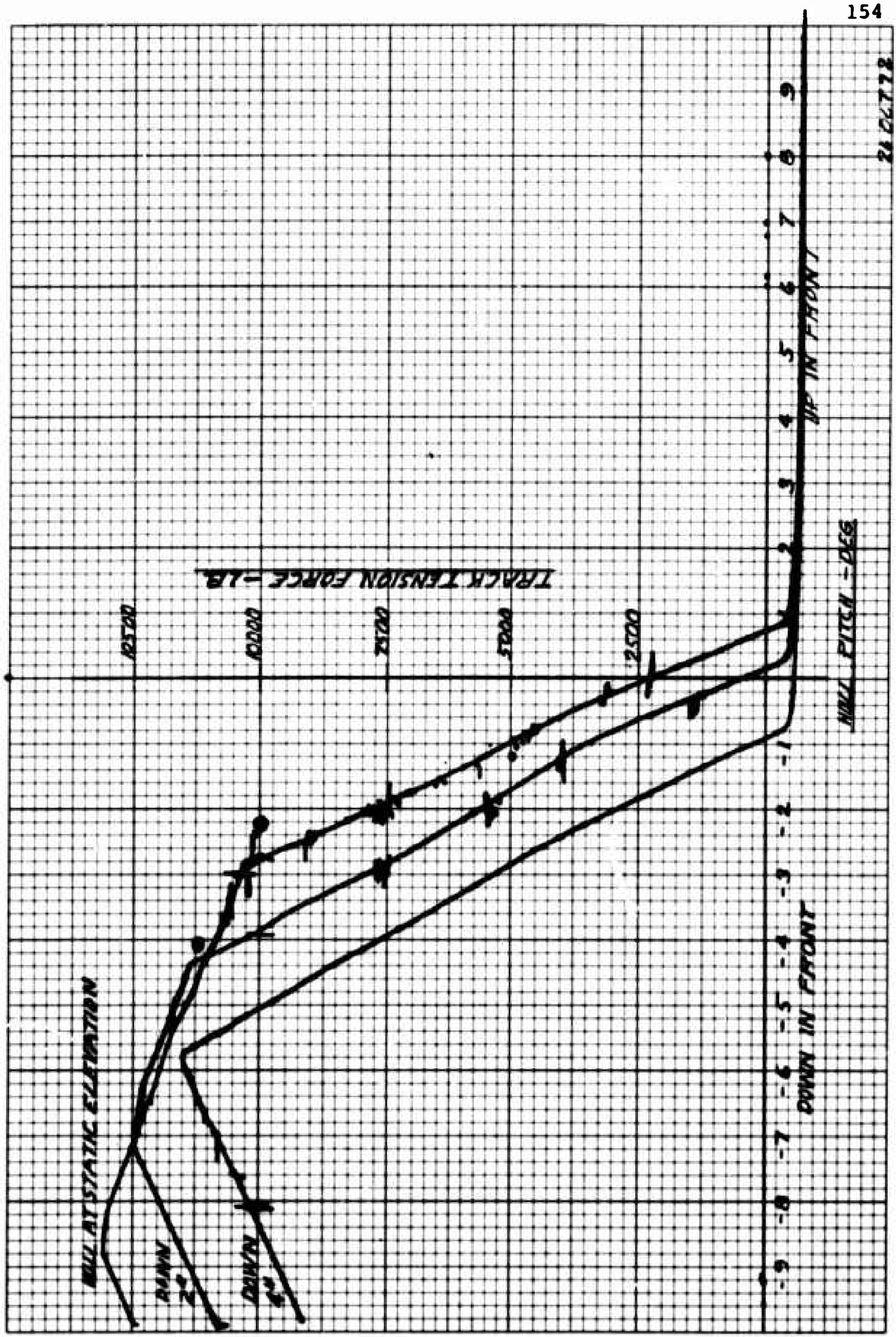
HULL AT STATIC ELEVATION
DOWN 2"
DOWN 4"
TRACK TENSION FORCE — LB
12500
10000
7500
5000
2500
HULL PITCH — DEG
DOWN IN FRONT
UP IN FRONT
-9 -8 -7 -6 -5 -4 -3 -2 -1
1 2 3 4 5 6 7 8 9
24 OCT 72

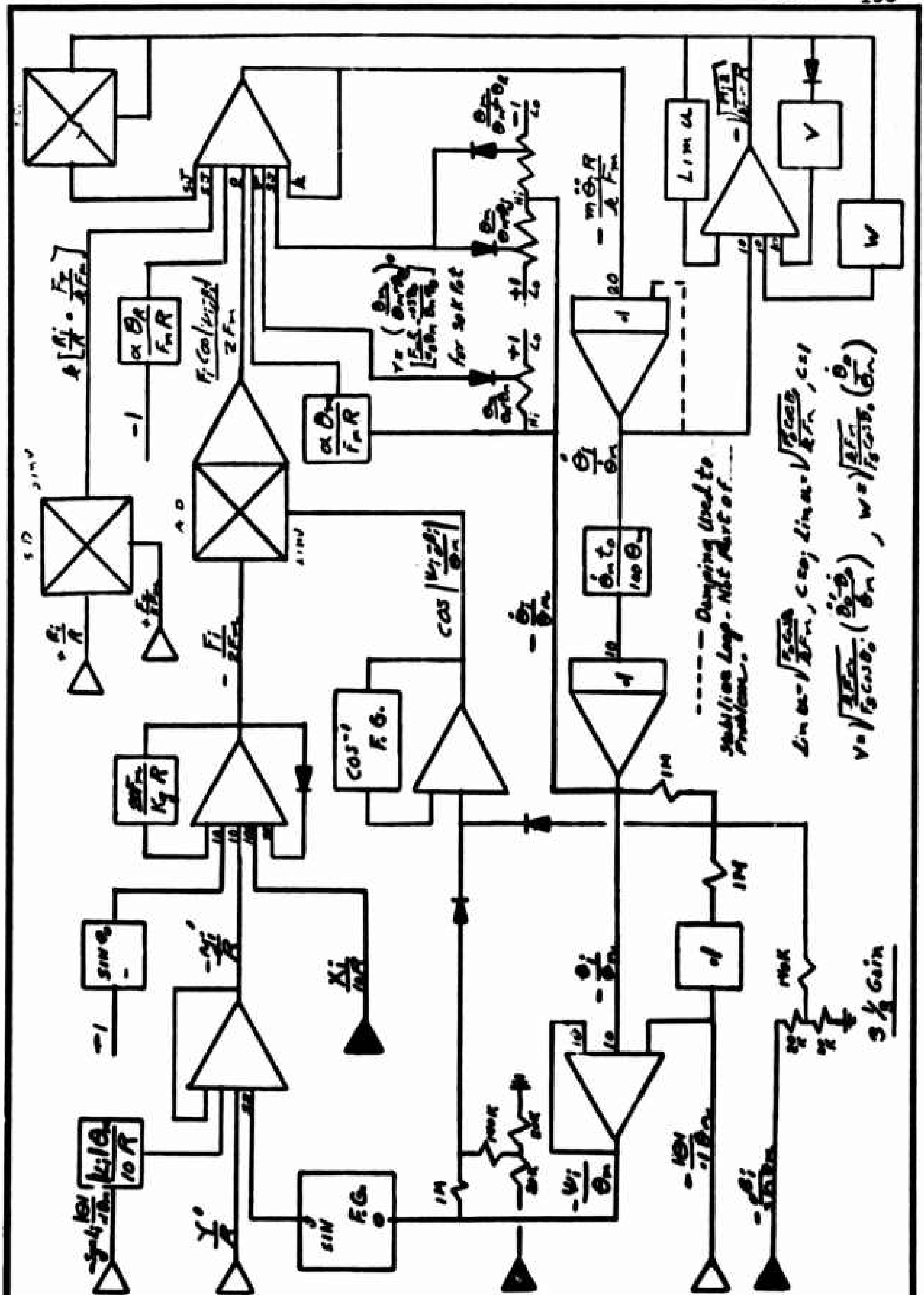
COS⁻¹ F.G.
F.G. SIN
Lim α
V
W
3 ½ Gain

Effective Track Tension Radius

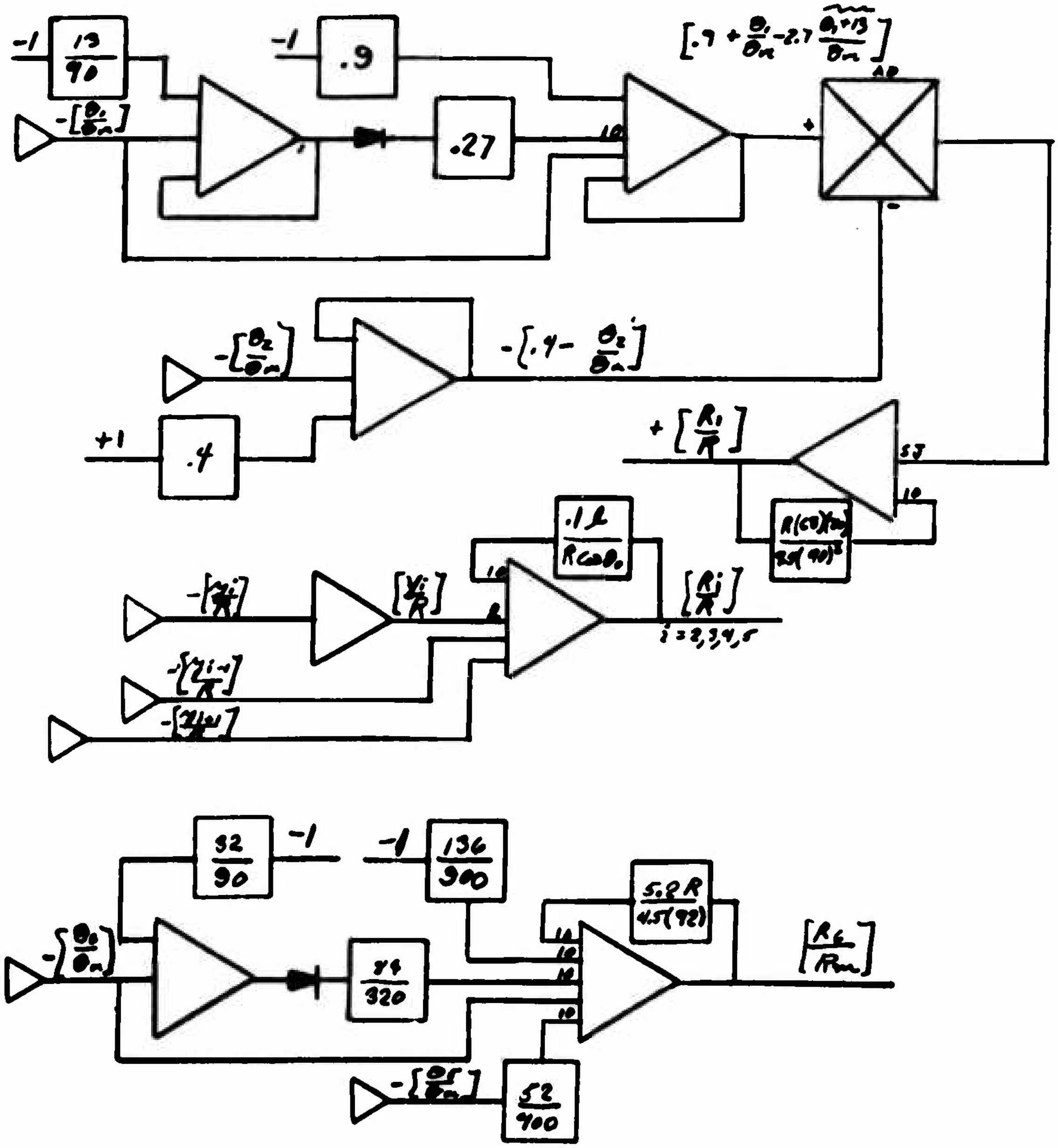

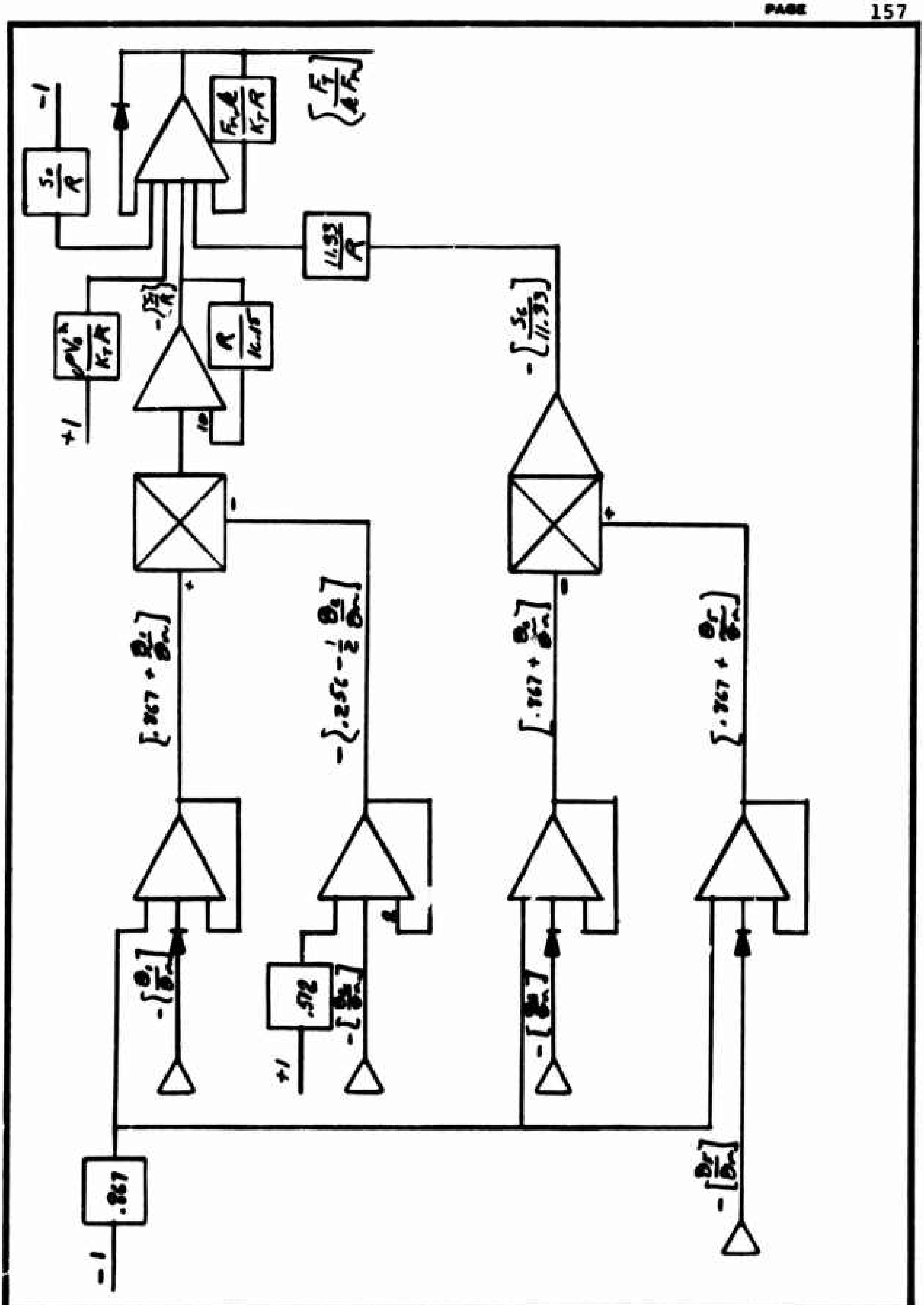

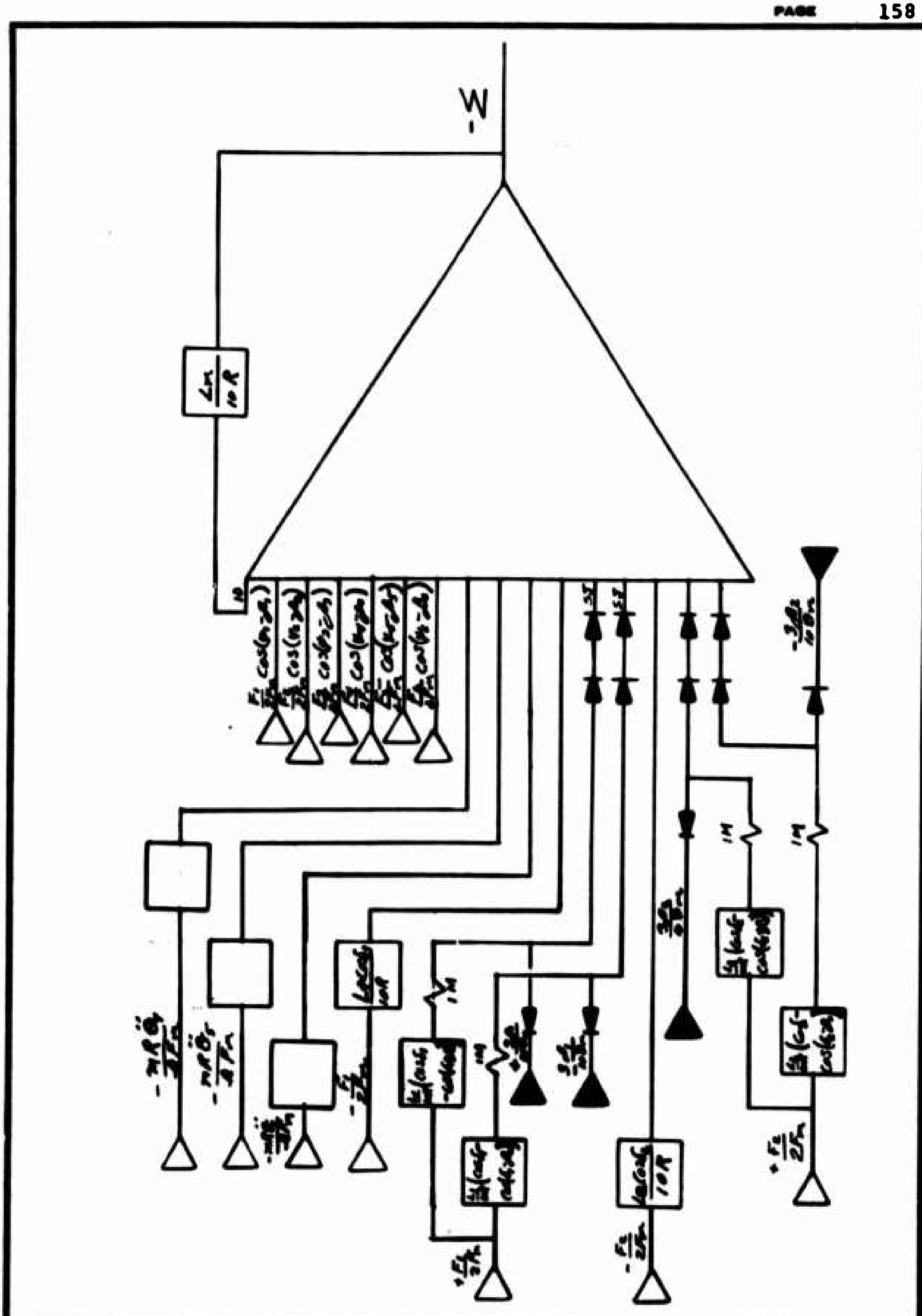

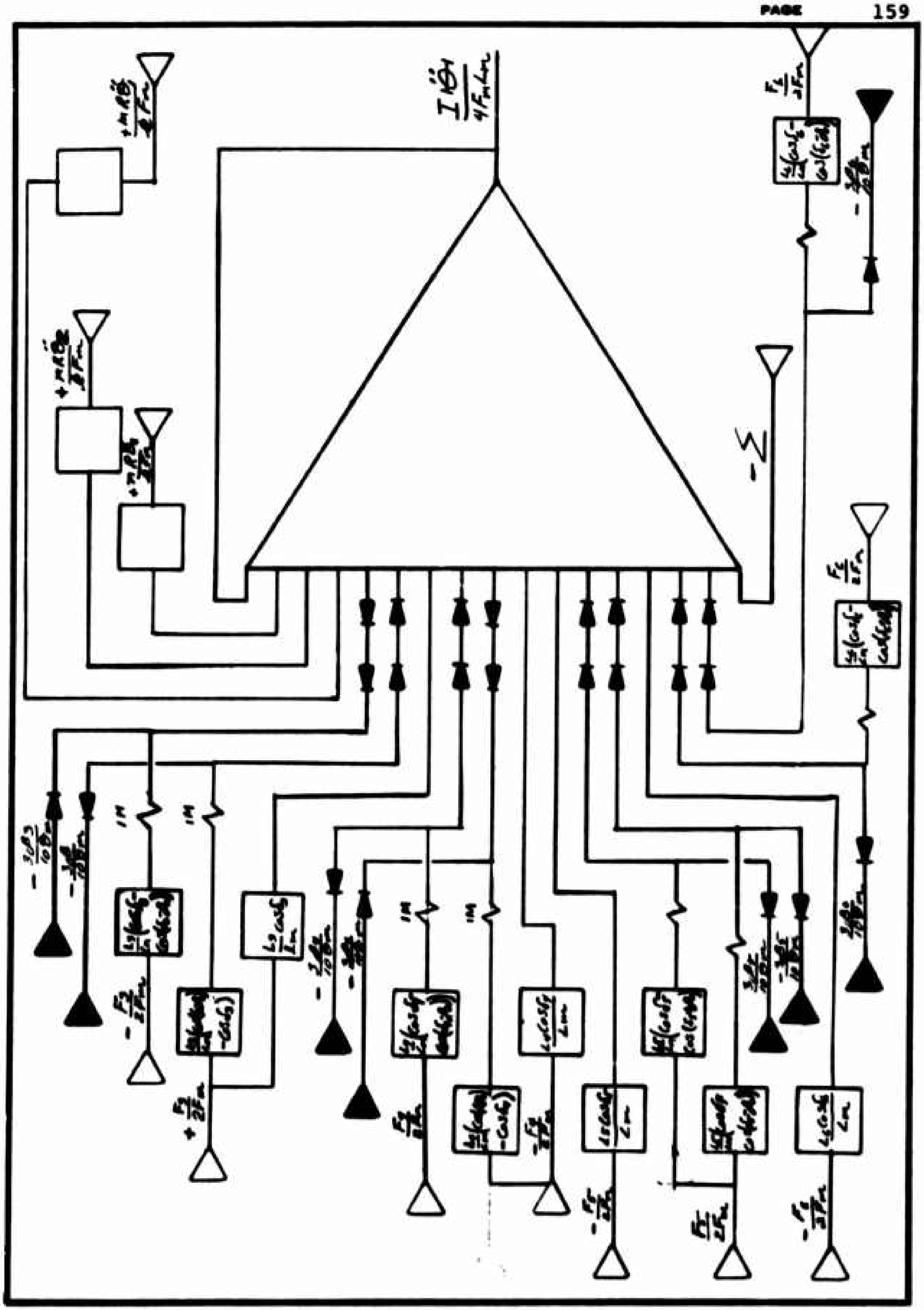

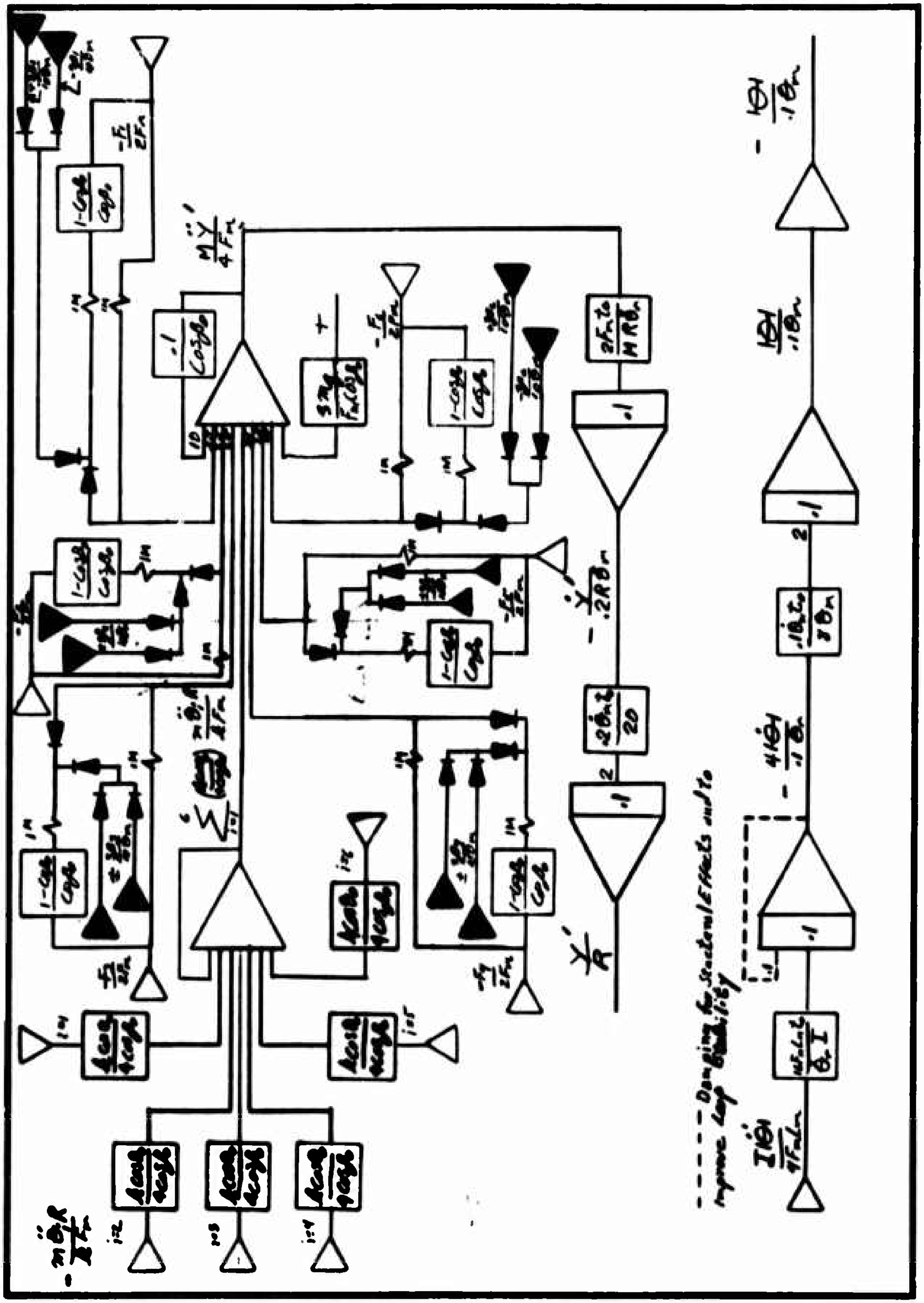

CIRCUIT VARIATIONS USED

Adaptive Damping (Pitch Rate)

Wheel #1

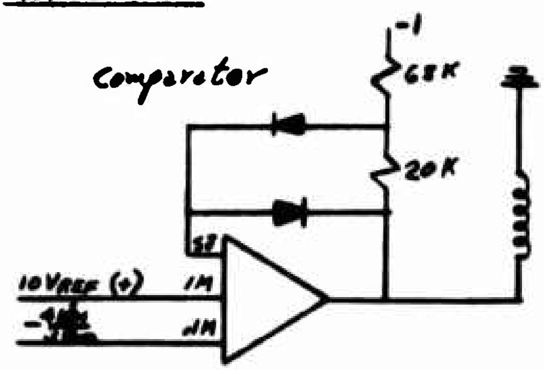

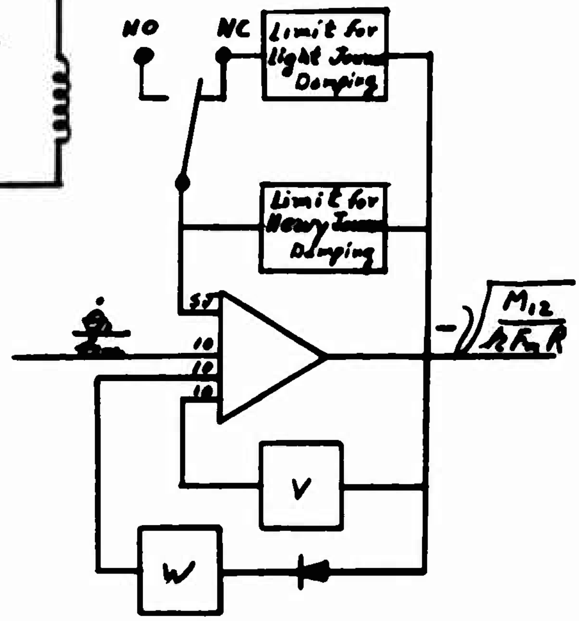

For Pitch Down Rates Greater than $\frac{\cdot 1.0\,\dot{\theta}_m V_{REF}}{400}$, the Light Damping Limit is Shut Off.

Note: Pitch-Up → $|\dot{\theta}|$ has a Negative Sign
Pitch-Down → $|\dot{\theta}|$ has a Possitive Sign

Wheel #6

The arrangement is similar to the above, except:

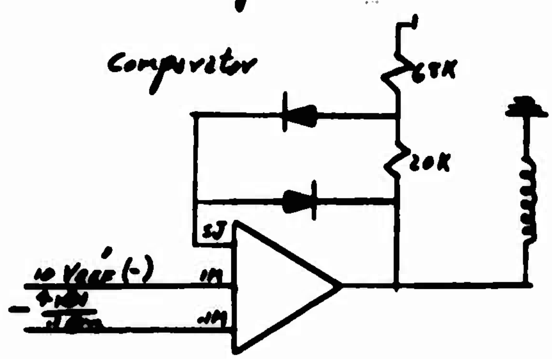

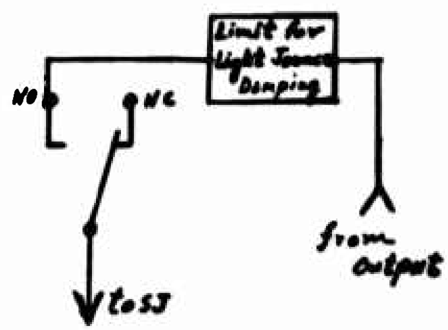

For Pitch Up Rates Greater than $\frac{\cdot 1.0\,V_{REF}}{400}$, the Light Damping Limit is Shut Off.

CIRCUIT VARIATIONS USED

Adaptive Damping (Pitch Rate + Heave Rate)

The circuits used to provide adaptive damping using heave rate in addition to pitch rate were the same as for pitch rate use alone, except that heave rate was summed with pitch rate. In the case of wheel #1 the normal sign of heave rate was used (heave rate = $\dot{Y}$, and is positive upward), so that a rising hull tended to keep the damping at a low level. The same requirement exists for wheel #6, but because of the difference in the use of the comparator, the inverse (−) sign of $\dot{Y}$ had to be used.

Heave rate was summed with pitch rate at various levels and thresholds (V_{REF} and V'_{REF}). Recorded Data was run with

$$\frac{9R}{L_w}\frac{\dot{Y}}{.2R\theta_n} - \frac{4\dot{\theta}_1}{.1\theta_n} < V_{REF}$$

shutting off low limit damping on wheel #1 and

$$-\left[\frac{9R}{L_w}\frac{\dot{Y}}{.2R\theta_n} + \frac{4\dot{\theta}_1}{.1\theta_n}\right] \geq V'_{REF}$$

shutting off low limit damping on wheel #6

L_w = wheel base = 168.5 in.
$V_{REF} = V'_{REF} = 0$ seemed to be the best choice

CIRCUIT VARIATIONS USED

Ground / Track / Road Wheel Interface Damping

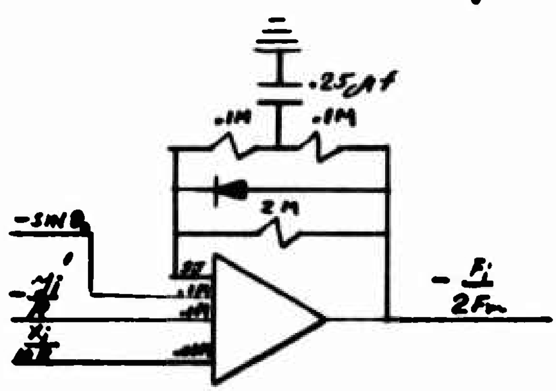

Equation

$$10\frac{y_i}{R} - 100\frac{x_i}{10R} + 10\,\sin\theta_0 = -\left[5.5\left(1+\frac{.0185S}{11}\right)\Big/\left(1+.0125S\right)\right]\frac{F_i}{2F_m}$$

Ignoring the constant part of the equation and defining $\Delta x = x_j - y_j$, we have

$$\Delta F_j = \frac{20F_m}{5.5R}\left[\frac{1+.0125S}{1+.00187}\right]\Delta x_j$$

The form desired for damping is

$$\Delta F_j = K_g\,\Delta x_j + C_g\,\Delta\dot{x}_j$$

Considering only the load term:

$$K_g = \frac{20F_m}{5.5R} = \frac{20(40000)}{5.5(15)} = \frac{800000}{82.5} = 9696.97\ \text{lb/in}$$

$$C_g = \frac{20(40000)(.0125)}{5.5(15)} = \frac{10000}{82.5} = 121.21\ \text{lb sec/in}$$

Damping Ratio (Ignoring torsion bar)

$$\zeta = \frac{C_g}{2\sqrt{K_g m}} = \frac{121.12}{2\sqrt{9696.97(.7)}} = \underline{.795}$$

PARAMETER AND NORMALIZING FACTOR VALUES

α	1000 IN.-LB./DEG., NOM., 750, 900, 1100, 2000 USED
α_B	6200 IN.-LB/DEG.
β_0	30 DEG.
δ_1	6.65 DEG.
δ_2	10.81 DEG.
δ_3	26.38 DEG.
δ_4	-38.08 DEG.
δ_5	-12.41 DEG.
δ_6	-7.14 DEG.
F_D	VARIOUS VALUES
F_D'	VARIOUS VALUES
F_m	40000 LB.
F_s	3333 1/3 LB.
g	386 IN./SEC^2
h	10.1 IN.
I	581000 IN.LB.SEC^2
k	2586
K_g	9697. LB/IN. ALSO USED 8889, 17777 LB./IN.
K_T	3000 LB./IN.
L_1	87.1979 IN.
L_2	54.308 IN.
L_3	22.728 IN.
L_4	-16.375 IN.
L_5	-46.987 IN.
L_6	-82.5095 IN.
ℓ	83 IN.
L_m	87.1979 IN.
m	.7 LB SEC^2/IN
M	103.6 LB SEC^2/IN.
ρ	70 LB./FT.
R	15 IN.
S_0	ADJUSTED TO LEVEL TANK AT REFERENCE SPEED
θ_c	78° NOM. DEPENDS ON α, θ_0, M, R
θ_J	21 DEG.
θ_R	78 DEG.

PARAMETER AND NORMALIZING FACTOR VALUES

θ_m	90 DEG. ($\pi/2$ RAD.)
θ_0	44° NOM., ALSO 39, 49 DEG.
$\dot{\theta}_0$	.322 RAD/SEC (.05 IN. ORIFICE)
$\dot{\theta}_0'$	17.65 RAD/SEC (.368 IN ORIFICE)
$\dot{\theta}_m$	68.304 RAD/SEC.
t_0	1
V_s	5, 10, 15, 20, 25, 30, 35 MPH, etc.

DAMPERS:

$PAR_A = F_D R \cos\theta_0$ DAMPER TORQUE

A	7.45 $IN.^2$ VANE AREA
R_A	3.179 IN. EFFECTIVE RADIUS.

$\dot{\theta} A R_A = 100 A_0 \sqrt{P}$ $P \leq$ LIM.

$A_0 = \pi/4 \, (D_0)^2$ ORIFICE AREA

D_0	.05 IN (ALSO .0582, .099 IN) BLEED
	.368 IN (ALSO .877 IN.) REBOUND ORIFICE

HULL INPUT APPROXIMATION FOR $\ddot{\theta}_I$ AND $\dot{\theta}_I$

C_1	1.0
C_2	.944
C_3	.888
C_4	.832
C_5	.776
C_6	.720
D_1	75.821 IN.
D_2	42.571 IN.
D_3	9.571 IN.
D_4	23.679 IN.
D_5	56.679 IN.
D_6	92.679 IN.

APPENDIX C

RATE GYRO SPECIFICATIONS NWL MODEL 925064

NWL PROCUREMENT SPECIFICATION	PS-333 February 1973

NATIONAL WATER LIFT CO., A Division of PneumoDynamics Corporation, KALAMAZOO, MICHIGAN

RATE GYRO SPECIFICATIONS
NWL Model No. 925064

Prepared by:

Checked by: W. J. Lubitz

Approved by:

C/C:

Released: Feb 5 73

R E V I S I O N S

LTR.	BY - DATE	PARA. OR PAGES	DESCRIPTION OF CHANGE
A	Taylor 2/16/73	8.3 9.7 12.2 15.0 18.1 8.5 & 8.6 8.10	36 ma was 75 ma; 17 ma was 15 ma. WVDC was WVD 0.075% max was 0.05% Was "Alignment of gyro in mount" ±70 deg/sec was ±10 deg/sec. Add winding Add (NWL to supply capacitor) Per ECO 62039
B	Taylor 6/19/73	1.0 8.6 8.10	Was Type: GR-G5-AH7 IS: GR-G5A-1.74N Was 1375+ j 6780 IS: 625 + j 3550 Was TBD IS: 0.22± 10% capacitor PER ECO 63149

REVISION LETTER OF THIS SPECIFICATION MUST APPEAR ON ITS APPLICABLE SOURCE CONTROL DRAWING

1.0 This specification covers Northrop Type GR-G5A-1.74N gyro. B

2.0 TEMPERATURE RANGE

2.1 Operating: -25°F to +165°F

2.2. Storage: -70°F to +165°F

3.0 NOMINAL RATE RANGE: ±100°/sec

4.0 STOPS SET AT: 100 to 120°/sec

5.0 OVER-RANGE: 500°/sec with no change in characteristics

6.0 NATURAL FREQUENCY: 55Hz nominal

7.0 SCALE FACTOR

7.1 At room temperature, measured at ±10°/sec: 54 to 60 MV/°/sec

7.2 Scale factor change with temperature: 0.02%/°F

8.0 PICKOFF

8.1 Excitation Voltage: 16 VRMS

8.2 Excitation Frequency: 5000 Hz

8.3 Excitation Current: 86 ma nominal untuned, 17 ma nominal after tuning A

8.4 Series Choke: None required

8.5 Primary winding impedance at room temperature: 41 + j 189 nominal A

8.6 Secondary winding impedance at room temperature: 625 + j 3550 nominal A B

8.7 Phase Angle

8.7.1 At room temperature: ±5°

8.7.2 Over operating temperature range: ±8°

8.8 Padding: As required

8.9 Load: 10,000 ohms in parallel with 1000 pf capacitor

8.10 Power Factor: 0.9 minimum with a 0.22 ±10% MFD capacitor connected across the primary (NWL to supply capacitor) B A

9.0 MOTOR

9.1 Excitation Voltage: 26 v TRMS, single phase

9.2 Excitation Frequency: 400 Hz

9.3 Excitation Waveform: Non-sinusoidal; QUASI square Wave

9.4 Power Plan

9.4.1 Starting: 3.5 watts maximum

9.4.2 Running: 3.0 watts maximum

9.5 Excitation Current

9.5.1 Starting: 125 ma maximum

9.5.2 Running: 110 ma maximum

9.6 Power Factor: Not less than 0.9

9.7 Phase splitting capacitor (to be supplied by NWL): 0.75 MFD at 100 WVDC A

9.8 Syncronization Time

9.8.1 At room temperature: 30 seconds maximum

9.8.2 Over the operating temperature range: 30 seconds maximum.

10.0 Damping Ratio over the operating temperature range: 0.5 to 1.0

11.0 MASS UNBALANCE: 0.05 °/sec/g maximum

12.0 HYSTERESIS

12.1 Definition: Hysteresis shall be calculated as the total width of the hysteresis loop at its widest point divided by total rate input used in generating the complete loop. For example, if a hysteresis loop is generated by operating the gyro first at 100°/sec CW then at 100°/sec CCW and it is found that the widest width of the loop is 4 mv while the outputs at 100°/sec are 5.98 and 5.92 volts the hysteresis shall then be calculated as:

$$HYS = \frac{(4)(10^{-3})}{5.98 + 5.92}(100) = 0.034\%$$

12.2 Value: 0.075% maximum A

13.0 Zero Offset with Output axis Up

13.1 At room temperature: ±0.2°/sec maximum

13.2 Shift over the operating temperature range: ±0.3°/sec maximum

14.0 AC NULL VOLTAGE

14.1 Total Null Voltage: 100 MVRMS maximum

14.2 Quadrature Null: TBD maximum

15.0 ALIGNMENT OF GYRO INPUT AXIS IN MOUNT A

15.1 Error: ±0.1 degrees maximum

15.2 Orientation: As shown in NWL drawing 925064

16.0 THRESHOLD: 0.01 deg/sec maximum

17.0 RESOLUTION: 0.01 deg/sec maximum

18.0 LINEARITY

18.1 Definition: The linearity error is defined as the difference between the measured output at any rate and the output as indicated by a straight line through the ±70 deg/sec points. A

18.2 Value: 0.5% of full scale plus 0.5% of the reading.

19.0 Self test Characteristics: No self test capabilities are required

20.0 DIELECTRIC STRENGTH

20.1 Once only: 250 VRMS, 60 Hz

20.2 Repeated: 150 VRMS, 60 Hz

21.0 OUTLINE CONFIGURATION: As shown in NWL drawing 925064

22.0 VIBRATION

22.1 Type: Random

22.2 Bandwidth: 1200 Hz (20 to 1200 Hz)

22.3 Density: 0.006 g^2/Hz

22.4 Amplitude: 3.8 g's peak (2.68 g's RMS) nominal

22.5 Gyro Error

22.5.1 During Vibration: Gyro to operate within spec.

22.5.2 After Vibration: No damage

23.0 ACCELERATION: These requirements are TBD

24.0 SHOCK

24.1 One-half sine, 40 g's peak, 45 MS: No damage after repeated exposure

24.2 Triangular, 10.5 g's peak, 100 MS: No damage after repeated exposure

25.0 EMI: MIL-STD-461A, Notice 4

26.0 MODULATION NOISE

26.1 0 to 1.4 Hz: Maximum allowable modulation noise increases linearly with frequency from zero at zero frequency to 0.05 deg/sec at 1.4 Hz.

26.2 1.4 to 20 Hz: 0.05 deg/sec maximum

26.3 20 to 100 Hz: 0.15 deg/sec maximum

27.0 LIFE: 1000 hours of operation minimum

DISTRIBUTION LIST
(As of March 1975)

Please notify USATACOM, AMSTA-RHM, Warren, Michigan 48090, of corrections and/or changes in address.

No. of Copies	
50	Commander U.S. Army Tank-Automotive Command Warren, MI 48090

ATTENTION:

Chief Scientist, AMSTA-CL (230)	(1)
Director of RD&E, AMSTA-R (200)	(1)
Deputy Director of RD&E, AMSTA-R (200)	(1)
Foreign Intelligence Ofc, AMSTA-RI (200)	(1)
Systems Development Division, AMSTA-RE (200)	(4)
System Engineering Division, AMSTA-RB (200)	(2)
Engineering Science Division, AMSTA-RH (200)	(6)
Armor & Components Division, AMSTA-RK (215)	(4)
Methodology Function, AMSTA-RHM (215)	(10)
Propulsion Systems Division, AMSTA-RG (212)	(3)
Canadian Forces Liaison Office, CDLS-D (200)	(1)
US Marine Corps Liaison Ofc, USMC-LNO (200)	(3)
Project Manager MICV, AMCPM-MCV (Dqr)	(2)
Product Manager XM861, AMCPM-CT (Dqr)	(2)
Project Manager, M60 Tank Dev (AMCPP-M60TD)Dqr	(2)
Project Manager XM-1, AMCPM-GCM (dqr)	(2)
Technical Library, AMSTA-RWL (200)	(3)
TRADOC Liaison Ofc, TRADOC-LNO (200)	(3)

2	Chief, Research Development and Acquisition Department of the Army Washington, DC 20310
1	Superintendent US Military Academy ATTN: Professor of Ordnance West Point, NY 10996
1	Commander US Army Logistic Center ATTN: ATCL-CC (Mr. J. McClure) Ft. Lee, VA 23801

1	Commander US Army Concept Analysis Agency Long Range Studies 8120 Woodmont Avenue Bethesda, MD 20014
1	Dept of the Army Office Chief of Engineers Chief Military Programs Team Rsch & Dev Office ATTN: DAEM-RDM Washington, DC 20314
2	Director US Army Corps of Engineers Waterways Experiment Station P.O. Box 631 Vicksburg, MS 39180
3	Director US Army Corps of Engineers Waterways Experiment Station ATTN: Mobility & Environmental Laboratory P.O. Box 631 Vicksburg, MS 39180
3	Director US Army Cold Regions Research & Engineering Lab ATTN: Dr. Freitag, Dr. W. Harrison, Library P.O. Box 282 Hanover, NH 03755
3	Commander US Army Materiel Command AMC Building, Room 8S56 ATTN: Mr. R. Navarin, AMCRD-TV 5001 Eisenhower Avenue Alexandria, VA 22333
2	President Army Armor and Engineer Board Ft. Knox, KY 40121
1	Commander US Army Arctic Test Center APO 409 Seattle, Washington 98733

2 Commander
US Army Test & Evaluation Command
ATTN: AMSTE-BB and AMSTE-TA
Aberdeen Proving Ground, MD 21005

2 Commander
Rock Island Arsenal
ATTN: SARRI-LR, Mr. Rankin
Rock Island, IL 61201

2 Commander
US Army Yuma Proving Ground
ATTN: STEYP-RPT, STEYP-TE
Yuma,Arizona 85364

1 Mr. Frank S. Mendez, P.E.
Technical Director
US Army Tropic Test Center
ATTN: STETC-TA
Box 942
Fort Clayton, Canal Zone 09827

1 Commander
US Army Natick Laboratories
ATTN: Technical Library
Natick, Massachusetts 01760

1 Director
US Army Human Engineering Laboratory
ATTN: Mr. Eckels
Aberdeen Proving Ground, MD 21005

2 Director
US Army Ballistic Research Laboratory
Aberdeen Proving Ground, MD 21005

3 Director
US Army Materiel Systems Analysis Agency
ATTN: AMXSY-CM, Messrs. D. Woomert, W. Niemeyer,
W. Criswell
Aberdeen Proving Ground, MD 21005

12 Director
Defense Documentation Center
Cameron Station
Alexandria, VA 22314

1 US Marine Corps
Mobility & Logistics Division
Development and Ed Command
ATTN: Mr. Hickson
Quantico, VA 22134

1 Mr. A. M. Wooley
West Coast Test Branch
Mobility and Support Division
Marine Corps Base
Camp Pendleton, CA 92055

1 Naval Sea Systems Command
Code PMS300A1
Department of the Navy
Washington, DC 20362

1 Naval Ship Research & Dev Center
Aviation & Surface Effects Dept.
Code 161
ATTN: E. O'Neal & W. Zeitfuss
Washington, DC 20034

1 Director
National Tillage Machinery Laboratory
Box 792
Auburn, Alabama 36830

1 Director
USDA Forest Service Equipment Dev Center
444 East Bonita Avenue
San Dimas, CA 91773

1 Dr. R. A. Liston
Director, Keweenaw Research Center
Michigan Technological University
Houghton, MI 49931

1 Engineering Societies Library
345 East 47th Street
New York, NY 10017

1 Dr. M. G. Bekker
224 East Islay Drive
Santa Barbara, CA 93101

1	Dr. I. R. Ehrlich, Dean for Research Stevens Institute of Technology Castle Point Station Hoboken, NJ 07030
2	Grumman Aerospace Corporation ATTN: Dr. L. Karafiath, Mr. E. Markow Plant 35 Bethpage, Long Island, NY 11714
1	Dr. Bruce Liljedahl Agricultural Engineering Department Purdue University Lafayette, IN 46207
1	Dr. W. G. Baker Dean, College of Engineering Universtty of Detroit 4001 W. McNichols Detroit, MI 48221
1	Mr. H. C. Hodges Nevada Automotive Test Center Box 234 Carson City, NV 89701
1	Mr. W. S. Hodges Lockheed Missile & Space Corporation Ground Vehicle Systems Department 50-24, Bldg 528 Sunnyvale, CA 94088
1	Mr. R. D. Wismer Deere & Company Engineering Research 3300 River Drive Moline, IL 61265
1	Oregon State University Library Corvallis, Oregon 97331
1	Southwest Research Institute ATTN: Mr. R. C. Hemion 8500 Culebra Road San Antonio, TX 78228

1 FMC Corporation
Technical Library
P.O. Box 1201
San Jose, CA 95108

1 Mr. J. Appelblatt
Director of Engineering
Cadillac Gamge Co.
P.O. Box 1027
Warren, MI 48090

2 Chrysler Corporation
Mobility Research Laboratory,
Defense Engineering
ATTN: Dr. B. VanDeusen, Mr. =. Cohron
Department 6100
P.O. Box 751
Detroit, MI 48231

1 Library
CALSPAN Corporation
Box 235
4455 Genessee Street
Buffalo, NY 14221

1 Mr. Sven E. Lind
SFM, Forsvaretsforskningsanstalt
Avd 2
Stockholm 80, Sweden

2 Mr. Rolf Schreiber
c/o Bundesamt Fuer Wehrtechnik
Und Beschaffung - KGII 7 -
5400 Koblenz
Am Rhein 2-6 Germany

1 Foreign Science & Technology Ctr
220 7th Street North East
ATTN: AMXST-GE1
Mr. Tim Nix
Charlottesville, Va 22901

1 General Research Corporation
ATTN: Mr. A Viilu
7655 Old Springhouse Road
Westgate Research Park
Mc Lean, VA 22101

1 Commander
US Army Materiel Command
ATTN: AMCRD-T (Dr. Norman Klein)
5001 Eisenhower Avenue
Alexandria, VA 22333

1 Commander US Army Materiel Command
ATTN: AMCRD-GV, Mr. Robert Green
5001 Eisenhower Avenue
Alexandria, VA 22333

179 UNCLASSIFIED

SECURITY CLASSIFICATION OF THIS PAGE (When Data Entered)

REPORT DOCUMENTATION PAGE

READ INSTRUCTIONS BEFORE COMPLETING FORM

1. REPORT NUMBER: 11893 (LL-146)

2. GOVT ACCESSION NO.

3. RECIPIENT'S CATALOG NUMBER

9

4. TITLE (and Subtitle)

6

Feasibility Analysis and Evaluation of an Adaptive Tracked Vehicle Suspension and Control System.

5. TYPE OF REPORT & PERIOD COVERED: Final Report,

6. PERFORMING ORG. REPORT NUMBER

7. AUTHOR(s)

10

Robert M. Salemka, National Water Lift Company
Dr. Ronald R. Beck, US Army Tank Automotive Comd

8. CONTRACT OR GRANT NUMBER(s)

15

DAAE07-72-C-0176

9. PERFORMING ORGANIZATION NAME AND ADDRESS

National Water Lift Company
2200 Palmer Avenue
Kalamazoo, Michigan 49001

10. PROGRAM ELEMENT, PROJECT, TASK AREA & WORK UNIT NUMBERS

16 DA-1Y062112A045
502C.55 8220

11. CONTROLLING OFFICE NAME AND ADDRESS

US Army Tank Automotive Command
Rsch, Dev & Engr Directorate
Warren, MI 48090

12. REPORT DATE

11 June 1975

12 181p.

13. NUMBER OF PAGES: 180

14. MONITORING AGENCY NAME & ADDRESS (if different from Controlling Office)

15. SECURITY CLASS. (of this report): UNCLASSIFIED

15a. DECLASSIFICATION/DOWNGRADING SCHEDULE

16. DISTRIBUTION STATEMENT (of this Report)

Approved for public release; distribution unlimited

17. DISTRIBUTION STATEMENT (of the abstract entered in Block 20, if different from Report)

18 TACOM, LL

18. SUPPLEMENTARY NOTES

19 TR-11893, 146

19. KEY WORDS (Continue on reverse side if necessary and identify by block number)

Computerized simulation
suspension devices
road wheels
tracked vehicles
damping
pitch (motion)

20. ABSTRACT (Continue on reverse side if necessary and identify by block number)

This study shows that adaptive control of the jounce damping characteristics of the first and last wheel of a tracked vehicle can cause a significant improvement in performance. This improvement resulted in an overall 30 percent reduction in average pitching rate of the hull, as measured on the simulation of the MICV vehicle traversing the JEA bump course.

Verification testing of the computer model with actual performance data of the

(SEE REVERSE SIDE)

DD FORM 1 JAN 73 1473 EDITION OF 1 NOV 65 IS OBSOLETE

UNCLASSIFIED

SECURITY CLASSIFICATION OF THIS PAGE (When Data Entered)

MICV vehicle showed good correlation of peak amplitudes and hull resonance. This data also confirmed that the actual dampers are working well below recommended levels.

A proposed method of mechanizing and testing the adaptive control on an actual vehicle is presented along with system schematics and preliminary performance specifications for the critical components.